Cellular effects of phosphoinositide derivatives on the actin cytoskeleton.

Thesis

CELLULAR EFFECTS OF PHOSPHOINOSITIDE DERIVATIVES ON THE ACTIN CYTOSKELETON

Beatrice Maria Filippi

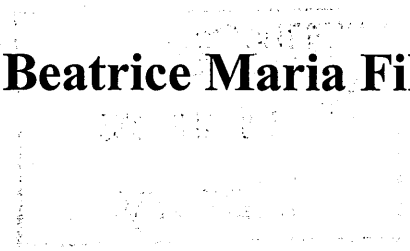

Discipline: Life science

Sponsoring establishment: Consorzio Mario Negri sud

Thesis submitted in accordance with the requirements of the Open University for the degree of Doctor of Philosophy

November 2005

DATE OF SUBMISSION 29 NOVEMBER 2005
DATE OF AWARD 06 MARCH 2006

To the memory of my father
and to my mother

ABSTRACT

The glycerophosphoinositols are water-soluble, biologically active phospholipase A_2 metabolites that are derived from phosphoinositides. The cellular concentrations of the glycerophosphoinositols have been shown to increase in hormone- and Ras-activated cells. Glycerophosphoinositol 4-phosphate (GroPIns4P) is the most active and well studied of the glycerophosphoinositols. When added exogenously, GroPIns4P can enter cells and affect various cellular functions, such as adenylyl cyclase (AC) activity (inhibition) and actin cytoskeleton organization (stimulation of ruffle and stress fibre formation). GroPIns4P acts at the level of the Rac1 and RhoA GTPases of the Rho family to form ruffle and stress fibres, and in addition, it increases the cytosolic fraction of GTP-bound Rac1 and favours its translocation to the plasma membrane.

In the present study, the mechanisms of action of the glycerophosphoinositols, with focus on GroPIns4P, have been characterized, with two potential mechanisms of action being revealed. On the one hand, GroPIns4P initiates a signal cascade that start from Src activation and leads to a phospholipase Cγ-dependent increase in intracellular Ca^{2+} and the consequent activation of Ca^{2+}/calmodulin kinase II (CaMKII); this kinase can, in turn, activate TIAM1, a specific exchange factor of Rac1 that is involved in Rac1-dependent ruffle formation. On the other hand, GroPIns4P increases the binding between GDP-bound Rac1 and TIAM1 in pull-down assays and interacts with a protein complex that co-immunoprecipitates with TIAM1, and which also contains CaMKII. These data suggest that besides the signalling pathway initiate by Src, GroPIns4P can favour the formation of a large protein complex that could provide the machinery important for ruffle formation.

The other activities of GroPIns4P, such as AC inhibition and stress fibre formation, are not modulated by the same pathway as ruffle formation, thus suggesting that GroPIns4P is a multifunctional compound that is able to modulate different cellular functions by acting through multiple targets.

TABLE OF CONTENTS

LIST OF FIGURE

LIST OF TABLE

CHAPTER 1

INTRODUCTION

1.1 Aim of the study

The glycerophosphoinositols are natural, water-soluble, cell-permeable and biologically active compounds. Their formation has been linked to Ras activation and their activity involves many different cellular events. Glycerophosphoinositol 4-phosphate (GroPIns4P) is the most active and well studied of the glycerophosphoinositols, and it is able to modulate actin cytoskeleton organization. Actin filaments provide the basic infrastructure for the maintenance of cell morphology, which includes functions such as adhesion, motility, exocytosis, endocytosis and cell division. Alterations in actin polymerization, or actin remodelling, have a pivotal role in regulating the morphological and phenotypic events of a malignant cell. The aim of this study is to define the mechanisms of action of the glycerophosphoinositols in actin cytoskeleton organization, with this analysis focused on GroPIns4P, the most active and well characterized glycerophosphoinositol.

1.2 Function and modulation of the actin cytoskeleton

This section will provide a general background about the organization of the actin cytoskeleton, focusing on the process of actin polymerization for cell protrusion (formation of lamellipodia, ruffles and stress fibers). This will allow to better understand the mechanisms of action of glycerophosphoinositols on actin cytoskeleton organization.

1.2.1 The cytoskeleton

The cytoskeleton contains a complex network of filamentous proteins that extends throughout the cytoplasm. It consists of an elaborate array of protein fibres that serve in functions such as establishing cell shape, providing mechanical strength, locomotion, chromosome separation in mitosis and meiosis, and intracellular transport of organelles. The cytoskeleton is made up of three kinds of protein filaments: microtubules, intermediate filaments and actin filaments (microfilaments) (Fig. 1.1).

Microtubules are straight, hollow cylinders with a diameter of about 25 nm; their length is variable, but they can grow up to 1000-times as long as they are thick. Microtubules are built by the assembly of heterodimers formed by α and β tubulin that polymerize and form a spiral structure. This polymerization of tubulin dimers is powered by the hydrolysis of GTP and can occur at each end of the microtubule, even if it is more rapid at the plus end. The filaments can then shrink at each end by the release of tubulin dimers (depolymerization), which occurs more rapidly at the minus end (Hunter and Wordeman, 2000).

Microtubules participate in a wide variety of cell activities, most of which involve motion. This motion is provided by protein motors, like the kinesins, most of which move towards the plus ends of microtubules and the dyneins, which move toward the minus ends; in all cases the energy for movement is provided by ATP hydrolysis. The rapid transport of organelles, like vesicles and mitochondria, along the axons of neurons takes place along microtubules, with their plus ends pointed towards the end of the axon (Mallik and Gross, 2004).

The movement of chromosomes in mitosis and meiosis takes place along the microtubules that make up the spindle fibres. Both kinesins and dyneins are used as motors, and the spindle fibres arise from the microtubule organizing centre (MTOC). The MTOC in animal cells is the centrosome, which is located in the cytoplasm just outside the nucleus. Before mitosis, the centrosome duplicates and the two centrosomes move apart

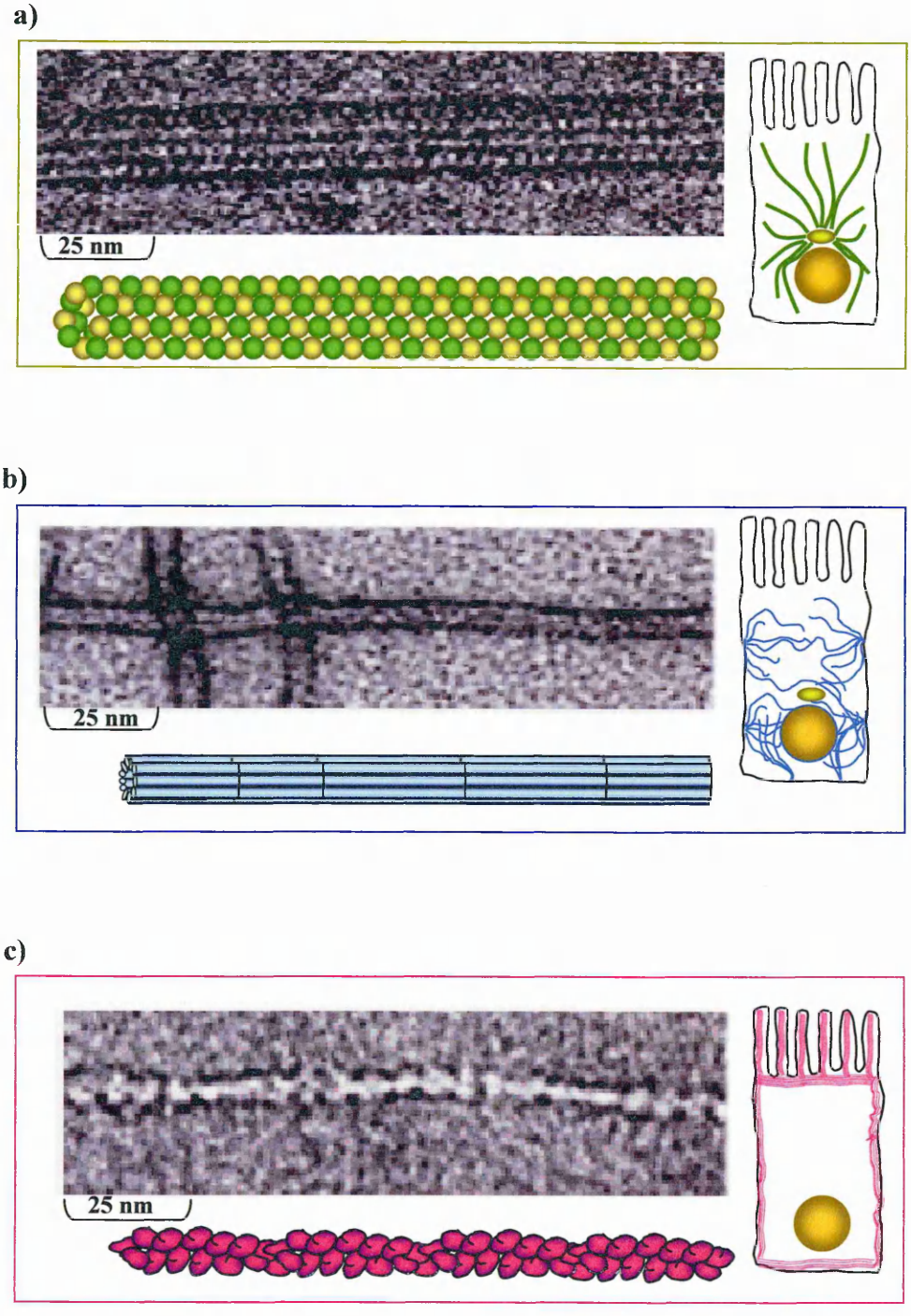

Figure 1.1 - Schematic representation of the structure of microtubules (a), intermediate filaments (b) and actin filaments (c) with the corresponding electro-microscopy images.

until they are on opposite sides of the nucleus (Dogterom et al., 2005). In addition to their role in spindle formation, centrosomes have other important roles in animal cells: as regulators of the correct signalling to proceed to S phase or cytokinesis. Each centrosome contains a pair of centrioles. The centrioles are built from a cylindrical array of nine microtubules, each of which has attached to it two partial microtubules. When a cell enters the cell cycle, and proceeds from G_1 to S phase, each centriole is duplicated. The centrioles appear to be needed to organize the centrosome in which they are embedded, and are also needed to make cilia and flagella (Silflow and Lefebvre, 2001).

The intermediate filaments are cytoplasmic fibres that are an average of 10 nm in diameter, and thus they are "intermediate" in size between actin filaments (8 nm) and microtubules (25 nm). There are several types of intermediate filaments, each of which is constructed from one or more characteristic proteins. The *keratins* are found in epithelial cells and also form hair and nails; the nuclear *lamins* form a meshwork that stabilizes the inner membrane of the nuclear envelope; the *neurofilaments* strengthen the long axons of neurons; and the *vimentins* provide mechanical strength to muscle (and other) cells. Despite their chemical diversity, intermediate filaments have similar roles in the cell, which involves providing a supporting framework within the cell. For example, the nucleus in epithelial cells is held within the cell by a basket-like network of intermediate filaments made of keratins. Different kinds of epithelia use different keratins to build their intermediate filaments. Over 20 different kinds of keratins have been described, although each kind of epithelial cell may use no more than two of them. Up to 85% of the dry weight of squamous epithelial cells can consist of keratins (DePianto and Coulombe, 2004).

Actin filaments are about 8 nm in diameter, and being the thinnest of the cytoskeletal filaments, they are also called microfilaments (in skeletal muscle fibres they are called "thin" filaments). Actin is the most abundant protein in the cytoplasm of mammalian cells, often amounting to 10 % to 20 % of the total cytoplasmic protein. Actin

filaments have many different functions in the cell: they form a layer just beneath the plasma membrane that provides mechanical strength to the cell, links transmembrane proteins (e.g. cell surface receptors) to cytoplasmic proteins, anchors the centrosomes at opposite poles of the cell during mitosis, and pinches dividing animal cells apart during cytokinesis. Moreover they can generate cytoplasmic streaming in some cells, generate locomotion in cells such as white blood cells and the amoeba, and interact with myosin ("thick") filaments in skeletal muscle fibres to provide the force of muscular contraction (Holmes et al., 1990).

Actin exists either as a globular monomer (called G-actin) or as a filament (designated F-actin). Different isoforms of G-actin can be found in cells: there are four α isoforms present in muscle cells, while the β and γ isoforms are formed in non-muscle cells. They are characterised by the presence of two different lobes separated by a deep cleft, where the Mg^{2+}/ATP complex is bound. F-actin has a polarity that is formed by the head-to-tail polymerization of asymmetric monomers. At the minus (pointed) end the ATP-binding cleft is exposed to the surrounding solution, and at the plus (barbed) end, the cleft is in contact with the neighbouring actin subunits (dos Remedios et al., 2003).

The first step in actin filament formation *in vitro* is called nucleation. In this low probability event, three actin monomers are believed to combine simultaneously, forming a thermodynamically unstable trimeric nucleus. Once a trimer is formed, this nucleus most frequently dissociates back into monomers. However, this nucleus occasionally survives long enough to permit the subsequent binding of additional actin molecules. As this elongation reaction proceeds *in vitro*, monomeric actin molecules (each containing ATP) are added one by one to both ends of the elongating nucleus, to form filaments. Monomer addition is more rapid at the plus end, and in the cell little or no monomer addition takes place at the minus end. After monomer incorporation into growing filaments, ATP-actin undergoes nucleotide hydrolysis to form ADP-actin subunits within the helical lattice of the filament. Once the actin filaments reach a steady-state length, ADP-actin monomers are

released from the minus ends of the filaments at the same rate as new ATP-actin monomers are added to the plus ends (Carlier et al., 1987). There is a dynamic equilibrium between the monomeric pool (G-actin) and the filaments (F-actin), which depends on the different rates of polymerization at the pointed and barbed ends. Barbed ends elongate 5-10-times faster than pointed ends. The critical monomer concentration is 0.1 μM at the plus ends and 0.8 μM at the minus ends. When the concentration of actin monomers is between 0.1 and 0.8 μM, the plus ends elongate and the minus ends dissociate (steady state). This situation in which the net length of actin filament is constant is known as actin treadmilling (Korn et al., 1987).

In the cell, two additional issues are important: first, actin monomer addition occurs mostly, if not exclusively, at the plus ends; and second, this process probably produces a pool of ADP-actin from which ATP-actin must be regenerated by exchange (not by direct phosphoryl transfer) with ATP in the cytoplasm. ATP-actin has a much higher affinity for the ends of actin filaments than ADP-actin does, and ATP-actin is the primary monomeric species of actin that adds to filament ends in the cell. Moreover, a multitude of actin binding proteins (ABPs) in the cell control the state of actin assembly and polymerisation events (dos Remedios et al., 2003).

1.2.1.1 Actin binding proteins

In the cell, the transition between G-actin and F-actin is very closely regulated by numerous different proteins. They can act by sequestering actin monomers, by favouring actin nucleation, by linking the actin filaments to the membrane, and by determining the position and orientation of actin bundles.

The capping proteins bind at the ends of actin filaments. Depending on whether they bind at the plus or minus end, different capping proteins may stabilize the filament or promote its disassembly (Carlier and Pantaloni, 1994).

Actin filaments may associate into bundles or networks via cross-linking proteins. Most cross-linking proteins are dimeric or have two actin-binding domains. Depending on the length of a cross-linking protein, or the distance between its actin-binding domains, actin filaments may be held close together in parallel bundles, or may be far enough apart to allow interactions with other proteins, such as myosin. ***Filamin*** is a V-shaped cross-linking protein; it causes actin filaments to associate in loose networks that give a gel-like consistency to some areas of the cytosol (Feng and Walsh, 2004). ***Spectrin*** is an actin-binding protein that forms an elongated tetrameric complex (Thomas, 2001). ***α-actinin*** is a bipolar linker that forms parallel bundles of actin filaments (Otey and Carpen, 2004).

The group of severing proteins contains ABPs that favour the dissociation of monomer from F-actin. ***Gelsolin*** functions in gel/sol transitions in the cytosol (Sun et al., 1999). When activated by Ca^{2+}, gelsolin severs an actin filament and caps the plus end, blocking filament regrowth. In the absence of Ca^{2+}, gelsolin does not bind actin, as Ca^{2+} causes a conformational change in gelsolin that exposes one of its actin-binding site. Actin contributes a Glu carboxyl group to one of the two Ca^{2+}-binding sites (Bryan and Kurth, 1984; Yin and Stossel, 1980). ***Cofilin*** is a member of a family of proteins called actin-depolymerising factors (ADFs) (Bamburg, 1999). Cofilin binds along the sides of actin filaments and distorts the helical twist, and under some conditions, cofilin can sever actin filaments (McGough et al., 1997). Cofilin promotes dissociation of G-actin-ADP (as a complex with cofilin) from the minus ends of actin filaments. Cofilin binding to G-actin-ADP inhibits ADP/ATP exchange, inhibiting actin polymerization. Phosphorylation of cofilin causes it to dissociate from G-actin, which can then undergo ADP/ATP exchange and add to the plus ends of F-actin. In some cases, actin polymerization may be triggered by signalling cascades that lead to the phosphorylation of cofilin (Theriot, 1997). ***Thymosin β4***, is a small acidic peptide (5 kDa) that forms a 1:1 complex with G-actin, and it is proposed to "buffer" the concentration of free actin, by maintaining a pool of monomeric actin. An increase in the concentration of thymosin β4 can promote

depolymerization of F-actin by lowering the concentration of free G-actin (Huff et al., 2001). ***Profilin*** has a role in regulating actin polymerization. It forms a 1:1 complex with G-actin and binds at the plus end, on the opposite side to the nucleotide-binding cleft, altering the conformation of G-actin and making its nucleotide-binding site more open to the cytosol. This promotes ATP/ADP exchange (Goldschmidt-Clermont et al., 1992). Profilin binds to some membrane elements involved in cell-cell signalling, suggesting that they may be important in controlling actin assembly. It can bind to phosphatidylinositol 4,5-bisphosphate ($PI4,5P_2$) at the plasma membrane, through proline-rich sequences that are commonly found in membrane-associated signalling proteins (Vasp, Mena, etc....) (Lassing and Lindberg, 1985; Witke, 2004). These interactions allow the localization of profilin to the plasma membrane without inhibiting its binding to G-actin. Profilin also promotes the assembly of actin, acting as an ATP/ADP exchange factor. It increases the local concentration of G-actin-ATP, the form that is able to polymerize. Profilin is the only ABP that allows ATP/ADP exchange (Carlier and Pantaloni, 1994).

1.2.1.2. Actin-nucleation-promoting factors

In vivo actin nucleation is dependent on the free barbed ends, which can arise by either *de novo* nucleation of filaments from a nucleation template, by uncapping of the barbed ends through the loss off the capping protein, or by severing of non-covalent bonds between monomers in filamentous actin, producing short filaments with free barbed ends.

The Arp2/3 complex is one of the major players for *de novo* synthesis of actin filaments. It is a conserved complex of seven polypeptides, two of which are actin-related proteins: Arp2 and Arp3. This complex is found in filament networks at Y-branches and in association with barbed ends at the leading edge of fixed cells. When is activated, it nucleates new actin filaments from the sides of existing filaments (Pollard and Beltzner, 2002). The exact mechanism by which the Arp2/3 complex nucleates actin is not

completely understood. Two models of actin nucleation by the Arp2/3 complex have been proposed, each of which is supported by experimental evidence (Condeelis, 2001):

1) The dendritic nucleation model proposes that the nucleation activity of the Arp2/3 complex to form a daughter filament is stimulated by binding to the sides of pre-existing actin filaments (Fig. 1.2). The new filament will be shorter than the pre-existing one (Pollard et al., 2000).
2) The protein barbed-end branching model proposes that the Arp2/3 complex binds to and branches free barbed ends, resulting in two new filaments with equal length (Fig. 1.2) (Pantaloni et al., 2000).

However actin nucleation can also start from:

3) Uncapping of barbed ends, through which Arp2/3 complex attaches and starts the polymerization (Barkalow et al., 1996);
4) Severing proteins, which create free barbed ends from pre-existing filaments. This is the case for the gelsolin Ca^{2+}-dependent severing activity (McGough et al., 1997). Also, ADF/cofilin induces the detachment of G-monomers from actin filaments that have free barbed ends. Moreover, it increases the concentration of free G-actin, enhancing the polymerization rate (Ghosh et al., 2004).

In all of these cases the net result is the formation of a complex actin meshwork, with actin filaments that cross each other, typical of lamellipodial structures (Small et al., 2002) (see Section 1.2.2).

The nucleation activity of Arp2/3 complex is regulated by multiple signalling pathways, through members of Wiskot-Aldrich-syndrome protein (WASP) family (Pollard and Borisy, 2003). There are at list six mammalian WASP family members, including WASP, N-WASP and four Scar/WAVEs. N-WASP can activate the Arp2/3 complex directly, and is recruited by Shigella and Vaccina viruses. Scar/WAVE is found in vertebrate cells and has been implicated in activating the Arp2/3 complex in lamellipodium formation; in fact, it localizes at their tips (Bompard and Caron, 2004).

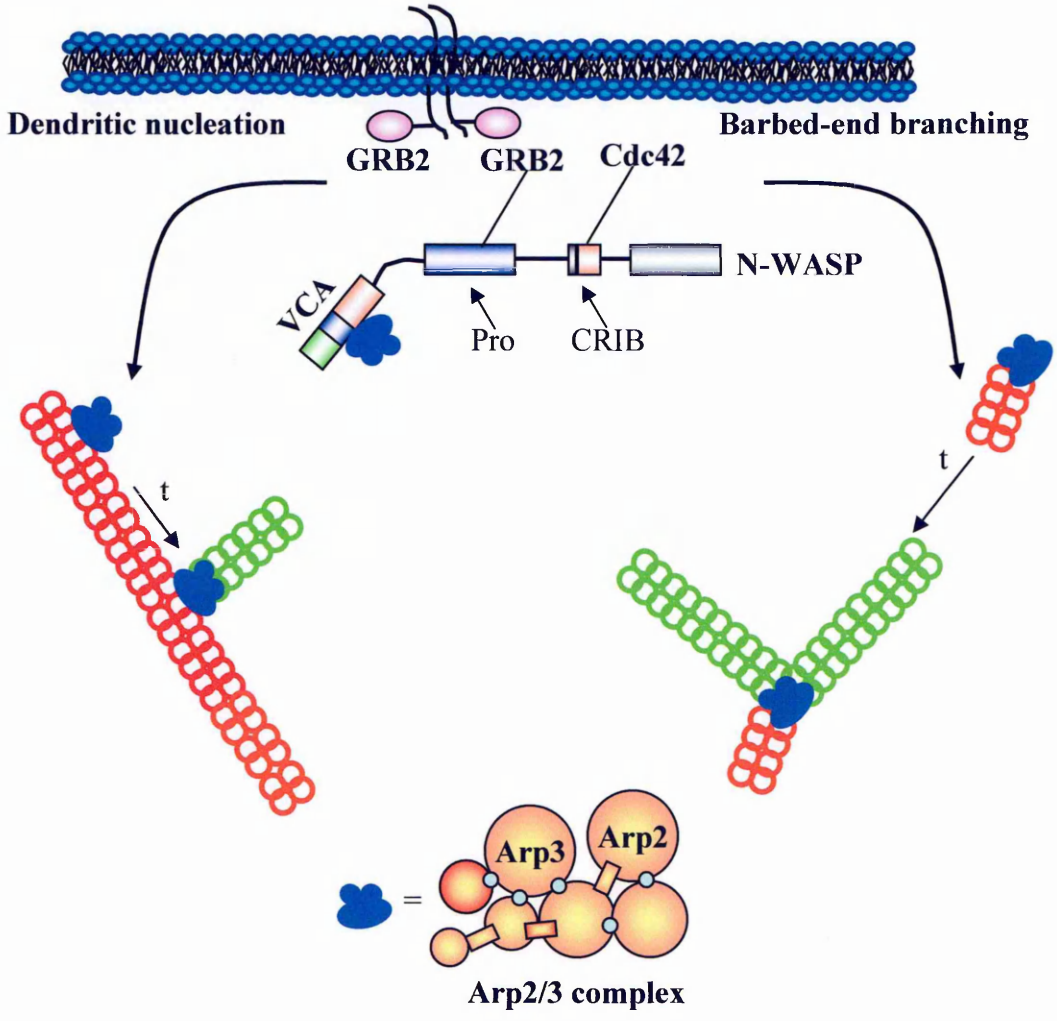

Figure 1.2 - Models of actin nucleation by the Arp2/3 complex. Left, the dendritic nucleation model proposes that the nucleation activity of the Arp2/3 complex to form a daughter filament (green) is stimulated by binding to the sides of pre-existing actin filaments (red). Right, the barbed-end branching model proposes that the Arp2/3 complex binds to and branches free barbed ends, resulting in two new filaments (green). The initial stimulation of nucleation activity, by binding of a protein from the WASP family to the Arp2/3 complex at cell membrane, is common to both models. The stimulatory complex is formed following binding to a G-protein, GRB2 or other ligands to N-terminal domains of WASPs. This changes the WASP conformation and allows binding of the VCA domain to the Arp2/3 complex (Condeelis et al., 2001) .

The initial stimulation of nucleation activity implies the binding of a protein from the WASP family to the Arp2/3 complex at the cell membrane. The stimulatory complex is formed following binding of a G-protein, or other ligand, to the N-terminal domains of WASPs. This changes the WASP conformation and allows binding of the verprolin-homology–cofilin-homology–acidic (VCA) domain to the Arp2/3 complex (Pollard and Borisy, 2003) (Fig. 1.3).

The signalling to actin at the leading edge of the lamellipodium implies that N-WASP is activated and targeted to the membrane. G-actin and the Arp2/3 complex bind the exposed COOH-terminal domain of N-WASP (VCA), forming a branching complex. Association of the branching complex with a filament leads to the formation of a branch, and the two branches grow at equal rates. N-WASP catalyzes several consecutive cycles of branching (Fig. 1.3) (see Section 1.2.2).

Ena/VASP (Vasodilator stimulating phosphoprotein) accumulates at the tip of lamellipodia and filopodia, corresponding to the sites of fast growing ends of actin filaments at the cell membrane. The amount of VASP recruited to the lamellipodium tips increased with the protrusion rate. More than a direct activator, this protein can function as a co-factor for actin nucleation (Pantaloni et al., 2001).

The Arp2/3 complex is not the nucleator of all actin filaments, as many cellular events that imply actin nucleation can occur also in the absence of this complex. At least some of these Arp2/3-independent structures are controlled by members of the ***formin*** family of proteins. Formins are a family of highly conserved eukaryotic proteins implicated in a wide range of actin-based processes, including cell polarization, cytokinesis, hair cell stereocilia formation, sperm cell acrosome formation and embryonic development (Ridley, 1999; Wasserman, 1998; Zeller et al., 1999). A distinct class of formins, the Diaphanous-related formins (Drfs) has been defined on the basis of their ability to interact with the activated GTP-bound form of a Rho-type GTPase through an N-

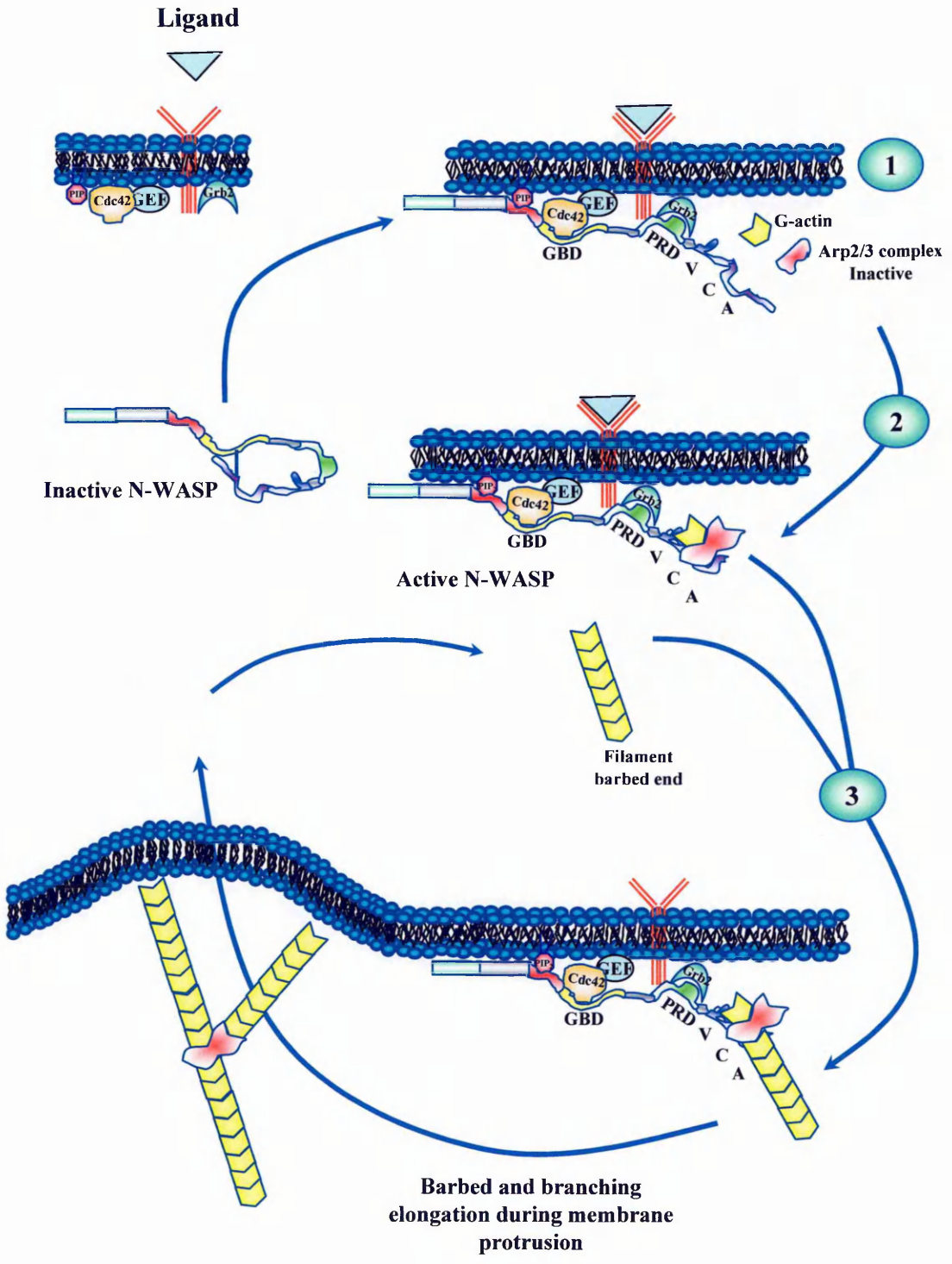

Figure 1.3 - Signalling to actin at the leading edge of the lamellipodium. N-WASP is activated and targeted to the membrane by signalling molecules (1). G-actin and the Arp2/3 complex bind the exposed COOH-terminal domain of N-WASP (VCA), forming a branching complex (2). Association of the branching complex with a filament leads to the formation of a branch (3). The two branches grow at equal rates. N-WASP catalyzes several consecutive cycles of branching (Pantaloni et al., 2001).

terminal Rho-binding domain (Evangelista et al., 1997; Habas et al., 2001; Imamura et al., 1997; Kohno et al., 1996; Watanabe et al., 1997). These Drfs are regulated by auto-inhibition through interaction between the diaphanous inhibitory domain (DID) and diaphanous auto-regulatory domain (DAD), and activated by Rho GTPase binding to GTPase-binding domains (GBD) (Alberts, 2001; Watanabe et al., 1999). This regulatory activity was originally characterized in mDia1, a mammalian ortholog of *Drosophila Diaphanous,* which has been linked to actin filament assembly in both *Drosophila* and yeast (Watanabe et al., 1999), and a consensus DAD domain is a general feature of Drfs (Alberts, 2001). Some formins may be regulated by other signalling pathways or different mechanisms. The formins are able to nucleate actin bundles starting from the G-actin/profilin complex. The polymerisation occurs along the actin filament and the result is the formation of long and thin actin fibres that differ from the classical actin branching induced by the Arp2/3 complex (Fig. 1.4 a). For example in fibroblasts, mDia1 is required for Rho-dependent stress fibre formation (Nakano et al., 1999).

1.2.2. Assembling the actin cytoskeleton for cell attachment and movement

Cell migration is a critical component of many physiological and pathological events, including development, wound repair, angiogenesis and metastasis (Price et al., 1997). In many cases, these events are mediated by cytokine, integrin and growth factor receptors that transmit a cascade of signals that are important for the regulation of the migration machinery (Keely et al., 1998). The driving force of cell movement is provided by the dynamic reorganization of actin cytoskeleton, directing protrusion at the front of the cell and retraction at the rear. The locomotory process for fibroblastic cells can be divided into essentially three independent sequential phases: (i) the polar extension of a leading lamella (**lamellipodium**) via the active motility of the anterior leading edge; (ii) the formation of anterior contacts with the underlying substrate (focal contacts); and (iii) the

retraction of the trailing tail into the advancing cell body (Condeelis, 2001; Raftopoulou and Hall, 2004). The lamellipodium is characterised by the presence of a dense actin meshwork and fine bundles containing microfilaments. It contains extensively branched arrays of actin filaments, oriented with their plus (barbed) ends toward the plasma membrane. Actin monomers are incorporated at the membrane, bordering the front of lamellipodium; there, the actin treadmilling is active and the continuous nucleation pushes the cell forward (Small et al., 1998). **Membrane ruffles** are often found on the cell surface and at the advancing front of lamellipodium. They consist of dynamic fluctuating movements of the membrane (membrane curling), formed by continuous attachment and detachment of the membrane at the leading edge and characterised by accumulation of actin and vinculin as precursors of focal contacts (Rinnerthaler et al., 1988). Ruffles are believed to serve as sites of actin polymerisation, endocytosis (dorsal ruffles), receptor tyrosine kinase signalling, protease activation and receptor internalization (circular ruffles) (Lauffenburger and Horwitz, 1996). **Filopodia or microspikes** are another characteristic feature that can be found at the front of a moving cell. These consist of long, thin and transient processes that extend out from the cell surface. Bundles of parallel actin filaments, oriented with their plus ends towards the filopodial tip, are cross-linked within filopodia by the small actin-binding protein fascin (Small et al., 2002). **Stress fibres** form when a cell makes stable connections to a substrate. Bundles of crosslinked actin filaments extend from the cell surface through the cytosol. In a spreading fibroblast, the ventral stress fibres are commonly extended from an anchoring site (focal adhesion) close to the cell edge, to one with a perinuclear location. Actin filaments, the plus ends of which are oriented towards the cell surface on opposite sides of the cell, can overlap in more interior regions of a cell, in antiparallel arrays (Small et al., 1998). Myosin mediates sliding of antiparallel actin filaments during contraction of stress fibres. α-Actinin can cross-link actin filaments within stress fibres, as well as within lamellipodia (Defilippi et al., 1999) (Fig. 1.4b).

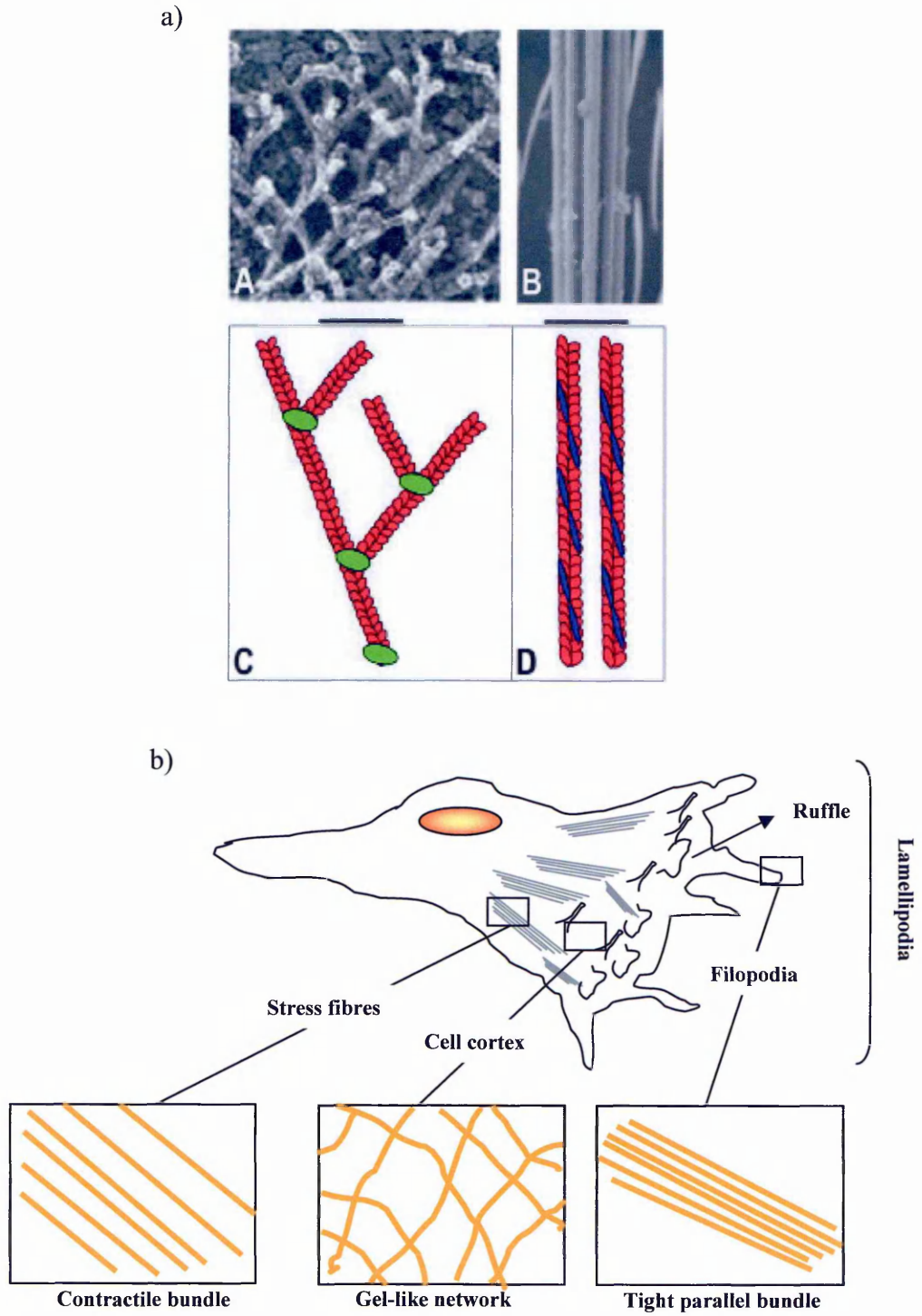

Figure 1.4 - Ultra-structure of Actin at the level of Lamellipodia and stress fibre. **a)** The branched actin networks found in fibroblast lamellipodia (A) and actin bundles in a bristle of *Drosophila melanogaster* (B) (bar, 0.1 μm); a schematic diagram showing branched (C) and unbranched (D) actin filaments. The Arp2/3 complex (green) crosslinks and stabilises branched filaments, whereas tropomyosin (purple) stabilises unbranched filaments (from Evangelista et al., 2003).
b) Schematic representation of the actin structures at the level of lamellipodia, filopodia end stress fibres in a moving cell.

New focal adhesions are formed within and at the base of the lamellipodium, probably from pre-existing focal contacts. These sites, which undergo localized actin bundling, are favourable templates for stress fibre formation (Small et al., 1998).

Many different signalling molecules have been implicated in actin remodelling, including MAPK (mitogen activated protein kinase) cascades, lipid kinases, phospholipases, Ser/Thr and Tyr kinases and scaffold proteins. However, a specific family of proteins plays a pivotal role in regulating this pathway, favouring one morphological feature versus another: the Rho family of GTPases.

1.2.3. The Rho family of GTPases.

Small GTP-binding proteins (G-proteins) are monomeric proteins with molecular masses of 20-30 kDa, which are grouped into the Ras superfamily. The Ha-Ras and Ki-Ras genes were first discovered as the v-Ha-Ras and v-Ki-Ras oncogenes of sarcoma viruses (Kirsten and Harvey sarcoma) in around 1980 (Chien et al., 1979; Shih et al., 1978). The cellular oncogenes were then identified in humans and their mutations were found in some human carcinomas (Hall et al., 1983). Now, more than 100 small G-proteins have been identified in eukaryotes from yeast to humans and classified within the Ras superfamily (Takai et al., 2001). The members of this superfamily are structurally classified into five families: the Ras, Rho, Rab, Sar1/Arf and Ran families. The functions of many small G-proteins have been elucidated: the Ras subfamily members (Ras proteins) of the Ras family mainly regulate gene expression; the Rho/Rac/Cdc42 subfamily members (Rho/Rac/Cdc42 proteins) of the Rho family regulate both cytoskeletal reorganization and gene expression; the Rab and Sar1/Arf family members (Rab and Sar1/Arf proteins) regulate intracellular vesicle trafficking; and the Ran family members (Ran proteins) regulate nucleo-cytoplasmic transport during G1, S, and G2 phases of the cell cycle and microtubule organization during the M phase (Takai et al., 2001).

These small G-proteins act as molecular switches, cycling between the GDP- and GTP-bound forms. When bound to GDP, they are inactive and when bound to GTP they undergo conformational changes that favour their interaction with downstream effectors. The GTP-bound form is converted by the action of the intrinsic GTPase activity to the GDP-bound form, which then releases the bound downstream effector.

The rate-limiting step of the GDP/GTP exchange reaction is the dissociation of GDP from the GDP-bound form. This reaction is extremely slow and therefore stimulated by a guanine nucleotide exchange factors (GEFs). A GEF first interacts with the GDP-bound protein and releases bound GDP, to form a binary complex of a small G-protein and the GEF. Then, the GEF in this complex is replaced by GTP to form the GTP-bound form. The GEFs are specific for each small G protein. Rho/Rac/Cdc42 and Rab proteins are also regulated by another type of factor, the Rho GDP dissociation inhibitors (GDIs) and Rab GDI, respectively. This regulator inhibits both the basal and GEF-stimulated dissociation of GDP by sequestering the GDP-bound form in the cytoplasm. The intrinsic GTP hydrolysis of the small GTPases is very slow and is enhanced by GTPase-activating proteins (GAPs). Most GAPs, such as Ras GAP and Rab3 GAP, are specific for each member or subfamily of small G-proteins, but some GAPs, such as p190, a GAP active on Rho/Rac/Cdc42 proteins, show a wider substrate specificity (Fig. 1.5) (Takai et al., 2001).

The major players in actin cytoskeleton modification are the small GTPase of the Rho family. When activated, they have a pivotal role in the regulation of actin cytoskeleton dynamics, gene transcription, cell-cycle progression and membrane trafficking (Kaibuchi, 1999). The mammalian Rho GTPases can be grouped into six different classes, consisting of the following members: Rho (RhoA, RhoB, RhoC), Rac (Rac1, Rac2, Rac3, RhoG), Cdc42 (Cdc42Hs, G25K, TC10), Rnd (RhoE/ Rnd3, Rnd1/Rho6, Rnd2/Rho7), RhoD, and TTF (Aspenstrom, 1999). The structure of Rho GTPases is widely conserved and comprises both invariant regions, which do not change their position and conformation whatever the nature of the bound guanine nucleotide, and two variable regions, which

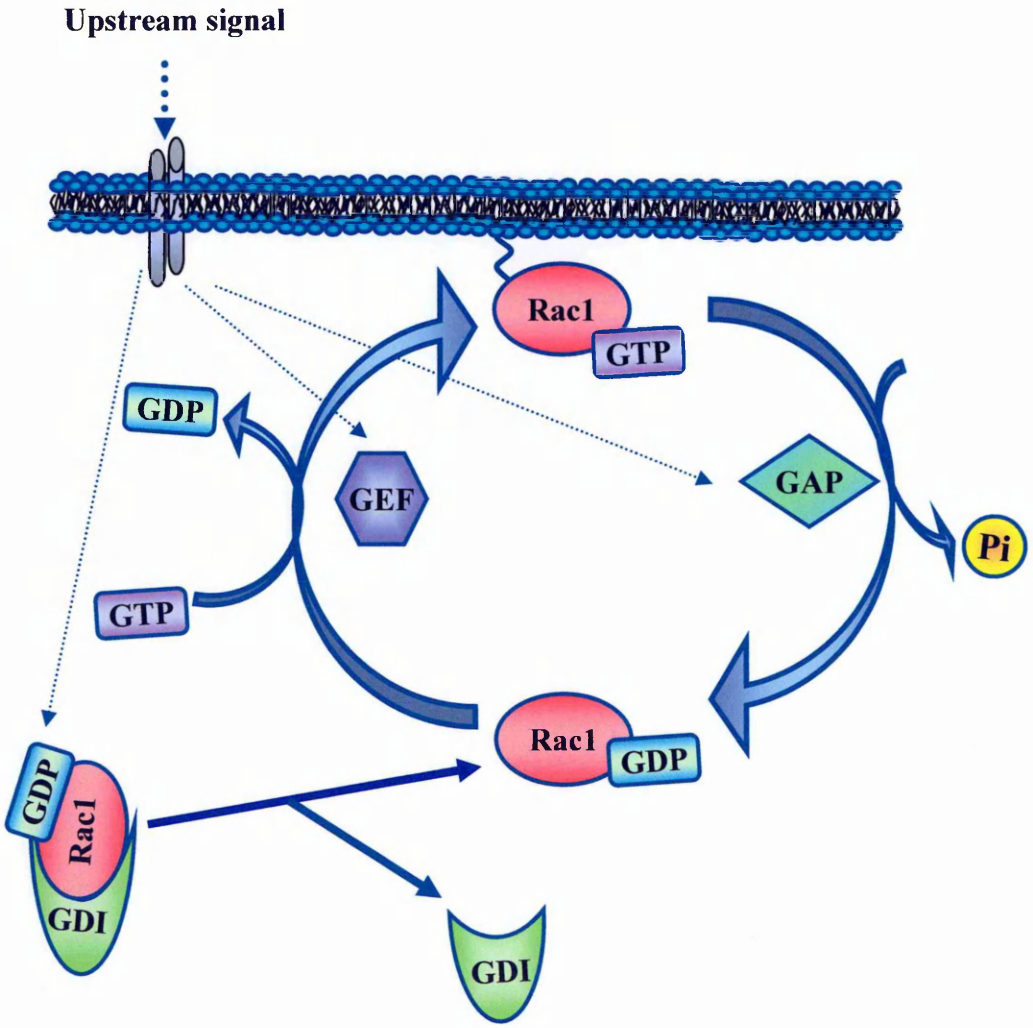

Figure 1.5 - The Rho GTPase cycle. Rho GTPases cycle between an active (GTP-bound) and an inactive (GDP-bound) conformation. In the active state, they interact with one of over 60 target proteins (effectors). The cycle is highly regulated by three classes of protein: in mammalian cells, around 60 guanine nucleotide exchange factors (GEFs) catalyse nucleotide exchange and mediate activation; more than 70 GTPase-activating proteins (GAPs) stimulate GTP hydrolysis, leading to inactivation; and four guanine nucleotide exchange inhibitors (GDIs) extract the inactive GTPase from membranes.

undergo structural changes upon GTP/GDP binding and that are called switch I (residues 40-51) and switch II (residues 68-81) (Paduch et al., 2001). Moreover, they undergo posttranslational modifications in the C-terminal region that are important for their intracellular localization. Rho GTPases are synthesized as cytosolic proteins, but they have the capacity to associate with membranes through their C-terminal CAAX motif that is prenylated and the polybasic region immediately upstream of this CAAX motif (Dvorsky and Ahmadian, 2004). Unlike the Ras proteins, the prenylated Rho proteins can be sequestered in the cytosol by their interaction with RhoGDI, and the capacity to cycle on and off the membranes conferred by this interaction is believed to be integral to their biological activity (Schmidt and Hall, 2002; Zheng, 2001).

The activation of small GTPases of the Rho family implies their translocation to the plasma membrane, and this event is strictly related to their dissociation from GDIs. Once at the membrane, the Rho GTPases can interact with the GEFs and exchange GDP for GTP. The GAPs then allow GTP hydrolysis and favour the inactivation of these GTPases (Moon and Zheng, 2003)(Fig. 1.5).

Rac1, RhoA and Cdc42 are the most studied GTPase of the Rho family. They are responsible for the formation of filopodia (Cdc42), lamellipodia with the corresponding focal contacts and ruffles (Rac1), and stress fibres and focal adhesions (Rho) (Ridley and Hall, 1992; Ridley et al., 1992). Their activation can be hierarchical such that Cdc42 activates Rac1 that activates RhoA, but this is not a common feature; down regulation of one G-protein upon the activation of another can also occur (Nobes and Hall, 1995). This feature is important during cell migration, when the three G-proteins are involved in different functions.

Rac1 is required at the cell edge to regulate actin polymerization and membrane protrusion. For efficient cell migration, this activity would be expected to be spatially restricted; in fact, a gradient of active Rac1 can be visualized in migrating fibroblasts with the highest concentrations at the leading edge (Kraynov et al., 2000). RhoA, on the other

hand, is believed to regulate the contraction and retraction forces required in the cell body and at the rear, and would be expected to follow an inverse distribution with respect to Rac1, even though this has not yet been directly demonstrated. Cdc42 is also important in cell migration because it establishes cell polarity. Inhibition of Cdc42 in cells at a wound edge cause a complete loss of polarity; cells protrude lamellipodia from all around their periphery, irrespective of whether there are cell-cell contacts. In addition, the Golgi apparatus reorientation to the anterior side of the nucleus, which is important to establish the direction of cell movement, does not occur (Mellor, 2004; Nobes and Hall, 1999).

1.2.3.1 Signalling upstream of the Rho family GTPases

The activation of the Rho family GTPases originates from complex signalling events that start at the level of the plasma membrane. Tyrosine kinase receptors (RTKs) like growth factor receptors (for platelet-derived growth factor-PDGF-, epidermal growth factor-EGF-, hepatic growth factor-HGF-, etc...), integrin related receptors, and also G-protein coupled receptors (GPCR) (like LPA receptors) have been shown to initiate a signal cascade that leads to Rho GTPase activation. The exact mechanisms by which the receptors signal to the Rho GEF and then to the Rho proteins in mammalian cells are poorly understood. However, studies on two GEFs, p115 RhoGEF and Sos, have produced two examples for how such links can be organized. It has been shown that the LPA activates RhoA to induce the assembly of focal contacts and stress fibres (Tapon and Hall, 1997). This pathway is mediated by the LPA-dependent activation of a G_{13} heterotrimeric G-protein, which can directly interact with p115RhoGEF (it contains an RGS domain, a regulator of G-protein signalling). This event can favour the activation of RhoA by this GEF (Gohla et al., 1998).

A model for Rac1 activation by RTKs relies on the fact that the activation of PDGF or insulin receptors leads to Ras activation by the Ras GEF domain of Sos. The

activated Ras can, in turn, trigger phosphoinositide 3-kinases (PI3K) to produce 3 phosphorylated phosphoinositides (see Section 1.4.1) which, by interacting with the pleckstrin homology (PH) domain (see Section 1.4.1.1) of Sos, unmask the Dbl-homology (DH) domain and render Sos into a functional Rac1 GEF. In addition to a Ras GEF at the C-terminus, Sos contains a Rho GEF domain DH in its N-terminus that has a GDP/GTP exchange activity specific for Rac. Besides Sos, many different GEFs exist and the pathway described above cannot explain their involvement in Rho GTPase activation. PI3K appears to have an important role though the formation of phosphatidylinositol (PI) 3,4,5,trisphosphate (PI3,4,5P_3) (see Section 1.4.1), which participates in the localization of many different GEFs at the plasma membrane. Each GEF has the ability to regulate distinct signalling pathways downstream of the Rho GTPases, thus directing their signal to a specific effector. For example the co-expression of GEFs such as TIAM1 (see section 1.2.3.2), Dbl (human oncogene from a diffuse B-cell lymphoma) (Eva and Aaronson, 1985), or FGD1 (the Cdc42 GEF responsible for Faciogenital Dysplasia) (Pasteris et al., 1994) with either Rac1 or Cdc42 showed that TIAM1 and Dbl can activate the kinase activity of p21-activated protein kinase 1 (PAK1) (Lim et al., 1996) but not that of c-Jun N-terminal kinase (JNK) (Hibi et al., 1993) whereas FGD1 was a potent activator of the JNK signalling pathway, although it evoked only a limited induction of PAK1 (Zhou et al., 1998). Another potential way to achieve specificity in Rho GTPase signalling can be provided by the activity of the RhoGDI family of proteins (see Section 1.2.3). There are indications that the dissociation of Rho-RhoGDI complexes requires the concerted action of GEFs like Dbl and proteins of the ezrin–radixin–moesin family of actin-binding proteins (Takahashi et al., 1998). Moreover, signalling that leads to an increase in intracellular Ca^{2+} ($[Ca^{2+}]_i$) could favour the detachment of RhoGDI from Rac1. It has been shown that Ca^{2+}-dependent activation of protein kinase C (PKC) can disrupt the Rac1-RhoGDI complex via phosphorylation of GDI. This event favours the translocation of Rac1 to the plasma membrane and consequently its interaction with the GEFs (Price et al., 1997).

In addition the p130Cas/CrkII/DOCK180 pathway is also known to activate Rac1 (Buday et al., 2002; Hasegawa et al., 1996). Crk signalling proteins have been implicated as participating in growth factor induced migration. The expression of oncogenic v-Crk or cellular Crk lead to an enhanced phosphorylation of Cas and paxillin, two proteins that are integral parts of focal adhesions (Feller, 2001). Crk, is an adaptor proteins that consist of SH2 and SH3 domains, and contain no catalytic activity. The SH2 domain binds the phosphotyrosine-containing proteins p130Cas (Crk-associated substrate) and the SH3 domains binds DOCK180 (180-kDa protein downstream of Crk), which is able to activate Rac1 (Gotoh et al., 1995).

1.2.3.2 TIAM1, a specific exchange factor for Rac1

TIAM1 was originally identified in T-lymphoma cells as an invasion- and metastasis-inducing gene. This gene encodes a specific exchange factor for Rac1, ubiquitously expressed and well conserved in different species. The human *TIAM1* gene shows a high degree of homology to its murine counterpart, and it is widely expressed (Habets et al., 1994). The protein possesses the characteristic DH-PH domain (Dbl homology, catalytic, domain combined with a C-terminal PH domain) combination that is always found in members of the Dbl-like family of exchange factors. The TIAM1 protein is 1,591 amino acids long and contains several distinct domains. It is myristoylated at its N-terminus and contains two N-terminal PEST (sequences that are rich in proline-P-glutamic acid-E- serine-S- and threonine-T-) domains. The N-terminal PH domain (PHn) together with a coiled-coil region and an adjacent sequence (PHn-CC-EX), are important for membrane localisation (Michiels et al., 1997; Stam et al., 1997). The PHn domain interacts with a high affinity with $PI3,4,5P_3$ over $PI3,4P_2$ and $PI4,5P_2$ at the plasma membrane (Stam et al 1997) (see Section 1.4.1.1). A Ras-binding domain (RBD) and a PSD-95/DlgA/ZO-1 (PDZ) domain are important for the interaction of TIAM1 with Ras

and other activators. The characteristic catalytic DH domain is related to the GEF activity of TIAM1 and is important for the Rac1-TIAM1 interaction (Worthylake et al., 2000). The C-terminal PH (PHc) domain cooperates with the catalytic DH domain in enhancing the GDP/GTP exchange of Rac1, favours the interaction of the DH domain with Rac1, and finally, determines the cytoskeletal localisation of TIAM1. The PHc domain does not bind the phosphoinositides, with the exception of a weak interaction with PI3P. Mutations in the PHc domain that abolished PI3P binding did not affect the *in vitro* GEF activity or the membrane localisation of TIAM1, but prevented the *in vivo* Rac1 activation (Baumeister et al., 2003) (Fig. 1.6).

Membrane translocation of TIAM1 is important for Rac1-dependent formation of membrane ruffles and also for JNK activation, in NIH 3T3 cells (Michiels et al., 1997). The PHn-CC-EX domain is crucial for this event, since it can interact with PI3K products at the level of the plasma membrane. Intriguingly, $PI3,4,5P_3$ production does not cause the translocation of the isolated PHn and PHc domains of TIAM1 to the plasma membrane, and PI3-kinase inhibition does not reduce the ability of C1199-TIAM1 (a truncated but still active form of TIAM1 that lacks the myristoylated region) to translocate to the plasma membrane and induce membrane ruffle formation. However, truncation of the PHc domain made C1199-TIAM1-induced membrane ruffling dependent on PI3K activity (Mertens et al., 2003).

Phosphorylation of TIAM1 is another event that may directly trigger the translocation and/or the activity of this GEF. TIAM1 was reported to be phosphorylated on threonine residues by Ca^{2+}/calmodulin kinase II (CaMKII) (see Section 1.3.4) and PKC *in vitro*; and upon treatment of Swiss 3T3 fibroblasts with LPA and PDGF *in vivo* (Fleming et al., 1999; Fleming et al., 2000). CaMKII, but not PKC, was able to stimulate TIAM1-induced nucleotide exchange on Rac1 *in vitro*. Moreover, upon LPA and PDGF stimulation, membrane translocation and threonine phosphorylation of membrane-bound TIAM1, can only be inhibited by KN-93, a CaMKII specific inhibitor, in NIH 3T3 cells

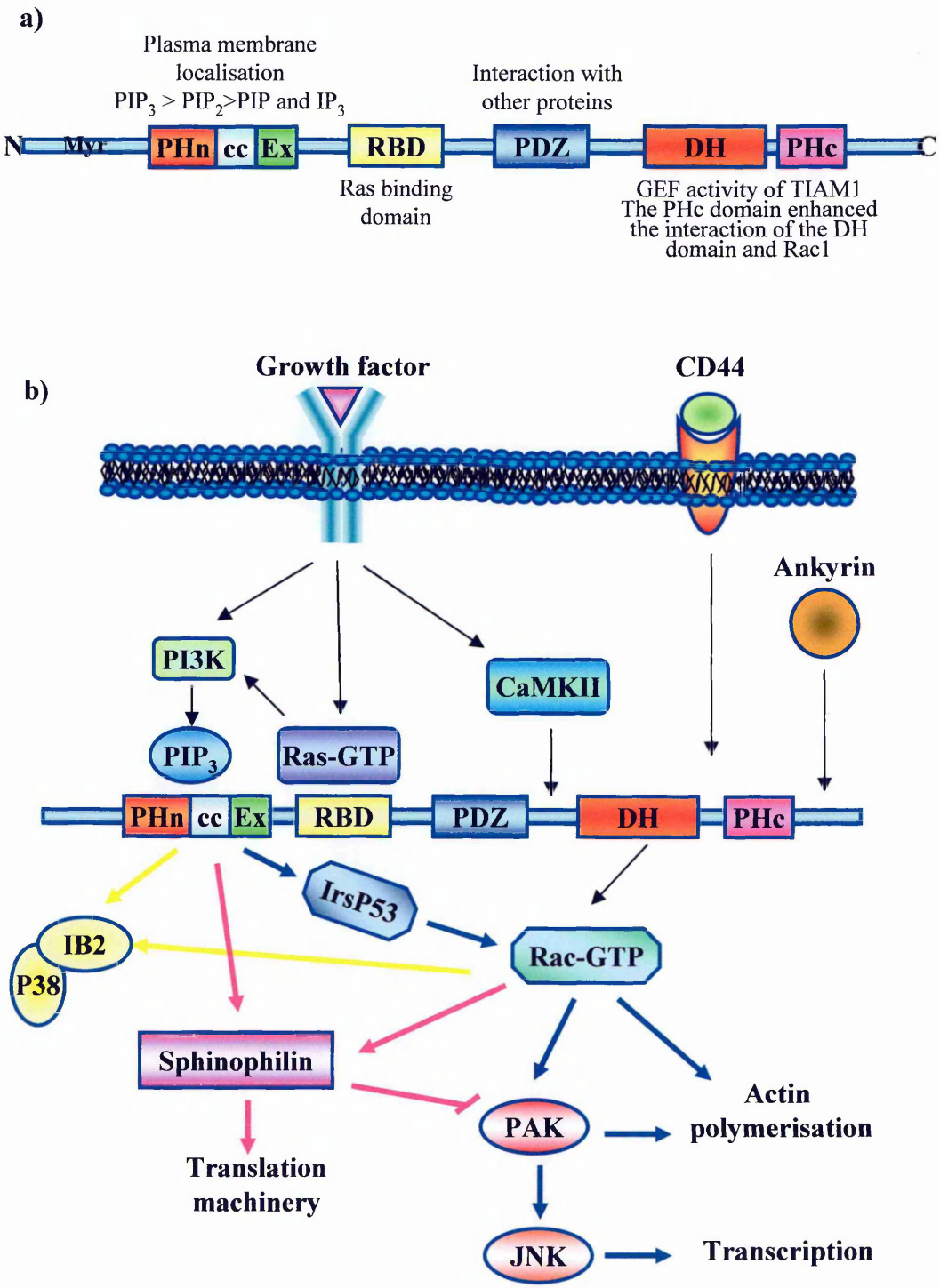

Figure 1.6 - Structure of TIAM1 and pathways in which it is involved. a) Domain structures of representative of TIAM1 (see Section 1.2.3.2 for explanations). **b)** Regulation of TIAM1 in intracellular signalling networks. It is regulated by diverse mechanisms including phosphorylation by CaMKII or related kinases, interaction with PI3K product PI3,4,5P_3, binding to cell surface molecule CD44 or cytoskeleton protein ankyrin, as well as direct binding to activated Ras.

(Buchanan et al., 2000). PKC phosphorylation probably does not have a direct role in TIAM1-Rac1 signalling.

Direct interaction with proteins that directly couple TIAM1 with Rac1 versus a specific signalling pathway, is another way to activate this GEF. Through its RBD domain, TIAM1 can interact directly with Ras in its active form (GTP bound). This complex causes the activation of TIAM1, and consequently, can cooperate to cause the synergistic formation of Rac1-GTP (Lambert et al., 2002). Thus, TIAM1 can function as a Ras effector and mediate Ras-dependent activation of Rac1 directly, in a PI3K-independent way.

The interactions of TIAM1 with different proteins can not only control its GEF activity, but also determine the downstream specificity of TIAM1-induced Rac1 signalling, as demonstrated by the following examples (Fig. 1.6):

1. Spinophilin was identified at the heads of dendritic spines, and it binds TIAM1 at the level of the PHn-CC-EX region, and localises to the plasma membrane. This protein can also bind P70 S6 kinase, a downstream effector of Rac1 that is involved in translation events. The binding with spinophilin targets TIAM1 and Rac1 at the level of P70 S6 kinase, favouring its downstream signalling. In contrast, spinophilin binding suppresses the ability of TIAM1 to activate PAK1 (Buchsbaum et al., 2003).
2. Ib2/JIP2 is a pancreatic β-cell/brain-specific protein, which is a scaffold for the MLK3-MKK3-P38-mitogen activated kinase (MAP) complex. It binds TIAM1 at the level of PHn-CC-EX and couples its signalling to P38 kinase, thus enhancing p38 MAP kinase signalling (Buchsbaum et al., 2002).
3. IRSp53 (Insulin receptor tyrosine kinase substrate p53), is known to link Rac1 and WAVE2, for lamellipodia protrusion (Miki et al., 2000). It interacts with the PHn-CC-EX region of TIAM1 and also binds Rac1 and

Cdc42. The interaction between TIAM1 and IRSp53 favours the formation of the IRsp53/Rac1 complex that activates WAVE2 through a direct interaction, thus forming lamellipodia. PDGF, which activates TIAM1, favours its interaction with IRSp53. Under normal conditions, IRSp53 overexpression causes filopodia formation by direct interaction with Cdc42. TIAM1 co-expression or PDGF stimulation shifts the signalling to Rac1 activation and lamellipodia protrusion (Connolly et al., 2005).

4. Another interactor of TIAM1 (through the PHn-CC-Ex domain) is the hyaluronic acid (HA) receptor isoform CD44v3. In parallel, the same domain of TIAM1 was shown to interact with the cytoskeletal protein ankyrin (Bourguignon et al., 2000). In fact, both CD44v3 and TIAM1 bind to the ankyrin repeat domains of ankyrin and both CD44v3 and ankyrin bind to the same domain of TIAM1. Based on these data, one can envisage that TIAM1 binds indirectly to CD44v3, using ankyrin as the hub. The significance of this interaction is still not clear, however.

1.2.3.3 Signalling downstream of the Rho GTPases

The cellular targets of Rac1 and Cdc42 that promote changes to the actin cytoskeleton have been the subject of intense investigation. Potential pathways for the transduction of signals from active Rac1 and Cdc42 to actin polymerization into lamellipodia and filopodia have been recently uncovered. The Ser/Thr kinase p65PAK is commonly activated either by Rac1 or Cdc42, and it is believed to play an important role in regulating actin dynamics and cell adhesion during migration. It regulates focal adhesion turnover, with the help of PIX (PAK-interactive exchange factor) and GRK (G protein coupled receptor kinase) interactor 1, for efficient integrin-dependent matrix adhesion during cell migration, to generate traction forces at the front of the cell (Manabe et al.,

2002; Obermeier et al., 1998). In addition, p65PAK phosphorylates and activates LIM kinase (LIMK), which in turn phosphorylates and inactivates cofilin (Arber et al., 1998; Edwards et al., 1999). The ability of cofilin to cycle between active (unphosphorylated) and inactive (phosphorylated) forms is a critical feature for promoting filament treadmilling at the front of migrating cells (Bamburg and Wiggan, 2002).

Cdc42 activates WASP and N-WASP directly and the lipid $PI(4,5)P_2$ is an essential cofactor (Rohatgi et al., 2000; Rohatgi et al., 1999). This activation stimulates the Arp2/3 complex, which can initiate actin polymerization either *de novo*, or at the barbed ends, and at sites of pre-existing filaments to form filopodia. Rac1 activates the Scar/WAVE family indirectly, and this involves IRSp53, which is known to link Rac1 and WAVE2 for lamellipodia protrusion (Miki et al., 2000). IRSp53 can also interact with Cdc42, and this interaction can favour the formation of a complex between IRSp53 and Mena, a member of Ena/VASP family, which can activate the Arp2/3 complex for actin polymerization and filopodia formation (Krugmann et al., 2001) (see also Section 1.2.1.2) (Fig. 1.7).

In the protruding lamellipodium, WAVE and Mena regulate actin polymerisation near the cell membrane and N-WASP regulates the formation of protruding filopodia (Nakagawa et al., 2001) (see Section 1.2.2). The GTP-bound form of Rac1 activates WAVE, which can then migrate to the lamellipodial edge through its N-terminal Scar homology domain (SHD). Subsequently, WAVE stimulates the Arp2/3 complex to promote actin filament nucleation and thus lamellipodia protrusion (Machesky et al., 1999). Mena is recruited around the fast-growing ends of actin filaments through the EVH2 domain (Ena/VASP homology domain) and supplies monomeric actin molecules to elongate actin filaments branched by the Arp2/3 complex. Its action modulates the speed of lamellipodium protrusion downstream of various receptors (Mullins et al., 1998). When Cdc42 is activated in the lamellipodium, N-WASP can bundle actin filaments into microspikes, and can then elongate them to produce protruding filopodia (Nakagawa et al., 2001) (Fig. 1.7)

For stress fibre and focal adhesion formation, many downstream effectors of Rho have been identified; in particular the mechanism of stress fibres formation has been associated to the activity of a Rho associated kinase (Ishizaki et al., 1997) and mDia (Watanabe et al., 1997). These two enzymes can cause the contraction of pre-existing filaments and de novo actin polymerization (see Section 1.2.1.2). The Ser/Thr kinase p160ROCK is involved in stimulating actin:myosin filament assembly and therefore contractility, as well as in detaching the rear of single migrating cells (Alblas et al., 2001; Nobes and Hall, 1999). In its active state, p160ROCK, like p65PAK, can phosphorylate and activate LIMK, which in turn phosphorylates and inactivates cofilin, leading to stabilization of actin filaments within actin:myosin filament bundles (Maekawa et al., 1999; Sumi et al., 2001). p160ROCK interacts with and phosphorylates the myosin binding subunit of myosin light chain phosphatase, and thereby inactivates it (Kawano et al., 1999). This leads to increased levels of myosin phosphorylation, which then can cross-link actin filaments and generate a contractile force that, at the rear of a migrating cell, promotes movement of the cell body (Mitchison and Cramer, 1996). On the other end mDia can bind RhoA and this interaction opens up and activates this scaffold protein. It cooperates with p160ROCK in the assembly of actin:myosin filaments, but its biochemical mechanism of action is still unclear (Uehata et al., 1997; Watanabe et al., 1999) (Fig. 1.7)

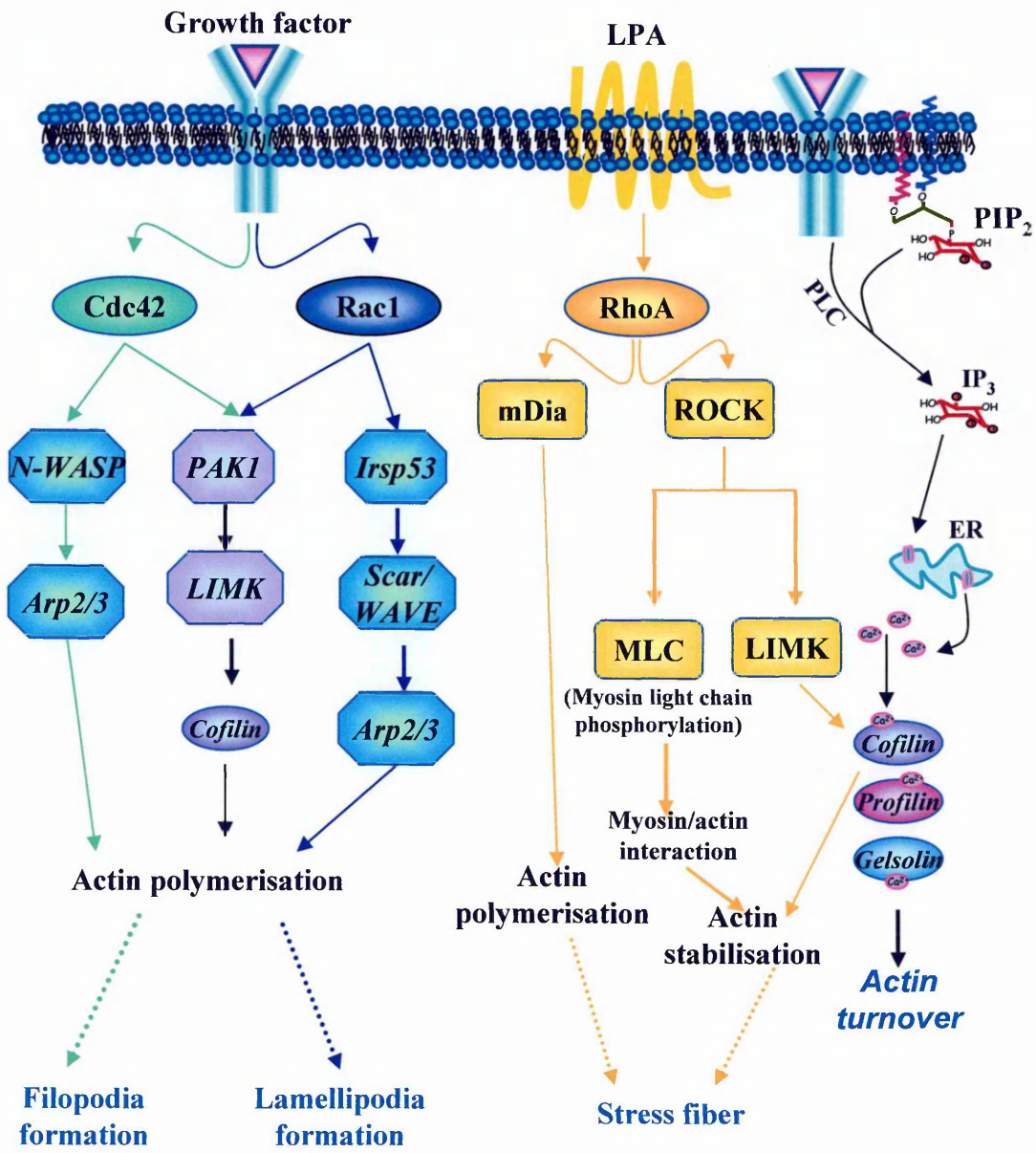

Figure 1.7 Schematic representation of the signalling cascade that leads to actin cytoskeleton modifications. For explanations see Sections 1.2.3.1 and 1.2.3.3.

1.3 Signalling enzymes

The glycerophosphoinositols have been shown to be biologically active in cells. A treatment with these compounds can initiate different signal cascades that involve many signalling enzymes. In details, the phospholipase A_2s (PLA_2s) are involved in the synthesis of the glycerophosphoinositols (Falasca et al., 1996) (see Section 1.4.3.1) and can be also inhibited by GroPIns4P and GroPIns (Corda et al., 2002). In addition the adenylyl cyclases (ACs) can be inhibited by treatment with GroPIns4P (see Section 1.3.3.2.1).

The aim of this study was to define the mechanism of action of the glycerophosphoinositols in actin cytoskeleton modulation, with a particular focus on GroPIns4P (the most active compound) (see Section 1.4.3.2.3). This analysis lead to the definition of a signal cascade that involves the activation of many enzymes such as Phospholipase Cs (PLCs), Ca^{2+}/calmodulin-dependent protein kinase II (CaMKII) and Src family kinases (as it will be demonstrated in Chapter 3).

This section will provide a general background about the structure and functions of both the signalling enzymes that are already known to be involved in the activity of GroPIns4P (PLA_2 and AC) but also that have been found to be important for the present study (PLCs, CaMKII and Src).

1.3.1 Phospholipase A_2

PLA_2 enzymes catalyse the hydrolysis of the *sn-2* ester linkage of the phospholipid substrate, resulting in the production of a free fatty acid, arachidonic acid (AA) in general, and the corresponding lysophospholipid.

The PLA_2s form a superfamily of enzymes divided in three different families, depending on their localization and activation. Within each family, different groups of PLA_2s are present. The family of secretory PLA_2s ($sPLA_2$) is formed by low molecular

weight (14-17 kDa), disulfide-linked secretory proteins, with a histidine residue at the catalytic centre and which require Ca^{2+} at mM concentration. The family of cytosolic PLA_2s ($cPLA_2$) consists of 85-110 kDa proteins localised in the cytosol of resting cells. Upon activation, they translocate to the Golgi complex and ER. There are at least four $cPLA_2$s (α, β, γ, δ) in mammals, all classified in the group IV and that all require Ca^{2+} at μM concentration for their activation (Dennis, 1994). From a structural point of view, they all contain two homologous catalytic domains, A and B, interspaced with a unique sequence. The C2 domain, important for Ca^{2+} binding, is conserved in the α, β and δ isoforms, whereas the γ isoform has a site of farnesylation at the C-terminus (Fig. 1.8). The third family comprises the other cytosolic forms of the PLA_2s that do not require Ca^{2+}. These are known as the $iPLA_2$s (Ca^{2+}-independent) and are classified as group VI (Dennis, 1997) (Table 1.1).

The Ca^{2+}-dependent and cytosolic $cPLA_2$s have been implicated in the production of arachidonic acid (AA) and in eicosanoid biosynthesis; their activation has been reported to be via cell surface receptors. Once activated these PLA_2s translocate from the cytosol to intracellular membranes (Golgi complex, ER), where the phospholipids are hydrolysed. The proposed model for cPLA2α activation implies cell-surface-receptor-dependent stimulation and a consequent $[Ca^{2+}]_i$ increase, followed by Ca^{2+} binding to the C2 domain that promotes cPLA2α translocation from the cytosol to the membranes. Upon membrane binding, major conformational changes in the enzyme take place to remove the lid from the active site (the catalytic cleft, in its inactive state, is covered by a lid containing an α-helix and a short turn) and to allow the fatty acyl chain of a substrate molecule to enter the active site (Bahnson, 2005).

Phosphorylation of cPLA2α by MAPK kinase, MAPKAP kinase and CaMKII are also important for its activity and the stabilisation of the active form at the membrane (Kudo and Murakami, 2002).

Families	Enzymes	Other names	Size (kDa)	Ca^{2+} requirement	Catalytic site	domains
$sPLA_2$	IB	Pancreatic PLA_2	14	mM	His/asp dyad	
	IIA	Synovial PLA_2	14	mM	His/asp dyad	
	IIC		15	mM	His/asp dyad	
	IID		14	mM	His/asp dyad	
	IIE		14	mM	His/asp dyad	
	IIF		16	mM	His/asp dyad	
	V		14	mM	His/asp dyad	
	X		14	mM	His/asp dyad	
	III		55	mM	His/asp dyad	
	XII		19	mM	His/asp dyad	
$cPLA_2$	IVA	$cPLA_2\alpha$	85	<μM	Ser/asp dyad	C2dom
	IVB	$cPLA_2\beta$	110	<μM	Ser/asp dyad	C2dom
	IVC	$cPLA_2\gamma$	60	none	Ser/asp dyad	
$iPLA_2$	VIA	$iPLA_2\beta$	85-88[b]	none	Ser/His/Asp triad	Ankyrin repeat
	VIB	$iPLA_2\gamma$	90	none	Ser/His/Asp triad	
PAF-AH	VIIA	Plasma-PAF-HA	45	none	Ser/His/Asp triad	
	VIIB	PAF-HA-II	40	none	Ser/His/Asp triad	
	VIIIA	PAF-HA-Iα_1-sub	30	none	Ser/His/Asp triad	
	VIIIB	PAF-HA-Iα_2-sub	30	none	Ser/His/Asp triad	

Table 1.1 - Classification of mammalian PLA_2 (from Kudo and Murakami, 2002).

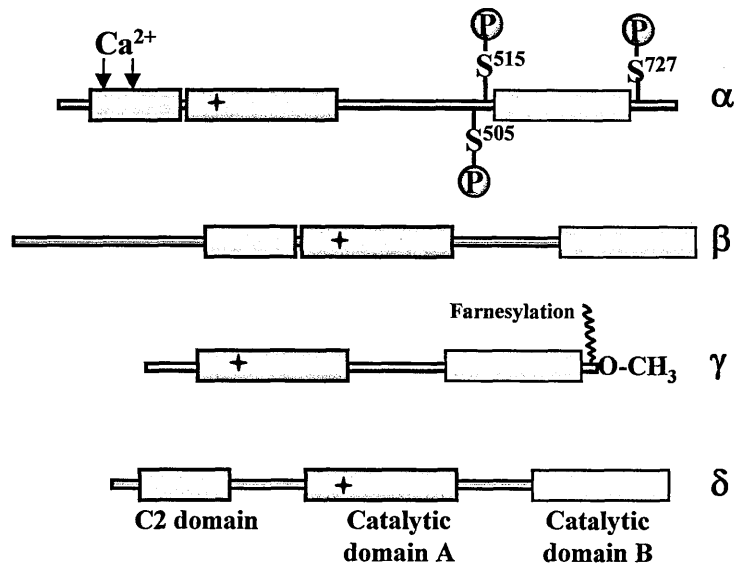

Figure 1.8 - Structure of $cPLA_2$s. Members of the $cPLA_2$/Group VI PLA_2 subfamily showing conserved domain and posttranslational modifications. Three functionally important serine residues can be phosphorylated in $cPLA_2$ (Hirabayashi et al., 2004).

1.3.2 Adenylyl cyclase

The adenylyl cyclases (ACs) are a family of enzymes that are responsible for cyclic AMP (cAMP) production. They are integral membrane proteins composed of twelve transmembrane segments and a large cytoplasmic (catalytic) loop. The N-terminal hydrophobic domain (M1) is organised into six membrane-spanning α-helices; this domain is followed by a 40-kDa cytoplasmic domain (C1) and by a second transmembrane (M2) domain; finally, there is a second cytoplasmic domain (C2). The two cytoplasmic domains form the catalytic core of the protein and interact together (Fig. 1.9) (Sunahara et al., 1996). The ten AC isoforms can be divided into five distinct families based on their amino-acid sequence similarities and functional attributes. The Ca^{2+}/CaM-sensitive forms are types AC1, AC3 and AC8. The Gβγ-stimulated forms are represented by AC2, AC4 and AC7. AC5 and AC6 are distinguished by their sensitivity to inhibition by both Ca^{2+} and $G\alpha_i$ isoforms ($G\alpha_o$, $G\alpha_{i1}$, $G\alpha_{i2}$, $G\alpha_{i3}$ and $G\alpha_z$). AC9 is the most divergent of the membrane-bound family and is highly insensitive to the diterpene forskolin. The last isoform is a soluble AC (sAC), and it is the most divergent of all the mammalian cyclases, as it is not membrane bound. In general, all membrane bound AC isoforms are found in, but not limited to, excitable tissues, such as neurons and muscle. Within the brain, AC isoforms localize to different, discrete, brain regions. Although most isoforms are widely expressed, AC1 and AC3 are expressed only in brain. The soluble cyclase is expressed predominantly in the testis, although splice variants have been identified displaying a broader distribution pattern (Cooper, 2003).

The activity of AC is mostly regulated by heterotrimeric G proteins and the Ca^{2+}/calmodulin (Ca^{2+}/CaM) complex. The hormonal activation of AC occurs primarily through receptors coupled to the stimulatory G protein, $G\alpha_s$; whereas the members of the $G\alpha_i$ family exert an inhibitory effect selectively on certain AC isoforms (AC6 and AC5). Interestingly $G\alpha_i$ does not compete with $G\alpha_s$ for the binding to the ACs. The heterodimer

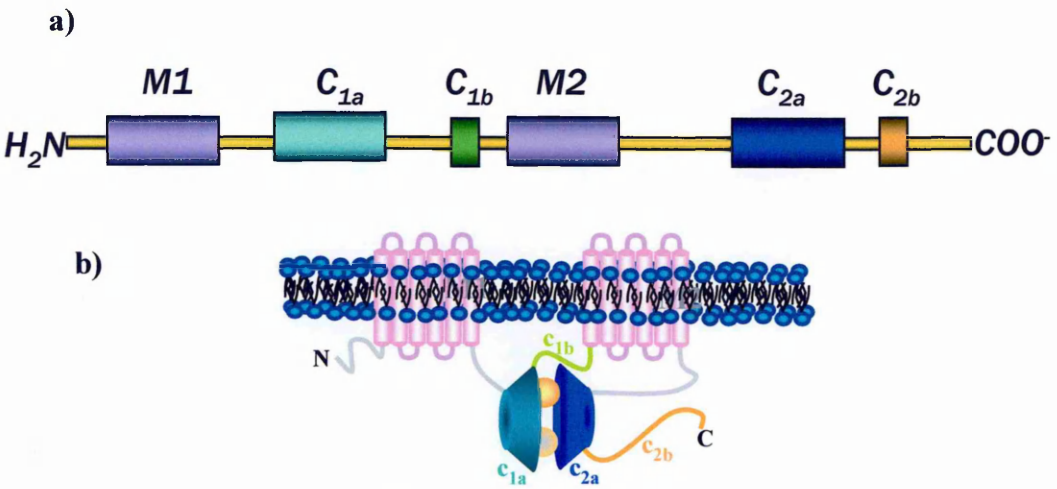

Figure 1.9 - Organisation of the AC. The figure represents the main structural features of mammalian ACs. **a)** The primary sequence of more than 100 amino acids is interrupted by a number of specialised domains. **b)** General topology and organisation of the enzyme. The N-terminus hydrophobic domain (M1) is organised into six membranes-spanning α-helices, this domain is followed by a 40-kDa cytoplasmic domain (C1) and by a second transmembrane (M2) domain; finally, there is a second cytoplasmic domain (C2). The two cytoplasmic domains form the catalytic core of the protein and interact together.

		Regulatory signals								
Isoform	Distribution	βγ	α_i	α_0	α_s	PKA	PKC	Forskolin	Ca/CaM	Ca^{2+}
II	Brain, lung	↑	n/e	n/e			↑	↑	n/e	
IV	Widely distributed	↑						↑		
VII	Widely distributed	↑					↑	↑		
V	heart>brain	↑	↓	n/e	↓	↓	↑	↑	n/e	↓
VI	Heart, brain> other tissues	n/e	↓	n/e		↓	↓	↑	n/e	↓
VIII	Neural tissue	n/e						↑	n/e	
I	Neural tissue	↓	↓	↓	↓			↑		
III	Predominantly olfactory	n/e	↓	n/e				↑		

Table 1.2 – Classification of the AC isoforms.

Gβγ can modulate the activity of AC either activating, as in the case of AC2, AC4 and AC7, or inhibiting, as for AC1 and AC8, the enzyme. Also, for the Ca^{2+}/CaM complex there is this dual effect, stimulatory at the level of some isoforms and inhibitory versus other isoforms. Other proteins, like protein kinases, are able to differently modulate AC activities (Table 1.2) (Sunahara and Taussig, 2002).

The product of AC is cAMP, the first second messenger that was identified, which is involved in the regulation of cell metabolism, cell shape and gene transcription (Sutherland, 1972) via reversible protein phosphorylation. Elevated levels of cAMP in the cell lead to activation of different cAMP targets. The main targets of cAMP are the cAMP-dependent protein kinases (cAPKs) (Walsh et al., 1968). However, not all of the effects of cAMP are mediated by a general activation of cAPKs; several cAMP-binding proteins have been described: the cAMP receptor of *Dictyostelium discoideum*, which participates in the regulation of development (Klein et al., 1988a); cyclic-nucleotide gated channels, which are involved in the transduction of olfactory and visual signals (Goulding et al., 1992; Kaupp et al., 1989); and the cAMP-activated guanine exchange factors Epac 1, 2, which specifically activate the monomeric G protein Rap (Kawasaki et al., 1998).

1.3.3 Phospholipase C

Many of the earliest key events in the regulation of various cell functions elicited by the interactions of many signalling molecules with their cell surface receptors trigger the hydrolysis of a minor membrane phospholipid, ($PI4,5P_2$), by PLC. This reaction produces two intracellular messengers, diacylglycerol (DAG) and inositol 1,4,5-trisphosphate (IP_3), which mediate the activation of (PKC) and $[Ca^{2+}]_i$ release, respectively.

In the late 1980s and early 1990s ten mammalian PLC isozymes were isolated and their corresponding DNAs sequenced (Rhee and Bae, 1997; Rhee et al., 1989). They have been divided in three subtypes, β, γ and δ; recently a new isoform has been identified

(PLCε) that contains several domains that are not present in any other known PLC (Lopez et al., 2001). The molecular mass of the PLCδ isozymes is ~85 kDa, that of the β and γ isoforms is in the range of 120-155 kDa, and that of PLCε is 230-260 kDa. The amino acid sequences of the PLC isozymes are relatively non-conserved, with the exception of two regions, known as the X and Y domains that form the catalytic core. These domains are comprised of alternating α-helices and β-strands and resemble an incomplete triose phosphate isomerase α/β barrel domain, which is important for the binding of the substrate and which requires Ca^{2+} for its catalytic activity. The sequence between the X and Y domains comprises 40 to 110 residues in the PLCβ and PLCδ and 190 residues in the PLCε. PLCγ has a larger region (~400 residues) that contains two Src homology 2 (SH2) domains and one Src homology 3 (SH3) domain, which bind phosphotyrosine (pTyr)-containing sequences and proline-rich sequences, respectively. The β, γ and δ isozymes all contain an N-terminal PH domain that is important for their membrane localization (see Section 1.4.1.1), and an EF-hand domain localized between the PH and the X domains. This EF-hand motif consists of a helix-loop-helix structure and serves as a flexible link between the PH domain and the rest of the protein. Another important domain is the C2 domain in the C-terminus; it binds Ca^{2+} and is fundamental for the activity of PLCδ. The PLCγ isozyme contain an additional PH domain that is split by the SH2/3 domains, while PLCβ shows a long C-terminal sequence (~45 amino acids) downstream of the Y domain. PLCε differs from the other types and has a Ras-exchange-factor-like domain (Ras-GEF) and a RBD (Fig. 1.10a) (Rhee, 2001)

Each PLC isoform is characterised by different regulation of the catalytic activity. The **PLCβ** isozymes are regulated by heterotrimeric GTP-binding proteins and function as effectors of GPCRs. In the classical G-protein model of PLC activation, the binding of an agonist triggers the receptor-catalysed exchange of GTP with the bound GDP on the α-subunit of the heterotrimeric G-protein. The GTP-α subunit then dissociates from the

membrane and binds PLCβ, increasing its catalytic activity. Alternatively, the βγ heterodimer can also bind alone or in cooperation with the α monomer and activate PLCβ. The activation comprises conformational changes and the translocation of PLCβ to the plasma membrane, in compartments enriched in PI3P (the specific ligand of the PLCβ-PH-domain) (Fig 1.10b) (Rebecchi and Pentyala, 2000). **PLCγ** is activated by growth factors, such as PDGF, EGF, and by immunoglobulin and cytokine receptor stimulation. Binding of a growth factor to its receptor results in dimerization of the receptor subunits, stimulation of the intrinsic tyrosine kinase activity, and the consequent auto-phosphorylation of the receptor. The recruitment of PLCγ results in the binding of its SH2 domain to a phosphorylated tyrosine on the receptor, then PLCγ is phosphorylated by the kinase activity of the receptor itself or of enzymes activated by it (as is the case with the non-receptor tyrosine kinases, like the Src family proteins) (Barfod et al., 2005; (Weiss, 1993). This phosphorylation is necessary but not sufficient for PLCγ activation. An important event is the tethering to the plasma membrane of PLCγ, operated by the interaction of the PH domain with the PI3K product $PI3,4,5P_3$ (Bae et al., 1998a). The activation of PI3K is also associated with RTK signalling. Besides this classical route, the activation of PLCγ can derive also from GPCR activation. One possibility is that ligand activation of the heterotrimeric G-protein βγ subunit results in an intracellular signal that induces the extracellular activation of a transmembrane metalloproteinase. This can lead to the extracellular processing of a transmembrane growth factor precursor, and to the release of the mature factor, which directly activates a RTK. Another possibility is a direct activation of an intracellular tyrosine kinase by an active Gα subunit (Fig. 1.10c) (Rhee, 2001). Independently of tyrosine phosphorylation, a direct binding of phosphatidic acid (PA) or arachidonic acid (AA) could be responsible for PLCγ activation (Hwang et al., 1996; Liu et al., 1999).

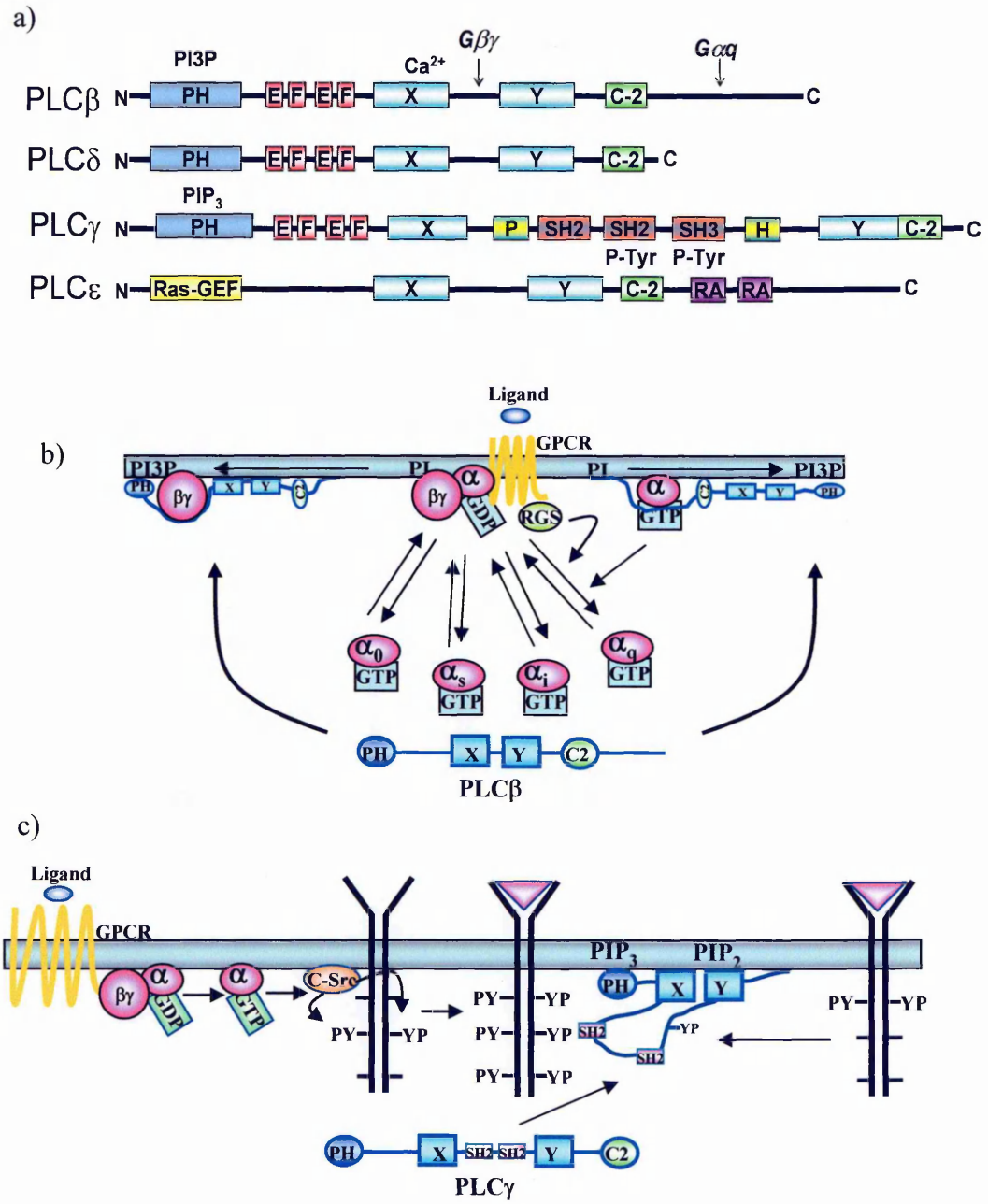

Figure 1.10 - Structure of PLCs and their pathways of activation. a) Domain organisation of the four types of PLC isozymes. The X and Y catalytic domains as well as the PH, EF-hand, C2, SH2, SH3, RasGEF, and RA domains are indicated in Section 1.3.3. **b)** GPCR-mediated activation of PLCβ isozymes. An agonist-occupied GPCR induces the exchange of GDP for GTP on the G protein α subunit and the subsequent dissociation of this subunit from the membrane-associated βγ dimer. The GTP-bound α subunits mediate the targeting of PLCβ to the membrane and activate it as a result of interaction with the C2 domain and downstream COOH-terminal region of the enzyme (*right*). The membrane-anchored βγ dimer also recruits PLC β by interacting with the PH and Y domains (*left*). The membrane localisation of PLCβ isozymes might be further promoted by interaction of the PH domain with PI3P (PI3P) generated in response to legation of the GPCR (from Rhee et al., 2001). **c)** PLCγ can be activated either by RTKs or by GPCR. The phosphorylated receptor RTK provides a structural scaffold for the assembly of a signalling complex that includes PLCγ. GPCR can trans activate the RTK through the activation of Src tyrosin kinases (from Rhee et al., 2001).

The mechanism by which the **PLCδ** isozymes are coupled to receptors remains unclear. Their affinity for Ca^{2+} is greater than that of the other isozymes. The binding of Ca^{2+} to the EF-hand domain promotes the association of the PH domain with $PI4,5P_2$ and the formation of a ternary complex containing the C2 domain, the phosphatidilseryne (the substrate) and Ca^{2+} also favours the activation of PLCδ (Yamamoto et al., 1999).

1.3.4 Ca^{2+}/calmodulin kinase II

The Ca^{2+}/calmodulin-dependent protein kinases (CaMK) are a family of Ser/Thr protein kinases that are activated upon binding to the Ca^{2+}/CaM complex. The family consists of CaMK I, II and IV and they have an extremely wide tissue distribution. The CaMKII group is encoded by four genes (α, β, γ, δ). The CaMKII isoforms share 80-90% identity, and the α and β isoforms are found mainly in neuronal tissues, while the γ and δ isoforms are broadly expressed (Braun and Schulman, 1995). CaMKII is a ubiquitously expressed protein kinase that transduces elevated Ca^{2+} signals in cells to a number of target proteins, ranging from ion channels to transcriptional activators. It is a multimeric enzyme composed of identical or mixed isoforms. The holoenzyme is an oligomeric protein comprised of twelve 50-60-kDa subunits that are arranged as two stacked hexameric rings. The various CaMKII subunits comprise an N-terminal catalytic region, a central regulatory domain containing an auto-inhibitory domain (AID), a Ca^{2+}/CaM binding motif, a variable sequence and the C-terminal subunit association domain that is required for oligomer formation (Morris and Torok, 2001) (Fig. 1.11a).

CaM is the most ubiquitous calcium-sensing protein, and it contains four "EF" hand motifs with high specificity for binding four Ca^{2+} ions. The Ca^{2+}/CaM complex interacts with the Ca^{2+}/CaM binding motif of CaMKII, favouring the activation of the enzyme. In the absence of bound Ca^{2+}/CaM, CaMKII is maintained in an inactive conformation because of an interaction of the AID with the catalytic domain of its own

subunit. The Ca^{2+}/CaM complex binds to a sequence that partially overlaps the AID, presumably causing a conformational change and thereby disrupting the interaction of the AID with the catalytic domain, and producing kinase activation. Upon activation by Ca^{2+}/CaM binding, the kinase undergoes an immediate autophosphorylation on Thr-286. This autophosphorylation occurs within the oligomeric complex (intramolecular) and between adjacent subunits (intersubunit) that have bound Ca^{2+}/CaM (Braun and Schulman, 1995). This rapid autophosphorylation on Thr-286 has two important regulatory consequences: first, the subsequent dissociation rate for Ca^{2+}/CaM upon removal of Ca^{2+} is decreased by several orders of magnitude; second, even after full dissociation of Ca^{2+}/CaM, the kinase retains its activity until a phosphatase dephosphorylates the Thr-286 (Ca^{2+}/CaM-independent or constitutively active). Thus, transient elevation of intracellular Ca^{2+} can give a prolonged response through the constitutive activity of auto-phosphorylated CaMKII. The Ca^{2+}/CaM binding site is also the main target of CaMKII inhibitors like KN-93, which leave the kinase in its inactive conformation (Fig. 1.11b) (Sumi et al., 1991)

CaMKII coordinates a large variety of cellular functions, such as carbohydrate metabolism, gene expression, membrane excitability, the cell cycle and changes in strength of neuronal communication that underlie learning and memory (Braun and Schulman, 1995). In NIH 3T3 cells, inhibition of CaMKII leads to cell cycle arrest in G1 and apoptosis, thus suggesting an involvement of CaMKII in cell-cycle progression, by transduction of signals from growth factors and/or survival factors (Tombes et al., 1995). CaMKII can be activated by growth factors, like PDGF, or ligands of GPCRs, like LPA; this activation can favour TIAM1 phosphorylation, Rac1 activation, and consequently, the modification of the actin cytoskeleton (Fleming et al., 1999; Fleming et al., 2000). A fraction of CaMKII is associated with the cytoskeleton as it can interact with α-actinin, myosin-V and F-actin, and in this way, it can phosphorylate many substrates (Bayer and Schulman, 2001). The signalling pathways initiated by cAMP can also produce an increase in $[Ca^{2+}]_i$ and thus activate

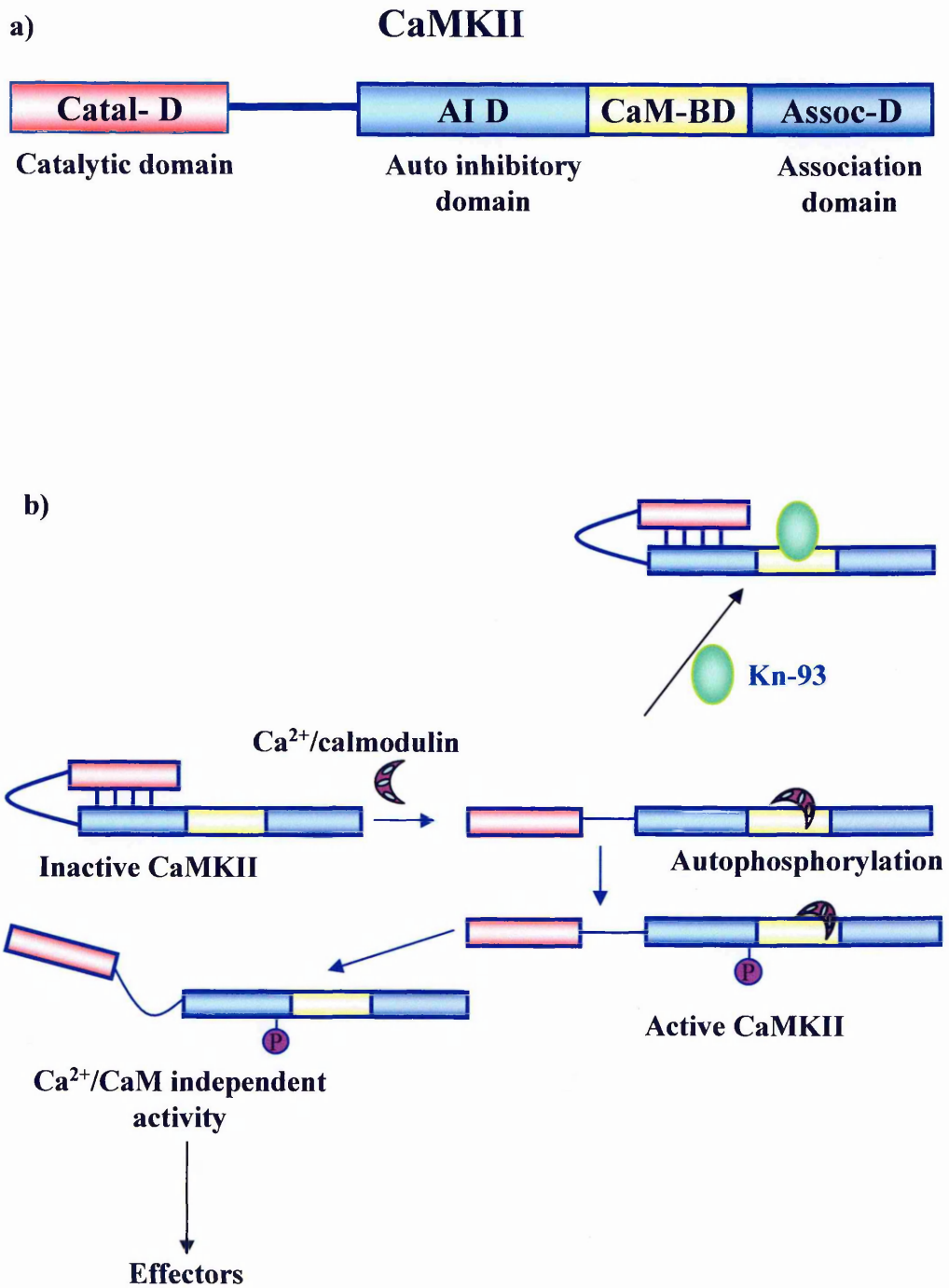

Figure 1.11 - Structure and mechanism of activation of CaMKII. a) Schematic representation of a CaMKII subunit, which is comprise of an N-terminal catalytic region, a central regulatory domain containing an auto-inhibitory domain (AID), a Ca^{2+}/CaM binding motif, a variable sequence and the C-terminal subunit association domain that is required for oligomer formation. **b)** Ca^{2+}/CaM-activation and mechanism of action of KN-93, a CaMKII specific inhibitor. It binds to the CaM binding site preventing the binding of the Ca^{2+}/CaM complex.

CaMKII (De Cesare et al., 1999). The final event is the stimulation of immediate early genes that are regulated by cAMP response elements (CREs), such as c-*fos* (Sheng et al., 1991). Phosphorylation of CREB (CRE binding protein) on Ser-133 is essential for transactivation, because it is required for binding of the ubiquitously expressed CREB binding proteins CBP and p300, which function as transcriptional co-integrators (De Cesare et al., 1999).

1.3.5 Src tyrosine kinases, downstream effectors of growth-factor signalling

The signalling pathways activated upon growth factor stimulation require several phosphorylation events. Receptor and non-receptor tyrosine kinases cooperate to transduce the signal to downstream targets. Among the non-receptor tyrosine kinases, the Src family plays a pivotal role in may different cellular events. The importance of this kinase stems from work on the *Rous sarcoma* virus that expresses the cancer-causing oncogene v-Src (an active form of Src) (Weiss et al., 1977). Src is the cellular homologue of v-Src in human, chicken and other animals. It derives from the *c-Src* cellular gene (the proto-oncogene), and its activity is regulated by intramolecular interactions controlled by tyrosine phosphorylation. Another way to modulate Src is through protein–protein interactions with sequences containing phosphotyrosine and proline-rich motifs, which bind the SH2-SH3 domains of Src (Martin, 2001).

The Src kinases are expressed ubiquitously, but brain, osteoclasts, and platelets express 5–200-fold higher levels of these proteins than most other cells (Brown and Cooper, 1996). In fibroblasts, Src kinases are bound to endosomes, perinuclear membranes, secretory vesicles and the cytoplasmic face of the plasma membrane, where they can interact with a variety of growth factor and integrin receptors (Roskoski, 2004). The Src kinases are controlled by tyrosine kinases, integrins, GPCR, antigen- and Fc-coupled receptors, cytokine receptors and steroid hormone receptors (Parsons and Parsons, 2004).

There are eleven members of the Src family kinase in humans. These are Blk, Brk, Fgr, Frk, Fyn, Hck, Lck, Lyn, Src, Srm, and Yes. Moreover, the human genome contains a Yes pseudogene (YESps). Src, Fyn, and Yes are expressed in all cell types, while Srm is found in keratinocytes, and Blk, Fgr, Hck, Lck and Lyn are found primarily in haematopoietic cells. Frk occurs chiefly in bladder, brain, breast, colon and lymphoid cells, whereas Brk occurs in colon, prostate, and small intestine (Roskoski, 2004).

In the structure of the protein, from the N- to C-terminus, it is possible to distinguish a regulatory region and a catalytic part. The regulatory region consists of a 14-carbon myristoyl group attached to an SH4 domain, then a unique domain, an SH3 domain that binds to proline-rich sequences of target proteins, an SH2 domain that binds to the regulatory p-Tyr-527 and an SH2-kinase linker. The catalytic part consists of a protein tyrosine kinase domain, which presents a bi-lobed structure. The smaller amino-terminal lobe (N-lobe) of the protein kinase is primarily involved in anchoring and orienting ATP; the G-rich loop forms part of the nucleotide-phosphate binding site. The larger carboxyl-terminal lobe (C-lobe) is responsible for binding the protein substrate. The catalytic site of Src lies in a cleft between the two lobes. Within each lobe is a polypeptide segment that has an active (when phosphorylated in Tyr-416) and restrained (α-helical non-phosphorylated) conformation. The two lobes move relative to each other and can open or close the cleft. Finally, there is a C-terminal regulatory segment that can be phosphorylated in Tyr-527 (Boggon and Eck, 2004) (Fig. 1.12a).

Src kinases are regulated by alternative phosphorylation/de-phosphorylation events: Tyr-416 is the main phosphorylation site of Src kinases that results in their activation *via* autophosphorylation. The Tyr-527 at the C-terminus, when phosphorylated by C-terminal Src kinase (CSK), cause the inhibition of Src kinases activity. The phosphorylated C-terminus interacts with the SH2 domain, causing the closed inactive structure of Src kinases (Fig. 1.12b). Protein-tyrosine phosphatases, such as cytoplasmic PTP1P, Shp1, Shp2 and several other transmembrane enzymes including PTPα, CD45, PTPε and PTPλ, can de-

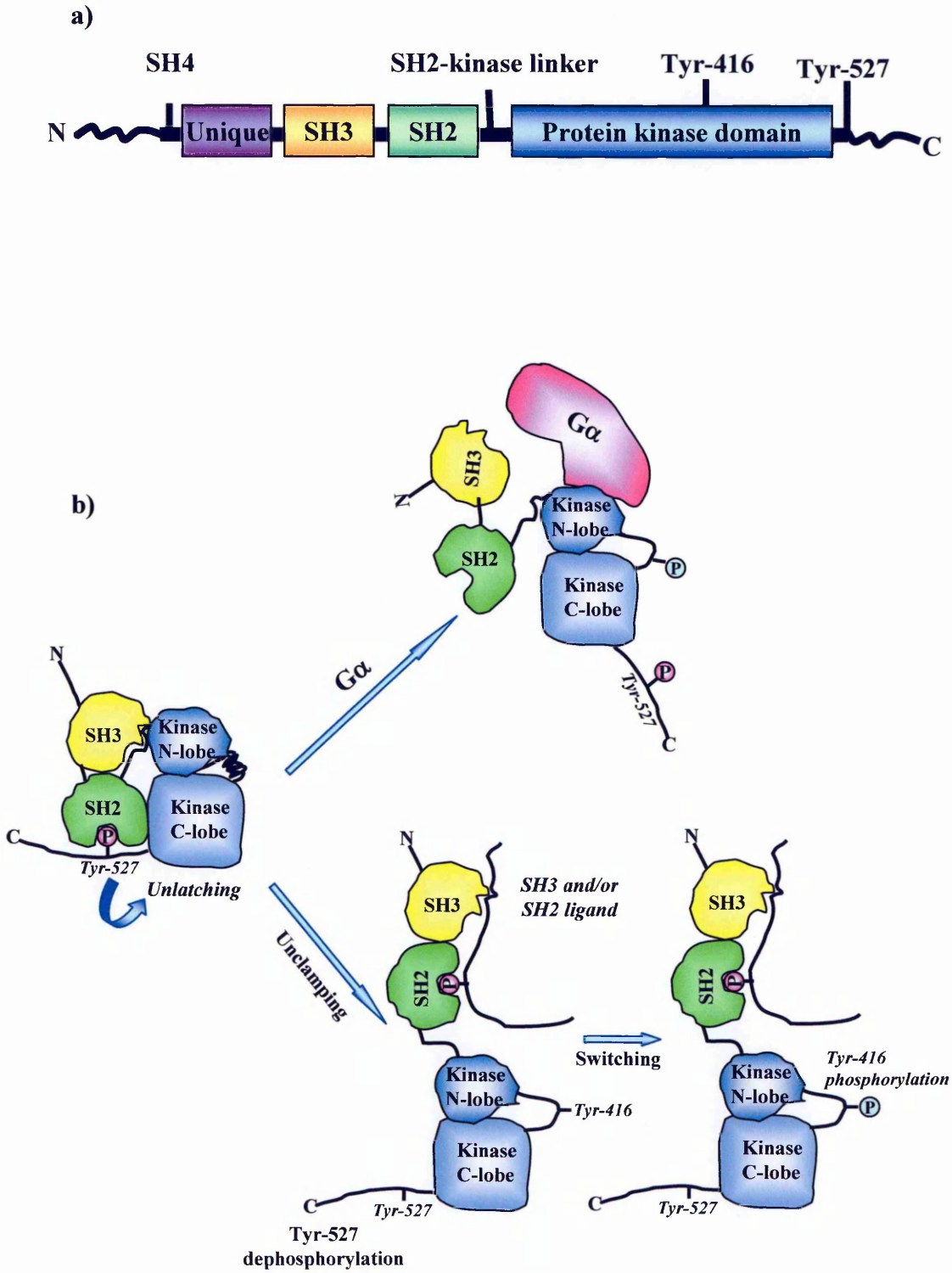

Figure 1.12 - Src structure and activation. a) Domain organisation of Src; The unique, SH4, SH3, SH2 and protein kinase domains are indicated in Section 1.3.5. **b)** Src activation by unlatching, unclamping, and switching. Or by direct interaction with Gα subunit of heterotrimeric G proteins. This figure is reproduced from Harrison, 2003 and Ma et al., 2000)

phosphorylate p-Tyr-527 (unlatching), causing the detachment of the SH2 domain, a consequent opening of the catalytic cleft (unclamping), and the autophosphorylation of Tyr-416, which stabilise the Src kinases in their active form (Fig. 1.3.5b) (Roskoski, 2004) Another way to modulate the activity of the Src kinases is via heterotrimeric G-proteins. It has been demonstrated that $G\alpha_s$ and $G\alpha_i$, but not $G\alpha_q$, $G\alpha_{12}$ or $G\beta\gamma$, directly stimulate the kinase activity of downregulated c-Src or Hck, another member of the Src family kinases. $G\alpha_s$ and $G\alpha_i$ bind to the catalytic domain (N-lobe) and change the conformation of Src, leading to increased accessibility of the active site to substrates. These data demonstrate that the Src kinases are direct effectors of G proteins (Ma et al., 2000) (Fig. 1.12b).

Src kinases activity during cell polarization and migration is important as an upstream signal to transduce growth-factor stimulation, for example by activating PLCγ or by activating Rac1 exchange factors, like PIX or VAV (Barfod et al., 2005), and also as a downstream effector of Rac1 and Cdc42 during peripheral actin and adhesion remodelling that is required for directional migration. The Src kinases are targeted to the peripheral adhesion sites, where they are able to convert Rho-dependent focal adhesions into smaller focal complexes along Rac1-induced lamellipodia (or Cdc42-induced filopodia) (Timpson et al., 2001)

1.4 The phosphoinositides and their aqueous derivatives

This section will provide a general background about the phosphoinositides, lysophosphoinositides and glycerophosphoinositols. A particular attention will be addressed on the metabolic pathway and the known functions of the glycerophosphoinositols.

1.4.1 The phosphoinositides

The phosphoinositides represent a minor fraction (approximately 10%) of the total membrane phospholipids (Toker, 2002), and they consist of a double acylated diacylglycerol moiety which is phosphodiesterified to *myo*-inositol, a six-carbon cyclic polyalcohol. The inositol headgroup contains five free hydroxyl groups with the potential to become phosphorylated. Thus, numerous derivatives of phosphatidylinositol (PI) that present single or multiple monoester phosphates in the inositol head group exist in cells, many with unique functions. To date, the following phosphoinositides have been identified in cells: PI-3-phosphate (PI3P), PI-4-phosphate (PI4P), PI-5- phosphate (PI5P), PI-3,4-bisphosphate ($PI3,4P_2$), PI-3,5-bisphosphate ($PI3,5P_2$), PI-4,5-bisphosphate ($PI4,5P_2$) and PI-3,4,5-trisphosphate ($PI3,4,5P_3$) (Takenawa and Itoh, 2001).

The phosphoinositides are mainly localised on the cytoplasmic side of the plasma membrane, where they are not likely to provide only a structural role, but where they also exert specific regulatory functions, such as agonist stimulated signal transduction. The phosphoinositides can interact specifically with a wide range of proteins, providing their translocation from one area of the cell to another, or producing conformational changes in the proteins, which can also result in modulation of the activity of the proteins. Alternatively, the phosphoinositides are substrates of different enzymes, including the phosphoinositide kinases (PIKs), phosphatases and phospholipases (see also Sections

1.3.1, 1.3.2) that can lead to the production of several second messengers that originated from the phosphoinositides. The result of these processes is that the phosphoinositide-protein interactions can initiate downstream signalling cascades leading to cell growth, proliferation, differentiation, death, secretion, vesicle trafficking, motility and intracellular metabolism (Toker, 2002).

The function of each phosphoinositide depends on when and where it is made, moved to and broken down within the cell. The synthesis of PI occurs in the ER, while the subsequent phosphorylation steps occur in post-ER compartments (Gehrmann and Heilmeyer, 1998; Loijens et al., 1996). Indeed, PIKs have been localised to most intracellular membrane compartments, including the plasma membrane, the nucleus, secretory granules, endosomes, the ER and Golgi complex.

Many PIKs were initially described as enzymatic activities, capable of transferring a phosphate to a specific position on the inositol ring of PI or its phosphorylated derivatives. Studies on purified enzymes led to categorisation into three main families: the PI3Ks, PI 4-kinases (PI4Ks) and PIP-5-kinases (PIP5Ks) (Fruman et al., 1998; Honda et al., 1999). Over the last decade the genes encoding several of these enzymes have been identified and sequence comparisons generally support the distinct classification of PI3Ks, PI4Ks and PIP5Ks. These enzymes phosphorylate, respectively, the D3, D4 and D5 positions of the inositol ring, thus forming the differently phosphorylated phosphoinositides. The phosphoinositide phosphatases act in the opposite direction to the PIKs, dephosphorylating the inositol ring. Three different classes of phosphatases exist: the 5-OH specific that eliminates the phosphate from position 5 of inositol (e.g. SHIP1-2), the 4-phosphate phosphatases that appear to participate in PI3K signalling, and the 3-OH phosphatases, like PTEN/MMAC1 (products of tumour suppressor genes), that are important for the conversion of $PI3,4,5P_3$ to $PI4,5P_2$ (Toker, 2002) (Fig. 1.13).

Each phosphoinositide exhibits a unique stereochemistry, and can elicit a distinct biological response. Indeed, the phosphoinositides pathways constitute perhaps the most

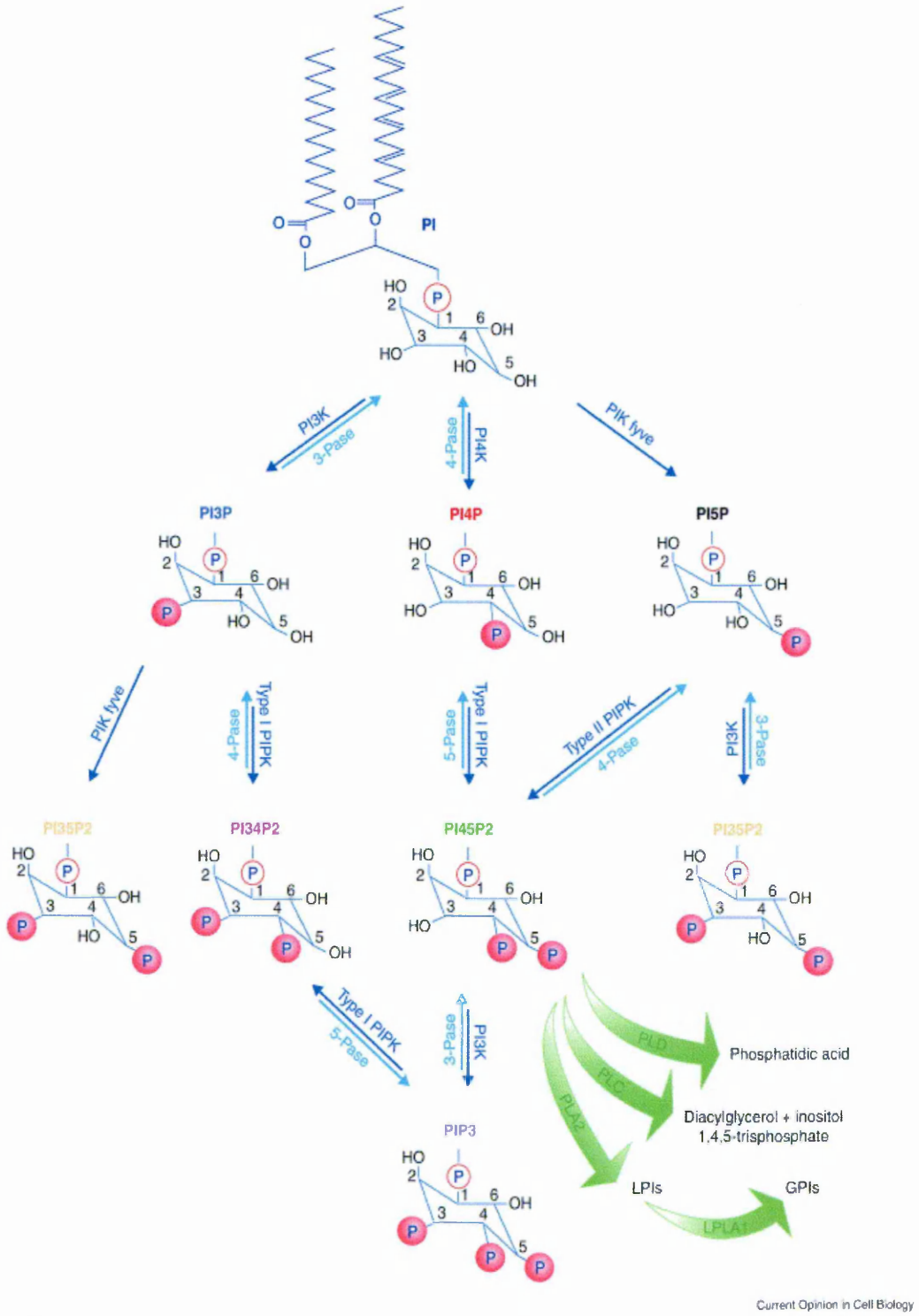

Figure 1.13 - Pathways of phosphoinositide synthesis and degradation (De Matteis et al., 2002). Blue and light-blue arrows indicate routes of phosphoinositide phosphorylation and dephosphorylation, respectively (note that some of these reactions are established *in vitro* but not yet *in vivo*). The phosphoinositides can be hydrolysed by PLC to generate IP_3 and DAG from $PI4,5P_2$; by PLA_2 to form the lysophosphoinositides; PLA/lysophospholipases ($LPLA_1$) to form the glycerophosphoinositols; and by phospholipase D (PLD) to form phosphatidic acid (Ching et al., 1999). PLC acts preferentially on $PI45P_2$, whereas the other phospholipases may act on the different PIs (for simplicity in the Figure, all the phospholipases are shown acting only on $PI4,5P_2$).

complex signalling network in the cell, and their location and specificity are of great importance.

1.4.1.1 The phosphoinositides as docking sites for proteins

As docking sites for proteins, the phosphoinositides can function as messengers themselves in the localisation and assembly of protein machineries. The differential localisation of these phosphoinositides is a pre-requisite for this function. The unphosphorylated form (PI) is the immediate precursor of all the phosphoinositides and localises to cytoplasmic membrane leaflets (Vanhaesebroeck et al., 2001). The most abundant monophosphorylated form is PI4P, produced by PI4K and resident in the Golgi complex; PI3P also localises in the Golgi complex, where it is involved in intracellular membrane trafficking. PI4,5P_2 is the most abundant bis-phosphorylated phosphoinositide, and is mostly enriched at the plasma membrane, where it is involved in clathrin cage assembly and actin polymerization, and where it is also hydrolyzed by the PLCs for the initiation of signal cascades (see also Section 1.3.1). PI3,4,5P_3, can be found on the plasma membrane but its detection is a result of extracellular or intracellular stimulation events, which leads to local increases of PI3,4,5P_3.

Several protein domains that bind to phosphoinositides with high affinity have been identified over the last few years. Among the best characterised are the FYVE (Fab1, YOTB, Vac1 and EEA1), PH (pleckstrin homology) and PX (Phox homology) domains (reviewed in Gillooly et al., 2001; Lemmon and Ferguson, 2000; Wishart et al., 2001). These domains recruit proteins to specific membrane regions in cells, via their interactions with phosphoinositides, and they can also serve as allosteric regulators of enzyme activities and protein-protein interactions. The localization of the phosphoinositides is strictly correlated to their function. All FYVE domains tested bind to PI3P, whereas PH and PX

domain display a variety of specificities. Surprisingly, there is little structural similarity between the different phosphoinositide-binding domains.

The **FYVE domain** was discovered in 1998 (Burd and Emr, 1998; Patki et al., 1998) as a specific recognition site for PI3P. This 65-residue module is known to exist in 37 human proteins, the majority of which have been implicated in endocytic/vacuolar membrane trafficking (e.g. EE1, Rabenosyn-5, Hrs proteins) (Gillooly et al., 2001) or in signalling (e.g. SARA) and cytoskeleton organisation (e.g. the Fdg family of proteins) (Takenawa and Itoh, 2001). The structure and specificity of the FYVE domains are conserved, consisting of a pair of small β-sheets and a short α-helix. Stabilisation is provided by two zinc ions, each contained by a cluster of four cysteines. The PI3P head-group fits into a shallow groove next to the first β-strand (Stenmark and Aasland, 1999).

PH domains are the most thoroughly characterized of the phosphoinositide recognition modules, and they have been adopted by a wide range of protein architecture and have a variety of different roles in signalling, cytoskeleton organization, membrane trafficking and lipid modification (Dowler et al., 2000; Kavran et al., 1998; Rameh et al., 1997). Their 120-residue sequence has been found in several hundred human proteins. The PH domain is formed by seven-stranded antiparallel β-sheets with a strong bend, which results in an orthogonal sandwich (Hyvonen et al., 1995). This domain also has a characteristic C-terminal α-helix that blocks one end of the twisted sheet. All the PH domains are electro-statically polarised, with the positively charged face coinciding with three variable loops connecting the β-strands. The loops are the most variable regions between different PH domains, and may account for their diversity in specificity and affinity for the phosphoinositides. A significant minority of PH domains binds specifically and tightly to one phosphoinositide (e.g. The PLCδ PH domain is specific for $PI4,5P_2$, the BTK and Grp1 PH domains are specific for $PI3,4,5P_3$); the rest of the PH domains associate weakly and promiscuously with several phosphoinositides.

The **PX domain** is a 125-residue module that was originally named through its presence in the $p40^{phox}$ and $p47^{phox}$ subunits of the neutrophil NADPH oxidase superoxide generating complex (Ponting, 1996). PX domains have now been found in at least 57 mammalian and 15 yeast proteins, including kinesins, phospholipases, protein kinases, SNAREs and sorting nexin (reviewed in Wishart et al., 2001). Analysis of the yeast Vamp7-PX domain by NMR spectroscopy has demonstrated that it has a specific PI3P-binding motif and this has a key role in regulating its subcellular localisation and function in vacuolar sorting (Cheever et al., 2001). The PX domain of cytokine-independent survival kinase, on the other hand, binds selectively to $PI3,5P_2$ and $PI3,4,5P_3$ (Song et al., 2001).

Other phosphoinositide binding domains include the **C2** (present in protein kinase C, PI3K , Rac GTPases and other enzymes) and **SH2** (present in Src, PLCγ and other enzymes) domains that are present in many kinases and phosphatases and have little specificity (Bae et al., 1998b; Rameh et al., 1995; Rameh et al., 1998). Nonetheless, these interactions are important for recruiting diverse cytosolic proteins to the plasma membrane in response to receptor activation.

1.4.1.2 The phosphoinositides as precursors of second messengers

One of the most important roles of the membrane phosphoinositides and their products is as second messengers that allow the transduction of information from extracellular stimuli into a given intracellular response. The phosphoinositide metabolites that are known to be important second messengers are IP_3 and DAG, both derived by the action of PLC enzymes on $PI4,5P_2$ (see Section 1.3.1). These two second messengers have independent mechanisms of action: IP_3 is classically associated with the increase in $[Ca^{2+}]_i$ and DAG activates several isoforms of PKC (Michell, 1992).

IP_3 increases $[Ca^{2+}]_i$ by opening a Ca^{2+} channel (IP_3 receptor) situated in the ER. The cytosolic Ca^{2+} concentration in resting cells is maintained at low levels (~100 nM) by enzymes that translocate Ca^{2+} ions across the plasma membrane or into intracellular stores. The cytosolic Ca^{2+} level is increased physiologically when cells are challenged with certain stimuli, such as hormones, growth factors, depolarisation or mechanical deformation. The Ca^{2+} ions can be released from intracellular stores or can enter the cell across the plasma membrane, or a combination of the two (Berridge et al., 2003). For mobilising $[Ca^{2+}]_i$ stores, IP_3 receptors are the main route in almost all cell types. IP_3 receptors are large (1200 kDa) tetrameric proteins, each subunit of which projects an amino-terminal domain into the cytoplasm; their membrane-spanning carboxy-terminal regions form an integral Ca^{2+} channel. IP_3 binding by the amino-terminal domains causes a conformational change that promotes channel opening (Bosanac et al., 2004). Up to 500 nM $[Ca^{2+}]_i$ works synergistically with IP_3 to further activate IP_3 receptors. At higher concentrations, $[Ca^{2+}]_i$ inhibits IP_3 receptor opening. The inhibition of IP_3 receptors by $[Ca^{2+}]_i$ is thought to be a crucial mechanism for terminating channel activity and thus preventing pathological $[Ca^{2+}]_i$ increase (Bootman et al., 2002).

DAG is one of the key lipid second messengers that are generated transiently following the stimulation of seven-transmembrane and tyrosine-kinase receptors. Binding of DAG to the C1 domains of the PKC isozymes of the classic (cPKCα, βI, βII and γ) and novel (nPKCδ, ϵ, η and θ) families results in their activation (Parekh et al., 2000). Phorbol esters, natural compounds that bind to C1 domains of PKC isozymes and thus mimic DAG action, affect cell proliferation, differentiation, survival and transformation (Ron and Kazanietz, 1999).

As discussed in full detail in Section 1.3.2, the PLA_2 enzymes catalyse the hydrolysis of the *sn-2* ester linkage of the phospholipid substrate, resulting in the production of a free fatty acid (generally AA), and the corresponding lysophospholipids. The AA is metabolized to prostaglandins by the cyclooxygenase pathway and to

leukotrienes by the 5-lipoxygenase pathway. In addition, AA and other unsaturated fatty acids are themselves important regulators of specific cellular processes, including the activation of PKC and PLCγ, the modulation of ion channels, and cell death (Hirabayashi et al., 2004). cPLA$_2\alpha$ has been shown to have a pivotal role in the biosynthesis of these inflammatory lipid mediators. Lysophospholipids concomitantly produced can be acetylated to generate platelet-activating factor (PAF), when the *sn-1* position of the phospholipid contains an alkyl-ether linkage. Other lysophospholipids are also reported to have several biological functions. These lipid mediators are implicated in the pathophysiology of asthma, arthritis and other inflammatory diseases (Kudo and Murakami, 2002).

The activity of PLA$_2$ is relevant to this study. The focus will be on a PLA$_2$ activity specific for the membrane phosphoinositides (PI-PLA$_2$). The main initial products are the AA and lysophosphoinositides. Starting from the lysophosphoinositides, the sequential hydrolysis of the fatty acid at the *sn-1* position leads to the production of the glycerophosphoinositols. This last event requires the activity of a lysolipase, or the action of cPLA$_2\alpha$ and cPLA$_2\gamma$, since both display lyso-phospholipase activity and can sequentially deacylate the *sn-2* and *sn-1* positions of these phospholipids (Leslie, 1991; Stewart et al., 2002). cPLA$_2\beta$ may not function as a PLA$_2$ but rather as a PLA$_1$ and lyso-phospholipase, for the sequential release of the *sn-1* and *sn-2* fatty acids (Song et al., 1999).

The cellular functions of the lysophosphoinositides and the glycerophosphoinositols will be described further in the following sections.

1.4.2 The lysophosphoinositides

The plasma membrane lysophosphoinositide pool is continuously deacylated/reacylated to maintain a constant concentration of the phosphoinositides.

Okuyama (Kobayashi et al., 1996) and colleagues indicated that the production and removal of lysophosphoinositides can occur by a Ca^{2+}-insensitive PI-specific PLA_1 that is coupled to a LPI-specific PLC. This activity is also accompanied by a $lysoPLA_2$ activity that produces glycerophosphoinositol (GroPIns) (Ueda et al., 1993). When exogenously added to cells, the lysophosphatidylinositol (LPI) can be metabolized to inositol 1:2-cyclic monophosphate (Ins1:2cP) by an extracellular PLC activity, or incorporated into the plasma membrane as a precursor of the phosphoinositides. The incorporated LPI can be further hydrolyzed to Ins1:2cP via a intracellular PLC-like activity and to GroPIns via a lysoPLA activity, depending on the cell system (Corda et al., 2002; Falasca et al., 1998) (Fig 1.14).

LPI has been reported to increase by 2-3-fold in K-Ras transformed thyroid cells in response to the increased activity of PLA_2. In addition, treatment with LPI can cause an increase in [^{3}H]-thymidine incorporation both in Ras-transformed and in differentiated thyroid cell lines (Falasca and Corda, 1994). These data suggest that LPI has a mitogenic activity and that its formation is responsible for the increase in cell growth that is typical of transformed cells.

A number of lysophospholipids have been reported to be mitogens in different cell systems. The best characterised of these is lysophosphatidic acid (LPA), which is known to be the agonist of a specific GPCR. It initiates a complex signal cascade that activates the small G-protein Rho and affects the organization of the actin cytoskeleton (Moolenaar, 1999). In addition, LPA is also a marker for, and induces proliferation of, breast and ovarian cancers (Goetzl et al., 1999; Xu et al., 1995). Lysophosphatidylcholine (LPC) is also a mitogen, and it is associated with vascular, inflammatory and autoimmune diseases (Asaoka et al., 1991) and ovarian cancer (Fang et al., 2000). It has also been shown that LPC activates a signalling cascade as the ligand for the immunoregulatory A2G receptor (a GPCR) (Kabarowski et al., 2001)

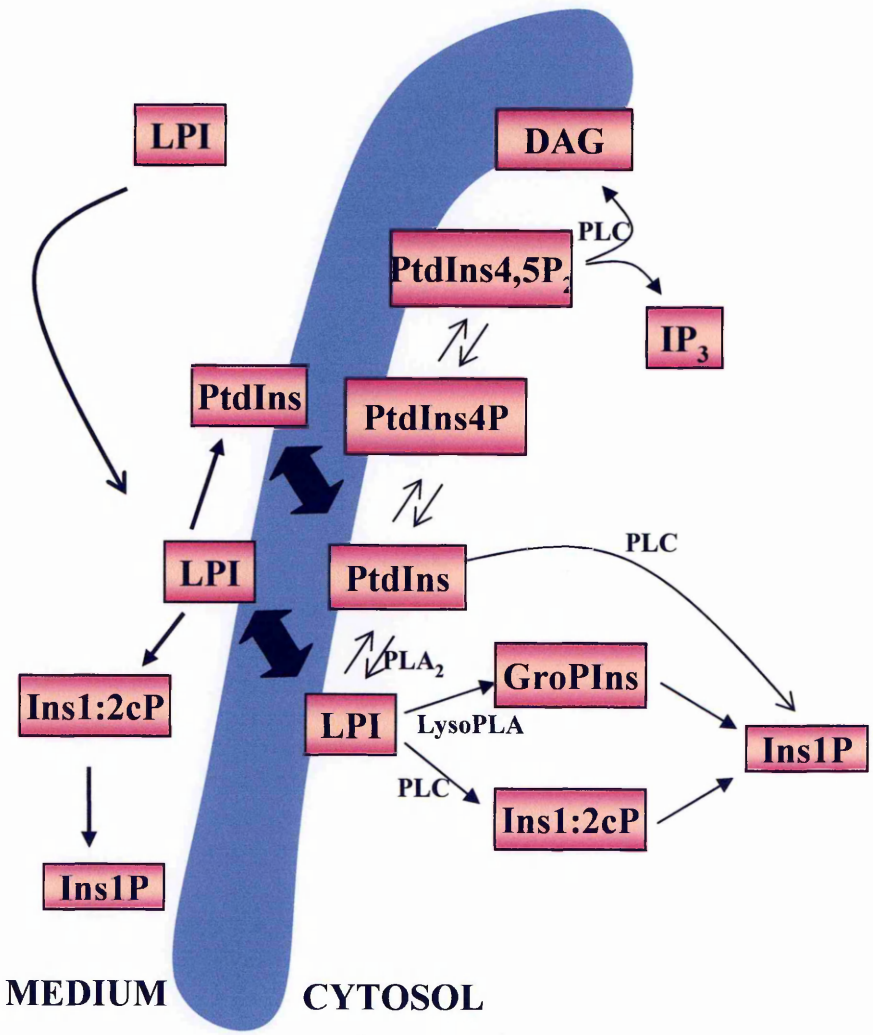

Fig. 1.14 - Main potential pathways of metabolism from extracellularly applied or extracellularly produced LPI. Potential receptor activation by LPI is not included (see Section 1.4.2 for details) (Corda et al., 2002).

The mitogenic activity of LPI is pronounced in Ras-transformed cells (thyroid cells and fibroblasts), while LPA is active also in normal cells. These lysophospholipids show different mechanisms of action that have allowed the exclusion of the presence of a unique receptor; moreover, LPI appears to be more active in cell systems in which it is also accumulated, thus suggesting that this compound can function as an autocrine modulator of cell growth. In fact it as been shown that in Ras-transformed fibroblasts (FRT-Fibro cells) and thyroid cells, LPI accumulates in the extracellular space. Thus, LPI accumulates inside the cell, and then is released and consequently activates its specific receptor (Falasca et al., 1998). The presence of a specific receptor for LPI is strongly suggested by the fact that suramin, a membrane-impermeant antagonist of growth factors, completely prevents LPI activity (Corda et al., 2002).

The mechanism of action of LPI in fibroblasts includes the activation of a PLC that leads to $[Ca^{2+}]_i$ increases, PLA_2 activation and AA release. These events produce AC inhibition and a decrease in cAMP (see Section 1.3.3). Also, in pancreatic cells it is possible to follow a similar effect, while in yeast the LPI activates AC and inhibits PLD. In thyroid cells the LPI pathway involves tyrosine kinase activation (Falasca and Corda, 1994; Falasca et al., 1995). These effects of LPI are all exerted at low micromolar concentrations (~10 μM), which are below its critical micellar concentration (~75 μM). An additional effect of LPI is to completely inhibit the Ras-GAP and neurofibromatosis type 1 proteins, but at concentrations of >100 μM (micellar form) (Falasca et al., 1995).

In summary, LPI is a mitogen that can act via a receptor-mediated mechanism. It is particularly active in transformed cells, which show an elevated concentration of lysophospholipids, and it can be accumulated in Ras-transformed cells more rapidly than in normal cells.

Besides LPI, the phosphorylated derivatives, the LPIPs such as LPI4P, LPI4,5P_2, which are produced upon deacylation of their corresponding phosphoinositides (PI4P and PI4,5P_2) can also be found in cells. Once formed, the LPIPs are rapidly dephosphorylated

to LPI, and there are no indications of the presence of a reacylation pathway (Corda et al., 2002; Palmer, 1986). In parallel to the dephosphorylation it is also possible to follow a deacylation by a LysoPLA$_2$ that produces the glycerophosphoinositols, GroPIns4P and GroPIns4,5P$_2$. In various cell types, it is possible to follow receptor and calcium-dependent GroPIns4P formation, and corresponding increase in LPI4P (Corda et al., 2002).

1.4.3 The glycerophosphoinositols

1.4.3.1 Metabolic pathway of the glycerophosphoinositols

The presence of GroPIns in cell extracts was originally seen in the 1960s and 1970s in early studies of phosphoinositides hydrolysis, when *in vitro* enzymatic activities relating to their formation were described (Irvine et al., 1978; Kemp et al., 1961). The formation of GroPIns was first described as requiring the combined action of a PLA$_2$ and a lysolipase. More recently, an extracellular phospholipase B that is able to deacylate both the *sn-1* and *sn-2* positions of phospholipids and that has been identified in the intestine of different mammalian species has been proposed (Chaminade et al., 1999). The formation of GroPIns and its monophosphorylated form, GroPIns4P, has been reported in several tissues and cell lines (Corda et al., 2002)(Table 1.3).

Of interest, there is the observation that both GroPIns and LPI accumulate in Ras-transformed cells. The cellular systems used were KiKi or KiMol cells, which are transformed by the K-Ras oncogene and which originated from a normal rat thyroid cell line (FRTL-5 cells). The effect of the transformation was a 6-fold increase in GroPIns. A parallel increase in membrane pools of phosphoinositides was also detectable in transformed cells, and this was related to a decrease in free cytosolic inositol. Furthermore, cell lines expressing temperature-sensitive mutants of oncogenic Ras display an

Table 2
Stimulation of glycerophosphoinositols production in cells

Tissue/cell preparation	Stimulant
Glycerophosphoinositols	
Peritoneal macrophages	Zymosan particles, concanavalin A
Platelets	Thrombin
Brain slices	Oxotremorine-M
Cerebral cortical slices	Carbachol, noradrenaline
Neutrophils	fMetLeuPhe, concanavalin A
C62B glioma cells	Acetylcholine
Kidney slices	Noradrenaline
Umbilical vein endothelial cells	Histamine
Uterine decidua cells	TPA
NIH 3T3 fibroblasts	Ras/src/met/trk/mos/raf/vav transformation
Rat-1	Ras transformation
RAW264.7 macrophages	Cholera and pertussis toxins
Vascular smooth muscle cells	Atrial natriuretic peptide
Thyroid slices	Thyrotropin, carbachol, noradrenaline
Vascular smooth muscle cells	Endothelin
Adrenal fasciculata reticularis cells	ACTH1-39
Precapillary resistance arteries	Spontaneous hypertension, noradrenaline
Kupffer cells	PAF
Thyroid cells	Thyrotropin, carbachol, ATP
Permeabilized pituitary GH3 cells	5′-CMP
HL60 cells	Differentiation (DMSO)
Kupffer cells	PAF, cholera toxin+PAF
Thyroid cells	Ras transformation
Normal and Ras-transformed thyroid cells	A23187
Myeloid blast cells	Differentiation (PMA)
Kupffer cells	Endothelin-3
T-helper cells	Tax transformation
Yeast	Glucose
HL60 cells	Differentiation (retinoic acid/GCSF)
HL60 cells	Differentiation (dihydroxyvitamin D_3)
Myeloid blast cells	Differentiation (spontaneous)
B and T lymphocytes	Maturation
Renal proximal tubule cells	Lindane
Various	Receptor stimulation
Hepatocytes	Pre-maturation
NG-108-15 cells	Differentiation (cAMP)
PC12 cells	Differentiation (NGF)
Various	Receptor stimulation
NIH 3T3 fibroblasts	PITPα transfection
Kupffer cells	PAF, A23187
RBL cells	A23187
GroPIns4P	
Precapillary resistance arteries	Spontaneous hypertension, noradrenaline
Yeast	Glucose
Thyroid cells	Ras transformation
Hepatocytes	Liver development
NG-108-15 cells	Differentiation (cAMP)
Fibroblasts	EGF/insulin/ATP/LPA/A23187
Thyrocytes	ATP/thyrotropin
PC12 cells	EGF/NGF
RBL cells	Antigen to IgE receptor
Rat heart	α1-adrenoceptor
RBL cells	A23187
Ras-transformed thyroid cells	A23187

Abbreviations are as used in text.
[a] C. Iurisci and D. Corda, unpublished data; see text.

Table 1.3 - Stimulation of GroPIns and GroPIns4P production in cells. From Corda et al., 2002.

accumulation of lysophosphoinositides and glycerophosphoinositols only at the permissive temperature. The modification in phosphoinositide pools and the parallel formation of GroPIns, were accompanied by striking changes in cell morphology (Alonso and Santos, 1990; Valitutti et al., 1991).

These increases in GroPIns and LPI appear to be related not only to Ras transformation, but more in general to the activation of Ras pathways. Hence, these compounds are formed upon the activation of receptors, including those coupled to Ras, and high GroPIns levels can be measured during cellular responses, such as with the differentiation of hepatic and neuronal cells, where Ras is activated (Corda and Falasca, 1996; Falasca et al., 1996). However, the correlation between Ras transformation and an increase in GroPIns has to be verified in individual cases, as was more recently examined by liquid chromatography-tandem mass spectrometry (to directly measure the GroPIns levels in cell extracts) (Berrie et al., 2002). Here the GroPIns levels in selected parental and Ras-transformed cells, as well as in some carcinoma cells, ranged from 44 to 925 μM, without increasing during transformation in all of the cell types (Table 1.4) (Berrie et al., 2002).

In some cellular system (such as Ras-transformed thyroid cells, epithelial cells and fibroblasts), the activity of PLA_2 is specific for the hydrolysis of the phosphoinositides, as the level of lysophosphoinositides is the only change seen after stimulation (the formation of LPC and lysophosphatidylethanolamine was not detectable). This suggests that a PI-specific PLA_2 is present in these cells (Corda and Falasca, 1996; Falasca and Corda, 1994). This enzyme deacylates the phosphoinositides at the *sn-2* position resulting in the production of AA; then a lysolipase (probably the same PLA_2 that can also display a lysolipase activity, see Section 1.4.1.2) deacylates the *sn-1* position of the glycerol backbone of phosphoinositides, thus forming the glycerophosphoinositols (Fig. 1.15a). As reported in Table 1.3, in many different cell types the formation of GroPIns has been associated with an ionophore (A23187)-dependent increase in $[Ca^{2+}]_i$ and with many of the

Cell line	GroPIns concentration (μM±SEM)	n^a(MS)	Derived inositol[b](mM)	n^c ([^{3}H])	Cell volume (pl ±SE)	Cell type
FRT-Fibro	172±25	7	1.1	11	1.62±0.14	Fibroblast
FRT-Fibro-Ha	925±155**	6	0.26	24	1.92±0.07	Fibroblast, H-*Ras* transformed
FRTL5	434±48	13	97.1	13	0.84±0.07	Thyroid
KiKi	272±34**	16	0.29	18	1.71±0.11	Thyroid, K-*Ras* transformed
PCCl3	144±3	5	25.3	20	0.97±0.03	Thyroid
PC-KiKi	133±12	6	30.4	10	0.97±0.02	Thyroid, K-*Ras* transformed
PC-Ha	44 ±3**	8	1.2	10	1.57±0.08	Thyroid, H-*Ras* transformed
PC-Src	90 ±7*	7	0.14	11	2.22±0.04	Thyroid, *Src* transformed
11+/+	433±40	8	10.6	17	4.39±0.23	Mouse embryo fibroblasts eps8+/+
4-/-	317±4*	6	3.6	16	1.82±0.04	Mouse embryo fibroblasts eps8−/−
Swiss 3T3	328±16	5	10.9	27	2.48±0.14	Fibroblast
293	439±12	3	ND	–	1.11±0.05	Kidney epithelial, adenovirus transformed
MDA	400±30	3	ND	–	1.53±0.10	Prostate epithelial adenocarcinoma
OVCAR3	200±22	3	133	9	2.20±0.03	Ovarian epithelial adenocarcinoma
MCF7	185±19	3	ND	–	1.64±0.10	Mammary epithelial adenocarcinoma
Hela	134±10	3	ND	–	1.39±0.08	Cervical epithelial adenocarcinoma
L cells	89 ±10	3	ND	–	0.74±0.19	Mouse fibrosarcoma

Table 1.4 - Intracellular GroPIns concentrations and relative inositol levels in selected cell lines. From Berrie et al., 2002

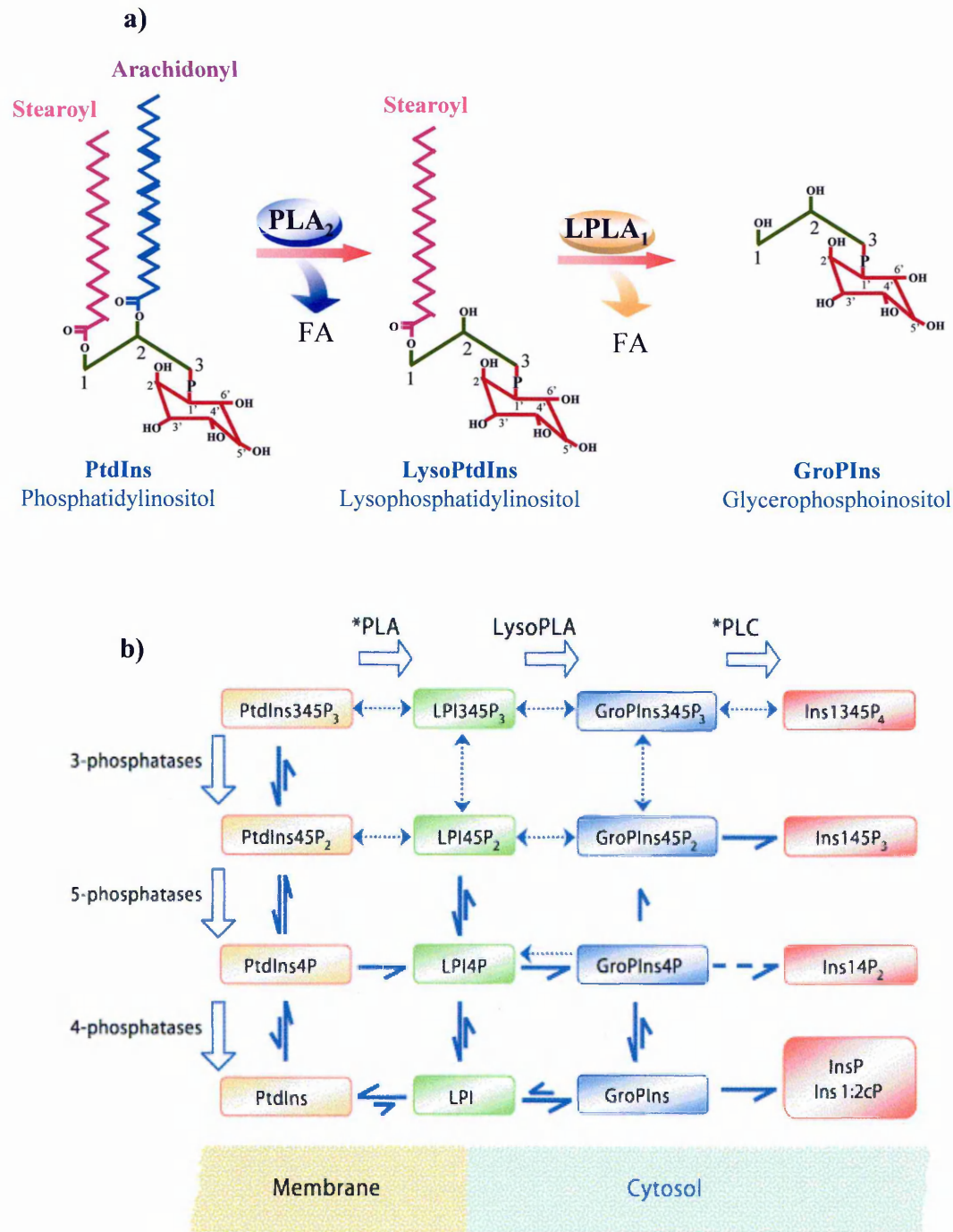

Figure 1.15 - Synthesis and metabolic pathway of the glycerophosphoinositols (Corda et al., 2002). **a)** Schematic representation of the formation of LPI and GroPIns from PI *via* the sequential actions of a PLA_2 and a $LysoPLA_1$ activity (see text for details). AA, arachidonic acid; SA, stearic acid; PLA_2, *sn*-2-specific phospholipase A; $LPLA_1$, *sn*-1-specific lysophospholipase A. **b)** A scheme for the known and potential metabolic interconversion pathways with particular reference to the lysophosphoinositides and the glycerophosphoinositols. Hollow arrows: direction of relevant enzymatic activities; asterisk: enzyme pathways known to be receptor activated; dotted arrows: potential metabolic pathways yet to be investigated; broken arrow: GroPIns4P is a reported substrate for PtdIns-specific PLCδ1 *in vitro* (Wu et al., 1997), but was not seen to undergo a PLC-like attack in Swiss 3T3 membranes in vitro (Berrie et al., 1999).

other stimuli used also implying an increase in $[Ca^{2+}]_i$, indicating that a Ca^{2+}-dependent cPLA2 is involved (Corda et al., 2002).

In Swiss 3T3 cell extracts, GroPIns can be formed through the dephosphorylation of GroPIns4P; this is the only detectable catabolic pathway for GroPIns4P (Berrie et al., 1999). The enzyme involved in the dephosphorylation is membrane associated, requires free Ca^{2+} (100-1000 nM) and is specific for GroPIns4P (Berrie et al., 1999). GroPIns4P can also be phosphorylated to GroPIns4,5P_2 by a Ca^{2+}-insensitive cytosolic enzyme. The reacylation to phosphoinositide has been found only for GroPIns, which can be converted into PI both in whole cells and in membrane fractions. A schematic representation of the known and potential metabolic pathways for the formation of lysophosphoinositides and glycerophosphoinositols is given in Figure 1.15b. While the amount of GroPIns detectable in normal and transformed cells is generally in the range of 44-925 μM, when GroPIns4P is formed, it represent less than 3% of the GroPIns levels (Corda et al., 2002). Thus it will normally range from 1 to 50 μM.

1.4.3.2 Biological activities of the glycerophosphoinositols

The glycerophosphoinositols are formed in many different cells types upon stimulation with growth factors, hormones and Ca^{2+}-ionophores. To understand their biological function, these compounds were given exogenously to cells and their potential actions on different signalling pathways were analyzed. The results of these studies are summarized below.

1.4.3.2.1 Adenylyl cyclase and PLA_2 inhibition

The biological activities and mechanism of action of the glycerophosphoinositols was originally characterised in thyroid cells. GroPIns4P was the only active compound, and it was able to inhibit AC (see Section 1.3.3). The first evidence was that in isolated

membranes of thyroid cells, AlF^-_4 (aluminium fluoride)-activated AC was inhibited by 48% by the addition of GroPIns4P, with an IC_{50} of 30 μM (Iacovelli et al., 1993). This GroPIns4P-dependent inhibition of AC was also seen in intact cells, when the AC was activated by cholera toxin (CTX) or thyrotropin: 50 μM GroPIns4P caused a 67% inhibition of CTX-activated AC and a 20% inhibition of thyrotropin-activated AC (with an IC_{50} of 14 μM). Both AlF^-_4 and CTX activate AC via heterotrimeric G-proteins. By mimicking GTP, AlF^-_4 causes the dissociation of the Gα subunit from the βγ dimer, while CTX ADP-ribosylates the $G\alpha_s$ subunit, favouring its activation (Gill and Meren, 1978). Thyrotropin is the main hormonal activator of AC in thyroid cells and it also acts through G-proteins. Based on these observations, it was proposed that GroPIns4P inhibits AC when it is activated by Gs proteins at least in the thyroid cell system. This proposal was supported by the demonstration that when AC was activated directly (by forskolin, which binds AC and causes structural changes that leads to its activation; Klein et al., 1988b), it was not inhibited by GroPIns4P. This AC inhibition also has a physiological relevance, as shown by thyrotropin-induced iodine uptake, which was inhibited by the treatment with GroPIns4P (Iacovelli et al., 1993). This GroPIns4P-dependent AC inhibition was then verified and confirmed in other cell lines, including smooth muscle cells, pituitary cells, pneumocytes, RBL cells and fibroblasts (Corda and Falasca, 1996; Falasca et al., 1997).

An additional correlation to cell function was seen in fibroblasts, were GroPIns4P potentiates EGF–stimulated cell growth, which is known to be inhibited by cAMP. Upon EGF treatment, the GroPIns4P concentration increases in a rapid and transient manner in Swiss 3T3 fibroblasts: a 2-4-fold increase was visible after 15 sec of treatment, with the maximal increase observed at 1 min (5-6-fold); within 2 min, the GroPIns4P levels return to basal (Falasca et al., 1997). The levels of GroPIns were not affected by this EGF treatment. This increase in GroPIns4P upon EGF treatment was observed also in other cell lines, like NIH 3T3, FRT-fibro and PC-12 cells. The mechanism by which this EGF treatment produced GroPIns4P was also investigated by applying a series of inhibitors, and

in particular, wortmannin (a PI3K inhibitor) was able to prevent GroPIns4P formation. The expression of a dominant-negative mutant of the small GTPase Rac1 also inhibited the formation of GroPIns4P, and a dominant-positive mutant resulted in an increase in basal GroPIns4P levels (Falasca et al., 1997). This could be explained by the fact that Rac1 is essential for EGF-induced PLA_2 activation (Peppelenbosch et al., 1995). In Swiss 3T3 cells, forskolin and CTX-dependent cAMP synthesis was inhibited by EGF. Exogenously added GroPIns4P also inhibited forskolin and CTX-activated AC in the same cell system, with an IC_{50} of 0.1μM (Fig. 1.16a) (Falasca et al., 1997). The EGF-dependent AC inhibition paralleled the changes in GroPIns4P levels: the maximal inhibition of cAMP was associated in time with the formation of GroPIns4P, which was maximal at 1 min and persisted for 30 min (Fig. 1.16b). Moreover, the extent of EGF-dependent AC inhibition was similar to that observed with exogenously added GroPIns4P and was prevented by the same inhibitors that blocked the production of GroPIns4P (Falasca et al., 1997). All these data suggested a potential role of GroPIns4P as second messenger, formed upon activation of the EGF-dependent Ras-Rac1 pathway that leads to PLA_2 activation, and finally to AC inhibition (Ras-PI3K-Rac1-PLA_2-GroPIns4P-cAMP↓).

Further indications that G-proteins can be a target of GroPIns4P come from the observations that GroPIns4P inhibits G_i-mediated activation of PLA_2 in thyroid cells, as does GroPIns, but not GroPIns4,5P_2. In FRTL5 thyroid cells, low micromolar concentrations of GroPIns and GroPIns4P inhibit purinergic- and adrenergic-receptor-induced AA release, which is known to involve the activation of G_i proteins (Berrie and Falasca, 2000; Corda et al., 2002). In line with these data, melittin- or calcium-induced AA release, which is G_i-independent, was not affected by either GroPIns or GroPIns4P (Corda et al., 2002). However, to date, there is no experimental evidence of a direct interaction of the glycerophosphoinositols with the G-proteins, as indicated by overlay and binding assays. The possible explanation of these effects of the glycerophosphoinositols

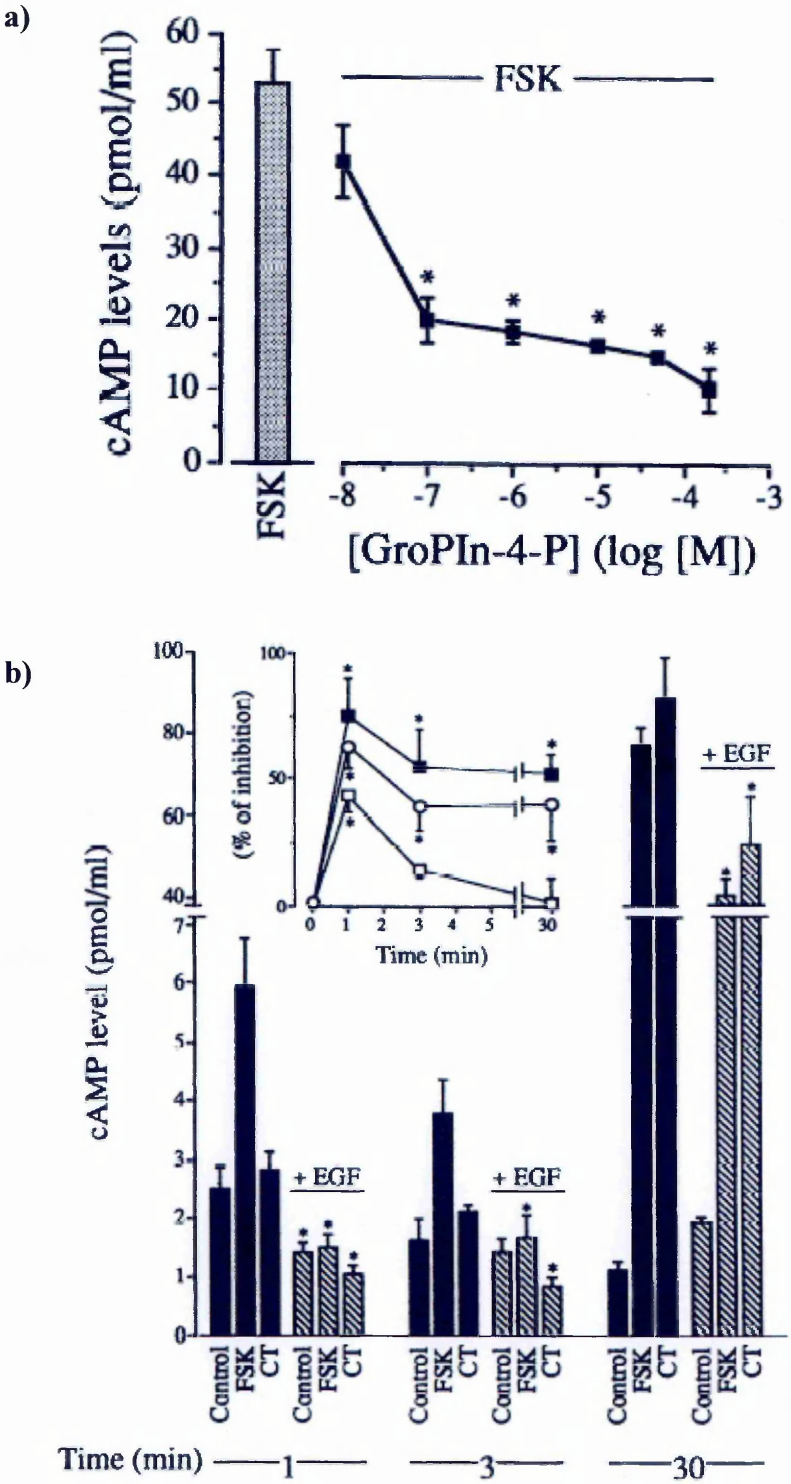

Figure 1.16 - GroPIns4P-dependent AC inhibition. a) GroPIns4P-dependent inhibition of forskolin-induced cAMP levels in Swiss 3T3 cells. Data are presented as pmol/ml. GroPIns4P was added at the indicated concentrations 60 min prior to forskolin; the incubation was then carried out for 30 min. Similar results were obtained by increasing the cAMP levels with 10 nM cholera toxin. **b)** EGF-induced inhibition of the basal, cholera toxin-induced, and forskolin-induced cAMP levels in Swiss 3T3 cells. Data are presented as pmol/well. The inset shows the percentage of inhibition induced by EGF over the basal (open squares), cholera toxin-stimulated (open circles) or forskolin-stimulated (closed squares) cAMP levels. (Falasca et al., 1997).

could relate to an action at the level of the regulatory proteins that can modulate the activity of the G-proteins (Corda et al., 2002).

1.4.3.2.2 Modulation of the actin cytoskeleton

As previously mentioned (Section 1.4.3.1), the formation of the glycerophosphoinositols has been correlated to Ras activation. Ras-dependent pathways are important for many proliferative cellular events, such as cell growth, proliferation, motility and invasion. The glycerophosphoinositols have not shown any clear direct effects on cell growth (Falasca et al., 1996) although other cell functions downstream Ras, like cell motility and invasiveness, were analysed. All these events require modification of the structure of the actin cytoskeleton. For this reason, a possible role for the glycerophosphoinositols in the organization of actin cytoskeleton was studied in Swiss 3T3 fibroblasts. Between the glycerophosphoinositols tested, the most powerful was GroPIns4P; its exogenous addition in serum-starved fibroblasts caused the rapid formation of membrane ruffles (detected within 1 min, and maximal at 2 min) followed by the formation of stress fibres (at 10-15 min) (Mancini et al., 2003) (Fig. 1.17). These effects were dose dependent: the 10-20% increase in ruffles after 1 μM GroPIns4P treatment reached an 80% increase when the concentration of GroPIns4P was 50-100 μM. These concentrations were also compatible with the evaluated cellular levels of GroPIns4P, which as mentioned before, is in the low μM concentration range (the basal level is less than 3% of GroPIns, which generally ranges from 44-925 μM), and increased by 1.5- to 6-fold after stimulation (Berrie et al., 2002; Corda et al., 2002). Under identical conditions, GroPIns and GroPIns4,5P_2 had no measurable effects. The possible products of GroPIns4P degradation (inositol 1-phosphate, inositol 4-phosphate and inositol 1,4-bisphosphate) or reacylation (LPI, LPI4P) were also tested but no effects on ruffle or stress fibre formation were seen (Mancini et al., 2003).

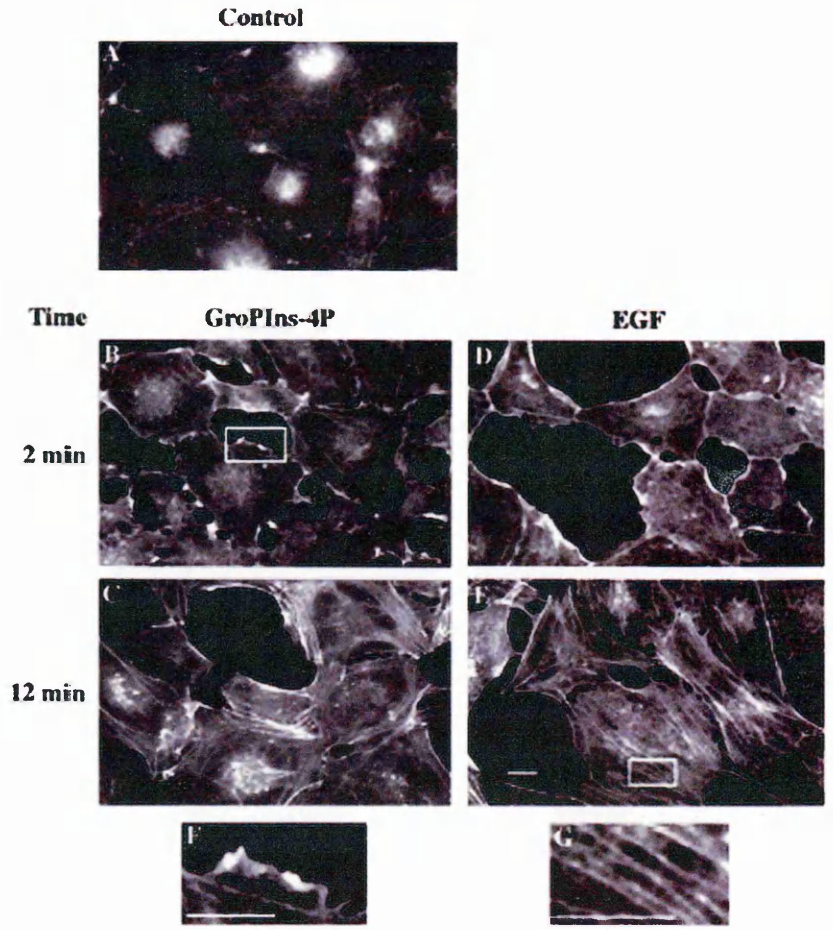

Figure 1.17- GroPIns4P and EGF-induced modifications of the actin cytoskeleton in Swiss 3T3 cells. Serum-starved Swiss 3T3 cells (A) were treated with either 50 μM GroPIns4P (B and C) or 20 ng/ml EGF (D and E) for 2 and 12 min, respectively. Cells were fixed and stained with TRITC-labelled phalloidin. (F and G) Higher magnification of the boxed areas in B and E, respectively. Bar =20 μm (Mancini et al., 2003).

Table 1. Effects of N17Rac, N17Cdc42, and *C. botulinum* C3 transferase microinjection on the GroPIns-4P-induced actin cytoskeleton reorganization

	Ruffles		Stress Fibers	
	Injected	Noninjected	Injected	Noninjected
N17 Cdc42				
GroPIns-4P (2 min)	21.9 ± 4.0	32.7 ± 6.0	29.7 ± 5.2	23.8 ± 10.1
GroPIns-4P (12 min)	0.7 ± 0.5	1.1 ± 0.8	73 ± 2.6	73.1 ± 4.9
N17 Rac				
GroPIns-4P (2 min)	0.7 ± 0.6*	36.7 ± 6.0	24.7 ± 6.5	22.0 ± 6.1
GroPIns-4P (12 min)	0	0.4 ± 0.3	56.9 ± 5.2	66.7 ± 7.7
C. botulinum				
GroPIns-4P (12 min)			10.6 ± 1.5*	40.8 ± 2.5

Serum-starved Swiss 3T3 cells microinjected with N17Rac, N17Cdc42, or *C. botulinum* C3 transferase were treated with GroPIns-4P (50 μM). Cells were fixed and stained with TRITC-labeled phalloidin as described under MATERIALS AND METHODS. Samples of control (noninjected) and injected cells from three to five independent experiments were subjected to double-blind morphological scoring as described under MATERIALS AND METHODS. An example of the actin structures identified as ruffles and stress fibers is shown in Figure 1 (F and G, respectively).

* Statistically significant difference $p < 0.05$ (injected vs. noninjected). A parallel scoring was also performed in control cells, resulting in a level of ruffling and stress fibers of 0.7 ± 0.2 and 4.1 ± 0.4, respectively. The total number of injected cells assessed under each condition ranged from 20 to 50, and equivalent numbers of noninjected cells were selected at random and also scored.

Table 1.5 - Effects of N17Rac, N17Cdc42, and *C. botulinum* C3 transferase microinjection on the GroPIns4P–induced actin cytoskeleton reorganisation (Mancini et al., 2003).

The investigation of the mechanism of action of GroPIns4P on ruffle and stress fibre formation revealed that the small G-proteins of the Rho family are involved (Mancini et al., 2003). As indicated in Section 1.2.3, the role of the small G-proteins of Rho family in the control of distinct actin structures has been extensively documented (Nobes and Hall, 1995). Cdc42 induces filopodia formation, Rac1 modulates the formation of lamellipodia and membrane ruffles and RhoA regulates the formation of stress fibres and focal adhesions (Ridley, 1998). The microinjection of serum-starved Swiss 3T3 cells with myc-tagged N17-Rac1 (a dominant negative mutant) completely abolished the activity of endogenous Rac1 and prevented Rac1-dependent cellular functions (Ridley et al., 1992). Under these conditions, GroPIns4P-dependent ruffle formation was completely inhibited, while stress fibres still formed. The dominant-negative construct for Cdc42 (N17-Cdc42), which completely abolishes the activity of endogenous Cdc42, had no influence on actin cytoskeleton modifications induced by GroPIns4P. To block the activity of endogenous RhoA, cells were microinjected with C. botulinum C3 transferase which ADP ribosylates and inactivates the RhoA proteins (Ridley and Hall, 1992). Under these conditions, stress fibre formation induced by GroPIns4P was completely prevented, but ruffles were still formed (Mancini et al., 2003). Together, these results led to the conclusion that GroPIns4P acts upstream of Rac1 and RhoA and requires active Rac1 (but not Cdc42 and RhoA) to form ruffles and active RhoA (but not Rac1 and Cdc42) to form stress fibres (Table 1.5).

The effects of GroPIns4P were similar in type, extent and time course to those of EGF. In serum-starved Swiss 3T3 cells, this growth factor was able to cause the rapid formation of membrane ruffles followed by stress fibres (within 10 min). Even if the final effects of EGF or GroPIns4P treatment were similar, the enzymes involved were different. EGF initiates a signalling cascade that involves the activation of PI3K and PLA_2, enzymes connected to the activation of Rac1 and RhoA (Nobes et al., 1995). Thus, EGF was completely blocked in the presence of either the PI3K inhibitor wortmannin or methyl arachidonil fluorophosphonate (MAFP), a cell-membrane permeant, irreversible inhibitor

of PLA_2 (Lio et al., 1996). Under the same conditions, GroPIns4P was still active (Mancini et al., 2003). Collectively, these results indicated that GroPIns4P modifies the actin cytoskeleton via a mechanism of action that is different from that of EGF, and suggested that GroPIns4P may act on a molecular target close to the activation of Rac1 and RhoA themselves.

The action of GroPIns4P on Rac1 has also been demonstrated in living cells. In Swiss 3T3 cells, GFP-tagged Rac1 showed a predominant cytosolic localisation upon serum starvation. During the first 2 min of stimulation of living cells with GroPIns4P (50 μM), a clear accumulation of Rac1-GFP became detectable at the plasma membrane, within specific structures exhibiting the morphology and dynamics typical of actin ruffles. When these cells were fixed and stained for actin with phalloidin, it appeared that actin and Rac1-GFP indeed colocalized in ruffles at the plasma membrane (Fig. 1.18). Within 12 min of treatment with GroPIns4P, Rac1-GFP assumed again a diffuse localization, and ruffles disappeared, while stress fibres were formed (Fig 1.18) (Mancini et al., 2003).

The effect of GroPIns4P on Rac1 was also evaluated by assessing the ability of this agent to activate Rac1 in living cells. The fraction of active (GTP-bound) Rac1 present in serum-starved Swiss 3T3 cells exposed to GroPIns4P (50 μM) was 2-fold higher than in untreated cells (near maximal, obtained by *in vitro* addition of 100 μM GTPγS). The activation of Rac1 was rapid and sustained in time (Fig 1.19), and GroPIns4P was already active at a 1 μM concentration, reaching a maximal 2-fold increase at 50 μM (Mancini et al., 2003) (Fig. 1.19). GroPIns and GroPIns4,5P_2 were also tested for their ability to activate Rac1, and surprisingly a certain degree of activation was detectable, but only when the cells were treated with a 100 μM concentration of these agents. The time course of activation also differed from that of GroPIns4P; both GroPIns and GroPIns4,5P_2 caused a rapid and transient activation of Rac1 (Fig 1.19). These data suggest that the duration and the extent of the Rac1 activation induced by these compounds, have important roles in initiating the signal cascade, leading to actin rearrangements and might reflect a different

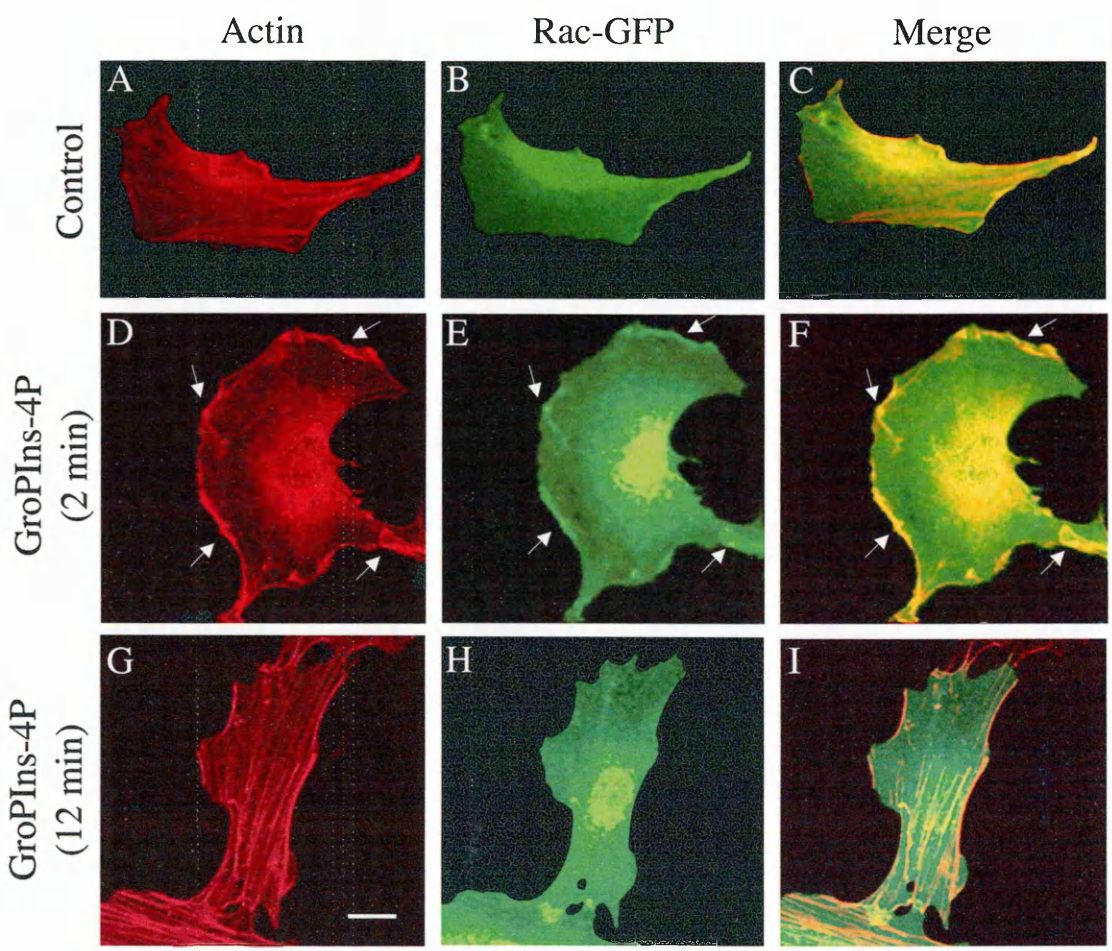

Figure 1.18 - Localisation of Rac1 and actin in GroPIns4P-induced membrane ruffles. Sub-confluent Swiss 3T3 cells were transfected with the pEGFP-Rac1 construct. Twenty-four hours after transfection, cells were treated with GroPIns4P (50 μM) for 2 min (D–F) or 12 min (G–I), fixed, and stained with TRITC-labelled phalloidin. Unstimulated control cells are shown in A–C. Arrowheads show areas of extensive membrane ruffles where Rac colocalised with F-actin (Mancini et al., 2003).

mechanism of activation. In line with this, agents which produce a transient activation of Rac1, such as LPA, do not induce ruffling like GroPIns and GroPIns4,5P_2 (Mancini et al., 2003). Thus, the duration and the extent of Rac1 activation is important for membrane ruffling, and could explain how only GroPIns4P is able to produce this response.

Analysis of the effects of GroPIns4P on the GDP/GTP exchange (GEF activity) and GTPase activity (GAP activity) of Rac1 have shown that GroPIns4P does not affect either the intrinsic GEF activity or the exchange activity enhanced by Rac1 GEF proteins. The intrinsic GAP activity of Rac1 and the GTPase activity enhanced by its GAP protein were also not affected by GroPIns4P (Mancini et al., 2003).

In conclusion, GroPIns4P activates intracellular molecular steps leading to a reorganization of the actin cytoskeleton via the activation of the small GTPase Rac1. This Rac1 activation is mediated by a mechanism that is different from that initiated by growth factors, and it is long-lasting. Because agents that produce a transient activation of Rac1 (such as LPA) do not induce ruffling, the latter feature is relevant for clarifying both the mode of Rac1 activation by GroPIns4P and the manner in which activated Rac1 leads to ruffling.

1.4.3.2.3 Inhibition of tumour cell invasion of the extracellular matrix.

The small G-proteins of the Rho family are involved in a variety of cellular events, such as differentiation, motility and secretion, many of which are important for tumour development and metastatic invasion (see Section 1.2.3). The ability of the glycerophosphoinositols to modulate Rho protein function was exploited in relation to the capacity of tumour cells to migrate toward a chemoattractant and to invade an extracellular matrix (ECM). ECM invasion is a complex process that occurs during morphogenesis, differentiation, cell migration, apoptosis and tumour invasion.

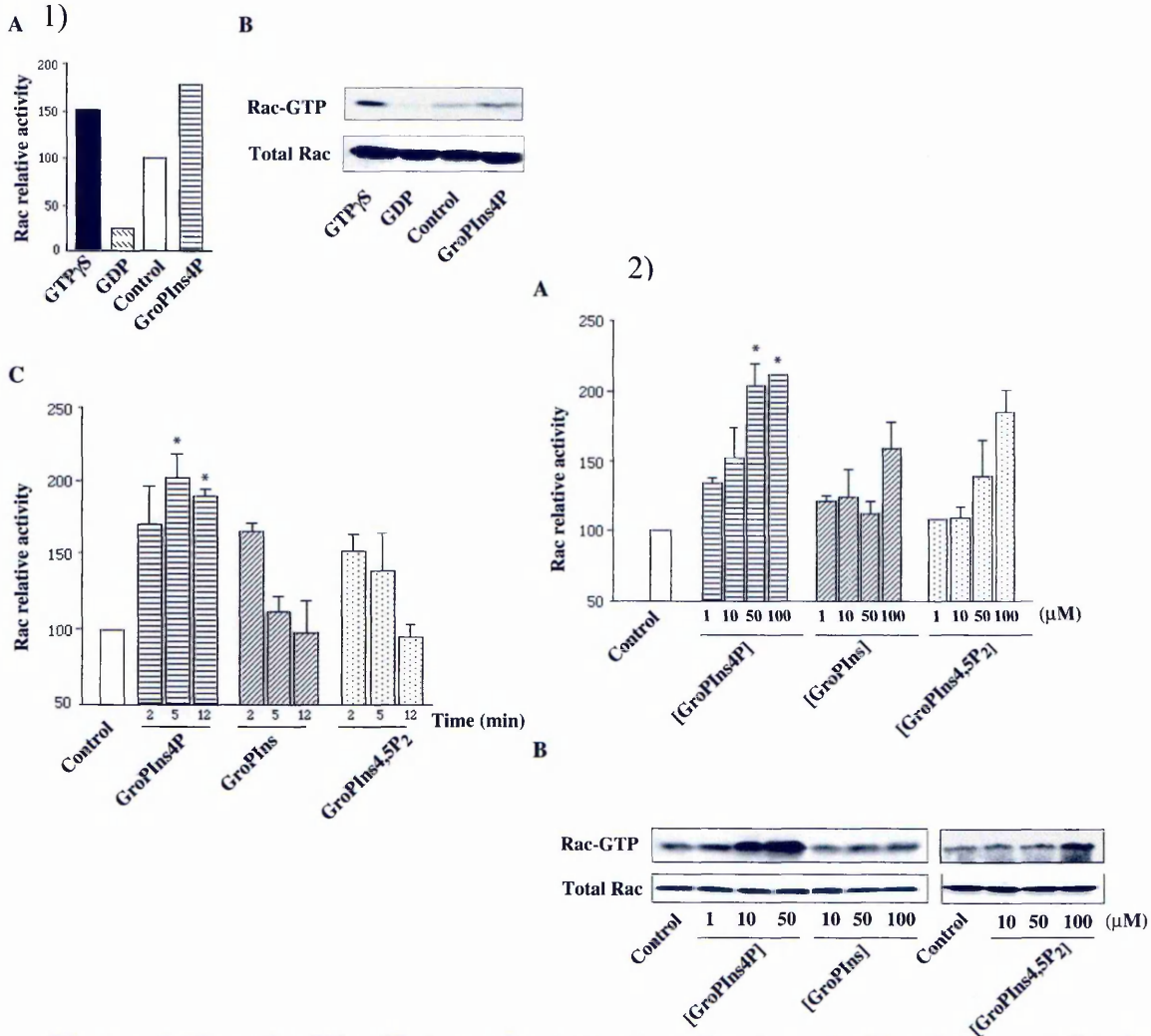

Figure 1.19 - GroPIns4P-dependent Rac1 activation. 1) Regulation of Rac1 activity by GroPIns4P. (A) Serum starved Swiss 3T3 cells were treated with 50 μM GroPIns4P for 2 min. Lysates from unstimulated and stimulated cells were processed and analyzed by Western blotting with an Ab against Rac1. Lysates from control cells were incubated with GTPγS (100 μM) or GDP (1 mM) for positive and negative controls, respectively. Rac1 relative activation was calculated as the amount of PBD (Pak binding domain)-bound Rac1 in stimulated cells, and normalised vs. the amount of Rac1 in unstimulated cells. (B) Western blots from one of the representative experiments showing activation of Rac1. (C) Time course of Rac1 activation by GroPIns, GroPIns4P, and GroPIns4,5P_2. Serum-starved Swiss 3T3 cells were treated with these stimuli (50 μM) for the indicated times. Rac1-relative activation was calculated as the amount of PBD-bound Rac1 in stimulated cells, and normalised vs. the amount of Rac1 in unstimulated cells. **2)** Dose response of GroPIns, GroPIns4P, and GroPIns4,5P_2 on Rac1 activation. (A) Serum-starved Swiss 3T3 cells were treated with the indicated amounts of GroPIns, GroPIns4P, or GroPIns4,5P_2 for 5 min; lysates from unstimulated and stimulated cells were processed and analyzed by Western blotting with an Ab against Rac1. Rac1-relative activation was calculated as the amount of PBD-bound Rac1 in stimulated cells, and normalised vs. the amount of Rac1 in unstimulated cells. (B) Western blots from one of the representative experiments showing the amount of activated Rac1 present in the affinity precipitations and the constant level of endogenously expressed Rac1 in the different cell lysates. (Mancini et al., 2003)

Treatment with GroPIns and GroPIns4P at the maximal active doses known to activate the Rho GTPases (50 μM) inhibited the migration of MDA and A375 cells through the ECM (48% and 50% inhibition, respectively). The ECM invasion implies two distinct events: the migration of cells and the degradation the matrix. The ability of the glycerophosphoinositols to affect one or both of these events was tested, and it was shown that GroPIns and GroPIns4P inhibited the total area of degradation of the matrix, from 10-20% (1 μM) to 60% (100 μM), both in MDA and A375 cells. However, the migration in a modified Boyden chamber (versus a chemoattractant, such as serum-free 3T3-cell-conditioned medium) was not influenced by either GroPIns or GroPIns4P. A possible effect of these compounds on cell adhesion to the substrates can be excluded, since the number of adhering cells (relative to the control) was not affected (Buccione et al., 2005)

GroPIns and GroPIns4P reduce the ability of cells to degrade the ECM. The bis-phosphorylated form of GroPIns, GroPIns4,5P_2, was ineffective in all of the assays (Buccione et al., 2005). The specialised cellular structures in which the ECM degradation occurs are the invadopodia (Chen, 1989). These are enriched in structural and signalling proteins, like the integrins, actin, the actin-binding proteins, the tyrosine kinases and the matrix metallo proteases (MMPs). No relevant changes in the structure and the proteins of invadopodia upon treatment with the glycerophosphoinositols were seen. However, the invadopodial machinery was less efficient in cells treated with GroPIns and GroPIns4P, thus implying that these compound act at a different level, altering the MMP secretion machinery or a component of invadopodia that is as yet unknown (Buccione et al., 2005).

1.4.4 Mechanism of action of the glycerophosphoinositols

The biological activities of the glycerophosphoinositols are related to G-proteins and cause many different cellular events (AC inhibition, Rac1 activation, modification of the actin cytoskeleton). An obvious question concerning the mechanism of action of these compounds derives from these data: whether they act directly on an intracellular target or

as agonists of a specific receptor. So far, studies conducted with GroPIns4P have shown that it does not bind to the plasma membrane specifically and with a high affinity. Instead, GroPIns4P crosses the plasma membrane to reach equilibrium rapidly with the cell cytoplasm (Berrie et al., 1999). The uptake of GroPIns4P was measured in Swiss 3T3 cells; it occurred very rapidly and reached equilibrium within 2-5 min. This rapid entry of GroPIns4P into Swiss 3T3 cells parallels the previously reported time courses of the intracellular effects of extracellularly applied GroPIns4P. The most likely explanation for this rapid cross-membrane equilibration of GroPIns4P is the presence of a GroPIns4P (or glycerophosphoinositol) transporter within the membrane. Indeed, a specific transporter for GroPIns in the yeast *Saccharomyces cerevisiae* has been described (Patton et al., 1995). In yeast the extracellular production of GroPIns is specific and regulated, and it is a major pathway for phosphoinositide metabolism; moreover, glucose stimulation of phosphoinositide metabolism leads to the production not only of GroPIns but also of GroPIns4P and GroPIns4,5P_2 within the yeast cell (Hawkins et al., 1993). This has thus led to the identification of the yeast GIT1 ORF that encodes a predicted Git1p protein of 57.3 kDa, which contains a sugar-transport motif and twelve membrane-spanning domains, and which represents the specific permease involved in the uptake of GroPIns in yeast (Patton-Vogt and Henry, 1998) While the presence and selectivity of an equivalent mammalian glycerophosphoinositol transporter remains to be confirmed, the rapid entry of GroPIns4P into Swiss 3T3 cells strongly suggests that the glycerophosphoinositols are taken up by mammalian cells through a similar mechanism to that used by yeast (Berrie et al., 1999).

1.5 Importance and potential implications of glycerophosphoinositols

The aim of this work is to characterise the mechanism of action of glycerophosphoinositols on actin cytoskeleton organization. The analysis was focused on the

GroPIns4P. The other two compounds (GroPIns and GroPIns4,5P_2) were tested in parallel mostly to verify the specificity of action of GroPIns4P.

The pathway of GroPIns4P-dependent ruffle formation is the best characterized in this work. The ruffle is a morphological feature visible mostly upon growth factor stimulation (see Section 1.2.2). The action of GroPIns4P can mimic the activity of growth factors even if it differs in the extent of the effects and the pathway activated. For example, EGF stimulation leads to ruffle formation in a PI3K dependent way, whereas GroPIns4P does not need this enzyme to do the same thing (Mancini et al., 2003).

The identification of the main targets of GroPIns4P will be important, as it will allow to extend the study also in other cellular systems. A part from the cytoskeleton modification, GroPIns4P is able to inhibit AC and, together with GroPIns, to inhibit PLA_2 and matrix degradation by melanoma cells. We cannot exclude that the mechanism of action is the same in these other events. On the other and it could be also possible that GroPIns4P has multiple targets and, depending on the cell type, it could produce different effects.

The results obtained from this study will allow the definition of the mechanism of action and the role of the glycerophosphoinositols in the regulation of the actin cytoskeleton, which might then lead to the identification of these compounds as potential leads for the development of pharmacologically active compounds. It will also allow us to determine whether they are potential second messengers involved in the transduction of receptor signalling.

CHAPTER 2

MATERIAL AND METHODS

2.1 Materials

Cell culture

NIH 3T3, HEK293T and SYF cells were from the American Tissue Type Collection (ATTC, USA). Human fibroblasts were kindly provided by the Istituto Dermatologico dell'Immacolata (IDI, Italy). Dulbecco's Modified Eagles Medium (DMEM), OptiMEM, calf serum (CS), penicillin, streptomycin, trypsin-EDTA, and L-glutamine were from GIBCO (UK). Foetal calf serum (FCS) was from Biochrom.

The *E. Coli* DH5α strain was from Stratagene. Tryptone and yeast extract were from Promega

Reagents

All the general laboratory salts were obtained at their maximal purities from Sigma-Aldrich (WI, USA). HEPES, paraformaldehyde, bovine serum albumin (BSA), saponin, glucose, leupeptin, aprotinin, phenylmethylsulfonyl fluoride (PMSF), antipain, phenanthroline, pepstatin, triethanolammine, ethylenediaminetetraecetic acid (EDTA), ethylene glycolbis (β-aminoethylether)-N,N,N',N' tetraacetic acid (EGTA), Tris [Hydroxymetyl] aminomethane•HCl (Tris•HCl), DL-dithiothreitol (DTT), tetanolysin, agar, glutathione, IPTG, sodium azide, Trypan Blue, ATP, GTP, GTP-γS, β-NAD^+ p-aminobenzamide-agarose and thrombin were from Sigma-Aldrich (WI, USA). MES (2[N-morpholino]ethansulphonic acid) and polyethylene glycol (PEG) 4000 were from Merk. Dextran T-500 was from Pharmacia. Hanks Balanced Salt Solution (10x) without Ca^{2+} and

Mg^{2+} ($HBSS^{=}$) and with Ca^{2+} and Mg^{2+} (HBSS) were from GIBCO. Perchloric acid, methanol, acetic acid, phosphoric acid and acetone were from Calbiochem (USA). Sterile water was from Diaco (Italy). The catalytic subunit of pertussis toxin (PTX) and the cholera toxin (CTX) were from Calbiochem (USA).

Plastic materials

All the plastic cell culture materials were from Corning (USA). Filters (0.45 and 0.2 μm) were from Amicon (USA). Glass-bottomed wells were from Mattek.

Instrumental equipment

The β-scintillation counter was from Beckman Coulter (LS 6500; USA). The vacuum filtration apparatus was from Millipore (USA). The electrophoresis and blotting apparatus were from Hoefer Scientific instruments, Germany. The Instant Imager was from Canberra Packard (CT, USA) and the gel dryer from Hoefer Scientific Instruments (Germany).

Microscopes: Axiophot microscope with a 100x 1.3 objective (Carl Zeiss, Jena, Germany). LSM 510 confocal microscope equipped with 40x and 63x objectives (Zeiss, Germany). IX70 microscope (Olympus, Hamburg, Germany) equipped with a TILL Photonics imaging system (Gräfelfing, Germany).

Plasmids

The pRK5myc, encoding RhoA, pGEX-4T-Rac1, encoding Rac1-GST and pGEX-4T, encoding GST, were kindly provided by Dr. A. Hall (University College London, London, UK). All of the TIAM1 expressing constructs and the corresponding deletion mutants (see Table 2.1) were kindly provided by Dr. I. Fleming (University of Dundee, Dundee, UK). The pSM-c-Src, encoding for wild-type Src, was kindly provided by Dr. S. Gutkind (NIH, Bethesda, USA). The pEGFPc1-Rac1, encoding for Rac1-GFP, was cloned

in this laboratory (Mancini et al., 2003). The pEGFP, encoding for GFP, was from Molecular Probes.

SDS-PAGE

The acrylamide-bisacrylamide stock solution was from Eurbio. Sodium dodecyl sulphate (SDS), Ponceau Red, Comassie Brilliant Blue, Tween-20, ammonium persulphate (APS), glycine and Trizma base were from Sigma-Aldrich (WI, USA). Pre-stained molecular weight markers were from Amersham Pharmacia Biotech AB (Sweden). Methanol, glycerol, silver nitrate, sodium thiosulfate, formaldehyde, citric acid and acetic acid were from Carlo Erba (Italy). N,N,N',N' tetramethylethylenediamine (TEMED) was from Bio-Rad (Germany). The Nitrocellulose filters were from Schleicher & Schuell (Germany). The 3MM paper was from Whatman (UK). Kodak X-Omat film (Amersham)

Antibodies and probes

The anti-Myc antibody (clone 9E10) was from Roche Diagnostics (Indianapolis, USA). Tetramethyl rhodamine isothiocyanate (TRITC)-labelled phalloidin and fluorescein isothiocyanate (FITC)-labelled phalloidin were from Sigma- Aldrich (St. Louis, USA). Fluo3-AM, and the Alexa 488- and Alexa 546-conjugated goat anti-rabbit and anti-mouse antibodies were from Molecular Probes. The secondary antibodies conjugated to horse radish peroxidase (HRP) and directed against mouse, rabbit and goat IgG were from Calbiochem (USA). The origins of the primary antibodies were specified in Tables 2.2 and 2.5.

Glycerophosphoinositols

GroPIns was from Euticals (Italy), while GroPIns4P and GroPIns4,5P_2 were prepared by Cristiano Iurisci (Department of Cell Biology and Oncology; Consorzio Mario Negri Sud Italy) by deacylation of their corresponding phosphoinositides (PI4P and

$PI4,5P_2$, respectively; from Avanti Polar Lipids, USA); the procedure is based on the original work of (Clarke and Dawson, 1981). For the [^{3}H]GroPIns4P, see radioactive compounds section below.

Stimuli and inhibitors

PDGF was from Upstate (USA), LPA from Avanti Polar Lipids. KN-93, U73122, U73433, PP2, SU6656 and Mowiol were from Calbiochem. Ionomycin, ATP, genistein and BAPTA-AM were from Sigma-Aldrich. PTX was kindly provided by Dr. R. Rappuoli (Chiron Vaccines, Siena, Italy).

Kits

The "CaMKII activity assay" kit and purified CaMKII were from Upstate. The "D-myo-inositol 1,4,5-trisphosphate (IP_3) [^{3}H] Biotrak assay system", the Cyclic AMP [^{3}H] assay system", the ECL reagents, the Glutathione-Sepharose™ 4B beads, the Protein-A Sepharose™ CL-4B beads and Protein-G Sepharose™ S4 fast flow beads were from Amersham Pharmacia Biotech. Lipofectamine/plus reagent was from GIBCO BRL (UK). The QIAGEN Plasmid Maxi Kit was from Qiagen (USA). The Protein Assay Kit was from Bio-Rad Laboratories (UK).

Radioactive compounds and solutions for the analysis

[γ^{32}P]ATP (3000 Ci/mmole; BLU/NEG502A), [γ^{35}S]GTPγS (1250 Ci/mmole, NEG030H), and the Filter Count and Ultima Gold scintillation fluids were from Perkin Elmer (USA). Cellulose nitrate membrane filters (45 μm) were from Whatman (England; UK). [^{32}P]NAD (specific activity 1000 Ci/mmol) was from Amersham Pharmacia Biotech (NJ, USA). [^{3}H]GroPIns4P was obtained by deacylation of [^{3}H]PI4P (ARC, USA; code number ART-185; specific activity 15-30 Ci/mmole), as originally described by Clarke and Dowson (1981) and carried out by Cristiano Iurisci

2.2 Cell culture

2.2.1 Growth media

HEK293T and SYF cells were grown in DMEM supplemented with 2 mM glutamine, 1 U/ml penicillin and streptomycin, and 10% FCS. NIH 3T3 cells, and human fibroblasts were grown in DMEM supplemented with 2 mM glutamine, 1 U/ml penicillin and streptomycin, and 10% CS. Complete media were prepared by adding the serum and antibiotics required to DMEM (1x) and filtering the mixture through a 0.2 μm filter.

2.2.2 Growth conditions

All cell lines were grown under a controlled atmosphere in the presence of 5% CO_2/95% air at 37 °C. Cells were grown in petri dishes until 90% confluence. The medium was removed and 0.25% trypsin solution was added for 2-5 min. The medium was added back to block the protease action, and the cells were collected in a plastic tube and centrifuged for 5 min at 200x *g*. The pellet was resuspended in fresh medium and placed into new petri dishes.

2.3 DNA preparation and cell transfection

2.3.1 Preparation of competent cells

Competent bacteria were obtained using the rubidium chloride method (Kushner, 1978). The DH5α *E. Coli* strain was streaked and incubated overnight on a plate of Luria Broth (LB; 10 g/l of tryptone, 5 g/l yeast extract and 10 g/l NaCl). The next day, one single colony was inoculated into 10 ml LB and grown overnight at 37 °C with shaking at 225 rpm. One ml of the overnight saturated culture was inoculated into 9 ml fresh LB and

grown until the optical density at 550 nm (OD_{550}) was 0.3. The bacteria were subcultured 1:20 into 100 ml pre-warmed LB and grown until an OD_{550} of 0.48. The cells were chilled on ice and centrifuged at 1000x *g* at 4 °C for 5 min. The supernatant was then removed, and the pellet was gently resuspended in 40 ml 30 mM potassium acetate, 100 mM RbCl, 10 mM $CaCl_2$, 50 mM $MnCl_2$, 15% (v/v) glycerol, pH 5.8. The bacteria were left on ice for 2 h, and then centrifuged and resuspended in 4 ml 10 mM MOPS, pH 7.0, 75 mM $CaCl_2$, 10 mM RbCl, and 15% (v/v) glycerol.

2.3.2 Transformation of bacteria by heat shock

Competent cells were thawed on ice and around 10 ng of plasmid added. After mixing, the cells were left on ice for 30 min and then heat shocked for 90 sec at 42 °C. After addition of 800 µl LB, the bacteria were grown at 37 °C for 45 min under constant shaking at 225 rpm. The culture was then plated on LB agar containing the appropriate selective antibiotics and incubated overnight at 37 °C. The next day, an isolated bacterial colony was picked from the plate and used to inoculate 2 ml of LB containing the appropriate antibiotics. Sterile glycerol was added to the bacterial culture (30%, v/v) for long-term storage at -80 °C.

Table 2.1 - List of plasmids

Plasmid	Fusion protein	Resistance	Application
pEGFP-Rac1	Rac1-GFP	Kanamycin	Eukaryote expression
pEGFP-c1	GFP	Kanamycin	Eukaryote expression
pcDNA-C1199-TIAM1	C1199-TIAM1-HA*	Ampicillin	Eukaryote expression
pMT_2-C1199-TIAM1	C1199-TIAM1-GST*	Ampicillin	Eukaryote expression
pEGFP-C1199-TIAM1	C1199-TIAM1-GFP*	Kanamycin	Eukaryote expression

pEGFP-ΔPHn-TIAM1	ΔPHn-TIAM1-GFP	Kanamycin	Eukaryote expression
pEGFP-ΔPHc-TIAM1	ΔPHc-TIAM1-GFP	Kanamycin	Eukaryote expression
pEGFP-ΔPH-TIAM1	ΔPH-TIAM1-GFP	Kanamycin	Eukaryote expression
pGEX-Rac1	Rac1-GST	Ampicillin	Bacteria expression
pGEX	GST	Ampicillin	Bacteria expression
pSM-c-Src	Src	Ampicillin	Eukaryote expression
pRK5 RhoA	RhoA-Myc	Ampicillin	Eukaryote expression

* C1199-TIAM1 is a mutant of TIAM1 that lacks the N-terminal myristoylated region, but that keeps the same behaviour as the wild-type protein (Michiels et al., 1997). It is easily transfectable compared to the full-length protein, and thus it is preferentially used for the studies in which TIAM1 is overexpressed.

2.3.3 DNA preparation

A single colony of transformed DH5α *E. Coli* bacteria was used to inoculate 500 ml LB that included the selective antibiotics. After a 15-20-h incubation, the bacteria were collected by centrifugation at 10600x *g* for 10 min at 4 °C and processed according to the "maxi plasmid purification protocol" of the "Qiagen-plasmid-kit". The DNA obtained was resuspended in TE buffer (10 mM Tris-HCl, 1 mM EDTA, pH 7.5) to a final concentration of 1 mg/ml and stored at 4 °C, or for long-term storage, at -20 °C.

2.3.4 Lipofectamine-based cell transfection

NIH 3T3 and SYF cells were transfected with the Lipofectamine/Plus reagent. The cells were seeded on glass coverslips in 24-well plates in normal culture medium, at a concentration suitable to have 50-70% confluence for transfection. About 24 h after seeding, a transfection mixture was prepared by first diluting the DNA with the PLUS solution and lipofectamine in separate polypropylene tubes, and followed by the mixing of

the two solutions by pipetting. For each well, 0.4 μg DNA and 4 μl PLUS were diluted in 150 μl OptiMEM (Gibco/BRL, NY, USA) and 1 μl lipofectamine was diluted in 150 μl OPTI-MEM. The two solutions were incubated for 15 min at room temperature (RT), and then were mixed together and incubated for a further 15 min at RT. Meanwhile, the cells were washed with OptiMEM medium. Then the final transfection mixture was added to the cells for 3 h. At the end of the incubation, 300 μl culture medium containing 20% CS was added to the cells for an additional 12 h. Finally, the solution was replaced with fresh medium.

2.3.5 Calcium-phosphate-based transfection

HEK293 cells were cultured in DMEM supplemented with 10% FCS and antibiotics (1 U/ml penicillin, 1 μg/ml streptomycin) and split 1:6 every 4-5 days. One day before transfection, the cells were subcultured into 15-cm petri dishes at a density of 5 $x10^4$ cells/cm^2. The cells were transfected using the calcium phosphate method (Graham and van der Eb, 1973; Jordan et al., 1996) where a HEPES-buffered solution was used to form a calcium phosphate precipitate that was layered directly onto the cells. The precipitate containing calcium phosphate and DNA was formed by slowly mixing an equal volume of HEPES-buffered saline (50 mM HEPES, 280 mM NaCl, 1.5 M Na_2HPO_4, pH 7.05) with a solution containing 2.5 M calcium chloride and the 25 μg DNA/15 cm dish. The resulting solution was added directly to the growth medium, and the cells were incubated for 16 h with the calcium phosphate precipitate under standard growth conditions. The precipitate was then washed out and the cells fed with complete medium for a further 48 h.

2.4 Immunofluorescence procedures

2.4.1 Solutions

PBS: 1.5 mM KH_2PO_4, 8 mM Na_2HPO_4, 2.7 mM KCl, 137 mM NaCl, pH 7.4.

Paraformaldehyde: 4% (w/v) paraformaldehyde was dissolved in heated PBS (65 °C) by adding a few drops of concentrated NaOH and the pH brought to 7.4 with 1 M HCl.

Blocking solution: 0.05% saponin, 0.5% BSA, 50 mM NH_4Cl in PBS.

Mowiol: 20 mg Mowiol were dissolved in 80 ml of PBS, stirred overnight and then centrifuged for 30 min at 12000x *g* to eliminate the unsolubilised particles.

Table 2.2 - List of the primary antibodies used for immunofluorescence:

Specificity (antibody name)	Source	Animal source	Dilution use
Anti-HA	Babco	mouse	1/100
Anti-Myc	Roche Diagnostics	mouse	1/100
Anti-TIAM1	Santa Cruz	rabbit	1/20
Anti-p-Src	Upstate	rabbit	1/500
Anti-c-Src	Santa Cruz	mouse	1/250

2.4.2 Cell treatments

Cells were seeded on glass coverslips in 24-well plates in normal culture medium at a concentration suitable for 70% confluence. The day after, the NIH 3T3 cells were serum starved using DMEM supplemented with 2 mM glutamine, 1 U/ml penicillin and streptomycin for 24 h. The SYF cells were serum starved with DMEM supplemented with 2 mM glutamine, 1 U/ml penicillin and streptomycin and 0.1% FCS for 12 h and the human fibroblasts were starved in DMEM supplemented with 2 mM glutamine, 1 U/ml penicillin and streptomycin for 12 h. Then the cells were treated with the different stimuli, in order to follow modifications to the actin cytoskeleton, and a number of inhibitors were applied to the cells to block specific pathways. Table 2.3 summarises the concentrations, times of stimulation, and specificities of all of the agents used.

Table 2.3 - List of the agents used to study actin cytoskeleton modifications

Compound	Application	Concentration and time of incubation	References
GroPIns4P	Ruffle and stress fibre formation, Rac1 activation and translocation to the plasma membrane	50 μM, for 2 to 30 min	Mancini et al., 2003
GroPIns	Rac1 activation	100 μM, for 2 to 30 min	Mancini et al., 2003
GroPIns4,5P$_2$	Rac1 activation	100 μM, for 2 to 30 min	Mancini et al., 2003
PDGF (Platelet derived growth factor)	Ruffle formation, Rac1 activation and translocation to the plasma membrane	10 ng/ml, for 5-10 min	Mellstrom et al., 1988
LPA (lysophosphatidic acid)	RhoA activation and stress fibre formation	10 μM for 5-15 min	Ridley et al., 1992
KN-93	CaMKII inhibitor	20 μM added 24 h before stimulation	Fleming et al., 1998; Sumi et al., 1991
BAPTA-AM	$[Ca^{2+}]_i$ chelator	20 μM added 30 min before stimulation	Fleming et al., 1998
U-73122	PLC inhibitor	5 μM added 10 min before stimulation	Bleasdale et al., 1990
U-73433	Inactive analogue of U-73122	5 μM added 10 min before stimulation	Bleasdale et al., 1990
PP2	Src inhibitor	10 μM added 10 min before stimulation	Bain et al., 2003
SU6656	Src inhibitor	10 μM added 10 min before stimulation	Bain et al., 2003
Genistein	RTK inhibitor	10 μM added 30 min before stimulation	Akiyama et al., 1987
PTX	To block $G\alpha_i$	5 nM added 24 h before stimulation	Pittman, 1984

2.4.3 Immunofluorescence analysis for ruffle and stress fibre formation

After the various treatments, the cells (NIH 3T3 or SYF) were fixed with 4% (w/v) paraformaldehyde for 15 min, permeabilised in blocking solution for 20 min, and then incubated with 0.1 μg/ml TRITC- or FITC-labelled phalloidin or for 45 min for

filamentous actin visualization (according to Mancini et al., 2003). All of these steps were carried out at RT, and coverslips were rinsed in PBS after each step. The coverslips were mounted by inverting them onto 15 µl of Mowiol. After 2 h at RT, the cells were examined with an Axiophot microscope using a 100x 1.3 objective (Carl Zeiss, Jena, Germany).

For the morphological scoring of cells, the samples from each independent experiment (performed in duplicate) were subjected to blind scoring for ruffle and stress fibre formation. As used by Mancini et al. (2003), the assessment was on the basis of a null score (zero) for the absence of the feature, followed by a score of one or two according to the level of response of each individual cell (one, partial response; two, full response). The cell phenotypes were quantified by counting 200 cells in each sample (potential maximum score =400). The data were then expressed as percentage scores (±SD) that represent the scores for each morphological feature expressed as percentages of the potential maximum scores. Scoring of the control cells was performed in the same way, evaluating the presence of the features of interest in untreated cells. Across the repeated independent experiments, data are given in the Figures, legends and text as percentages of each response with respect to the individual controls for a given pattern of response.

2.4.4 Immunofluorescence analysis for protein localization

NIH 3T3 and SYF cells were transiently transfected by Lipofectamine/Plus with GFP-, Myc- or HA-tagged constructs (see Table 2.1); while human fibroblasts were not transfected, they were used to follow endogenous Src. After cell starvation (see Section 2.3.3), the time courses of effects of different stimuli in the absence and presence of different agents (see Table 2.3) were followed. The cells then were fixed in 4% paraformaldehyde (w/v) for 15 min, permeabilised in blocking solution, and for filamentous actin visualisation, incubated with 0.1 mg/ml TRITC- or FITC-labelled phalloidin for 45 min (according to Mancini et al., 2003), for the cells overexpressing

GFP-tagged constructs. When the cells were transfected with constructs that can be visualised with an antibody (or non-transfected in the case of human fibroblasts), after permeabilisation, they were incubated with the specified antibodies diluted in blocking solution (see Table 2.2 for the list and dilutions of antibodies used in this study) for 2-3 h at RT. After incubation with the primary antibody, cells were washed three times in PBS and incubated with a fluorescent-probe (Alexa 488 or Alexa 546)- conjugated secondary antibody directed against the constant region of the primary IgG molecule, for 1 h at RT. Secondary antibodies were diluted 1:400 in blocking solution. Finally, the actin was stained with TRITC- or FITC-phalloidin as detailed above. Coverslips were mounted in Mowiol on microscope slides. To check the specificity of the GFP-tagged constructs, the same experiments were performed also with cells overexpressing GFP. This always showed a nuclear and cytoplasmic localisation for GFP that did not change upon treatment.

The samples were then analysed and quantified blind on a laser scanning microscope: the samples were observed by an LSM 510 confocal microscope equipped with a 63 x objective (Zeiss, Germany). Optical confocal sections were taken at 1 Airy unit with a resolution of 512x512 pixels and exported as JPEG files. The quantitative evaluation of the immuno-staining patterns was performed on at least 50 cells per sample in at least three independent experiments, each performed in duplicate. The results are given in the Figures, legends and text, as percentages of cells displaying a given pattern.

2.5 Measure of $[Ca^{2+}]_i$

2.5.1 Procedure

NIH 3T3 cells were plated into glass-bottomed wells (Mattek) at $4x10^5$ cells/well in normal culture medium at concentrations suitable for 50-70% confluence. The day after, the cells were incubated with 4 μM Fluo3-AM (a dye that fluoresces upon binding to Ca^{2+};

excitation wavelength, 488 nm) in a HEPES-buffered saline solution containing 10 mM HEPES, pH 7.0, 137 mM NaCl, 5 mM KCl, 4 mM $MgCl_2$, 3 mM $CaCl_2 \cdot 2H_2O$ and 25 mM glucose, for 30 min at 37 °C (Klepeis et al., 2001). After two washes in the HEPES-buffered saline solution, the cells were placed in an open well with 1 ml HEPES solution, and positioned on the stage of a IX70 microscope (Olympus, Hamburg, Germany) equipped with a TILL Photonics imaging system (Gräfelfing, Germany). For each experiment, the cells were scanned for at least 30 sec to establish a base-line fluorescence reading before the addition of the different stimuli (see Table 2.4). The live imaging was carried out by taking two sequential movies: the first one taken each 200 msec for 2 min (to monitor any rapid Ca^{2+} variations) and the second then taken each sec for 6 min, to monitor what happened up to 8 min from the treatment. In each time-lapse movie, the increase in fluorescence obtained upon stimulation was seen as a gradual change in colour (from blue to red, as minimal and maximal fluorescence levels, respectively). In each experiment, the NIH 3T3 cells were added with the HEPES-buffered saline solution and monitored to check that no spontaneous $[Ca^{2+}]_i$ rise occurred. Then GroPIns4P and the other stimuli were added as necessary (see Table 2.4). Between each stimulation, the cells were washed with the saline solution to allow the $[Ca^{2+}]_i$ to return to physiological concentrations. For each sample, from 5 to 12 cells were monitored for at least 8 min. A series of agents were applied before the stimulation (the same as used also to modulate ruffle formation; see Table 2.3).

To prevent the influx of extracellular Ca^{2+}, cells were incubated in a Ca^{2+}-free HEPES-buffered saline solution (10 mM HEPES, pH 7.0, 137 mM NaCl, 5 mM KCl, 4 mM $MgCl_2$, 1 mM EGTA, 25 mM glucose) for 30 min prior to the stimuli adition.

Table 2.4 - List of the stimuli used for $[Ca^{2+}]_i$ measurements

Compound	Application	Concentration	References
GroPIns4P	Ruffle and stress fibre formation, Rac1 activation and translocation to the plasma membrane	50 μM	Mancini et al., 2003
GroPIns	Rac1 activation	100 μM	Mancini et al., 2003
PDGF (Platelet derived growth factor)	Activation of PLCγ through TRK signalling	10 ng/ml	Secrist et al., 1990
ATP	Activation of PLCβ through GPCR signalling	100 μM	Giovannardi et al., 1992
Ionomycin	Create pores at the level of the plasma membrane	10 μM	Beeler et al., 1979

2.5.2 Image analysis

Each cell was selected at random and the fluorescence of each frame was calculated by the TILL Photonics imaging system. The background signal was determined from the average of three different areas adjacent to the cell. The fluorescence values were transferred to Microsoft Excel to perform the calculations, and after the background subtraction, they were plotted as increases in fluorescence per second.

The estimation of fluorescence intensity of Fluo3-AM is shown as the pseudoratio (ΔF/F) indicated by the following formula: ΔF/F0=[(F-F0)/(F0-B)] where F is the maximal level of fluorescence obtained upon stimulation, F0 is the fluorescence under basal conditions and B is the background fluorescence (Klepeis et al., 2001; Takahashi et al., 1999). Apart from dye saturation, ΔF/F0 is thought to approximately reflect the $[Ca^{2+}]_i$ if there is no change in dye concentration, intracellular environment or path length (Svoboda et al., 1997). The lag phase (time between the stimulation and the increase in $[Ca^{2+}]_i$), the time of stimulation (duration of the effects of the stimulus) and the percentage of

responsive cells were also measured. The results are given in Table 3.1, 3.2 and 5.1 and they represent the means of all of the experiments performed.

2.6 Enzymatic activity assays

2.6.1 CaMKII activity assay

The activity of CaMKII was measured by the "CaMKII activity assay" kit (Upstate). NIH 3T3 cells were plated at 3.5 x10^5 cells/well in 6-well plates, and the day after they were starved in DMEM, 0.1% BSA. After 20 h of starvation, the cells were stimulated with 50 μM GroPIns4P and 10 ng/ml PDGF. The treatment with BAPTA was performed as indicated in Table 2.3. After stimulation, the cells were harvested, lysed with 30 passes through a 27-gauge needle, and centrifuged at 2000x *g* for 3 min at 4 °C. The CaMKII assay was performed using from 2 to 5 μg of lysate proteins, per sample. The CaMKII activity was measured by monitoring the phosphorylation of a synthetic CaMKII substrate (autocamtide-2) in the presence (calcium-dependent activity) or absence (calcium-independent activity) of calcium and calmodulin, as provide by the CaMKII activity assay kit. The assays were conducted in a total volume of 50 μl, containing final concentrations of 20 mM MOPS, pH 7.5, 25 mM β-glycerophosphate, 1 mM Na-orthovanadate, 1 mM DTT (ADB buffer), 0.5 μM PKA and PKC inhibitor peptides, 1 μCi [γ^{32}P]ATP and 20 μM total ATP, 75 mM Mg^{2+} and 500 μM autocamtide-2 substrate. When the assay was performed in the absence of Ca^{2+}, 5 mM EGTA was added to the ADB buffer (ADBI buffer) and when the assay was performed in the presence of Ca^{2+}, 2 mM $CaCl_2$ was added to the ADB buffer (ADBII buffer). After 10 min at 30 °C, 25 μl of each samples were spotted onto P81 phosphocellulose paper squares, which were then air-dried for 1 min. The squares were washed 3 times in 40 ml 0.75% phosphoric acid for 5 min each, and once in 20 ml acetone for 5 min. The radioactivity associated with the dried

paper squares was quantified by scintillation counter by using Ultima Gold scintillation fluid (PerkinElmer). The results given in the Figures are presented as percentages of maximal CaMKII activation, obtained by performing the assay in the presence of the ADBII buffer.

The same assay was performed starting from cell lysates and purified CaMKII, instead of intact cells. Here the cells were seeded into 6-well plates. The day after, the cells were harvested and lysed (30 passes through a 27-gauge needle) in ADBI buffer with added protease inhibitors (0.5 μg/ml leupeptin, 2 μg/ml aprotinin, 0.5 mM phenanthroline, 2 μM pepstatin and 1 mM PMSF). The assay with the purified enzyme was performed with 0.25 μg of purified CaMKII incubated with 50 μM GroPIns4P. Then the assays to determine the activity of CaMKII were performed following the same procedure described above.

2.6.2 TIAM1 phosphorylation by CaMKII

These assays were conducted using the same conditions used for the CaMKII activity assay (Section 2.6.1). The reaction was carried out in a total volume of 50 μl, containing final concentrations of 20 mM MOPS, pH 7.5, 25 mM β-glycerol phosphate, 1 mM Na-ortovanadate, 1 mM DTT, 0.5 μM PKA and PKC inhibitor peptides, 1 μCi [γ^{32}P] ATP and 20 μM total ATP, 75 mM Mg^{2+}, 1 mM $CaCl_2$. Ten μl of the immunoprecipitated TIAM1-HA (see Section 2.8.3) were incubated in the buffer for 45 min at 30 °C. To stop the reaction, 40 μl of 4 x Laemmli sample buffer were added to each sample. After 5 min of boiling, the samples were loaded onto a 10% polyacrilamide gel (see Section 2.7). The Western blotting was quantitatively analysed for the level of TIAM1 phosphorylation using an Instant Imager (Packard Instruments Co.). The same assay was performed using

purified TIAM1-GST (2 μg) (see Section 2.9.2) and purified CaMKII (0.25 μg) (Upstate), instead of the immunoprecipitate.

2.6.3 IP_3 measurements

NIH 3T3 cells were plated at 3.5 $x10^5$ cell/well in 6-well plates, and the day after they were starved in DMEM, 0.1% BSA. After 20 h of starvation, the cells were stimulated for 2 to 15 min with 50 μM GroPIns4P at 37 °C, or with other stimuli, including thrombin (5 IU/ml), PDGF (10 ng/ml) and ATP (100 μM). The treatments were performed in DMEM, with 20 μM LiCl. For the experiments performed with cell lysates, the NIH 3T3 cells were harvested and lysed by 30 passes through a 27-gauge needle, in a buffer containing 20 mM HEPES, pH 7.4, 3 mM EGTA, 0.2 mM EDTA, 0.83 mM $MgCl_2$, 1.5 mM $CaCl_2$, 20 mM NaCl, 30 mM KCl, 1 mM DTT, 20 mM LiCl and protease inhibitors (0.5 μg/ml leupeptin, 2 μg/ml aprotinin, 0.5 mM phenanthroline, 2 μM pepstatin and 1 mM PMSF). Then the cells were treated as described above. The reaction was stopped by adding 20% perchloric acid for the IP_3 extraction and the samples were left 20 min on ice, before being centrifuged for 20 min at 2000x *g* at 4 °C. The pH was adjusted to 7.0 with KOH in the presence of phenol red as a pH indicator. After a second centrifugation step, the intracellular concentrations of IP_3 were measured using the "D-myo-inositol 1,4,5-trisphosphate (IP_3) [^{3}H] Biotrak assay system" from Amersham.

When the experiments were performed with cell lysates, anti-PLCβ and anti-PLCγ antibodies (20 μg/ml; as described in Ferry et al., 2001) were added prior to performing the stimulation, to selectively block the PLCβ or PLCγ. Then the assays were performed as described above.

The quantification of IP_3 provided by the kit is based on competition between [^{3}H] IP_3 (the tracer) and unlabelled IP_3 (produced by the samples) for the interaction with a

binding protein, prepared from bovine adrenal cortex. For each experiment, a standard curve with known IP_3 concentrations was performed, and the quantity of IP_3 present in the samples was extrapolated from the curve (as described in the kit). Once the pmols of IP_3 per sample had been calculated, the results were plotted as percentage increases versus the control (untreated sample).

2.6.4 Adenylyl cyclase assays

NIH 3T3 cells were grown to confluence in 12-well plates in complete growth medium. The cells were washed twice with HBSS and then stimulated with CTX (10 nM) for 30 min at 37 °C in HBSS containing 0.4% BSA, 10 mM HEPES and 0.5 mM 3-isobutyl-1-methylxanthine (pH 7.4), in the absence or presence of GroPIns4P (50 μM) or LPA (10 μM). The treatment with PTX (5 nM) was done 24 h prior to the stimulation of the cells. The intracellular cAMP content of the NIH 3T3 cells was extracted with ethanol and measured using a commercial radioimmunoassay ("Cyclic AMP [^{3}H] assay system"; Amersham) and the experiments were performed in triplicate. For each experiment, a standard curve with known cAMP concentrations was performed, and the quantity of cAMP present in the samples extrapolated from the curve (as described in the kit). The results are expressed as pmols cAMP/well.

2.6.5 Src activity assay

Human fibroblasts or NIH 3T3 cells were plated into 6-well dishes ($1.5x10^5$ cells/well). The day after, the cells were serum starved (see Section 2.4.2) for 20 h and then subjected to stimulation with GroPIns4P and PDGF (see Table 2.2). After this treatment, the cells where lysed in 150 μl buffer containing 60 mM Tris-HCl, pH 7.4, 30 mM β-glycerophosphate, 50 mM β-mercaptoethanol, 1 mM Na_3VO_4, 2% SDS, 10% glycerol and

protease inhibitors (0.5 μg/ml leupeptin, 2 μg/ml aprotinin, 0.5 mM phenanthroline, 2 μM pepstatin and 1 mM PMSF). Finally, after the addition of 50 μl of Laemmli sample buffer (4x), the samples were sonicated for 10 sec and processed for SDS-PAGE and Western blotting (see Section 2.7) with anti-p-Src, anti-c-Src or anti-Yes antibodies (see Table 2.5 for dilutions).

2.7 SDS-PAGE preparation and analysis

2.7.1 SDS-PAGE

Solutions

1) Acrylamide-bisacrylamide mixture: 40% (w/v) acrylamide-bisacrylamide (37.5:1)
2) Running buffer: 200 mM glycine, 20 mM Trizma base, 4 mM SDS pH 8.3;
3) Laemmli sample buffer (1x): 125 mM Trizma base, 4% SDS, 20% glycerol, 10% β-mercaptoethanol, pH 6.8.

Assembly of polyacrylamide gels

Two 16 cm x 15 cm glass plates were assembled to form a chamber using two 1.5 mm plastic spacers lined up with the lateral edges of the glass plates. This chamber was fixed using two clamps and then mounted on a plastic base that sealed the bottom.

The 'running' polyacrylamide gel was prepared by mixing H_2O, 40% (w/v) acrylamide-bisacrylamide solution, 1.5 M Tris-HCl, pH 8.8, 10% (w/v) SDS, in order to have the selected concentrations of acrylamide and 375 mM Tris-HCl, 0.1% (w/v) SDS. Then, 0.06% (w/v) APS and 0.06% (v/v) TEMED were added; the solution was pipetted and poured in the gap between the plates, leaving ~5 cm for the stacking gel. Soon after pouring, the gel was covered with a layer of 375 mM Tris-HCl, pH 8.8, and left at RT for

~1 h. The Tris-HCl layer was removed after gel polymerisation. The 'stacking' polyacrylamide gel was prepared by mixing H_2O, 40% (w/v) acrylamide-bisacrylamide solution, 0.5 M Tris-HCl, pH 6.8, 10% (w/v) SDS, in order to have 4% (w/v) acrylamide, 125 mM Tris-HCl, 0.1% (w/v) SDS. Then, 0.1% (w/v) APS and 0.07% (v/v) TEMED were added, and the solution was pipetted and poured onto the 'running' gel. Immediately, a 15-well comb was inserted between the glass plates and this was left to polymerise for 1 h at RT.

Sample preparation

Samples were prepared by adding an equal volume of 4x Laemmli sample buffer and boiling for 5 min; they were then loaded into the wells. The lateral wells were loaded with 10 µl pre-stained molecular weight standards (Amersham). The chamber was then assembled into the electrophoresis apparatus (Hoofer Scientific Instruments, Germany), and the electrophoresis was carried at a constant current of 8 mA (for overnight runs) or 30-40 mA (for 4-h runs).

2.7.2. Silver Staining

Polyacrylamide gels were soaked in fixing solution (methanol: acetic acid: H_2O 50:5:45) for 20-30 min with stirring, washed twice with H_2O (2 min per wash), and then left in H_2O for 1 h on a shaking platform. The gels were then incubated for 1-2 min in sensitizing solution (0.02 % sodium thiosulfate) and rinse with two washes of H_2O (30 sec each). Finally, the gels were incubated with the staining solution (0.1% silver nitrate) for 30 min and developed with the developing solution (0.04% formaldehyde in 2% sodium carbonate). The development was quenched by adding 1% acetic acid, and the gels were dried in a gel dryer.

2.7.3 Coomassie Brilliant Blue staining

Gels were incubated in staining solution (50% methanol, 40% H_2O, 10% acetic acid and 500 mg Coomassie Brilliant Blue/1 l) for 2 h, washed and then destained with 30% methanol, 10% acetic acid in H_2O. The gels were dried in a gel dryer.

2.7.4 Western blotting

Solution:

1) "Transfer buffer": 20 mM Trizma base, pH 8.3, 200 mM glycine;
2) Blocking buffer: 50 mM Tris-HCl, pH 7.5, 3% BSA (or alternatively 5% dry skim milk), 0.05% Tween-20, 150 mM NaCl;
3) TTBS: 50 mM Tris-HCl, pH 7.5, 0.05% Tween 20, 150 mM NaCl;
4) TBS: 50 mM Tris-HCl, pH 7.5,150 mM NaCl.

Nitrocellulose blotting

The polyacrilamide gels were soaked for 15 min in transfer buffer, together with two pieces of 3MM paper (Whatmann, UK) and one of nitrocellulose (Schleicher&Schuell). The gel was assembled into a sandwich as follows: first a sheet of filter paper was covered with the nitrocellulose, the gel was then placed onto the nitrocellulose, and finally, a second sheet of filter paper was placed on the gel. This sandwich was then assembled into the blotting apparatus (Hoefer Scientific Instruments, Germany) and the transfer was carried out at 500 mA. At the end of the run (typically 4-5 h), the sandwich was disassembled and the nitrocellulose was soaked in 0.2% Ponceau Red, 5% acetic acid for 5 min, to visualise the protein. The filters were then rinsed with 5% acetic acid to remove excess unbound dye.

Immunodetection of antigens

The nitrocellulose filters were cut into strips with a razor blade. The strips were incubated in blocking buffer for 30 min at RT, then with antibodies directed against the proteins of interest, which were diluted at the appropriate concentrations in the blocking solution. A list of antibodies used in this study and their working dilutions is provided in Table 2.5. Incubations with the primary antibodies were carried out for 2 h at RT, or overnight at 4 °C. At the end of this incubation, the antibodies were removed and the strips washed with TTBS for 3 x 3 min. The strips were incubated for 1 h with the appropriate HRP-conjugated secondary antibodies (1:5000 in TTBS, 3% BSA) and washed 2 x 3 min with TTBS and 2 x 3 min with TBS. At the end of the washing, the strips were incubated with the ECL developing solution according to the manufacturer instructions, for ECL-based detection visualised by autoradiography.

Table 2.5 - List of the antibodies used for Western blotting

Specificity (antibody name)	Source	Animal source	Dilution
Anti-HA	Babco	mouse	1/1000
Anti-GFP	Our Department	rabbit	1/20000
Anti-TIAM1	Santa Cruz	rabbit	1/500
Anti-p-Src	Upstate	rabbit	1/1000
Anti-c-Src	Santa Cruz	mouse	1/1000
Anti-Yes	Santa Cruz	mouse	1/1000
Anti-GST	Our Department	rabbit	1/10000

2.8 Cytosol overexpressing TIAM1

2.8.1 Cytosol preparation

The cell cytosol was prepared according to (Self and Hall, 1995) from HEK293T cells transfected with constructs overexpressing C1199-TIAM1 (henceforth referred as TIAM1 for brevity) or its deleted mutants, either HA or GFP tagged (see Table 2.1), by the

calcium phosphate method (Section 2.2.6). The cells were plated in seven 15 cm petri dishes, transfected the day after, and then after 48 h of transfection the cells were lysed by vortexing in a buffer containing 25 mM Tris-HCl, pH 7.6, 100 mM NaCl, 10 mM $MgCl_2$, 1% glycerol and 1% NP-40, and then centrifuged 30 min at 90,000x *g*. The supernatant was recovered, its protein concentration evaluated by a protein assay kit (Bio-Rad, see Section 3,7.2), and then it was aliquoted and frozen at -80°.

2.8.2 Evaluation of protein concentrations

Protein concentrations were evaluated using a commercially available protein assay kit (Bio-Rad Laboratories, UK), according to the manufacturer instructions.

2.8.3 Immunoprecipitation of TIAM1

The TIAM1-Ha-overexpressing cytosol (220 μg) was diluted in a buffer containing 25 mM Tris-HCl, pH 7.6, 100 mM NaCl, 10 mM $MgCl_2$, in a final volume of 200 μl. The lysate was then incubated with 1.5 μg of an antibody against the HA tag (Babco), overnight at 4 °C in a rotating wheel. The day after, 12 μl of 75% protein G (high affinity for antibodies raised in mouse) was added to the samples for 2 h in a rotating wheel. The immunoprecipitation of the GFP-tagged mutants was performed as for the HA-tagged construct, although the cytosol (220 μg) was pre-cleared with a 1 h-incubation with 50% protein A at 4 °C in a rotating wheel. Then the antibody against GFP (2 μg) was incubated overnight, and the day after, it was precipitated with 12 μl of 50% protein A (high affinity for antibodies raised in rabbit). After the incubations, the samples were centrifuged at 800x *g* for 10 min at 4 °C and washed 4 times in the dilution buffer. Finally an SDS-PAGE was

run and the amount of immunoprecipitated protein, was determined by Western blotting (Section 2.7) and quantified by NIH imaging program.

2.9 Fusion protein preparation

2.9.1 Purification of glutathione S-transferase (GST) fusion proteins

All the GST-fusion constructs (cloned in p-GEX vectors) were purified using the Glutathione-Sepharose™ 4B beads (Amersham Pharmacia Biotech AB, Sweden) according to the instructions of the manufacturer. The DH5α *E. Coli* strain harbouring the GST-fusion protein of interest was grown in LB (500 ml) plus ampicillin (60 mg/ml) until the OD_{600} was about 0.7-0.9. At this point, the fusion protein was induced for 2 h at 37 °C with 1 mM IPTG. The cells were harvested by centrifugation at 400x *g* for 10 min at 4 °C, and then resuspended in 20 ml 20 mM Tris-HCl, pH 7.6, 100 mM NaCl, 5 mM $MgCl_2$, 0.5% NP-40, 10 μM GDP, 1 mM DTT in the presence of a cocktail of protease inhibitors (0.5 μg/ml leupeptin, 2 μg/ml aprotinin, 0.5 mM phenanthroline, 2 μM pepstatin and 1 mM PMSF) (according to Mancini et al., 2003). The suspension was stirred for 30 min, and then sonicated three times for 1 min, on ice. The lysed cells were centrifuged at 12,000x *g* for 10 min at 4 °C. Meanwhile, 1.2 ml of a Glutathione-Sepharose resin was diluted up to 10 ml in ice-cold lysis buffer without DTT and protease inhibitors, to remove the preservative, and centrifuged at 2000x *g* for 5 min at 4 °C. The supernatant was discarded, and the resin was resuspended in the buffer. This procedure was repeated twice. The supernatants from the bacterial lysates were added to the Glutathione-Sepharose resin and incubated for 30 min at 4 °C on a rotating wheel. The beads were washed with 3 x 20 ml of the buffer used also for the resin, and poured into a column. Protein elution was started by the addition of 500 μl 50 mM Tris-HCl, pH 8.0, 150 mM NaCl, 5 mM $MgCl_2$, 1 mM DTT, 10 μM GDP and 5 mM glutathione (elution buffer). Five hundred μl was collected

(fraction 1) and this procedure was repeated four times. The fractions containing the protein were quantified using the BioRad Protein Assay Kit (BioRad), and 2 µl of each fraction were analysed by SDS-PAGE and stained with Coomassie Brilliant Blue or silver stained. The fractions were then dialysed overnight against a buffer containing 10 mM Tris-HCl, pH 7.6, 20 mM $MgCl_2$, 0.1 mM DTT.

2.9.2 Purification of TIAM1-GST from HEK293T cells

TIAM1 was purified from HEK293T cells that had been transiently transfected with pMT_2-C1199-TIAM1 plasmid encoding for TIAM1-GST (according to Fleming et al., 1997, with some modifications). The cells were plated in ten 15 cm petri dishes and transfected by the calcium phosphate method with TIAM-GST (as described in Section 2.3.5). After 72 h of transfection, the cells were collected and then resuspended in the lysis buffer (5 mM DTT, 1% Triton X-100, 10 mg/ml leupeptin, 10 mg/ml antipain, 1 mM PMSF in 1x PBS). The cells were then lysed with 20 passes through a 27-gauge needle, and centrifuged for 5 min at 10,000x *g* at 4 °C. The supernatant was diluted 1/10 with PBS, 5 mM DTT, and incubated overnight with the glutathione resin (50%). The day after, the resin was recovered by centrifugation for 5 min at 1,000x *g* at 4 °C, and then washed 3 times with PBS, 5 mM DTT. The elution was carried out in 50 mM Tris-HCl buffer, pH 7.4, containing 10 µM reduced glutathione. Two sequential elutions of 1 ml each were performed, and these eluates were dialysed overnight against 1 l PBS. Ten µl of each fraction was then analysed by SDS-PAGE and stained with Coomassie Brilliant Blue or silver stained.

When TIAM1-GST was used in the pull-down assay, the GST was removed by thrombin. This cleavage was done instead of elution from the glutathione beads, in a buffer containing 50 mM Tris-HCl, pH 8.0, 150 mM NaCl, 2.5 mM $CaCl_2$ and 10 IU thrombin. The beads were incubated for 2 h at RT on a rotating wheel, and then centrifuged at 1000x

g for 10 min at 4 °C. The supernatant containing the cleaved TIAM1 was then incubated for 30 min at RT with 20 µl of a resin that binds thrombin (p-aminobenzamide-agarose), to eliminate this enzyme, and then centrifuged at 1000x *g* for 10 min at 4 °C. The supernatant obtained in this way was dialysed overnight against 1 l PBS (see Section 2.4.1) at 4 °C.

2.10 Membrane preparation

2.10.1 Solutions

Potassium phosphate buffer (PFB; 200 mM, pH 7.4): 1.36 g K_2HPO_4 and 1.14 g K_2PO_4 dissolved to 50 ml in H_20.

Protease inhibitors: 2.0 µg/ml aprotinin, 0.5 µg/ml leupeptin, 2 µM pepstatin, 0.5 mM phenanthroline, 1 mM PMSF.

Hypotonic buffer: 10 mM TES, pH 7.0, 1 mM EDTA.

Sucrose buffer: 10 mM TES, pH 7.5, 250 mM sucrose.

PTX treatment was performed on intact cells as described in Table 2.2, 24 h prior to the preparation of the membranes.

2.10.2 Plasma membranes

Plasma membranes were prepared following the procedure described by (Gettys et al., 1994), with some modifications. NIH 3T3 cells at 80-90% confluence (6 x 10^8 cells for each preparation) were washed with $HBSS^=$, and then lysed with a Teflon glass Potter homogeniser in hypotonic buffer. The unbroken cells and nuclei were removed by low speed centrifugation at 400x *g* for 5 min at 4 °C, and the crude membranes were collected from the supernatant with a centrifugation for 20 min at 48,000x *g* at 4 °C. The pelletted membranes were re-suspended in the sucrose buffer, at a final concentration of *ca.* 100-150

mg/ml. Two hundred mg membranes were mixed to a 14 g pre-weighted aqueous two-phase system composed of 5.12 g 20% dextran T-500, 2.56 g 40% polyethylene glycol 4000, 0.4 ml 200 mM PFB, pH 7.2, 1.6 ml 1 M sucrose and distilled water. Separation was achieved by centrifugation at 2500x *g* for 20 min at 4 °C. The upper phase was removed and repartitioned against a fresh lower phase, while to increase the yield of the plasma membranes, the lower phase was extracted with a fresh upper phase. Finally, the two upper phases containing the plasma membranes were combined, diluted 5-fold in sucrose buffer, and collected by centrifugation at 20,000x *g* for 30 min at 4 °C. The purified plasma membranes were re-suspended at 1 mg/ml in 25 mM HEPES, pH 7.4, 150 mM NaCl, 1 mM EDTA, and protease inhibitors, and stored at -80 °C.

2.10.3 Total membranes

NIH 3T3 cells at 80-90% confluence (6 x 10^8 cells for each preparation) were washed with $HBSS^=$, harvested using $HBSS^=$ with 5 mM EGTA, and centrifuged at 500x *g* for 5 min at 4 °C. The pellet was then resuspended in hypotonic buffer and lysed by three steps of sonication (15 sec each). The lysate was centrifuged at 700x *g* for 10 min at 4 °C, to eliminate the unbroken cells, and then at 90,000x *g* for 90 min at 4 °C, to recover the total membranes. The pellet was resuspended in 20 mM HEPES, pH 7.4, with protease inhibitors.

2.10.4 PTX-dependent ADP-ribosylation of $G\alpha_i$ in plasma membranes

The ADP-ribosyltransferase activity was measured following the incorporation of radioactive ADP-ribose into the membrane components. The ADP-ribosylation assay was carried out following the procedure described by Lupi et al. (2000), with some modifications. Samples (5 μg NIH 3T3 plasma membranes) were incubated with 50 μl

ADP-ribosylation buffer (50 mM PFB, pH 7.4, 5 mM $MgCl_2$, 4 mM DTT, 10 μM GTPγS, 700 μM β-NAD^+ and 4.5 μCi [^{32}P]NAD) for 60 min at 37 °C in the presence of the catalytic subunit of PTX (100 nM), to allow the ADP-ribosylation of the α_i subunit of the heterotrimeric G proteins. The reaction was terminated by diluting the samples with 50 μl Laemmli sample buffer (2x), and analysed by 12% SDS-PAGE. The proteins were electroblotted (as described in Section 2.7.4), and the filters were exposed to Kodak X-Omat film (Amersham).

2.11 Pull-down assays

2.11.1 Pull-down assay with cell cytosol overexpressing TIAM1-HA

The cell cytosol was prepared from HEK293T cells that had been transfected with pcDNA-1199-TIAM1 vector, encoding for TIAM1-HA, as described in Section 2.8.1. Ten μl lysate was first diluted (1:15) in the reaction buffer (25 mM Tris-HCl, pH 7.6, 100 mM NaCl, 10 mM $MgCl_2$), and then cleared with the 50% glutathione resin for 1 h at 4 °C on a rotating wheel, and incubated for 10 min at 37 °C with 50 μM GroPIns4P. Finally, 4 μg purified Rac1-GST or purified GST (Section 2.8.2), 10 μl 50% glutathione resin and 20 μl 2 mg/ml BSA (final volume 200 μl) were added to the samples, which were then incubated for 1 h at 4 °C on the rotating wheel. The pellets were recovered by centrifugation at 800x *g* for 6 min at 4 °C, and after 3 washes with the reaction buffer, they were analysed by immuno-blotting with the anti-TIAM1 antibody (see Section 2.7). The amount of TIAM1-HA co-immunoprecipitated with Rac1-GST was quantified by the NIH imaging programme (densitometric analysis).

2.11.2 Pull-down assay with purified TIAM1

Two μg of the purified TIAM1 protein (see Section 2.8.3) were incubated for 10 min at 37 °C with 100 μM GroPIns4P, then 2 μg purified Rac1-GST or GST, 10 μl 50% glutathione resin and reaction buffer (20 mM Tris-HCl, pH 7.6, 100 mM NaCl, 200 mg/ml BSA, 1 mM $MgCl_2$, 1 mM DTT and 1% Triton X-100) were added to the samples (final volume 200 μl). Finally, the samples were incubated on a rotating wheel for 1 h at 4 °C. The pellets were recovered by centrifugation at 800x *g* for 6 min at 4 °C, and then after 3 washes with the reaction buffer they were analysed by immuno-blotting with the anti-TIAM1 antibody (see Section 2.7). The quantification of the densitometry of the bands was performed using the NIH imaging programme.

2.12 Uptake experiments

2.12.1 Cell permeabilisation with tetanolysin

Solutions

1) Tetanolysin solution: Tetanolysin was dissolved in sterile water to a final concentration of 1 μg/μl.
2) HGI buffer: 20 mM PIPES, 2 mM NaATP, 4.8 mM $Mg(CH_3COO)_2$, 150 mM potassium glutamate, 2 mM EGTA, 1 mM DTT (added just before the experiment) and KOH to obtain pH 7.0.

Procedure

The NIH 3T3 cells were permeabilised with tetanolysin (Sigma) by a procedure adapted from Riese et al. (2002). The cells were detached from the petri dish by scraping, then counted, divided into samples of 6 $x10^6$ cells (to be divided again into samples of 1.6 $x10^6$ cells for the uptake experiments), and washed with 6 ml/sample HGI buffer. The cells

were then incubated for 10 min at 37 °C with 2.4 μg tetanolysin, 1 mM DTT and 2 mM ATP in HG1 buffer and then washed with ice-cold HGI buffer. The level of cell permeabilisation was quantified by penetration of Trypan Blue (at 4 mg/ml).

2.12.2 GroPIns4P uptake in cells and binding in to membranes

2.12.2.1 GroPIns4P uptake in intact and permeabilised cells

The GroPIns4P uptake was performed according to Patton-Vogt and Henry (1998) and Berrie et al. (1999). Intact or permeabilised (see Section 2.12.1) NIH 3T3 cells (1.5 $x10^6$) were harvested and resuspended in 150 μl growth medium plus 10 mM HEPES, pH 7.5, and incubated with 150 μl growth medium plus [^{3}H]GroPIns4P (9 $x10^4$ cpm/sample), 10 μM GroPIns4P and 10 mM HEPES for 10 min at RT. The samples were then spotted onto nitrocellulose filters (0.45 μm cellulose nitrate membrane filters; Whatman), and washed three times with a buffer containing HBSS, 2 mg/ml BSA and 10 μM GroPIns4P in a vacuum filtration apparatus. The binding at time 0 was calculated by separately spotting cells and [^{3}H]GroPIns4P on the same nitrocellulose filter. The non-specific binding to the filters was calculated by spotting the radioactive mixture directly onto the filters without the cells, and this was subtracted from the total bound [^{3}H]GroPIns4P obtained for each sample. Each experiment was carried out in quadruplicate. The filters were dissolved in Filter Count (Perkin Elmer) and then counted to an error of ±2% in a β-scintillation counter (Beckman). The dpm obtained were then converted into total pmols of GroPIns4P bound to the sample and plotted. This was done considering the specific activity of the [^{3}H]GroPIns4P, the amount of [^{3}H]GroPIns4P bound per sample, the ratio between the [^{3}H]GroPIns4P and GroPIns4P, and the concentration of GroPIns4P.

2.12.2.2 GroPIns4P binding to membranes

The conditions applied in the uptake assay (Section 2.12.4) were used to follow the binding of GroPIns4P to membranes. The experiment was performed using the same amount of total membrane and plasma membranes that should be present in the cells used for the uptake experiment described in Section 2.12.2. The approximate amount of total membrane present in a single cell, was calculated by preparing total membranes from a known number of cells and then dividing the amount of membrane obtained for the number of starting cells. Thus, the theoretical amount of membrane present in a single NIH 3T3 cell is about 80 pg (amount of proteins). The uptake assay was performed with 1.5 x 10^6 cells per sample, and thus the amount of total membrane and plasma membranes would be 120 μg proteins and 6 μg proteins respectively (in general, the plasma membrane represents 5% of the total membranes; Gettys et al., 1994). The membranes were extracted from NIH 3T3 cells following the procedure described in Section 2.9, and the assay was performed as described in Section 2.12.2.

2.13 Binding assays

2.13.1 GTPγS binding

The GTPγS binding was performed according to (Wieland et al., 1994). Plasma membranes of NIH 3T3 cells (5 μg) untreated and treated with 5 nM PTX for 24 h, were incubated for 30 min at 30 °C in a buffer containing 50 mM triethanolammine, pH 7.3, 5 mM MES, 1 mM EDTA, 5 mM $MgCl_2$, 143 mM NaCl, 0.16% BSA, 10 μM GTP, and 4 nM [γ ^{35}S]GTPγS (2 x10^5 cpm/sample), in the presence of 50 μM GroPIns4P or other stimuli, including Mas 7 (25 μM), and LPA (10 μM), in a final volume of 100 μl. The non-specific binding was measured by adding GTPγS to samples to a final concentration of 10 μM. The reaction was stopped by adding 2.5 ml ice-cold washing buffer (50 mM Tris-HCl,

pH7.3, 1 mM EDTA and 5 mM $MgCl_2$). Then the samples were filtered through 0.45 μm filters (cellulose nitrate membrane filters; Whatman) and washed three times with 2.5 ml ice-cold wash buffer in a vacuum apparatus. Finally, the filters were collected, dissolved in Filter Count (Perkin Elmer) and counted to an error of ±2% in a β-scintillation counter (Beckman). The results in the Figures are plotted as percentage increases over the untreated samples.

2.13.2 Binding of GroPIns4P to immunoprecipitated TIAM1

Cell cytosols overexpressing different constructs of TIAM1 or its deletion mutants that were HA or GFP tagged (see Table 2.1 and Section 2.7.1) were used to immunoprecipitate the corresponding fusion proteins through the HA or GFP tags, as described in Section 2.7.3. The immunoprecipitates (already attached to Protein A or G depending on the tag) were incubated with GroPIns4P for 45 min at 37 °C in a buffer containing 25 mM Tris-HCl, pH 7.6, 100 mM NaCl, 10 mM $MgCl_2$, GroPIns4P in a range of 0.1-50 μM and [^{3}H]GroPIns4P 0.1 μM (at 9x10^{4}cpm/sample) in a final volume of 100 μl. Then the samples were centrifuged for 5 min at 3000x *g* at 4 °C, washed 3 times with the same buffer (25 mM Tris-HCl, pH 7.6, 100 mM NaCl, 10 mM $MgCl_2$) and the resin was counted on a β-scintillation counter using Ultima Gold scintillation fluid (PerkinElmer). The non-specific binding was calculated by immunoprecipitating the wild-type cytosol from HEK293T cells with the anti-HA antibody (in the case of the immunoprecipitation of TIAM-HA), or by immunoprecipitating GFP from cytosol overexpressing GFP with the anti-GFP antibody (in the case of the immunoprecipitation of TIAM1-GFP or its deletion mutants).

The Kd values (dissociation constants) for GroPIns4P were calculated using the Prism programme, according to the equation: B=(FxBmax)/(Kd+F), where F is the ligand

that is not bound to the receptor, B is the receptor that has radioligand bound to it, and Bmax is the total amount of receptor present (i.e., the maximum number of binding sites).

The following assumptions have to be taken in account for this calculation: i) only a small fraction of the radioligand binds; thus, its free concentration is almost identical to the total concentration added. ii) There is no cooperativity; thus, the binding of a ligand to one binding site does not alter the affinity of the ligand for another binding site. iii) The conditions are left to reach equilibrium. iv) The binding is reversible and follows the law of mass action.

The Kd for GroPIns4P versus immunoprecipitated TIAM1 value was calculated considering only the specific binding seen at the lower μM GroPIns4P concentrations (up to 10 μM) because with the increase in the concentration of GroPIns4P to 50 μM, the variability of the data through this procedure rendered the values of the specific binding difficult to estimate with any significance.

The samples were counted to a ±2% error and the dpm were converted into total pmols of GroPIns4P bound. This calculation was as explained in Section 2.12.2.

2.13.3 Binding of GroPIns4P to purified TIAM1-GST and Rac1-GST

Purified TIAM1-GST (2 μg) (see Section 2.8.3) or Rac1-GST (2 μg) (see Section 2.8.2) were used instead of the immunoprecipitate in the same binding assay as in Section 1.13.2. The assay buffer, containing 10 μM GroPIns4P and 0.1 μM [^{3}H]GroPIns4P (9 x10^{4}cpm/sample), and the times of incubation where the same as those used in Section 2.13.2. However, two different approaches were used to determine if GroPIns4P binds directly to TIAM1-GST or Rac1-GST:

1) TIAM1-GST was incubated with the assay buffer and then precipitated through the glutathione resin, to separate the unbound fraction. The non-specific binding was calculated by using purified GST instead of TIAM1-

GST. The resin was counted on a β-scintillation counter using the Ultima Gold scintillation fluid (PerkinElmer). The samples were counted to an error of ±2% and the dpm converted into total pmols of GroPIns4P bound (Section 1.12.2).

2) TIAM1-GST or Rac1-GST were incubated in the assay buffer and then spotted onto nitrocellulose filters, which were then washed twice using a vacuum apparatus, with 25 mM Tris-HCl, pH 7.6, 100 mM NaCl, 10 mM $MgCl_2$, 200 μg/ml BSA. Also in this case, GST was used to evaluate the non-specific binding. Finally the filters were collected, dissolved in Filter Count scintillation fluid (PerkinElmer) and counted to an error of ±2% in a β-scintillation counter. The dpm were converted into total pmols of GroPIns4P bound (Section 1.12.2).

2.13.4 Liposome-binding assay.

The GST-PH fusion proteins were expressed in *E. coli* (BL-21) and purified using Glutathione-Sepharose™ 4B beads (Amersham Pharmacia Biotech AB, Sweden). Liposomes of defined lipid compositions were generated by co-dissolving the appropriate lipids in 1:1 chloroform:methanol containing 0.1% HCl. The lipid mixtures contained phosphatidylcholine (PC) alone or in combination with 2% $PI45P_2$ (Kavran et al., 1998). The liposomes were prepared by initially drying the lipids under a stream of nitrogen, followed by a high vacuum, and then rehydration of the dried mixtures by bath sonication in PBS, to a final total lipid concentration of 10 mM. The lipids were subjected to at least 10 cycles of freezing (liquid N_2) and thawing (bath sonication), until optical clarity was achieved. The different PH domains were incubated with the liposomes at RT for 15 min, and then they were ultracentrifuged at 100,000x *g* for 30 min at 4°. After centrifugation, both the supernatants and the vesicle pellets were assayed for protein content. Competition assays

were then performed by Stefania Mariggiò (Department of Cell Biology and Oncology; Consorzio Mario Negri Sud, Italy), and the ability of the water-soluble glycerophosphoinositols to compete with PtdCho/ $PI45P_2$-lipid vesicles for the binding to PH domains was calculated (Kavran et al., 1998).

2.14 Statistical analysis

All experiments are presented as the means of duplicate or triplicate determinations that were repeated at least three times. Statistical analysis was carried out using the paired Student's *t* test, calculated by the "Prism GraphPad" programme.

CHAPTER 3

SIGNALLING CASCADE INVOLVED IN GLYCEROPHOSPHOINOSITOL 4-PHOSPATE INDUCED ACTIN RUFFLE FORMATION.

3.1 Introduction

GroPIns4P can modulate the actin cytoskeleton organization acting at the level of the small GTPases of the Rho family: when added exogenously to serum-starved Swiss 3T3 cells, it stimulates a Rac1-dependent rapid formation of membrane ruffles followed by RhoA-dependent stress fibres formation. Moreover, GroPIns4P increases the cytosolic fraction of GTP-bound Rac1 and favours its translocation to the plasma membrane, without altering its intrinsic GTP-binding or GTPase activity (Mancini et al., 2003). The action of GroPIns4P is specific, since under identical conditions GroPIns and GroPIns4,5P_2 had no measurable effects.

To study the mechanism responsible for the modulation of the actin cytoskeleton operated by GroPIns4P, the methodological approaches taken were:

1) Immunofluorescence analysis of the intracellular localization of small GTPases involved in actin cytoskeleton remodelling, of other proteins involved in their regulation and of the actin cytoskeleton.
2) *In vitro* assays to study specific enzymatic activities potentially modulated by GroPIns4P as well as second messenger production.
3) *In vivo* imaging of Fluo-3 loaded cells to measure intracellular calcium levels.

These approaches should allow the understanding of a complex signalling pathway that is activated upon cell treatment with GroPIns4P and that leads to ruffle formation.

3.2 GroPIns4P and Rac1

3.2.1 General description

The GroPIns4P-dependent Rac1 activation was investigated in Swiss 3T3 cells (Mancini et al., 2003). Exogenously added GroPIns4P induces a rapid translocation of Rac1-GFP to the plasma membrane and produces a sustained and nearly maximal activation of Rac1, increasing the GTP-bound fraction of Rac1 (Mancini et al., 2003). GroPIns and GroPIns4,5P_2 are also able to increase the amount of GTP-bound Rac1 in the cell, but only transiently and at a concentration a least of 100 μM (Fig. 1.9, Chapter 1) (Mancini et al., 2003). GroPIns4P is the only compound able to initiate the signal cascade that leads to actin reorganization, thus suggesting that the duration and the extent of Rac1 activation could play an important role in this pathway, as discussed in the introduction (Section 1.4.3.1).

Swiss 3T3 cells are not easily transfectable, which makes them unsuitable for further investigations into the activity of the glycerophosphoinositols. I therefore tested NIH 3T3 cells, which transfect well, for GroPIns4P-dependent ruffle and stress fibre formation and GFP-Rac1 translocation to the plasma membrane. In addition, I examined whether the reported ability of GroPIns and GroPIns4,5P_2 to transiently activate Rac1 could produce the translocation to the plasma membrane of this small G protein.

3.2.2 GroPIns4P triggers ruffle formation and Rac1-GFP translocation to the plasma membrane in NIH 3T3 cells

In order to verify whether GroPIns4P could modulate the actin cytoskeleton also in NIH 3T3 cells in a way that could be comparable to what is reported for Swiss 3T3 cells (Mancini et al., 2003), immunofluorescence experiments of ruffle and stress fibre formation were performed. Serum starved NIH 3T3 cells were treated with 50 μM

GroPIns4P or 10 ng/ml PDGF for different times (from 2 to 30 minutes), stained with TRITC-labelled phalloidin for filamentous actin visualization and subjected to blind morphological scoring, as described in Section 2.4.3.

Within 2 minutes of addition, GroPIns4P produced a clear increase in membrane ruffles (a 2.3-2.5-fold response versus control) both on the dorsal side of the cell and at the leading edge of the lamellipodium (Fig. 3.1a). This feature persisted for up to 5 min (1.4 fold increase) of treatment and then disappeared (Fig. 3.1b). A five min treatment with PDGF produced a 3.9-fold increase in the same kind of ruffles and the appearance of circular ruffles (or called waves) that are transient, actin-based dorsal membrane structures that can provide a structural base for force generation, and which function as indicators of cellular transition from a static to a motile state (Buccione et al., 2004) (Fig. 3.1a). The different effects of these two compounds underlined a divergence in their mechanism of action.

Both Swiss 3T3 and NIH 3T3 cells had a similar time course for GroPIns4P-dependent membrane ruffle formation; the appearance of stress fibres was instead delayed and less evident in NIH 3T3 cells (within 15-20 min there was a 1.7-fold response over the control in stress fibres) when compared to Swiss 3T3 (within 12 min a 3-4-fold response) (Mancini et al., 2003) (Fig. 3.1b).

In Swiss 3T3 cells the formation of membrane ruffles was associated with the translocation of Rac1-GFP to the plasma membrane (Mancini et al., 2003). The same event could be followed also in NIH 3T3 cells. Rac1 GFP tagged was transfected in NIH 3T3 cells and, after 24 h of serum starvation, 50 μM GroPIns4P or 10 ng/ml PDGF were added for different times (as described in Section 2.4.4). Within 2 min of treatment, Rac1-GFP localised at the plasma membrane and in particular in membrane ruffles and remained there for at least 15 min (as showed also for Swiss 3T3 cells). In basal conditions, only 32% of cells shown a localization of Rac1 at the plasma membrane, whereas upon stimulation with GroPIns4P Rac1 localised at the level of plasma membrane in the 75% of

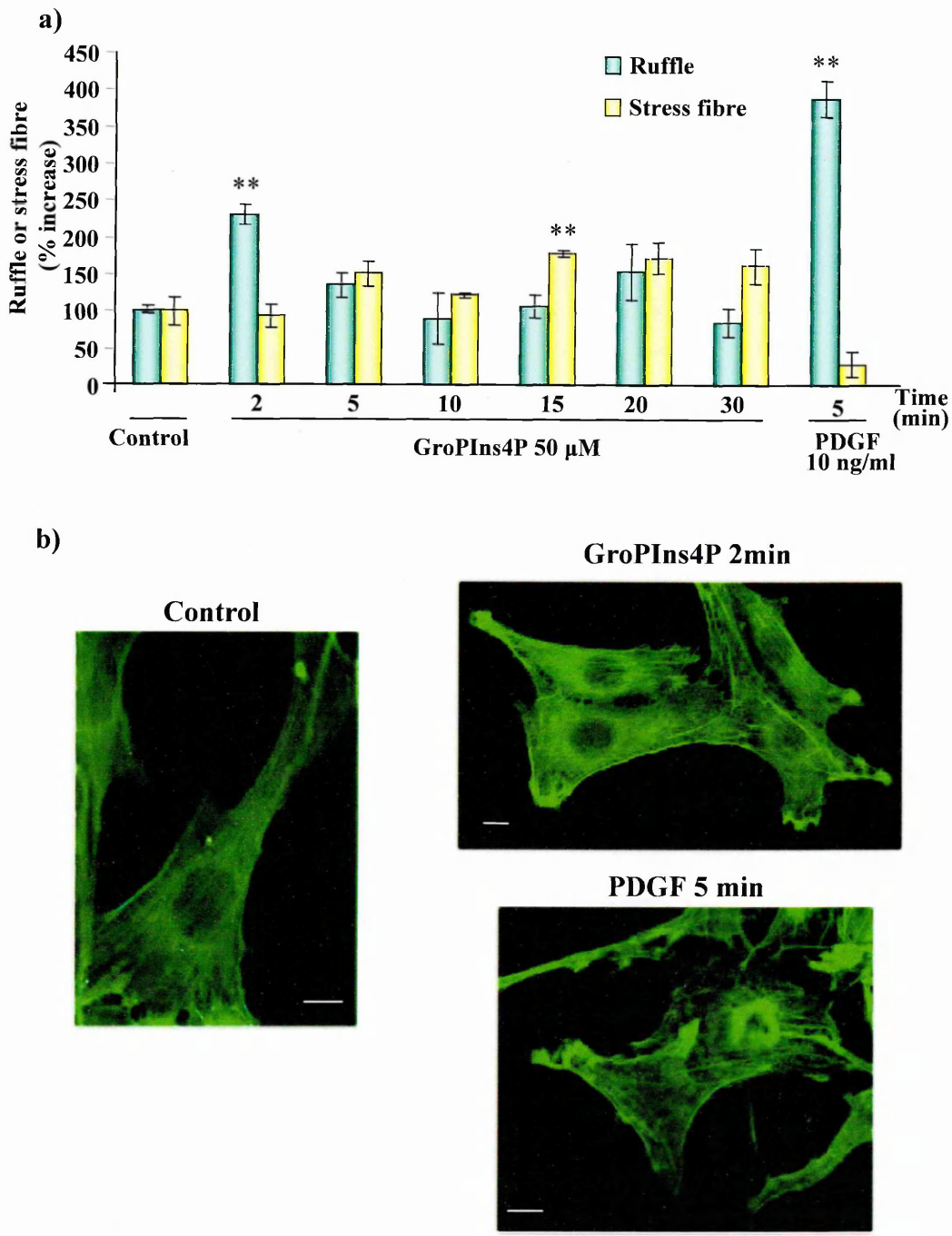

Figure 3.1 - GroPIns4P-dependent ruffle and stress fibre formation in NIH 3T3 cells. a) Serum starved NIH 3T3 cells were treated with 50 µM GroPIns4P for different times (from 2 to 30 min) or 10 ng/ml PDGF for 5 min. Cells were fixed and stained with FITC-labelled phalloidin and quantified blind for the extent of ruffle and stress fibre formation as described in Section 2.4.3.The results shown are the means (±SD) of three independent experiments, each performed in duplicate. **b)** Representative images of GroPIns4P- and PDGF-dependent modification of actin cytoskeleton in NIH 3T3 cells. Bar=20 µm

*P <0.05, **P <0.01, versus control (Section 2.14)

cells (Fig. 3.2a, b).

The behaviour of these two cell lines is therefore similar, but the NIH 3T3 cells have the advantage of being easy transfectable. For this reason these cells were used for the investigation of the mechanism of action of GroPIns4P.

3.2.3 GroPIns and GroPIns4,5P_2 do not induce the translocation of Rac1 to the plasma membrane.

A treatment with 50-100 μM GroPIns or GroPIns4,5P_2 of Swiss 3T3 cells did not produce any ruffle formation, despite, these two compounds are able to induce a small (50% increase) and transient activation of Rac1 (if compared with the 100% increase produced by GroPIns4P) (Mancini et al., 2003). Even if weak, this Rac1 activation could be sufficient to induce its translocation to the plasma membrane. To test this possibility, the extent of Rac1-GFP localisation to the plasma membrane upon treatment with GroPIns and GroPIns4,5P_2 was analysed in NIH 3T3 cells.

The cells, transfected with Rac1-GFP and serum starved, were stimulated with 100 μM GroPIns or GroPIns4,5P_2 for different times (from 2 to 20 min). TRITC-phalloidin was used for filamentous actin visualization and the localization of Rac1-GFP was analysed by confocal microscopy. Short-term treatment with GroPIns or GroPIns4,5P_2 (2-5 min) did not produce any translocation of Rac1-GFP to the plasma membrane. A longer incubation (15-20 min), resulted in a partial re-localisation of Rac1-GFP to the plasma membrane in 45-55% of the treated cells (a 1.5-1.6 fold response over the basal level). However, this was a weak and delayed effect when compared with that observed upon GroPIns4P treatment (Fig. 3.3). These data supported the conclusion that the rapid effect of Rac1 translocation and ruffle formation produced by GroPIns4P cannot be mimicked by other similar compounds like GroPIns and GroPIns4,5P_2.

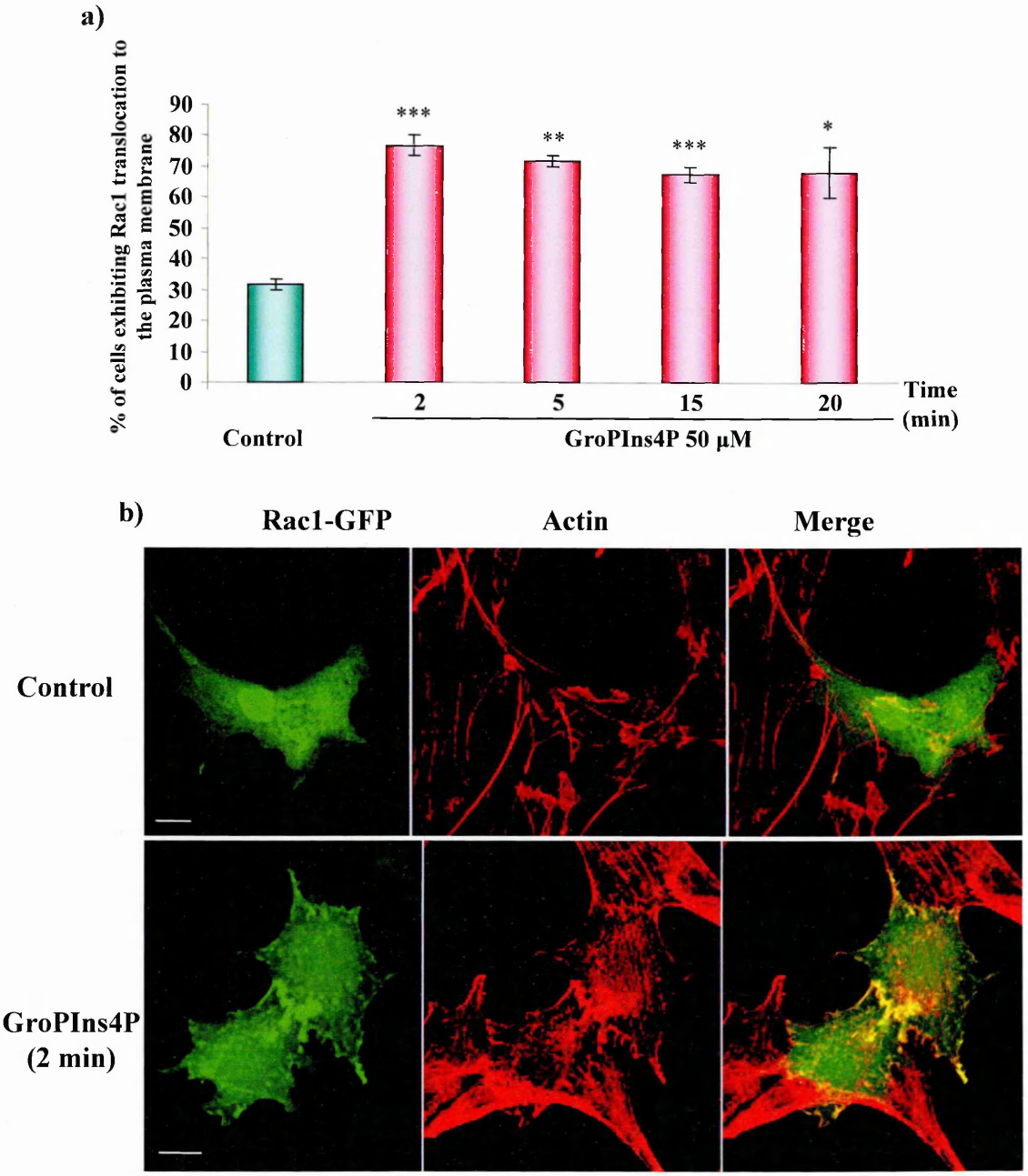

Figure 3.2 - GroPIns4P-dependent translocation of Rac1-GFP to the plasma membrane in NIH 3T3 cells. a) Sub-confluent NIH 3T3 cells were transfected with the pEGFP-Rac1 construct as described in Section 2.3.4. Twenty-four h after transfection, cells were serum starved for 24 h and then were treated with GroPIns4P (50 µM) for 2 to 20 min, fixed, and stained with TRITC-labelled phalloidin. The percentage of cells showing plasma membrane localisation of Rac1 was quantified blind as described in Section 2.4.4. The graph represents the mean (±SD) of three independent experiments, each performed in duplicate. **b)** Localisation of Rac1-GFP and actin in GroPIns4P-induced membrane ruffles. Bar=20 µm
*P <0.05, ** P <0.01, ***P <0.001, versus control (Section 2.14)

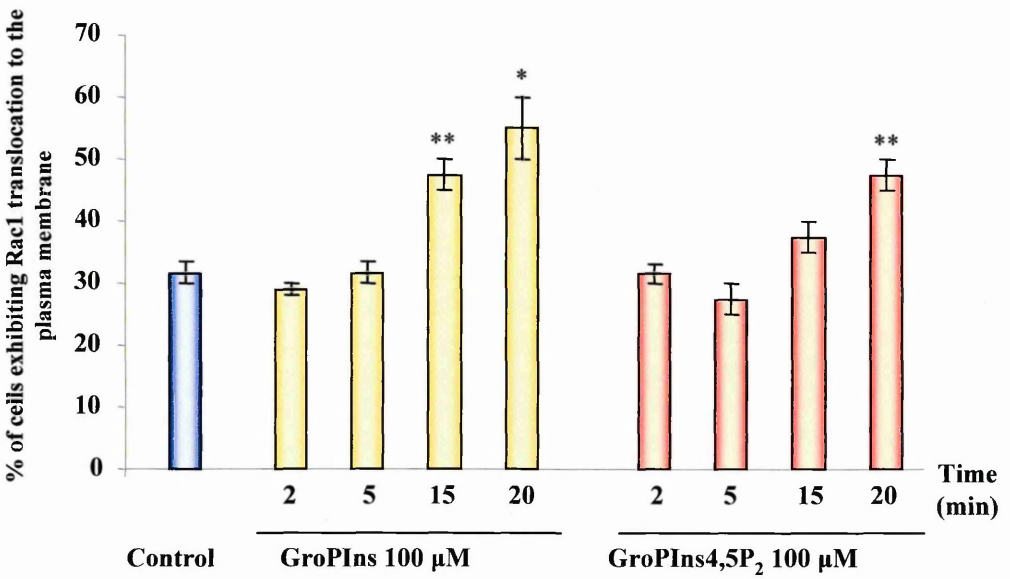

Figure 3.3 - Quantification of GroPIns and GroPIns4,5P_2-dependent Rac1-GFP translocation to the plasma membrane. Sub-confluent NIH 3T3 cells were transfected with the pEGFP-Rac1 construct as described in Section 2.3.4. Twenty-four h after transfection, cells were serum starved for 24 h and then were treated with GroPIns or GroPIns4,5P_2 (100 µM) for 2 to 20 min, fixed and stained with TRITC-labelled phalloidin. The amount of cells showing plasma membrane localisation of Rac1 was quantified blind as described in Section 2.4.4. The graph represents the mean (±SD) of two independent experiments, each preformed in duplicate. *P<0.05, **P<0.01, versus control (Section 1.14).

3.2.4 Conclusion

When exogenously added to Swiss 3T3 and NIH 3T3 cells, GroPIns4P produces a sustained activation of Rac1, followed by an increase of 2.3-fold versus the control of membrane ruffles. These features identify a site of actin polymerization and are associated with cell protrusion (linear ruffles at the leading edge of lamellipodium), macropinocytosis or receptor internalization (dorsal ruffles or waves) (see Section 1.2.2; Buccione et al., 2004). The GroPIns4P-dependent activation of Rac1 also results in both an increase in GTP-bound Rac1 and in its translocation to the plasma membrane. These changes can be easily followed both in Swiss 3T3 (Mancini et al., 2003) and in NIH 3T3 cells. In contrast GroPIns and GroPIns4,5P_2 do not produce any increase in membrane ruffle formation and even if they can generate a weak and transient activation of Rac1, this is not enough to give a significant stimulation that can cause a rapid and sustained translocation of Rac1 to the plasma membrane, which is necessary for ruffle formation.

3.3 TIAM1 is involved in GroPIns4P-dependent Rac1 activation and ruffle formation.

3.3.1 General description

The activation of Rac1 implies its GDP/GTP exchange, catalyzed by a specific GEF. Many different GEFs specific for Rac1 exist in nature (TIAM1, VAV1-2, PIX, STEF), each one expressed in different cell type. One of the most studied and well expressed both in Swiss 3T3 and NIH 3T3 cells is TIAM1. The gene encoding for TIAM1 was originally identified in T-lymphoma cells as an invasion and metastasis-inducing gene (Habets et al., 1994), and the function associated to it was the exchange activity specific for Rac1. This protein contains two PH domains, one at the N-terminus that binds

$PI3,4,5P_3$ and is important for its plasma membrane translocation, and one at the C-terminus that cooperates with the catalytic Dbl homology domain in enhancing the GDP/GTP exchange of Rac1. Plasma membrane-translocation of TIAM1 is required for Rac1-dependent membrane ruffling and also JNK activation in NIH 3T3 cells (Michiels et al., 1997). TIAM1 activity is also modulated by phosphorylation, and in particular, CaMKII-dependent phosphorylation is important for its plasma membrane translocation and enhances its exchange activity (Fleming et al., 2000) (see Section 1.2.3.2). The involvement of TIAM1 in Rac1 activation and ruffle formation, together with its high expression levels both in Swiss and NIH 3T3 cells, supported the hypothesis that TIAM1 could be involved in the pathway activated by GroPIns4P that leads to Rac1 activation. To see if this is the case, immunofluorescence experiments in NIH 3T3 cells transfected with TIAM1-GFP were performed.

3.3.2 GroPIns4P induces the translocation of TIAM1 to the plasma membrane

TIAM1 is a cytosolic protein that translocates to the plasma membrane upon activation. Once at the plasma membrane it interacts with Rac1 and catalyzes GDP/GTP exchange (as discussed in Section 1.2.3.2). In order to see if GroPIns4P could induce the translocation of TIAM1 to the plasma membrane, immunofluorescence experiments were preformed. NIH 3T3 cells were transfected with pEGFP-C1199-TIAM1, a construct that encodes for a GFP-tagged mutant of TIAM1 that lacks the N-terminal myristoylated region, but that keeps the same behaviour of the wild type protein (Michiels et al., 1997). For brevity the expressed protein is referred to throughout as TIAM1-GFP. After transfection, the cells were serum starved and treated with 50 μM GroPIns4P or 10 ng/ml PDGF for different times. The samples were analysed for the extent of C1199-TIAM1-GFP (henceforth referred as TIAM1-GFP for brevity) translocation and quantified in a blind fashion on a laser control scanning microscope (LSM510) with a 63 x objective (as

described in Section 2.4.4). Within 2 minutes of stimulation, GroPIns4P produced a translocation to the plasma membrane of TIAM1-GFP in 55% of transfected cells (a 2.5 response as compared to untreated samples). At 10 minutes TIAM1 was redistributed in the cytosol (Fig. 3.4 a). Similarly to Rac1, also TIAM1 was found associated with membrane ruffles, as shown in Figure 3.4b. This result was in line with the previous observations that GroPIns4P induces Rac1-GFP translocation to the plasma membrane in the same time frame (Mancini et al., 2003) and supported the hypothesis that GroPIns4P needs an active TIAM1 to activate Rac1. The extent of TIAM1 translocation to the plasma membrane mediated by GroPIns4P was comparable to that of PDGF, which caused a 2.6 fold response (Fig. 3.4a).

In parallel, the effect of GroPIns on TIAM1-GFP translocation to the plasma membrane was analysed. The experiment was performed in NIH 3T3 cells transfected with TIAM1-GFP and then treated with GroPIns. The effect of GroPIns was compared with that of GroPIns4P. Upon treatment with GroPIns, no significant translocation of TIAM1 to the plasma membrane was observed (Fig. 3.5).

The data confirmed that the mechanism of action of GroPIns4P is unique and cannot be mimicked by other similar compounds like GroPIns.

3.3.3 TIAM1 and Rac1 co-localize at the plasma membrane upon GroPIns4P treatment.

The direct interaction of TIAM1 and Rac1 at the plasma membrane favours the activation of Rac1 and consequently ruffle formation (Mertens et al., 2003). The effect of GroPIns4P at the level of Rac1 and TIAM1 activation had been followed independently by immunofluorescence experiments (as previously described), but there was no direct proof that Rac1 and TIAM1 could co-localize at the plasma membrane upon treatment with GroPIns4P. To see if this was the case, immuno-fluorescence assays in NIH 3T3 cells co-

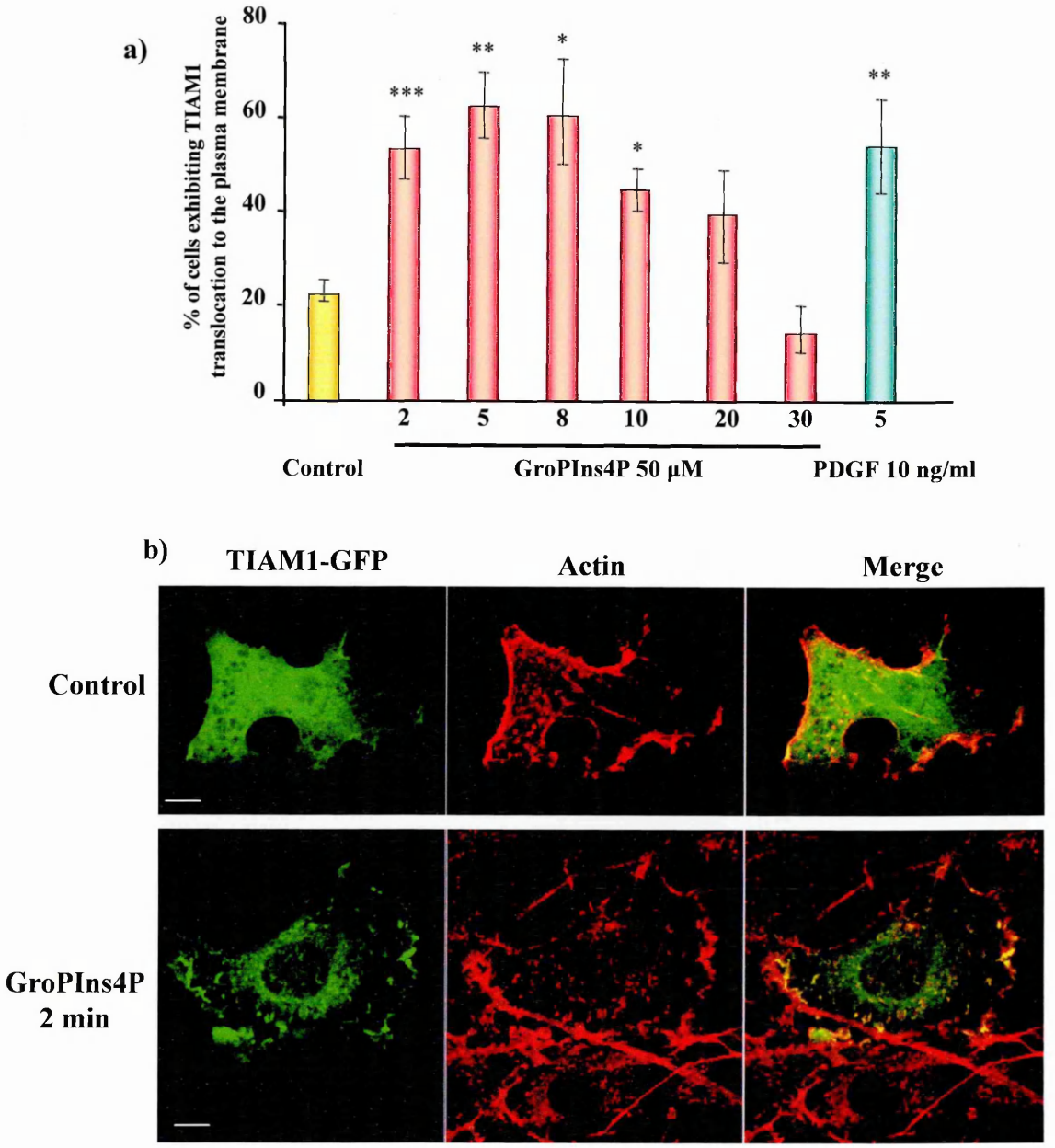

Figure 3.4 - GroPIns4P-dependent translocation of TIAMT1-GFP to the plasma membrane. a) Time-course of stimulation with 50 µM GroPIns4P in NIH 3T3 cells. Sub-confluent NIH 3T3 cells were transfected with the pEGFP-c1199-TIAM1 construct as described in Section 2.3.4. Twenty-four h after transfection, cells were serums starved for 24 h and then were treated with GroPIns4P (50 µM) for 2 to 20 min or 10 ng/ml PDGF for 5 min, fixed, and stained with TRITC-labelled phalloidin. The percentage of cells showing plasma membrane localisation of TIAM1 was quantified blind as described in Section 2.4.4. The bars show the means (±SD) of four independent experiments, each performed in duplicate. **P*<0.05, ***P*<0.01, ****P*<0.001 (Section 1.14).
b) Localisation of TIAM1-GFP and actin in GroPIns4P-induced membrane ruffles. Bar=20 µm

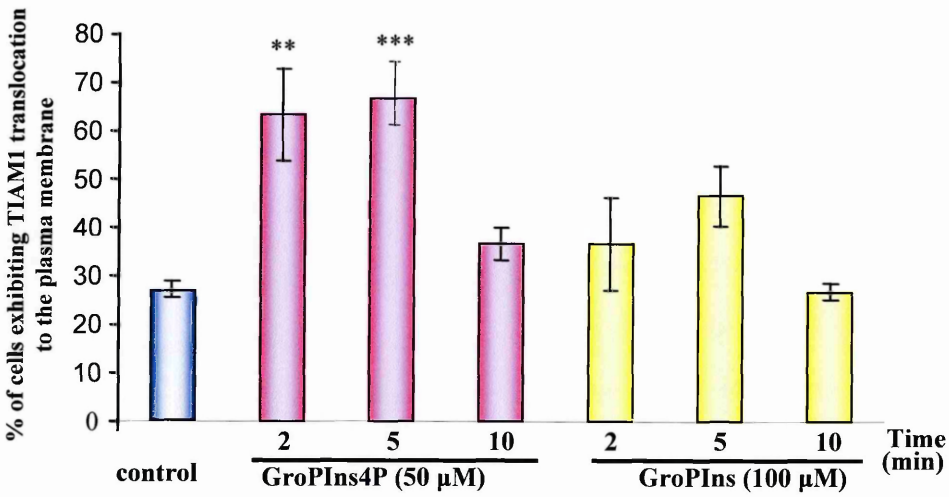

Figure 3.5 - Effect of GroPIns in TIAM1-GFP translocation to the plasma membrane. Time-course of stimulation with GroPIns and GroPIns4P in NIH 3T3 cells. Sub-confluent NIH 3T3 cells were transfected with the pEGFP-c1199-TIAM1 construct as described in Section 2.3.4. Twenty-four h after transfection, cells were serum starved for 24 h and then were treated with GroPIns4P (50 µM) or GroPIns (100 µM) for 2 to 10 min, fixed and stained with TRITC-labelled phalloidin. The percentage of cells showing plasma membrane localisation of TIAM1 was quantified blind as described in Section 2.4.4. The bars show the means (± SD) of two independent experiments, each performed in duplicate. $^{**}P<0.01$, $^{***}P<0.001$ (Section 1.14).

transfected with pEGFP-Rac1 and pcDNA-C1199-TIAM1 were performed. The two constructs encodes for Rac1-GFP and C1199-TIAM1-HA (henceforth referred as TIAM1-HA for brevity) respectively. GroPIns4P was able to induce the translocation of both Rac1-GFP and TIAM1-HA to the plasma-membrane and the two proteins co-localised in the same membrane structures within 2 min of treatment (Fig. 3.6). This co-localization supported the idea that TIAM1 could be the exchange factor activated by GroPIns4P for stimulating Rac1-dependent ruffle formation.

3.3.4 Effect of GroPIns4P on the PH-domain deleted mutants of TIAM1

The localization of TIAM1 at the membrane depends on the interaction of its N-terminal PH domain with $PI3,4,5P_3$ and $PI4,5P_2$. A deletion mutant that lacks this PH domain (ΔPHn-TIAM1-GFP) is not able to translocate to the plasma membrane (Fleming et al., 2000). The C-terminal PH domain of TIAM1 cooperates with the dbl homology (DH) domain in the interaction between Rac1 and TIAM1, but it is not important for its translocation to the plasma membrane (Fleming et al., 2000). In order to understand if the absence of one or both PH domains of TIAM1 could affect the ability of GroPIns4P to translocate TIAM1 to the plasma membrane, the PH-domain-deleted mutants of TIAM1 were overexpressed and analysed in the immunofluorescence assay. Those mutants that selectively lacks the N-terminal PH domain (ΔPHn-TIAM1), the C-terminal PH domain (ΔPHc-TIAM1) or both (ΔPH-TIAM1) were expressed in vectors that contain the GFP tag (Fig. 3.7a). PDGF was used in this experiment to follow the correct localisation of the constructs (Fleming et al., 2000).

The absence of the N-PH domain resulted in a loss of the ability of TIAM1 to translocate to the plasma membrane both in PDGF and in GroPIns4P-treated samples (Fig 3.7b). As expected, the ΔPHc-TIAM1-GFP was able to translocate to the plasma membrane upon treatment with GroPIns4P but, if compared with the full length TIAM1, it

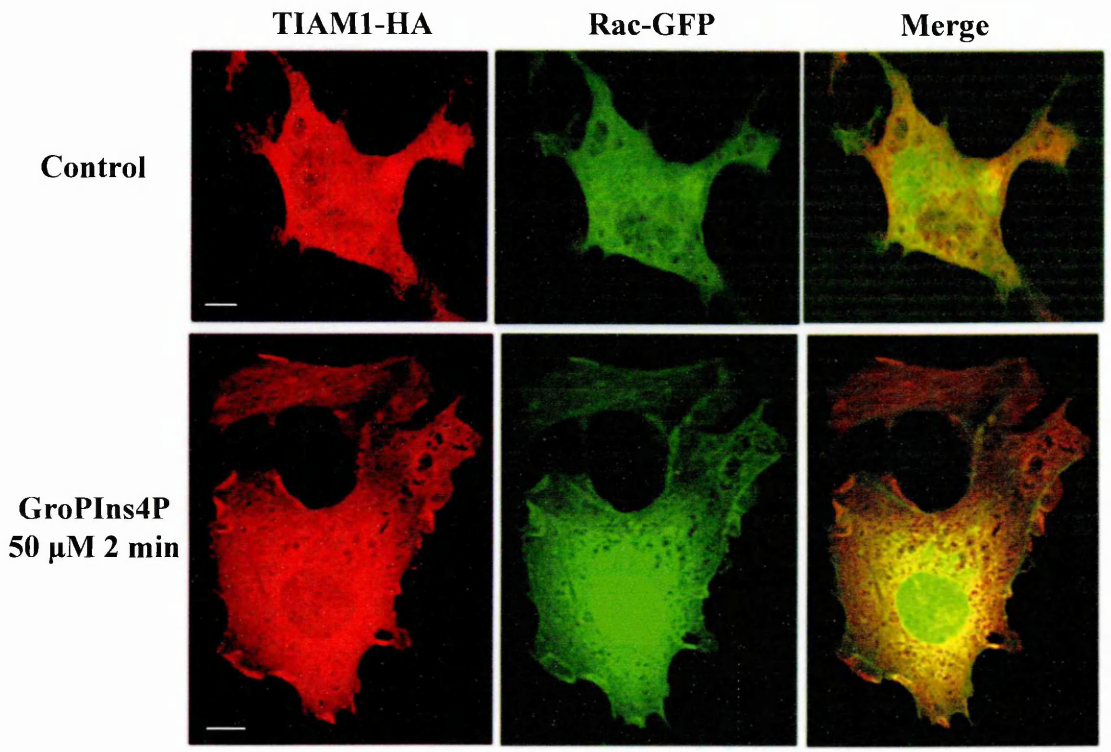

Figure 3.6 - Co-localisation of Rac1 and TIAM1 at the plasma membrane. Sub-confluent NIH 3T3 cells were transfected with the Rac1-GFP and TIAM1-HA construct as described in Section 2.3.4. Twenty-four h after transfection, cells were serum starved for 24 h and then were treated with GroPIns4P (50 µM) 2 min, fixed and stained with Ab-anti HA (Babco). The plasma membrane localisation of TIAM1 and Rac1 was analysed by confocal microscopy (as described in Section 2.4.4). The pictures are representative of three independent experiments. Bar=20 µm

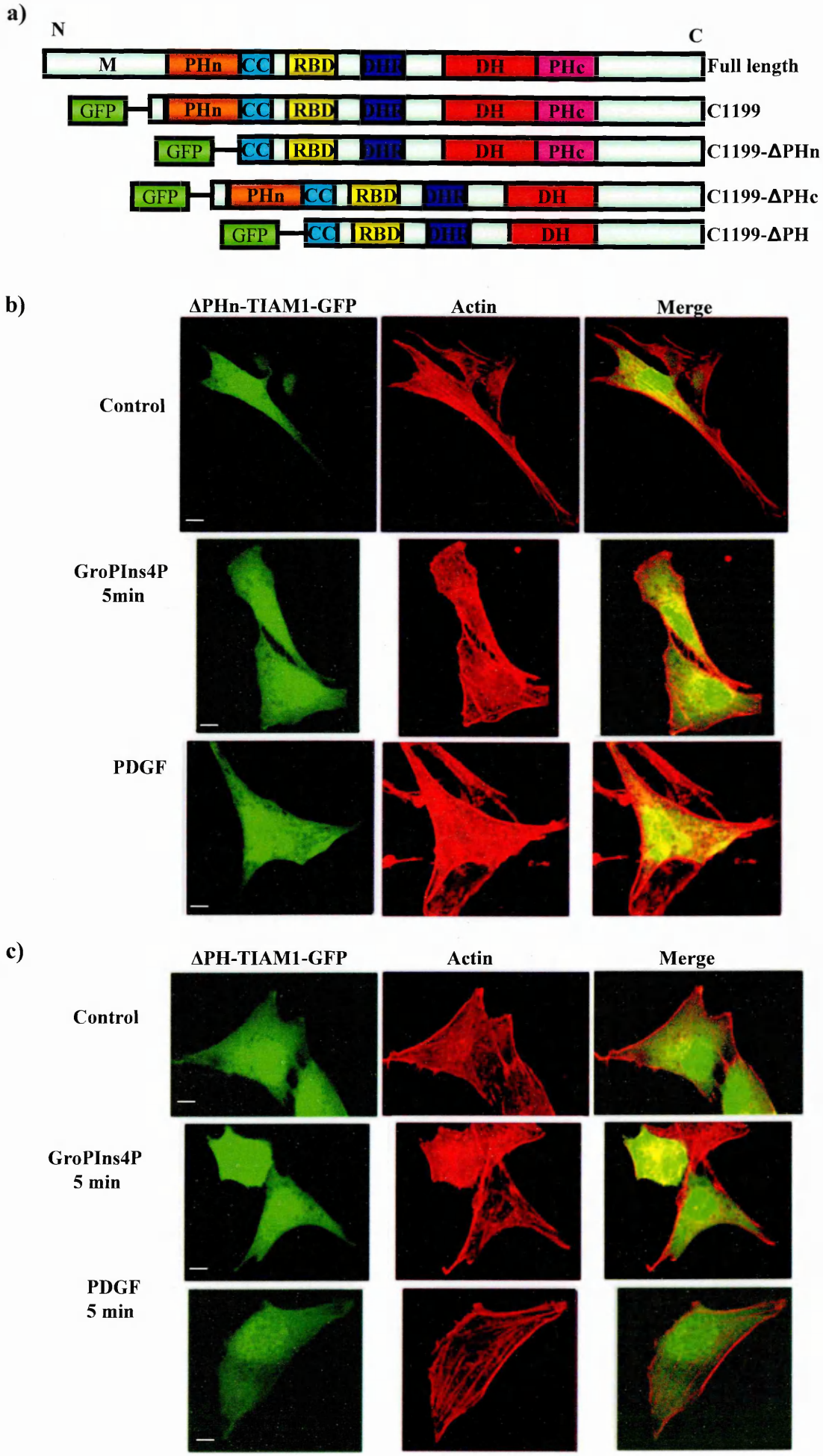
a)
N
C
M
PHn
CC
RBD
DH
PHc
Full length
GFP
C1199
C1199-ΔPHn
C1199-ΔPHc
C1199-ΔPH
b)
ΔPHn-TIAM1-GFP
Actin
Merge
Control
GroPIns4P
5min
PDGF
c)
ΔPH-TIAM1-GFP
Actin
Merge
Control
GroPIns4P
5 min
PDGF
5 min

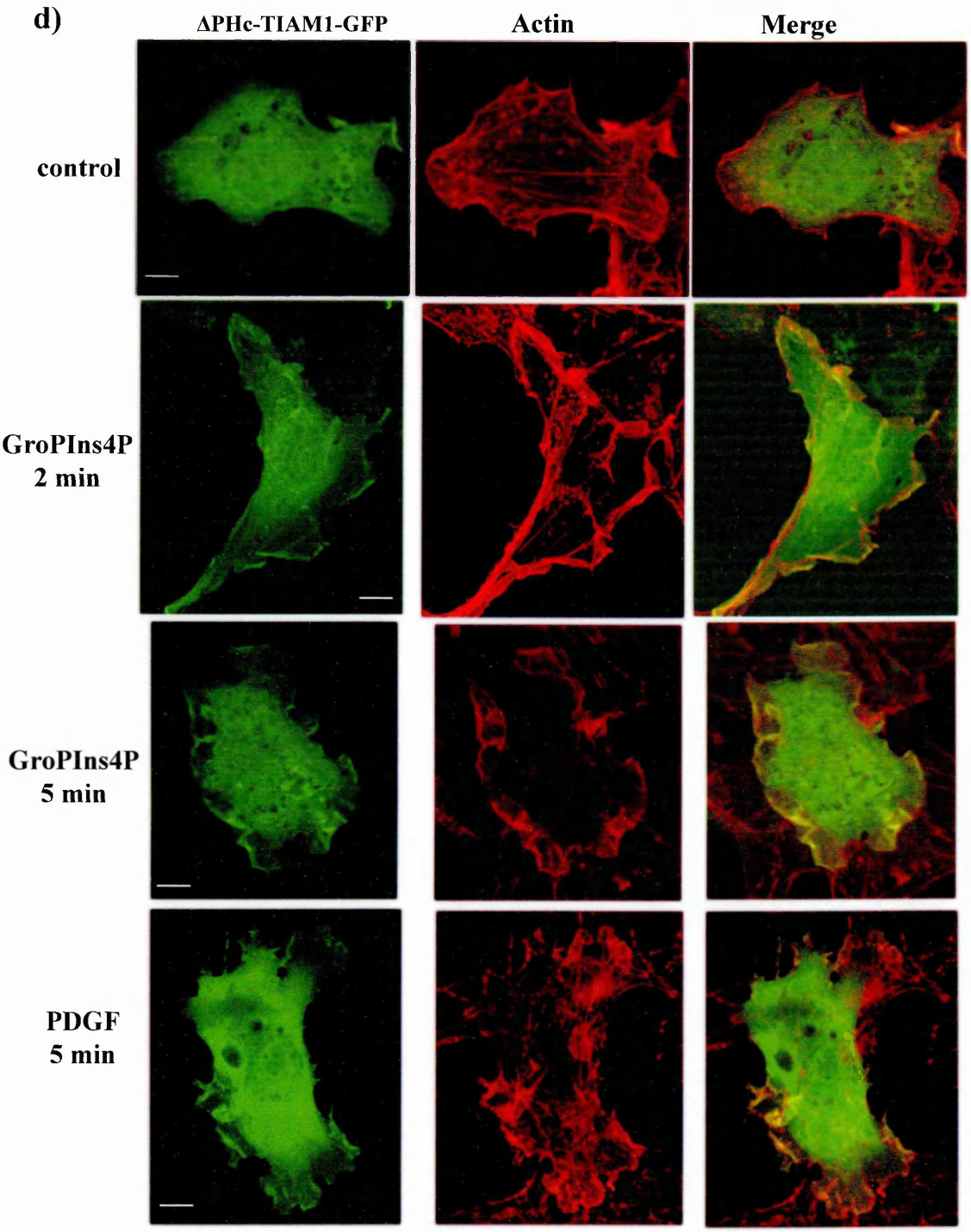

Figure 3.7 - Sub-cellular localisation of PH-domain-deleted mutants of TIAM1. Scheme of the construct overexpressing TIAM1 deleted mutants, GFP tagged (**a**). Sub-confluent NIH 3T3 cells were transfected with the pEGFP-ΔPHn TIAM1 (**b**); ΔPHc-TIAM1 (**d**) ΔPH-TIAM1 (**c**) as described in Section 2.3.4. Twenty-four h after transfection, cells were serum starved for 24 h and then were treated with GroPIns4P (50 μM) for 2 min (d) and 5 min (b, c and d), fixed, and stained with TRITC-phalloidin. The plasma membrane localisation of TIAM1 was analysed by confocal microscopy (as reported in Section 2.4.4). The pictures are representative of two independent experiments. Bar=20 μm

needed at least 5 min of stimulation with GroPIns4P to localize to the plasma membrane. PDGF, applied for 2 to 10 min, was also able to induce the translocation of the C-PH domain–deleted mutant of TIAM1 to the plasma membrane (Fig. 3.7d). The behaviour of the ΔPH-TIAM1-GFP was similar to the ΔPHn-TIAM1: it was always cytosolic and the stimulation with GroPIns4P or PDGF did not produce any changes in its localisation (Fig. 3.7c).

3.3.5 The membrane translocation of TIAM1 induced by GroPIns4P is inhibited by the Ca^{2+}/calmodulin kinase II inhibitor KN-93

The effect of GroPIns4P on TIAM1 translocation to the plasma membrane was comparable to that of PDGF (Fig. 3.4a). It is well known that PDGF activates TIAM1, inducing its translocation to the plasma membrane as well as an increase in Rac1-GTP and membrane ruffling, in a CaMKII-dependent way (Buchanan et al., 2000; Fleming et al., 1999). This kinase phosphorylates TIAM1 on threonine residues and this phosphorylation favours its translocation to the plasma membrane (see Section 1.3.4) (Buchanan et al., 2000). To see if this kinase could be involved in the GroPIns4P-dependent activation of TIAM1, KN-93, a CaMKII specific inhibitor that binds the Ca^{2+}/CaM binding site of the enzyme so preventing its activation (see Figure 1.3.4b; Sumi et al., 1991), was applied to NIH 3T3 cells before performing immunofluorescence analysis.

The cell were treated for 24 h with medium that contained KN-93 (20 μM) and lacked serum, before the addition of GroPIns4P. The experimental condition used were the most suitable to obtain a complete blockage of CaMKII in the cells as reported in Fleming et al. (1998). Treatments with 50 μM GroPIns4P for 2 to 10 min and 10 ng/ml PDGF for 5 min were performed and the samples were analysed for the extent of TIAM1-GFP translocation as described in Section 2.4.4

The translocation of TIAM1-GFP to the plasma membrane induced by GroPIns4P was completely prevented by the presence of the KN-93 as shown in Figure 3.8a,b. This inhibition was comparable with that observed in the samples treated with PDGF in the presence of KN-93. CaMKII is therefore involved in GroPIns4P-dependent TIAM1 translocation to the plasma membrane.

3.3.6 Conclusion

GroPIns4P affects TIAM1 translocation to the plasma membrane. TIAM1-GFP translocates to the plasma membrane after 2 minutes of stimulation with GroPIns4P and at 10 minutes it starts to redistribute in the cytosol. This event is visible in parallel with the translocation of Rac1 to the plasma membrane and precedes ruffle formation. Treatment with GroPIns4P also produces a co-localization of Rac1 and TIAM1 to the plasma membrane thus confirming the hypothesis that the translocation of Rac1 and its exchange factor TIAM1 could be a key point in understanding the mechanism by which GroPIns4P produces an increase of membrane ruffling. GroPIns4P-dependent TIAM1 translocation requires the N-terminal PH domain. The inhibition of CaMKII by its specific inhibitor KN-93, prevents the translocation of TIAM1 to the plasma membrane induced by GroPIns4P, thus suggesting that this enzyme is an important effector for GroPIns4P.

3.4 GroPIns4P increases Ca^{2+}/calmodulin kinase II activity

3.4.1 General description

CaMKII is an oligomeric protein comprised of twelve 50-60-kDa subunits arranged as two stacked hexameric rings. The various CaM Kinase II subunits are characterise by an

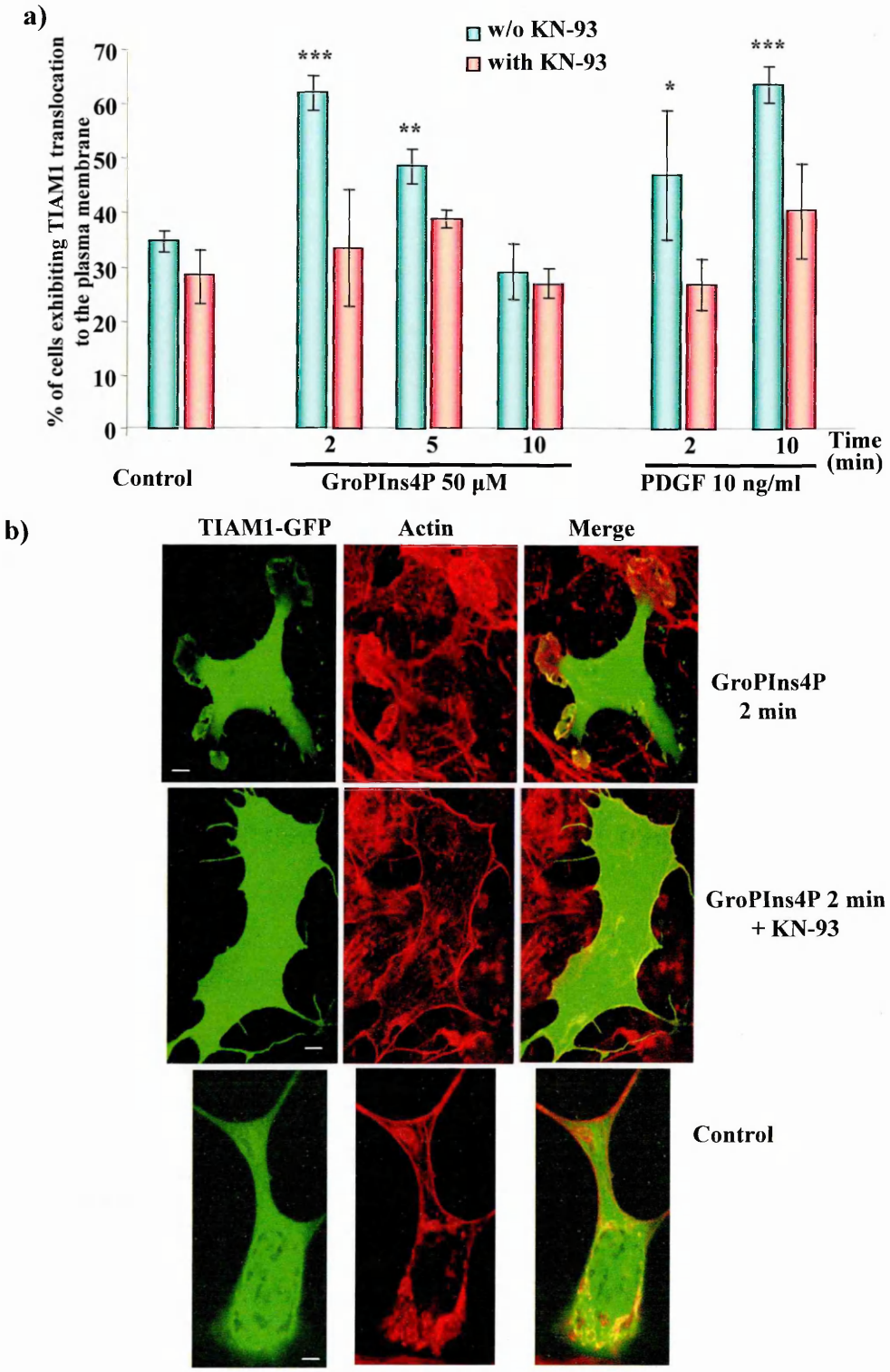

Figure 3.8 - Effect of GroPIns4P on TIAM1-GFP localisation in the presence and absence of KN-93. a) Sub-confluent NIH 3T3 cells were transfected with the pEGFP-c1199-TIAM1 construct as described in Section 2.3.4. Twenty-four h after transfection, cells were serum starved for 24 h and treated in parallel with KN-93 (20 µM), then were treated with GroPIns4P (50 µM) for 2 to 10 min or 10 ng/ml PDGF for 5 min, fixed and stained with TRITC-labelled phalloidin. The percentage of cells showing plasma membrane localisation of TIAM1 was quantified in blind as described in Section 2.4.4. The bars show the means (±SD) of four independent experiments, each performed in duplicate. *P<0.05, **P<0.01, versus control (Section 1.14). **b)** Localisation of TIAM1-GFP and actin in GroPIns4P-induced membrane ruffles, in the presence and absence of KN-93. Bar=20 µm

N-terminal catalytic region, a central regulatory domain containing an auto-inhibitory domain, a Ca^{2+}/CaM (calcium calmodulin complex) binding motif, a variable sequence and the C-terminal subunit association domain (Morris and Torok, 2001). The binding of the Ca^{2+}/CaM complex at the Ca^{2+}/CaM binding site allows an opening of the conformation of this kinase that exposes the catalytic site. The auto-phosphorylation that follows leads to a permanent activation of the kinase also in the absence of Ca^{2+} (for further information see Section 1.3.4 of the introduction and Figure 1.3.4 b).

The presence of active CaMKII is important for GroPIns4P-dependent translocation of TIAM1 to the plasma membrane. In order to see if GroPIns4P can activate this kinase, CaMKII activity assays were performed in NIH 3T3 cells.

3.4.2 GroPIns4P increases the Ca^{2+}/calmodulin kinase II activity

The CaMKII activity assay (kit from upstate) monitors the ability of the CaMKII present in a cell lysate to phosphorylate the autocamtide-2 substrate; this is a peptide corresponding to the auto-phosphorylation sequence of CaMKII. Intact NIH 3T3 cells were treated with 50 μM GroPIns4P or 10 ng/ml PDGF, lysed in a buffer that does not contain Ca^{2+} (ADBI) and then tested for CaMKII activity as described in Section 2.6.1 This procedure allows the measurement of the stimulus-dependent kinase activation. The fact that the kinase assay was performed in the absence of Ca^{2+} means that it was the proportion of auto-phosphorylated CaMKII in the lysate that was assessed. The level of maximal activation was evaluated by lysing the cells with a buffer containing 2 mM free Ca^{2+} (ADBII in Section 2.6.1). This Ca^{2+} concentration caused the activation of all the CaMKII enzymes present in the cell lysate, thus allowing the calculation of the maximal CaMKII activation level. The extent of CaMKII activation upon stimulation was expressed as percentage of the maximum (as described in Section 2.6.1).

GroPIns4P produced a rapid (within 90 sec) and transient increase of CaMKII activity: the percentage of activation expressed as a percentage of maximal activity was 13% in basal conditions and 24% after GroPIns4P stimulation (a 1,7-fold response over the basal). Within 5 min the level of CaMKII activation went back to the basal condition. PDGF (10 ng/ml) produced a 1,8-fold response in CaMKII activity versus the control within 150 sec of treatment (Fig. 3.9).

Ruffle formation can be visualised after a 2 min treatment with GroPIns4P and the activation of the CaMKII after 1 min and 30 sec; thus these two events could be considered as two sequential steps of the same pathway. The GroPIns4P-dependent activation of the CaMKII could be the starting point for TIAM1/Rac1 activation and ruffle formation.

3.4.3 CaMKII activity assay with cell lysates and purified CaMKII

The GroPIns4P-dependent CaMKII activation represented above was observed in intact cells. The molecular mechanism involved remained to be identified. Several possibilities could be taken into consideration: a direct interaction between GroPIns4P and the kinase; the involvement of other proteins (like PLC) that could be activated by GroPIns4P and consequently favour an increase in $[Ca^{2+}]_i$ that allowed the activation of the kinase; an extracellular action of GroPIns4P via receptor activation that initiates a signalling cascade in the cell.

If GroPIns4P acts like an agonist via a receptor, it should induce an increase in $[Ca^{2+}]_i$ that leads to CaMKII activation (Braun and Schulman, 1995). In a cell lysate, the Ca^{2+} stores are destroyed, thus it is not possible to create a signalling event due to agonist stimulation that triggers the release of Ca^{2+} from ER. To see if GroPIns4P can interact with a cell surface receptor, it was added directly to the cell lysate; under this condition the compound should be active only if it acts directly on the kinase and not through a receptor-dependent signalling. The cells were lysed in ADBI buffer (without Ca^{2+}) and then treated

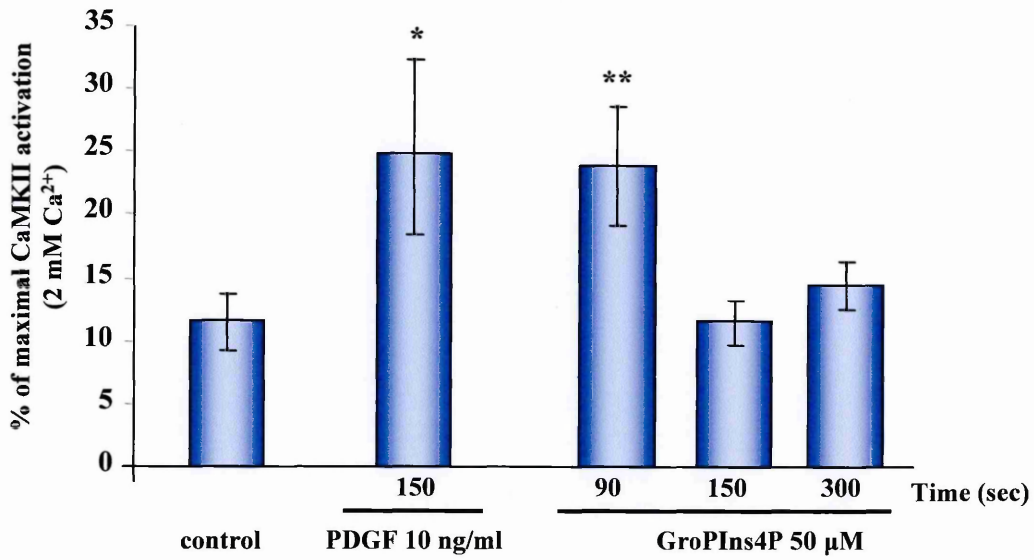

Figure 3.9 - GroPIns4P-dependent activation of CaMKII. NIH 3T3 cells were serum-starved for 20 h, treated with 50 µM GroPIns4P for 90, 150 or 300 sec, or PDGF for 150 sec and 300 sec, then lysed in a Ca^{2+}-free buffer (see Section 1.6.1). The cell lysate obtained in this way was used for the CaMKII activity assay. The extent of CaMKII activation is expressed as percentage of the maximal activation obtained when the cells were lysed in the presence of 2 mM free-Ca^{2+}. The bars are the means (±SD) of three independent experiments, each performed in duplicate. *P <0.05, **P <0.01, versus control (Section 1.14).

with GroPIns4P for different times at 37 °C, and subjected to the CaMKII activity assay. The activity of CaMKII was not affected by GroPIns4P when the treatment was done in NIH 3T3 cell lysate (Fig. 3.10a). This data indicated that GroPIns4P could act at the level of a membrane receptor or *via* an intracellular target that initiates a signalling pathway, which is impaired when the cells are lysed.

The above experiment was performed by lysing the cells in a buffer without Ca^{2+}, but it could not be excluded that the Ca^{2+} is important for the activity GroPIns4P. Thus a second set of experiments was performed by applying three different Ca^{2+} concentrations: without free Ca^{2+} (to evaluate the basal level), 0.5 μM free Ca^{2+} (an intermediate concentration in which the kinases present in the cell lysate are partially activated; Fig. 3.10b) and 2 mM free Ca^{2+} (to evaluate the maximal level of kinase activation) (Fig. 3.10c). In all these conditions GroPIns4P was not effective, however this data suggested that a direct interaction between GroPIns4P and CaMKII is probably not the mechanism involved in the kinase activation pathway.

In order to confirm that GroPIns4P does not activate the kinase by direct interaction, the activity assay was performed with purified CaMKII instead of cell lysate. The purified enzyme was pre-incubated with GroPIns4P at 30 °C for 10 min prior to performing the activity assay: no effect of GroPIns4P was observed, thus excluding a direct activation of the kinase under these conditions (Fig. 3.11).

3.4.4 Conclusion

GroPIns4P produce an increase in CaMKII activity only when added to intact cells. This activation is lost both when GroPIns4P is added directly to cell lysates or to the purified kinase. These data suggests that GroPIns4P does not act directly on the kinase but that there is another element involved in a step upstream of this activation. Indeed,

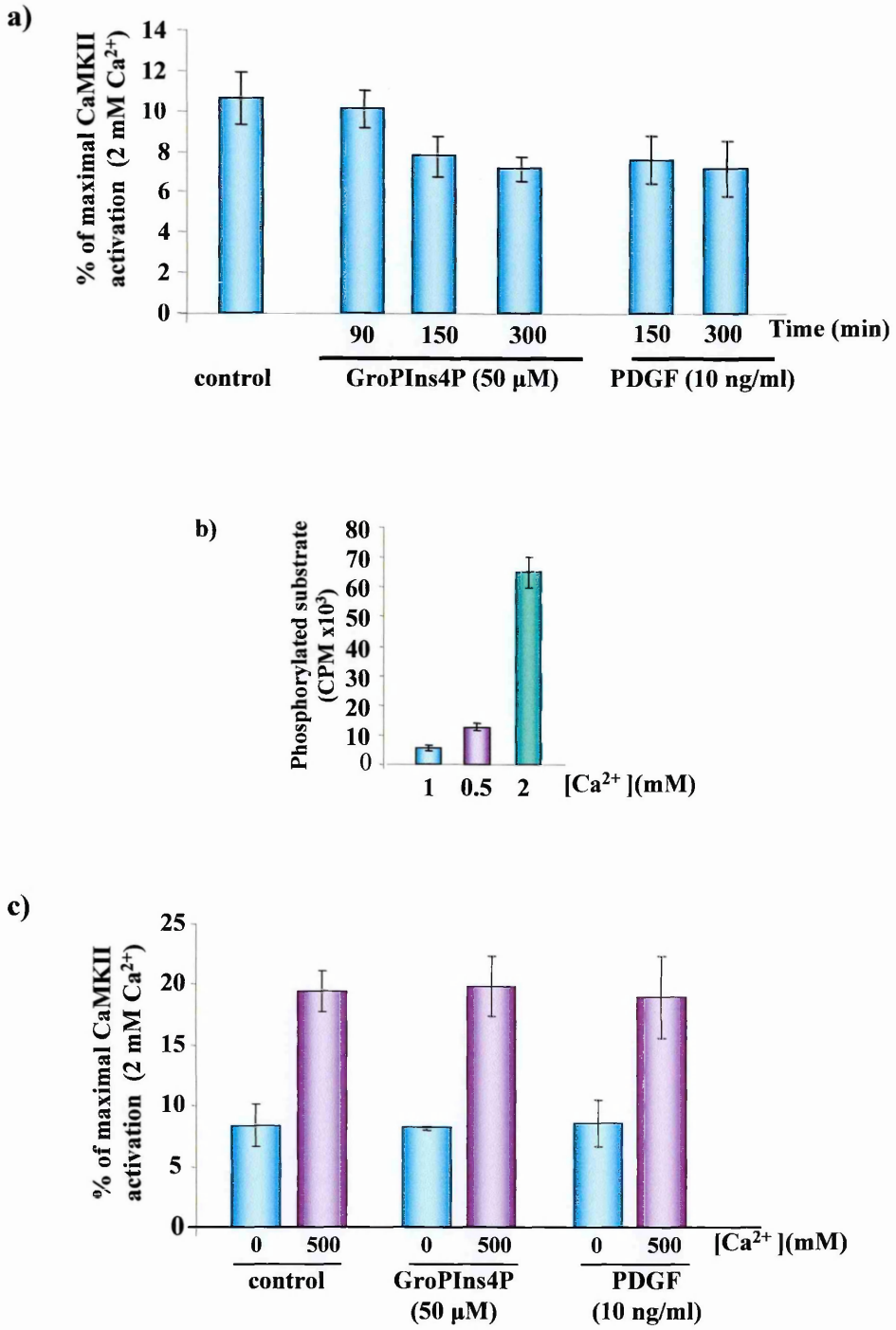

Figure 3.10 - CaMKII activity assay with cell lysate. NIH 3T3 cells were lysed in assay buffer ADBI (see Section 2.6.1), then the lysate were incubated at 37 °C with 50 µM GroPIns4P or 10 ng/ml PDGF prior to performing the CaMKII activity assay. **a)** The experiment was performed in a Ca^{2+} free assay buffer and the samples were treated for different times (from 90 sec to 5 min) with GroPIns4P or PDGF. **b)** Basal CaMKII activity at 3 different Ca^{2+} concentrations (0 Ca^{2+}, 500 nM or 2 mM); the CPM represents the amount of [^{32}P]phosphate attached to the substrate. **c)** The cells were lysed in buffers with three different free Ca^{2+} concentrations (0 Ca^{2+}, 500 nM or 2 mM), then were treated for 90 sec with GroPIns4P or PDGF. The values are reported as percentage of maximal activation that is evaluated when the concentration of Ca^{2+} is maximal (2 mM). The bars are the means (±SD) of two independent experiments, each performed in duplicate.

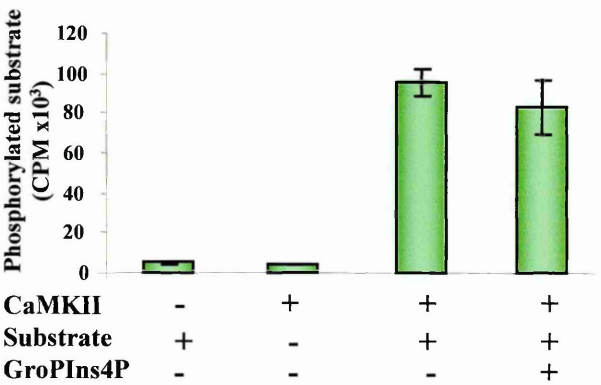

Figure 3.11 - CaMKII activity assay with purified CaMKII. The activity of purified CaMKII was tested by using the assay kit (Section 2.6.1). The effect of GroPIns4P on the kinase was evaluated by incubating the compound at 50 μM concentration with the CaMKII for 10 min at 30 °C prior to performing the activity assay. The bars are the means (±SD) of two independent experiments, each performed in triplicate.

GroPIns4P could be a ligand for a specific (still unknown) receptor, or it could activate an intracellular target that could lead to CaMKII activation, perhaps by increasing the $[Ca^{2+}]_i$.

3.5 Effect of intracellular Ca^{2+}chelation

3.5.1 CaMKII activity assay in the presence of BAPTA

The activation of CaMKII involves an increase in $[Ca^{2+}]_i$ that, once complexed with calmodulin, interacts with CaMKII allowing conformational changes that favour the auto-phosphorylation of the enzyme and consequently its activation (Braun and Schulman, 1995). It could be hypothesized that GroPIns4P activates the kinase by modulating the $[Ca^{2+}]_i$ concentration. In order to see whether changes in $[Ca^{2+}]_i$ are involved in GroPIns4P-dependent activation of CaMKII, the CaMKII activity assay was performed in the presence of BAPTA-AM, an intracellular calcium chelator. Twenty μM BAPTA-AM (a concentration suitable to cause a complete blockage of CaMKII activity; Fleming et al., 1998) was added to NIH 3T3 cells 30 min before stimulation, to allowed its incorporation inside the cells. The treatment with GroPIns4P was performed for 90 sec (enough to see an increase in CaMKII activity) and compared with PDGF treatment, which is known to activate CaMKII by increasing $[Ca^{2+}]_i$ (Fleming et al., 1998) (see Section 2.6.1).

GroPIns4P, as well as PDGF, were not able to activate the kinase when the intracellular calcium was chelated (Fig. 3.12). From these data it was clear that GroPIns4P needs $[Ca^{2+}]_i$ to activate the kinase.

3.5.2 TIAM1 translocation to the plasma membrane in the presence of BAPTA.

As described above, TIAM1-GFP over-expressed in NIH 3T3 translocates to the plasma membrane upon stimulation with GroPIns4P, and this translocation is blocked by

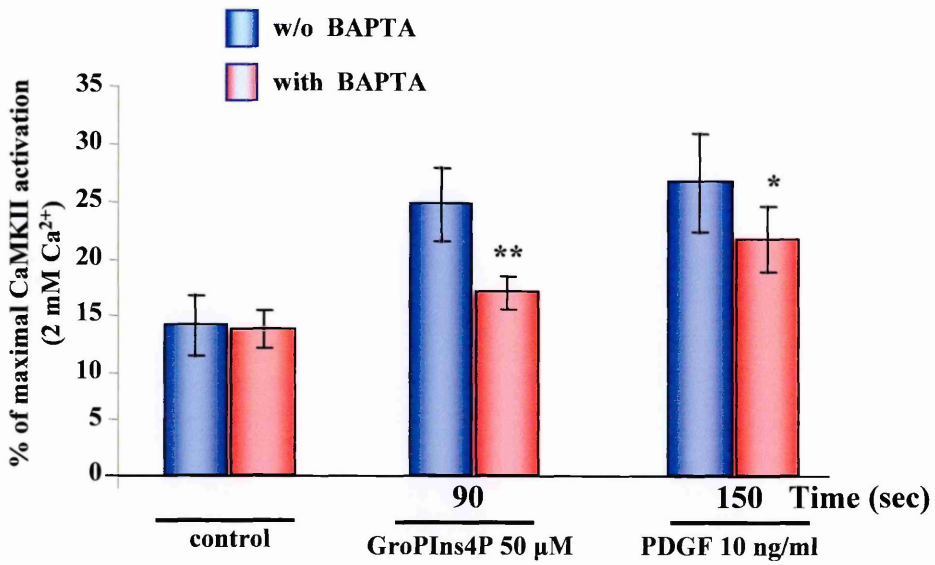

Figure 3.12 - CaMKII activity assay in the presence or absence of BAPTA. NIH 3T3 cells were serum-starved for 24 h and pre-incubated 30 min with BAPTA (20 µM) before treatment with GroPIns4P (50 µM) for 90 sec or PDGF (10 ng/ml) for 150 sec. The cells were then lysed in a Ca^{2+}-free buffer (as described in Section 2.6.1), and the cell lysate was tested for CaMKII activity. The extent of CaMKII activation is expressed as a percentage of the maximal activation obtained when the cells were lysed in the presence of 2 mM free-Ca^{2+}. The bars are the means (±SD) of three independent experiments, each preformed in duplicate. *P>0.07 **P<0.05, versus samples without BAPTA (Section 1.14).

the CaMKII-inhibitor KN-93. Moreover, NIH 3T3 cells treated with GroPIns4P shows an increase in the CaMKII activity and this increase does not occur when $[Ca^{2+}]_i$ is chelated by BAPTA. Taken together, this data suggested that the GroPIns4P-dependent TIAM1 translocation to the plasma membrane requires an increase in $[Ca^{2+}]_i$ concentration that in turn activates the CaMKII. However, there was no direct proof that $[Ca^{2+}]_i$ was important for the GroPIns4P-dependent translocation of TIAM1 to the plasma membrane. To test this possibility directly, immuno-fluorescence experiments were performed using NIH 3T3 cells transfected with TIAM1-GFP and treated with BAPTA-AM before stimulation with GroPIns4P. The cells were treated with GroPIns4P for 2 to 5 min and then the samples were analysed for the extent of TIAM1-GFP translocation (see Section 2.4.4).

In line with initial observations (figure 3.13), in the presence of the calcium chelator, GroPIns4P was not able to induce TIAM1-GFP translocation to the plasma membrane. The Figure 3.13 shows the quantification of the extent of TIAM1 translocation to the plasma membrane in the presence and absence of BAPTA (3.13a), also with two representative images of cells (3.13b). This treatment also prevented the membrane ruffling (3.13b).

3.5.3 Conclusion

The chelation of $[Ca^{2+}]_i$ completely abolished the effects of GroPIns4P by both preventing the CaMKII activation and the translocation of TIAM1 to the plasma membrane. This observation supported the idea that GroPIns4P needs free $[Ca^{2+}]_i$ for its activity. A possible model that could explain the action of GroPIns4P could be that treatment with GroPIns4P produces an increase in $[Ca^{2+}]_i$ that activates CaMKII, which phosphorylates TIAM1 favouring its translocation to the plasma membrane. Thus, by chelating the $[Ca^{2+}]_i$, these events are impaired.

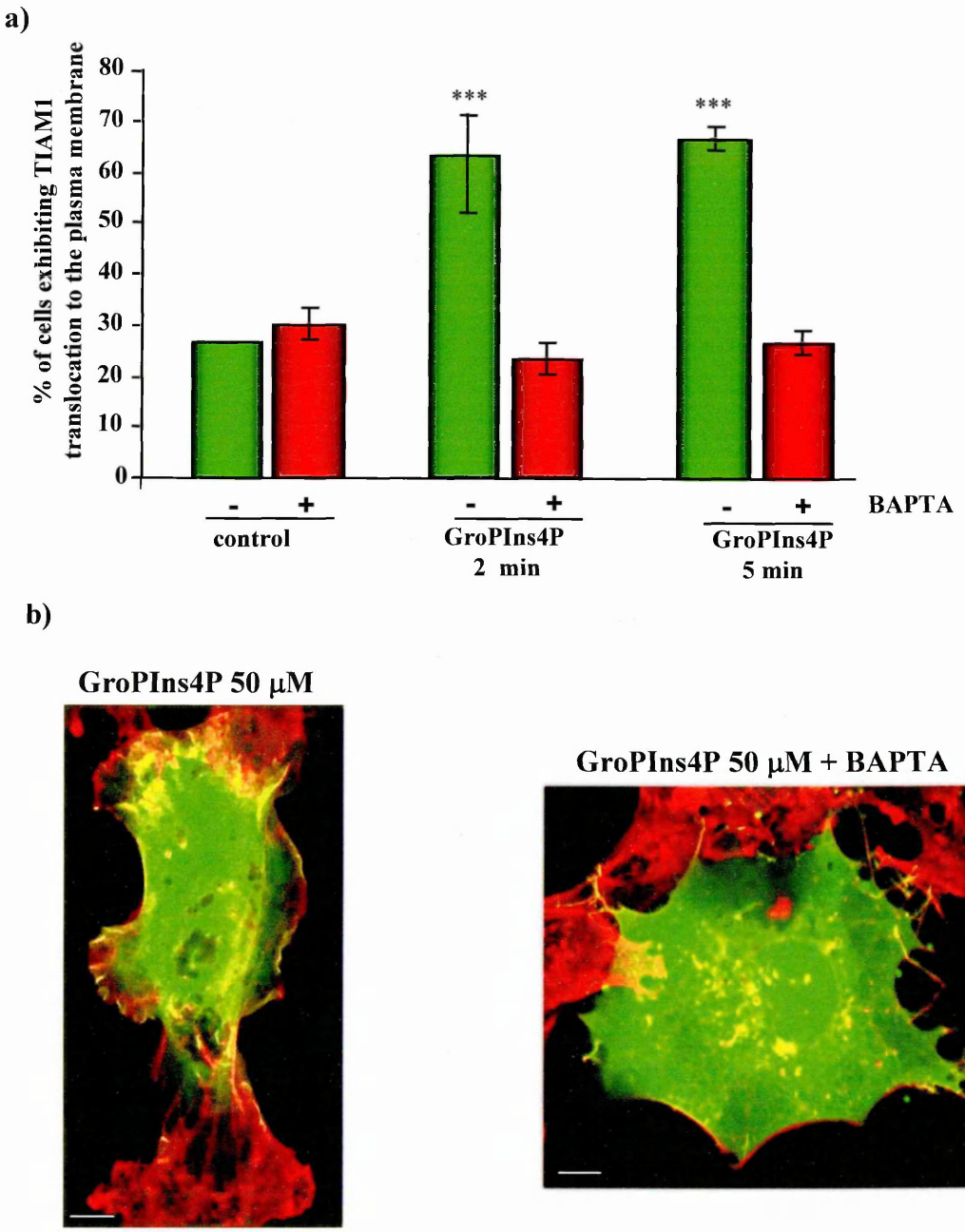

Figure 3.13 - Effect of BAPTA on GroPIns4P-dependent TIAM1 translocation to the plasma membrane. a) Sub-confluent NIH 3T3 cells were transfected with the pEGFP-c1199-TIAM1 construct as described in Section 2.3.4. Twenty-four h after transfection, cells were serum starved for 24 h and then were treated with 20 μM BAPTA for 30 min prior to being stimulated with GroPIns4P (50 μM) for 2 or 5 min. After fixation, cells were stained with TRITC-labelled phalloidin. The percentage of cells showing plasma membrane localisation of TIAM1 was quantified in blind as described in Section 2.4.4. The bars are the means (±SD) of two independent experiments, each performed in duplicate. ***P<0.001, versus control (Section 1.14). **b)** Localisation of TIAM1-GFP and actin in GroPIns4P-induced membrane ruffles, in the presence and absence of BAPTA. Bar=20 μm

3.6 GroPIns4P modulates the intracellular Ca^{2+} concentration

3.6.1 General description

The data described above suggested that the $[Ca^{2+}]_i$ could be the key element in GroPIns4P-dependent Rac1/TIAM1 activation and ruffle formation. GroPIns4P could activate CaMKII by increasing the concentration of $[Ca^{2+}]_i$. For this reason, cell imaging was performed in NIH 3T3 cells labelled with Fluo3-AM, a dye that fluoresces upon Ca^{2+}-binding. Cells were imaged using an Olympus IX70 microscope equipped with a TILL Photonics imaging system. After loading with the dye, NIH 3T3 cells were treated with GroPIns4P and the change in $[Ca^{2+}]_i$ levels measured as an increase in fluorescence (as described in Section 2.5). This technique allowed the measurement of any rapid and transient $[Ca^{2+}]_i$ variation within single living cell.

3.6.2 GroPIns4P increases intracellular Ca^{2+} levels

NIH 3T3 cells were plated in 100 mm dishes, and the following day were loaded with Fluo3-AM for 30 min in a HEPES-buffered saline solution and then placed on the stage of microscope (as described in Section 2.5.1). The live imaging was performed by taking two sequential movies: a first one taken each 200 ms for 2 min (to monitor any rapid $[Ca^{2+}]_i$ variation) and a second one taken each sec for 6 min, to see what happened within 8 min from the stimulation. So that the basal level of fluorescence at the initial state was known, the treatment with GroPIns4P (50 μM) was performed 30 sec after the beginning of the movie. In each time lapse movie, the increase in fluorescence obtained upon stimulation was represented by a gradual change in colour (from blue to red as minimal and maximal fluorescence level, respectively) (Fig. 3.14 a). Each cell was selected and the fluorescence of each frame calculated by the TILL Photonics imaging system. The

background signal was determined from the average of three different areas adjacent to the cell. The fluorescence values, after background subtraction, were then plotted as an increase in fluorescence per second.

For each experiment a series of controls were performed: PDGF (10 ng/ml) and ATP (100 μM) were added for the receptor-induced $[Ca^{2+}]_i$ increase, and ionomycin (10 μM) for ionophores-mediated Ca^{2+} entry (and to obtain the maximal calcium level). In each experiment NIH 3T3 cells were treated with GroPIns4P and then washed with buffer in order to allow the $[Ca^{2+}]_i$ to return to the physiological concentration (see Section 2.5.1). Other stimuli were then given to evaluate the level of $[Ca^{2+}]_i$ increase upon receptor-dependent stimulation (PDGF and ATP), or the maximal $[Ca^{2+}]_i$ increase obtained with non-physiological stimuli (ionophores). These effects were then compared with that obtained upon treatment with GroPIns4P. For each sample, from 5 to 12 cells were monitored for at least 8 min.

$[Ca^{2+}]_i$ can be estimated from measurements of the Ca^{2+} indicator fluorescence at maximal and minimal $[Ca^{2+}]_i$ (Fmax and Fmin), obtained by adding ionophores and Ca^{2+} chelators respectively. The single wavelength measurements, performed with the Fluo3-AM (a nonratiometric Ca^{2+} indicator), do not allow the $[Ca^{2+}]_i$ to be calculated. Fmax and Fmin cannot be obtained unless the dye concentration is precisely estimated or in vivo calibration is performed in the same cell. The estimation of fluorescence intensity of such nonratiometric Ca^{2+} indicators has been often reported not as $[Ca^{2+}]_i$, but as the pseudoratio (ΔF/F) indicated by the following formula: ΔF/F0=[(F-F0)/(F0-B)] where F is the maximal level of fluorescence obtained upon stimulation, F0 is the fluorescence at the basal condition and B is the background (Klepeis et al., 2001; Takahashi et al., 1999). Apart from dye saturation, ΔF/F0 is thought to approximately reflect the $[Ca^{2+}]_i$ if there is no change in dye concentration, intracellular environment or path length (Svoboda et al., 1997) (See Section 2.5.2).

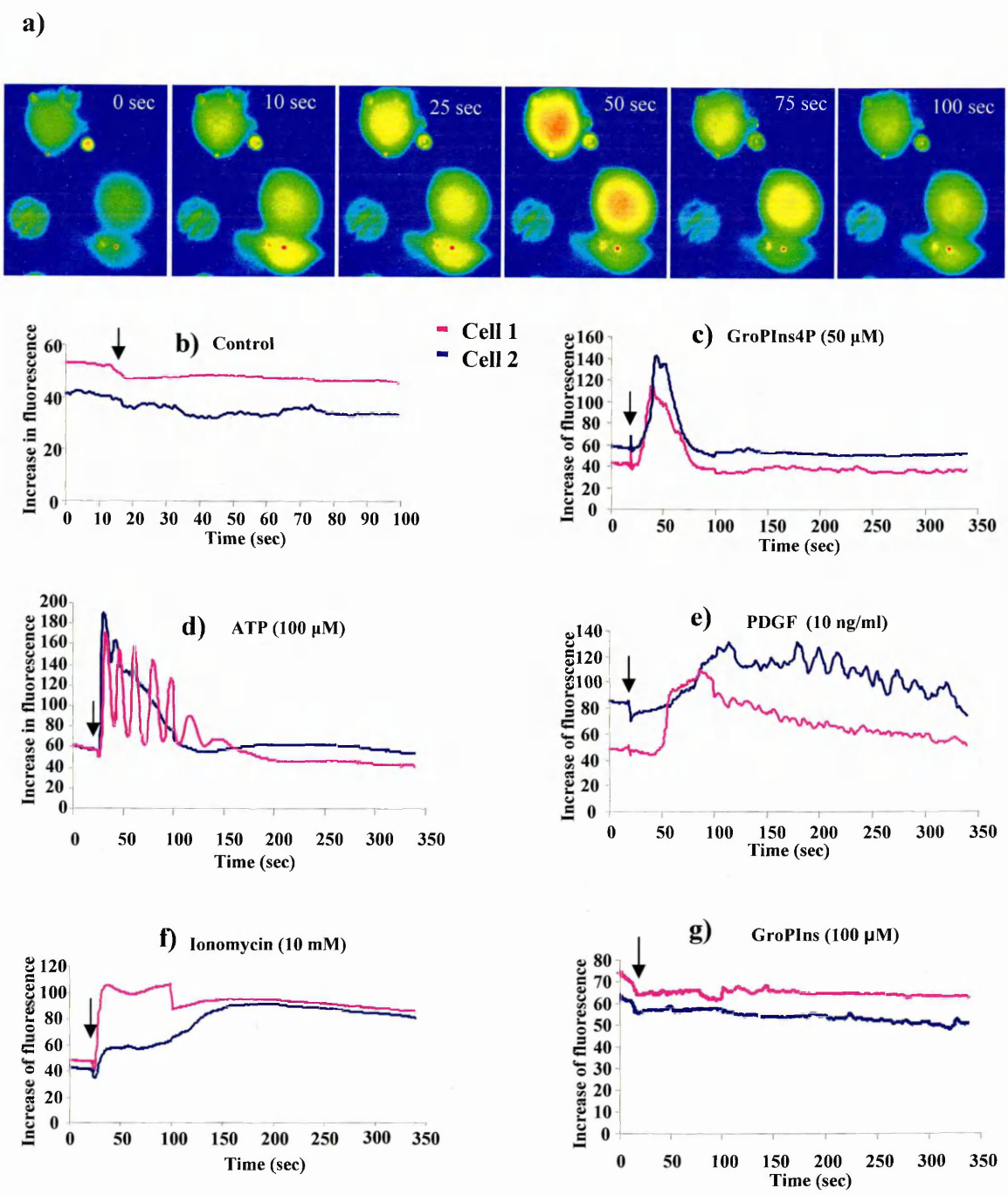

Figure 3.14 – Till photonics live imaging of fluo3-AM loaded NIH3T3 cells. Cells were incubated with 4 µM fluo3-AM for 30 min at 37 °C. After two washes in HEPES-buffered saline solution, the cells were positioned on the stage of a Till Photonic microscope (as described Section 2.5.1). For each experiment, the cells were scanned for 30 s to establish a base-line fluorescence reading before the sequential addition of the stimuli. All incubations were carried out while continuously scanning the cells every 200 ms for two min (first movie) and each second for 6 min (second movie) (as explained in Section 2.5.1). **a)** Selected frames from the time lapse movie obtained upon 50 µM GroPIns4P stimulation. The following plots represents the kinetics of $[Ca^{2+}]_i$ increase caused by 50 µM GroPIns4P (**c**), 100 µM ATP (**d**), 10 ng/ml PDGF (**e**), 10 µM ionomycin (**f**) and 100 µM GPI (**g**). The effect of HEPES buffer addition is represent in **b**. The arrows indicate the time point in which the stimulus was given to the cell. Each plot represents the behaviour of two cells (pink and blue)

In order to quantify the effect of GroPIns4P and compare it with the other stimuli, the fluorescence variation was calculated as the pseudoratio ΔF/F. The Lag phase (Time between the stimulation and the increase of Ca^{2+}), the time of stimulation (duration of the stimulus) and the percentage of responsive cells were also measured (Table 3.1).

The treatment with GroPIns4P (50 μM), produced a ΔF/F of 1.08±0.14 in approximately 58% of the cells analysed per sample (Fig. 3.14 c, Table 3.1). The Ca^{2+} increase obtained was rapid (within 25 sec) and transient (the $[Ca^{2+}]_i$ increase persisted for 30-50 sec); then the intracellular calcium concentration went back to the basal level. Figure 3.14 a shows selected frames from the time lapse movie obtained upon GroPIns4P stimulation. GroPIns4P was also active at lower concentration than 50 μM, but the stimuli were given to the cells at a concentration suitable for obtaining the highest response (according to Mancini et al., 2003).

ATP was applied to the cells in a range of concentration from 1 to 100 μM , to identify the condition that caused the maximal cellular response. Thus, 100 μM ATP was used routinely in all subsequent experiments. The treatment with ATP caused a ΔF/F of 1.52±0.09 in the 82% of the cells, a few seconds after its addition, then there was a prolonged oscillation in $[Ca^{2+}]_i$ (Fig. 3.14 d Table 3.1). The effect of PDGF (10 ng/ml) was similar to GroPIns4P for the ΔF/F (0.94±0.08) and for the number of responsive cells per sample (65%), whereas, the appearance of the Ca^{2+} spike was delayed (100-120 sec after the treatment) and more prolonged (100 sec) (Fig. 3.14 e, Table 3.1). Ionomycin produced a ΔF/F of 1.33±0.16 in the 96% treated cells. It showed the same rapid Ca^{2+} increase as seen in ATP-treated cells, but the rise was more sustained (250 sec) (Fig. 3.14 f, Table 3.1). Upon stimulation with ATP and ionomycin the level of fluorescence reached the saturation, thus the ΔF/F0 value could not be considered proportional to the increment in $[Ca^{2+}]_i$. In fact, the formula used to calculate the ΔF/F0 can approximately reflect the $[Ca^{2+}]_i$ variation only when the increase in fluoresce does not reach saturation

	ΔF/F0	LAG PHASE (s)	TIME OF STIM (s)	% OF CELLS
Control	**0.06 ± 0.16**			**2.5 ± 8**
GroPIns4P	**1.08 ± 0.14*****	**25 ± 4**	**45 ± 16**	**58 ± 3**
PDGF	**0.94 ± 0.08*****	**122 ± 16**	**247 ± 112**	**65 ± 9**
ATP	**1.52 ± 0.09*****	**8 ± 1**	**115 ± 7**	**82 ± 3**
Ionomycin	**1.33 ± 0.16*****	**18 ± 3**	**249 ± 13**	**96 ± 1**
GPI	**0.06 ± 0.03**			**0**

Table 3.1 - Quantification of the $[Ca^{2+}]_i$ increase. The effect of GroPIns4P (50 μM), ATP (100 μM), PDGF (10 ng/ml), ionomycin (10 μM) and GroPIns (100 μM) in increasing $[Ca^{2+}]_i$ levels was calculated as changes in fluorescence relative to the base line [pseudo ratio: ΔF/F0=(F-F0)/(F0-B)]. Lag phase (time between the stimulation and the increase of Ca^{2+}), the time of stimulation (duration of the stimulus) and the percentage of responsive cells were also measured (as described in Section 1.5.2). The number of responsive cells is given as percentage of the total number analysed per sample. ATP, PDGF and ionomycin were used as positive controls. The numbers represents the mean (±SE) of at least 10 independent experiments for GroPIns4P and of 5-8 experiments for the other stimuli. ***$P<0.001$, versus control (Section 1.14).

(Svoboda et al., 1997). In the case of GroPIns4P and PDGF, the increase in fluorescence did not reach the saturation, thus the values of ΔF/F0 calculated could reflect the real changes in $[Ca^{2+}]_i$.

Comparing the effect of GroPIns4P with the other stimuli, it was clear that the extent of $[Ca^{2+}]_i$ increase produced by GroPIns4P was high enough to activate a signalling pathway, similar to PDGF treatment. On the other hand, the kinetics were different, as suggested by the divergence in the duration of the $[Ca^{2+}]_i$ rise and the time of response. GroPIns (100 μM) was also tested for the ability to increase the $[Ca^{2+}]_i$ but it was not active (Fig. 3.14 g, Table 3.1).

The rapid and transient increase in $[Ca^{2+}]_i$ produced by GroPIns4P could be considered as an early event that allowed CaMKII activation and TIAM1 translocation to the plasma membrane.

3.6.3 Characterization of GroPIns4P-dependent Ca^{2+} increase

The results described above led me to perform experiments aiming at elucidating the mechanism by which GroPIns4P increases the intracellular calcium concentration. In order to see if the increase in $[Ca^{2+}]_i$ depends on the liberation of Ca^{2+} from the intracellular stores, the same experiment was performed in a Ca^{2+}-free buffer containing 1 mM EGTA (as described in Section 2.5.1; Klepeis et al., 2001). In the absence of extracellular Ca^{2+} it was possible to create an inverse gradient that favoured the exit of $[Ca^{2+}]_i$ (more concentrated inside) from the cell. In this condition, all the signals that caused the opening of Ca^{2+} channels or that mimic these channels by creating pores on the plasma membrane (ionomycin), instead of increasing $[Ca^{2+}]_i$, produces a complete Ca^{2+} depletion. Whereas agonists like ATP and PDGF that produce and increase in $[Ca^{2+}]_i$ by acting at the level of intracellular stores, are still active (Kuriyama et al., 1991; Ryu et al., 2003).

The treatment with GroPIns4P caused an increase in $[Ca^{2+}]_i$ levels also in the presence of EGTA, and so the action of GroPIns4P should not lead to the influx of extracellular Ca^{2+}, but is likely to activate the liberation of Ca^{2+} from intracellular stores (endoplasmic reticulum-ER) (Fig. 3.15 a, Table 3.2). In the same experiment, treatment with ionomycin (10 μM) caused a complete depletion of $[Ca^{2+}]_i$ (Fig. 3.15).

The release of Ca^{2+} from the ER can be controlled by $[Ca^{2+}]_i$ itself or by a variety of messengers and molecules such as IP_3, cyclic ADP ribose (cADPR), nicotinic acid adenine dinucleotide phosphate (NAADP) and sphingosine-1-phosphate (S1P) that either stimulate or modulate the release channel from the internal stores (Berridge et al., 2003). The possible involvement of IP_3 in the GroPIns4P-dependent pathway was analysed. Many stimuli such as growth factors, cytokines, and hormones can function through phospholipase C (PLC) to generate IP_3, which in turn stimulates the release of Ca^{2+} by acting at the level of IP_3 receptors at the ER (see Section 1.3.1). GroPIns4P could act at the PLC level generating IP_3 from $PI4,5P_2$ or directly at the level of the IP_3 receptor at the ER.

A specific inhibitor of PLCs (U-73122) was applied to the cells at a concentration of 5 μM, in order to completely prevent their activation (Bleasdale et al., 1990). In this way, the possible action of GroPIns4P at the level of these enzymes was tested. The result was a complete inhibition of GroPIns4P-dependent $[Ca^{2+}]_i$ rise (Table 3.2).

The inactive analogue of U-73122 (U-73443) was also tested in the assay and, as expected, the GroPIns4P-dependent $[Ca^{2+}]_i$ release was not blocked (Table 3.2). Thus, GroPIns4P acts at the intracellular level to produce an increase of $[Ca^{2+}]_i$ and a PLC is involved in the GroPIns4P-dependent pathway of $[Ca^{2+}]_i$ mobilisation. Under the same inhibitory conditions, ATP and PDGF were also not able to increase the $[Ca^{2+}]_i$ (Table 2).

PLCs can be activated by several mechanisms: PLCβ is activated by interaction with Gα or βγ subunits of heterotrimeric G-proteins, upon G-protein coupled receptor (GPCR) activation, whereas the PLCγ is tyrosine phosphorylated upon activation of tyrosine kinase receptors (RTK) (Rebecchi and Pentyala, 2000); see also Section 1.3.3).

a)

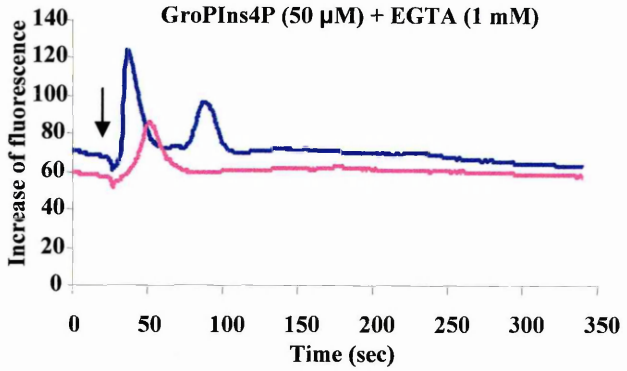

b)

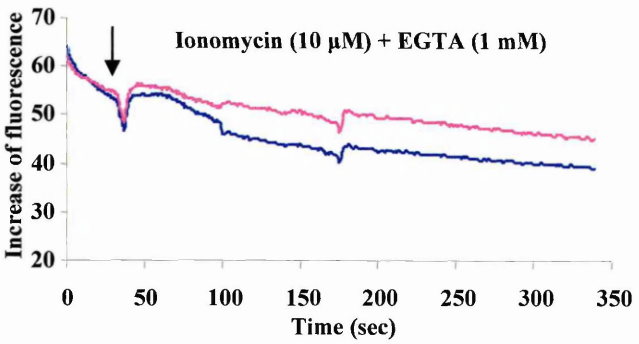

Figure 3.15 - Till photonics live imaging of fluo3-AM loaded NIH 3T3 cells. Cells were incubated with 4 µM fluo3-AM, for 30 min at 37 °C. After two washes in HEPES-buffered saline solution, the cells were positioned on the stage of a Till Photonic microscope (as described in Section 2.5.1). For each experiment, the cells were scanned for 30 sec to establish a base-line fluorescence reading before the sequential addition of the stimuli. All incubations were carried out while continuously scanning the cells every 200 msec for two min (first movie) and each second for 6 min (second movie) (as explained in methods). The plots represents the kinetics of $[Ca^{2+}]_i$ increase caused by 50 µM GroPIns4P **(a)** or 10 µM ionomycin **(b)** in the presence of 1 mM EGTA. The arrows indicate the point in which the stimulus was given to the cell. Each plot represents the behaviour of two cells (pink and blue)

	ΔF/F0	LAG PHASE (s)	TIME OF STIM (s)	% OF CELLS
EGTA GroPIns4P	0.94 ± 0.13***	19 ± 5	75 ± 17	81 ± 6
U-73122 GroPIns4P	0.05 ± 0.0 1	0	0	0
U-73122 PDGF	0.08 ± 0.06	0	0	0
U-73122 ATP	0.07 ± 0.10	0	0	0
U-73443 GroPIns4P	1.1 ± 0.3	20 ± 4	13 ± 9	56 ± 6
Genistein GroPIns4P	0.29 ± 0.06	54 ± 15	138 ± 23	22 ± 16
Genistein PDGF	0.19 ± 4	7 ± 2	70 ± 2	5 ± 3
Genistein ATP	1.16 ± 0.23***	6 ± 1	69 ± 11	78 ± 5
SU6656 /PP2 GroPIns4P	0.03 ± 4	0	0	0
SU6656/PP2 PDGF	0.08 ± 4	0	0	0
SU6656/PP2 ATP	0.75 ± 0.3***	6 ± 1	80 ± 11	90 ± 5

Table 3.2 - Effect of inhibitors in GroPIns4P-dependent $[Ca^{2+}]_i$ increase. The $[Ca^{2+}]_i$ was calculated as changes in fluorescence relative to the base line [pseudo ratio: ΔF/F0=(F-F0)/(F0-B)]. The lag phase (time between the stimulation and the increase of $[Ca^{2+}]_i$), the time of stimulation (duration of the stimulus) and the percentage of responsive cells were also measured (as described in Section 2.5.2). The number of responsive cells is given as percentage of the total number analysed per sample. The inhibitors used are EGTA (1mM), U-73122 (5μM), genistein (10 μM) and SU6656 or PP2 (10 μM). ATP (100 μM), and PDGF (10 ng/ml) were used as positive controls. The numbers represents the mean (±SE) of 6 different experiments.***$P<0.001$, versus control (Section 1.14).

GroPIns4P could act at different levels, via a receptor, directly on PLC, on heterotrimeric G-proteins or on a tyrosine kinase.

Using genistein, an inhibitor of receptor and non-receptor tyrosine kinases, it was possible to prevent the GroPIns4P-induced increase in $[Ca^{2+}]_i$ (Table 3.2). NIH 3T3 cells were treated for 30 min with 10 μM genistein (a concentration suitable to obtain a complete blockage of cellular tyrosine kinases; Akiyama et al., 1987) before stimulation with 50 μM GroPIns4P. The specificity of the inhibitor was assessed by treating the cells with PDGF, which activated RTK, and ATP which is an agonist of GPCR. As expected, the PDGF did not induced any $[Ca^{2+}]_i$ rise whereas ATP was still active in the presence of genistein (Table 3.2). This data indicated that the action of GroPIns4P is through a phosphorylation-dependent signal and probably could involve a PLCγ, known to be activated upon tyrosine kinase-dependent phosphorylation (Rhee, 2001).

The identification of the tyrosine kinase that could be activated by GroPIns4P was achieved by using a set of specific inhibitors. The addition of SU6656 or PP2 (Src family kinases specific inhibitors) at a concentration of 10 μM (suitable to have a specific inhibition of Src family kinases; Bain et al., 2003) completely prevented the increase in $[Ca^{2+}]_i$ levels produced by the stimulation with GroPIns4P in NIH 3T3 (Table 3.2). In the same assay, ATP was still able to increase the $[Ca^{2+}]_i$ thus confirming that the inhibitor has a specific effect; whereas the PDGF pathway was completely blocked (Table 3.2), the Src family kinases could be a good candidate as target for GroPIns4P. It remained to be determined if there was a direct activation of the kinase by GroPIns4P or whether there was another unknown element that could mediate the GroPIns4P-dependent Src family kinase activation and $[Ca^{2+}]_i$ increase.

3.6.4 Conclusion

GroPIns4P is able to induce a rapid and transient increase in $[Ca^{2+}]_i$ concentration

acting at the intracellular level. Using PLC inhibitors like U-73122 the effect of GroPIns4P was blocked, thus implying that a PLC is involved in the GroPIns4P-dependent pathway of $[Ca^{2+}]_i$ mobilisation. The GroPIns4P-dependent increase in $[Ca^{2+}]_i$ was also prevented by the addition of Genistein, a tyrosine kinase inhibitor. This data suggests that PLCγ could be involved in this pathway. Among the tyrosine kinases, the Src family of tyrosine kinases is the best candidate as mediator of GroPIns4P activity.

3.7 GroPIns4P increases IP_3 concentration in cells

3.7.1 General description

The GroPIns4P-dependent increase in $[Ca^{2+}]_i$ involves the action of a PLC and a tyrosine kinase since inhibitors of these enzymes cause a block in its activity. To confirm the involvement of a PLC in the GroPIns4P-dependent $[Ca^{2+}]_i$ increase, the intracellular concentration of IP_3 was measured. Intact cells or lysates of NIH 3T3 cells were treated with 50 μM GroPIns4P and the intracellular concentration of IP_3 measured using an IP_3 assay kit (see Section 2.6.3).

3.7.2 GroPIns4P increases IP_3 production both in intact and lysed NIH 3T3 cells

After treating NIH 3T3 cells with GroPIns4P, the IP_3 was extracted by the perchloric acid method (see Section 2.6.3). Then, the "D-myo-Inositol 1,4,5-trisphosphate (IP_3) [^{3}H] Biotrak assay system" from Amerhsham was used to determine the concentration of IP_3. Stimuli like thrombin (5U/ml), PDGF (10ng/ml) or ATP (100μM) were used to asses the viability of the assay (as described in Section 2.6.3).

The quantification of IP_3 provided by the kit is based on competition between [^{3}H] IP_3 (the tracer) and unlabelled IP_3 produced by the samples for the interaction with a

binding protein, prepared from bovine adrenal cortex. Since the binding protein for IP_3 was also able to bind the GroPIns4P with an affinity 5000-times lower than that of IP_3, this generated a potential source of error. This figure was obtained by performing a competition binding assay between IP_3 and an increasing concentration of GroPIns4P. The concentration of GroPIns4P added to the sample was 50 μM in a volume of 200 μl, which corresponds to 4 nmol, and the amount of IP_3 produced by stimulation ranges from 0.2 to 7 pmol, thus the non specific binding of GroPIns4P to the resin could partially compete with the IP_3, therefore altering the calculation of the IP_3 concentration. For this reason, the GroPIns4P-dependent increase in IP_3 was compared with an untreated sample to which the same amount of GroPIns4P as used for the stimulation was added just for the quantification step.

In intact cells, a 15% increase in IP_3 upon 2 min of treatment with GroPIns4P could be identified; this effect was comparable with that obtained with PDGF (25% increase), whereas ATP and thrombin produced a higher increase in IP_3 (70 and 100%, respectively), as shown in Figure 3.16. This data confirmed that the Ca^{2+} increase produced by GroPIns4P in NIH 3T3 cells is due to the activation of a PLC.

The increase was even higher using cell lysates; in this case the cells were harvested and subjected to mechanical lysis (as described in Section 2.6.3) before being stimulated with the various stimuli. After 5 min of treatment with GroPIns4P, a 20% increase in IP_3 was seen and by increasing the time of incubation to 15 min an 80% increase could be observed (Fig. 3.17). Even if the GroPIns4P-dependent increase in IP_3 concentration was seen in cell lysates as well as in whole cells, it could not be excluded that a potential action of GroPIns4P was *via* receptor, since the mechanical lysis did not uncouple receptors from their related PLCs. This was demonstrated by the increase in IP_3 concentration induces by thrombin (from 40% after 5 min to 150% within 15 min), an agonist of PAR family receptors (GPCR), in the same lysate used for the previous experiments (Fig.3.17).

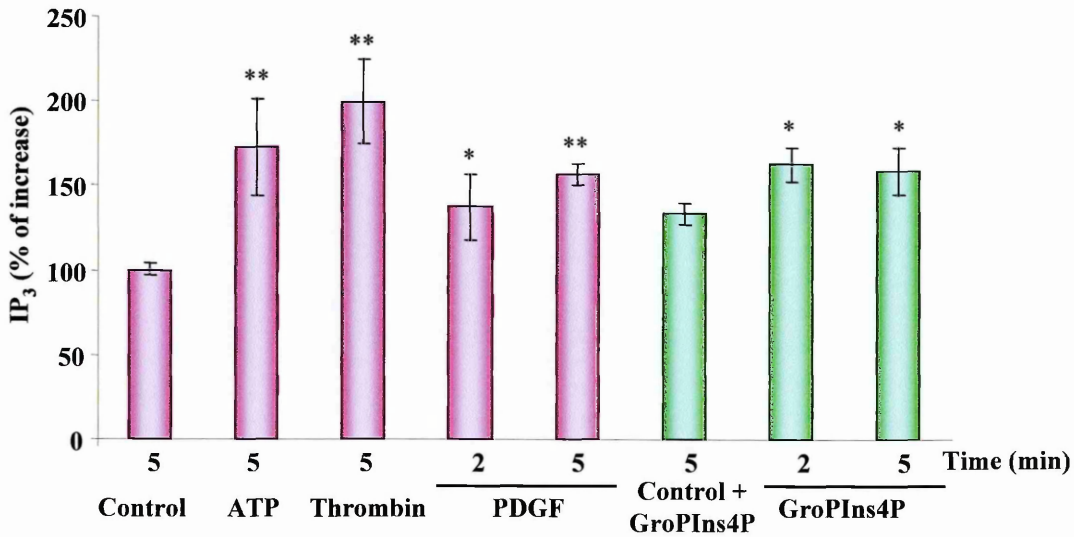

Figure 3.16 - Quantification of IP_3 production in intact cells. NIH 3T3 were treated with 50 μM GroPIns4P, 10 ng/ml PDGF, 100 μM ATP or 5 IU/ml Thrombin for different times at 37 °C. The reaction was stopped by adding 20% perchloric acid and the samples were left 20 min on ice. Then the samples were collected, centrifuged and the pH adjusted to 7.0 with KOH. After a second centrifugation step the samples were ready to be measured by a kit (as described in Section 2.6.3). The columns represent the average of at least 4 different experiments calculated as increase over basal (control); the bars represent the SD. The specific basal level for GroPIns4P is the untreated sample with GroPIns4P added immediately before IP_3 measurement.
*P<0.05, **P<0.01, versus control (Section 1.14). Each P value for GroPIns4P-treated samples was calculated in respect to their specific basal level.

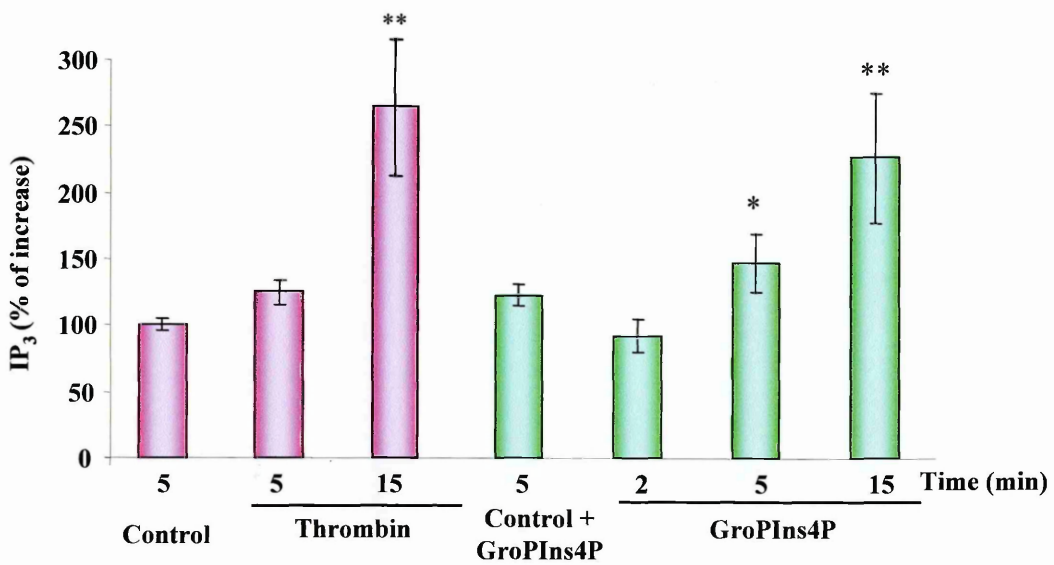

Figure 3.17 - Quantification of IP_3 production in cell lysates. NIH 3T3 were lysed and then treated with 50 μM GroPIns4P, 10 ng/ml PDGF or 5 U/ml Thrombin for different times at 37 °C. The rest of the assay was similar to the experiment performed with intact cells (Fig. 3.16). The columns represent the average of at least 4 different experiments calculated as increase over basal (control); the bars represents the SD. The specific basal level for GroPIns4P is the untreated sample with GroPIns4P added immediately before IP_3 measurement.
*P<0.05, **P<0.01, versus control (Section 1.14). Each P value for GroPIns4P-treated samples was calculated in respect to their specific basal level.

3.7.3 GroPIns4P acts through PLCγ for IP_3 production

In order to understand which PLC could be involved in GroPIns4P-dependent IP_3 increase, the same IP_3 assay was performed blocking selectively the PLCβ or γ with specific antibodies (Ferry et al., 2001): NIH 3T3 cell lysates were incubated with GroPIns4P for 15 min at 37°C in the presence or absence of 20 μg/ml of anti-PLCβ and anti-PLCγ antibody (the same concentration used in Ferry et al., 2001). The selectivity of the antibodies was assessed by treating the lysates with thrombin: this agonist was selectively blocked only by the anti-PLCβ-Ab that is coupled with the PAR family of GPCR, whereas the anti-PLCγ-Ab was ineffective (Fig, 3.18a).

The GroPIns4P-dependent increase in IP_3 was completely prevented by the presence of the anti-PLCγ-Ab and partially by the antibody for PLCβ. As shown in figure 3.18 b the GroPIns4P-dependent increase in IP_3 was 80% in normal conditions and 40% when the PLCβ was inhibited, whereas no increase in IP_3 production was observed in the absence of PLCγ activity. This set of experiments showed that PLCγ is the most responsible for the GroPIns4P-dependent IP_3 production. In contrast, PLCβ gives only a partial contribution. Thus GroPIns4P should activate the PLCγ, probably via phosphorylation. In fact, the inhibition of GroPIns4P dependent increase in $[Ca^{2+}]_i$ generated by genistein and Src family kinases inhibitors indicated that there is a kinase involved in the pathway.

3.8 GroPIns4P and Src family kinases

3.8.1 General description

The inhibition of Src family kinases completely impaired the GroPIns4P-induces $[Ca^{2+}]_i$ increase in NIH 3T3 cells. This data strongly suggested that GroPIns4P can activate

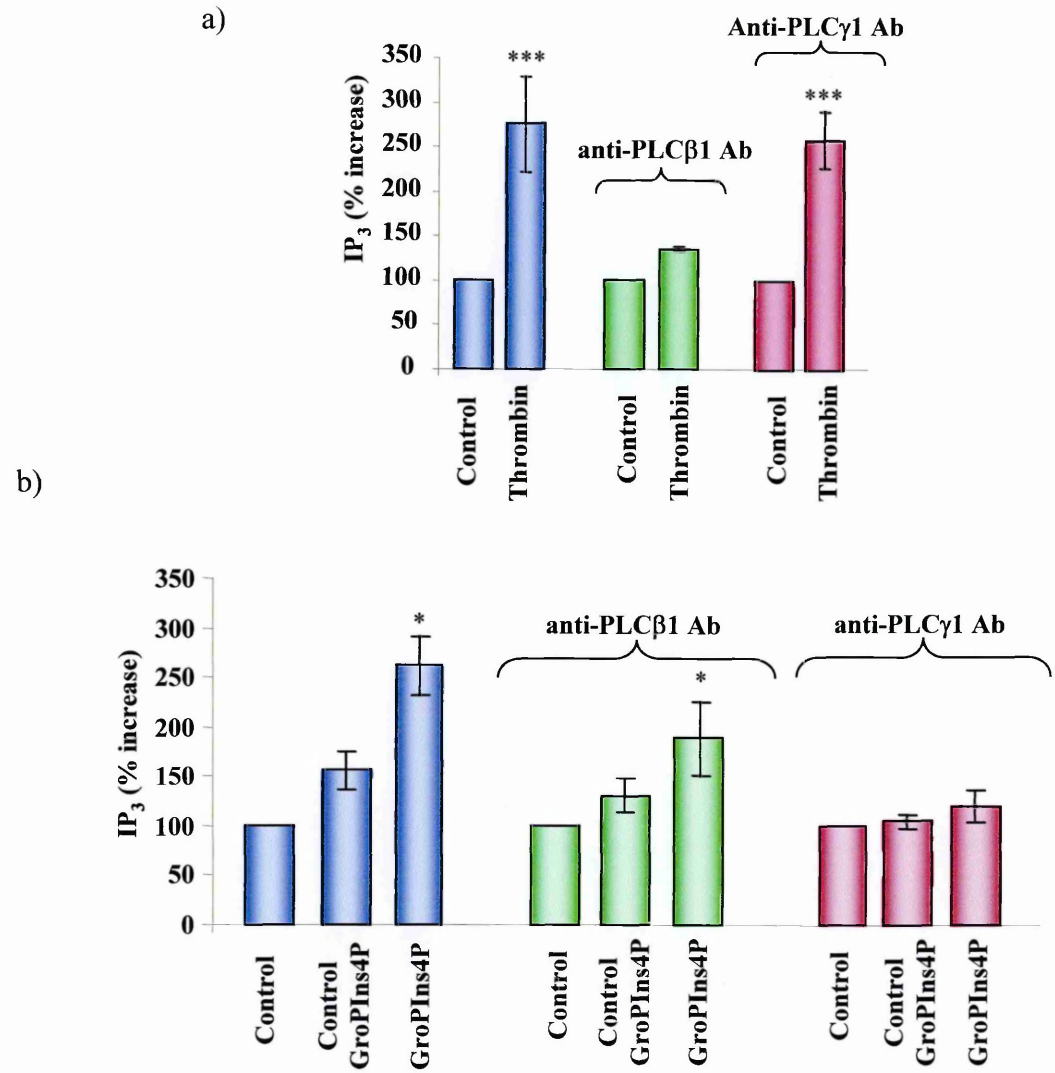

Figure 3.18 - Quantification of IP_3 production in the presence of anti-PLCβ1 and anti-PLCγ1 antibodies. NIH 3T3 cell lysate was incubated with anti-PLCβ1 and anti-PLCγ1 antibodies (20 μg/ml) as described in Section 2.6.3, then treated with 5 IU/ml thrombin (**a**) or 50 μM GroPIns4P (**b**) for 15 min. The rest of the assay was similar to the experiment performed with intact cells (Fig. 3.16). The columns represent the average of three independent experiments represented as increase over basal (control); the bars represents the SD. The specific basal level for GroPIns4P is the untreated sample added with GroPIns4P immediately before the IP_3 measure. *P<0.05, ***P<0.001, versus control (Section 1.14). Each P value for GroPIns4P-treated samples was calculated in respect to their specific basal level.

Src kinases, but there was no direct proof that a treatment with GroPIns4P leads to an increase in active Src kinases in the cells. These enzymes, when active, are phosphorylated at Tyr416 (Roskoski, 2004) (see Section 1.3.5). Thus, the amount of active Src kinases present in the cells was followed with a specific antibody that exclusively recognises p-Tyr416 (from Upstate) both by immunofluorescence and western blotting. This antibody was not selective for the three ubiquitously expressed isoforms of the Src family (Src, Fyn and Yes; see Section 1.3.5).

3.8.2 GroPIns4P activates Src kinases and induces their translocation to the plasma membrane both in Human Fibroblasts and NIH 3T3 cells

When Src kinases are activated, they undergo conformational changes that allowed the autophosphorylation of Tyr416 and favour their interaction with many different substrates (see Section 1.3.5). The formation of lamellipodia and ruffles also implies the activation of Src kinases and their translocation at the level of plasma membrane, which is visible by immunofluorescence as an increase in the staining of p-Src at the tip of lamellipodia and ruffles (Timpson et al., 2001).

We took advantage of human fibroblasts, a cellular system in which the conditions for following the activation of endogenous Src family kinases both by immunofluorescence and western blotting have been well established in a laboratory in this department (Sallese's lab. unpublished data). The cells were treated with 50 μM GroPIns4P or 10 ng/ml PDGF and then stained for p-Src with a specific antibody, and for actin with FITC- phalloidin. Within 2 min of treatment with GroPIns4P or performing a 5 min treatment with PDGF, an increase in lamellipodia and ruffles was visible in human fibroblast cells and p-Src localised at the tip of lamellipodia (Fig. 3.19 a). In parallel, an increase in p-Src level was observed also by western blotting. Human fibroblasts were treated with GroPIns4P and PDGF, then the cells were lysed and the amount of active

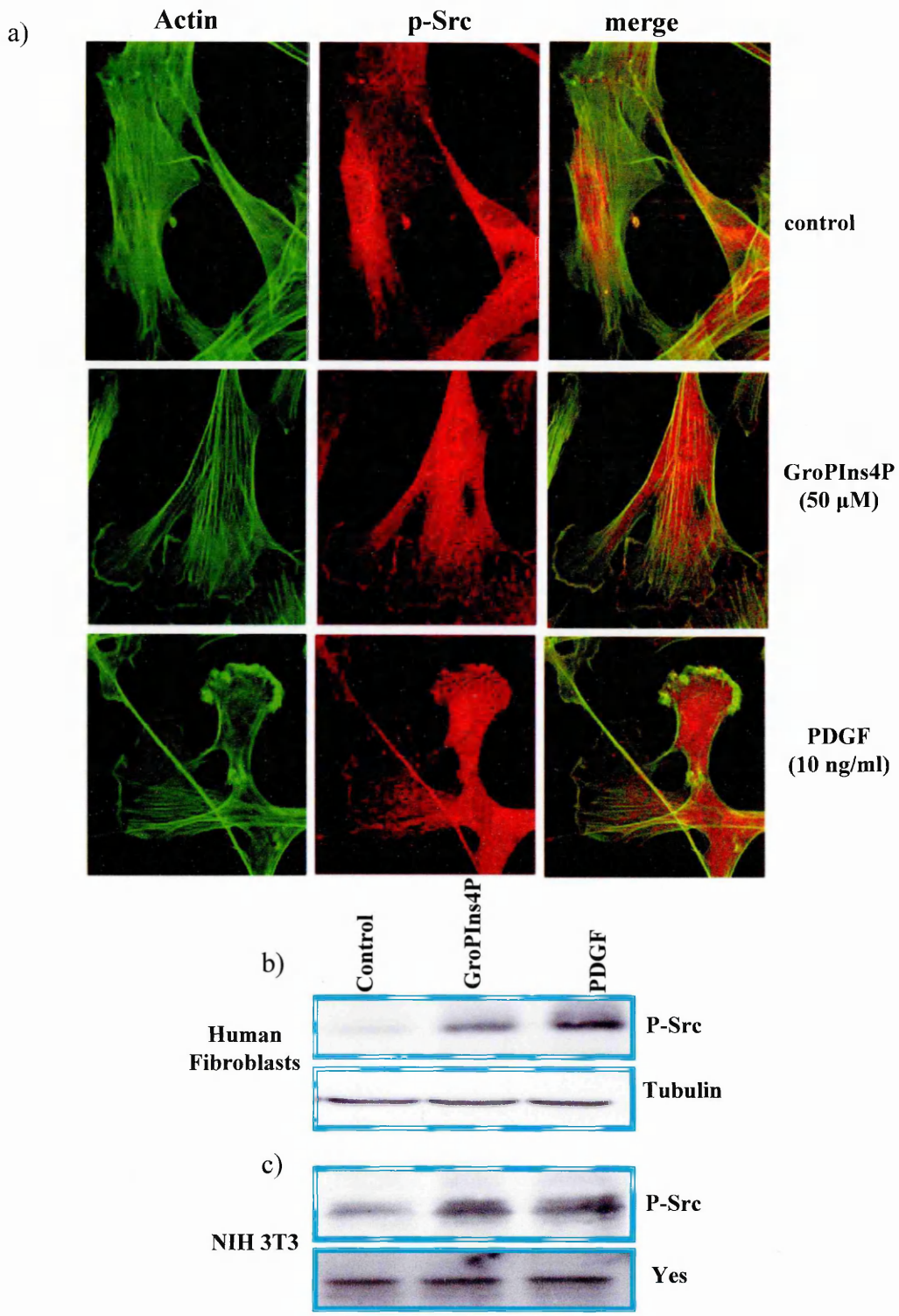

Figure 3.19 - GroPIns4P-dependent Src family kinases activation. a) Human fibroblasts were treated with 50 µM GroPIns4P or 10 ng/ml PDGF, fixed and then stained for p-Src with a specific antibody and for actin with TRITC-phalloidin (as described in Section 2.4.4). Bar=20 µm **b)** After stimulation, the same cells were lysed and the amount of active (phosphorylated) Src analysed by western blotting with the anti-p-Src antibody (see Section 2.6.5). **c)** NIH 3T3 were treated with 50 µM GroPIns4P or 10 ng/ml PDGF. The cells were lysed and the amount of active (phosphorylated) Src analysed by western blotting (see Section 2.6.5).
a-b were preformed in collaboration with Teodoro Pulvirenti from the Sallese's laboratory (our department)

(phosphorylated) Src analysed by western blotting using the anti-p-Src antibody (as described in Section 2.6.5). GroPIns4P double the amount of p-Src in the cells (Fig. 3.19b). The band of p-Src that was modulated by GroPIns4P was of 50 kDa and therefore corresponded to the Src isoform of Src family.

The same approaches were tested in NIH 3T3 cells, but unfortunately the Ab anti p-Src does not work for immunofluorescence in this cell system, because it generated too much non-specific binding. In contrast with the western blot approach it was possible to follow a strong increase in p-Src upon treatment with GroPIns4P also in NIH 3T3 cells (Fig. 3.19 c). However, in this case the p-Src band corresponded to a protein that is at least 66 kDa, whereas p-Src was at 50 kDa in human fibroblasts. Looking at the other isoforms of Src, Yes has a molecular weight of 66 kDa, and with an anti-Yes antibody it was possible to confirm that the band recognised by the Ab anti p-Src and that appears to be modulated by GroPIns4P, corresponded to Yes in NIH 3T3 cells (Fig. 3.19 c).

These data confirmed the initial hypothesis that GroPIns4P can activate Src family kinases and this activation could also be associated with $[Ca^{2+}]_i$ increase and, consequently ruffle formation.

3.9 Effect of different inhibitors on GroPIns4P-dependent ruffle formation

3.9.1 General description

The pathway elucidated so far shows that the translocation of TIAM1 to the plasma membrane depends on an increase in $[Ca^{2+}]_i$ that leads to the activation of the CaMKII, a kinase that phosphorylates TIAM1, allowing its activation. In turn, TIAM1 is able to activate Rac1, favouring the formation of membrane ruffles. All those events can be mediated by GroPIns4P.

While it was shown that the $[Ca^{2+}]_i$ increase and the translocation of TIAM1 are impaired when one element of the pathway is blocked with specific inhibitors (KN-93 for CaMKII, U-73122 for PLCs, SU6656 and PP2 for Src kinase), there was no parallel experimental evidence that those inhibitors prevented the GroPIns4P-induced membrane ruffle formation. For this reason the ability of GroPIns4P to induce membrane ruffling in NIH 3T3 cells treated with U-73122, KN-93 and SU6656 was analysed.

3.9.2 U-73122 prevents the GroPIns4P-dependent ruffle formation

Serum starved NIH 3T3 cells were subjected to 10 min treatment with 5 μM U-73122 before stimulation with 50 μM GroPIns4P (2 min, enough to follow ruffle formation) or 10 ng/ml PDGF (5 min stimulation). The extent of ruffle formation was analysed as for the other experiments and quantified in blind conditions (as described in Section 2.4.3).

The inhibition of PLCs reduced both the GroPIns4P- and PDGF-dependent ruffle formation by 70 % (from 2.5-fold response in normal condition to 1.45-fold response in the presence of the inhibitor). A residual 30% activity was still present also upon treatment with U-73122 (Fig. 3.20). The ability of PDGF to induce membrane ruffles was also strongly reduced by U-73122; it produces a 3.8-fold increase in ruffle under normal conditions and a 2-fold increase in the presence of the inhibitor (Fig. 3.20). To verify that the effect of the inhibitor was specific, the inactive analogue (U-73343) was also used. Treatment with 5 μM U-73343 (the same concentration used for U-73122) did not prevent the formation of membrane ruffles induced by GroPIns4P and PDGF (Fig. 3.20). The blockage of PLCs implies that that the increase of $[Ca^{2+}]_i$ produced by GroPIns4P is prevented. Under these conditions also ruffle formation is strongly reduced. Together these two observation implies that the $[Ca^{2+}]_i$ increase is an important event that precedes the signalling pathway that leads to GroPIns4P-dependent ruffle formation. In the figure 3.20b,

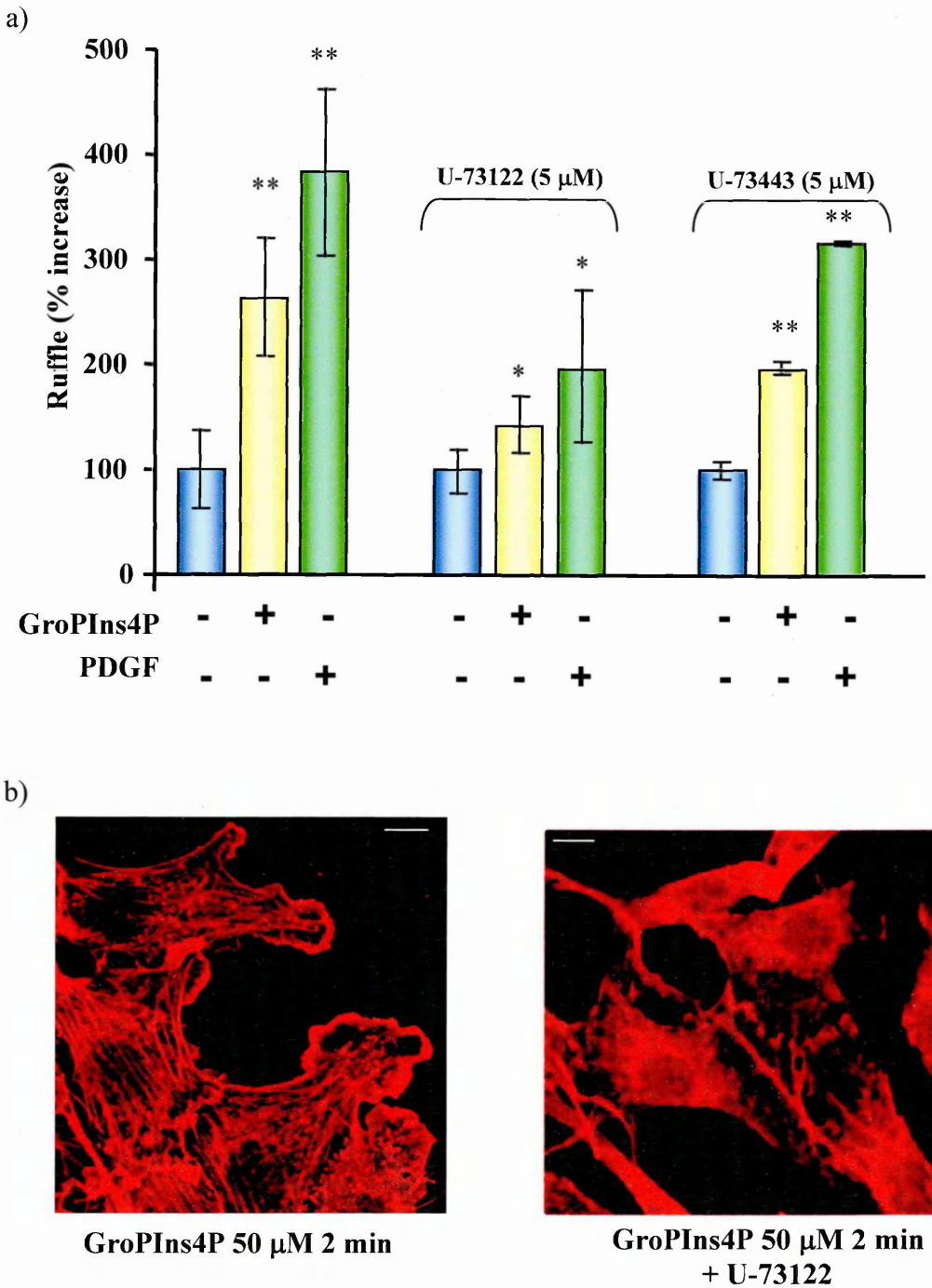

Figure 3.20 - Effect of PLCs inhibitors in GroPIns4P-dependent ruffle formation. Serum starved NIH 3T3 cells were incubated with 5 μM U-73122 or U-73343, and then treated with 50 μM GroPIns4P for 2 min or 10 ng/ml PDGF for 5 min. Cells were fixed and stained with TRITC-labelled phalloidin and quantified blind for the extent of ruffle formation as described in Section 2.4.3 The results shown are average (±SD) of three independent experiments, each performed in duplicate. *P<0.05 **P<0.01 ***P<0.001, versus control (Section 1.14). **b)** Representative images of GroPIns4P-dependent modification of the actin cytoskeleton in the presence and absence of U-73122, in NIH 3T3 cells. Bar =20 μm

two representative images of cells treated with GroPIns4P (50 μM) in the presence and absence of U-73122 (5 μM) are shown.

3.9.3 KN-93, PP2 and SU6656 prevent the GroPIns4P-dependent ruffle formation

To test the involvement of CaMKII and Src kinases in GroPIns4P-dependent ruffle formation, serum starved NIH 3T3 were treated with CaMKII (KN-93) or Src (PP2 and SU6656) inhibitors prior to being incubated with 50 μM GroPIns4P (2 min), PDGF 10 ng/ml (5 min) or 10 μM PMA (Phorbol 12-Myristate 13-Acetate) (5 min).

KN-93 completely prevented ruffle formation induced both by GroPIns4P and PDGF (Fig. 3.21). PMA, which binds to and activates protein kinase C causing Rac1 activation and ruffle formation in a CaMKII-independent way (Ridley and Hall, 1992), was still active also in the presence of KN-93. The two inhibitors of Src gave a significant but not complete inhibition (Fig. 3.21) both for GroPIns4P and PDGF-dependent ruffle formation (70% decrease).

As shown in figure 3.21, under normal conditions GroPIns4P caused a 2.5-fold increase versus the control in membrane ruffles, PDGF a 3.6-fold increase and PMA a 1.7-fold increase. Upon treatment with KN-93, the GroPIns4P effect was completely blocked and PDGF could induce only a 1.5-fold increase in ruffles, whereas PMA was still able to induce a 1.7-fold increase. On the other hand, the treatment with Src inhibitors caused only a 1.5-fold increase in ruffles upon GroPIns4P treatment and a 2-fold increase upon PDGF treatment.

This result indicated that CaMKII plays a fundamental role in the GroPIns4P-dependent ruffle formation, whereas blocking Src kinases lead to incomplete inhibition. There was still a 30% residual activity that could be explained by a possible incomplete blockage of the kinase produced by the inhibitor. However, the $[Ca^{2+}]_i$ increase induced by GroPIns4P was completely prevented by the same concentration of inhibitors used for the

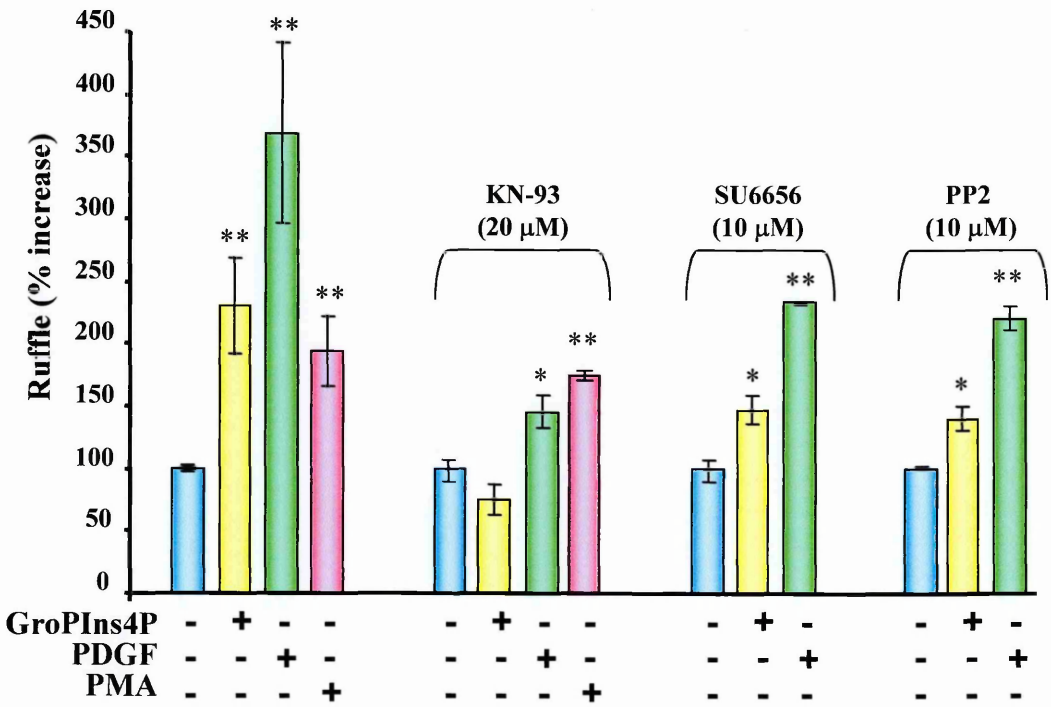

Figure 3.21 - Effect of CaMKII and Src inhibitors in GroPIns4P-dependent ruffle formation. Serum starved (24 h) NIH 3T3 were treated with KN-93 (24 h) or Src inhibitors (PP2 and SU6656) (15 min) and then incubated with 50 μM GroPIns4P (2 min), PDGF 10 ng/ml (5 min) or 10 μM PMA (5 min). The cells were then fixed and stained with TRITC-labelled phalloidin and quantified blind for the extent of ruffles formation as described in Section 2.4.3. The results shown are the means (±SD) of three independent experiments, each performed in duplicate.*P<0.05 **P<0.01, versus control (Section 1.14).

assay of ruffle formation. In addition, by blocking both the PLCs and Src kinases, the same 70 % inhibition could be obtained. Probably, beside Src, there is another element able to influence the pathway of GroPIns4P-dependent ruffle formation acting the level of CaMKII.

3.9.4 GroPIns4P is not able to induce ruffle formation in SYF cells (deficient for Src, Fyn and Yes)

In order to confirm the involvement of Src kinases in GroPIns4P-dependent ruffle formation by a different approach, a cell line which lacked Src, Fyn and Yes (SYF cells) was used. This cell line was derived from mice in which Src, Fyn and Yes have been knocked out, which displays severe developmental abnormalities and lethality by E9.5. PDGF-dependent chemotaxis and cell cycle progression is not altered in this cell line, whereas integrin-dependent cell motility in a wound healing assay is retarded (Klinghoffer et al., 1999).

In principle, if the Src family kinases are important in the pathway that is activated by GroPIns4P to produce membrane ruffles, in the knock out fibroblasts this compound should not be active. On the other and, if Src kinases are not the only tyrosine kinase family activated by GroPIns4P and Src activity could be replaced by other kinases, GroPIns4P should be able to induce ruffles also in this knock out system. This is the case for PDGF, which is still active in the absence of Src, Fyn and Yes (Klinghoffer et al., 1999).

Serum starved SYF cells were treated with GroPIns4P (50 μM) for different times (2 to 10 min), PDGF (10 ng/ml) for 5 min or PMA (10 μM) for 5 min, then were fixed and stained with TRITC-phalloidin for actin visualization (see Sections 2.4.2 and 2.4.3). GroPIns4P was not able to induce ruffles formation in SYF cells, whereas the membrane ruffle were still formed upon treatment with PDGF or PMA (Fig. 22a,b). This data

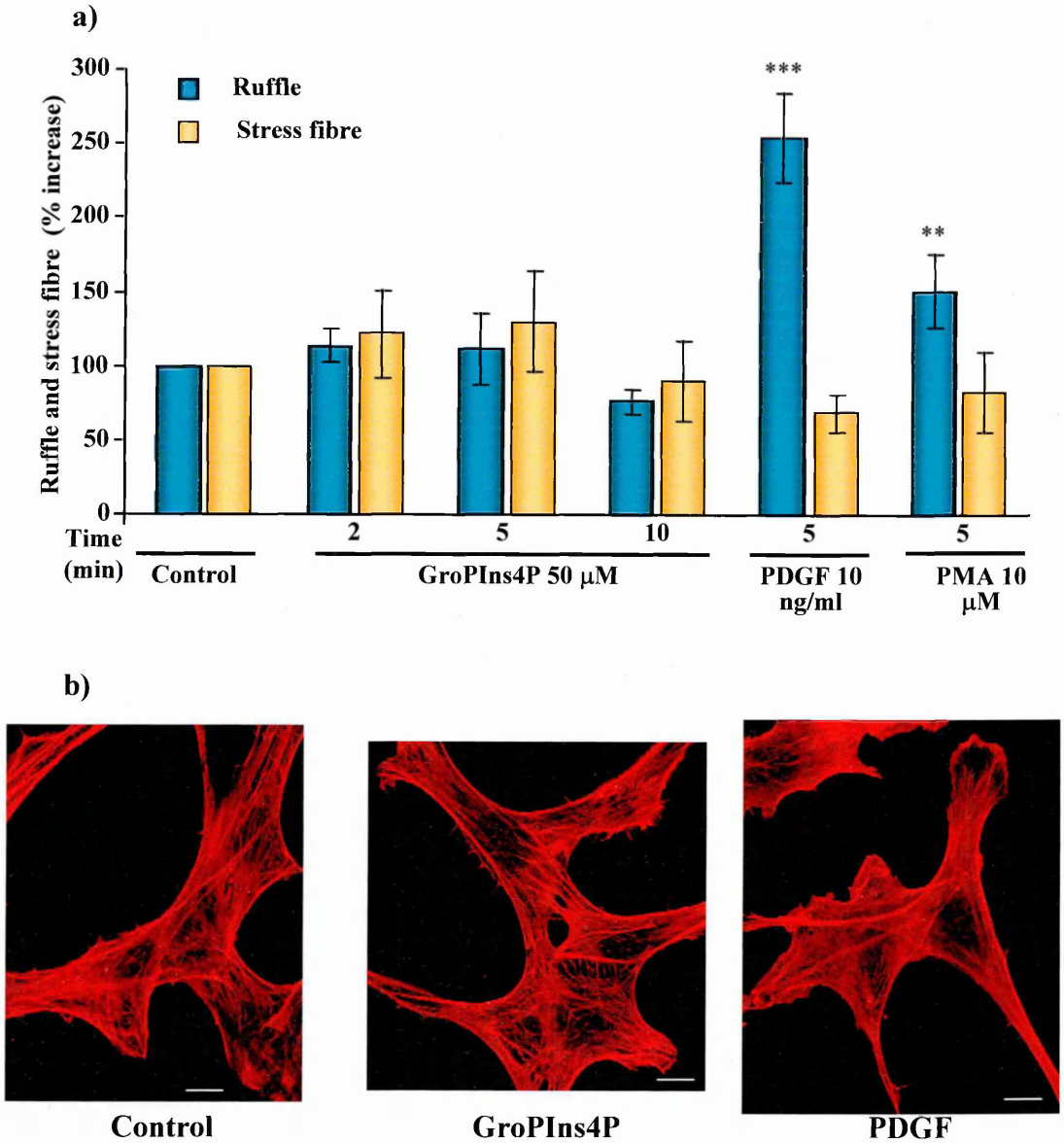

Figure 3.22 - GroPIns4P–dependent ruffle formation in SYF cells. a) SYF cells were serum starved for 12 h in DMEM, 0.1 % foetal bovine serum; then were treated with 50 μM GroPIns4P for different times (from 2 to 30 min), 10 ng/ml PDGF for 5 min or 10 μM PMA for 5 min. Cells were fixed and stained with TRITC-labelled phalloidin and quantified blind for the extent of ruffles formation as described in Section 2.4.3. The results shown are means (±SD) of two independent experiments, each performed in duplicate. $^{**}P < 0.01$ $^{***}P < 0.001$, versus control (Section 1.14).
b) Representative images of GroPIns4P- and PDGF-dependent modification of the actin cytoskeleton in SYF cells. Bar=20 μm

suggested that Src is a key element for the activity of GroPIns4P.

In support of these data, the transfection of c-Src in SYF cells restored their ability to from ruffles upon GroPIns4P treatment (Fig. 3.23). In this case, the cells were transfected with an expression vector for c-Src, then starved and treated with GroPIns4P (50 μM) or PDGF (10 ng/ml). The extent of ruffle formation was quantified by observation of the transfected cells. GroPIns4P as well as PDGF, induced a 2.5-fold increase versus control of membrane ruffles as shown in figure 3.23. If the effect of GroPIns4P was restored by the expression of c-Src, the effect of PDGF was not increased upon transfection, thus indicating that its receptor is coupled with another TyrK in this cell system.

3.9.5 Conclusion

In NIH 3T3 cells the inhibition of PLCs, as well as Src family kinases inhibition, prevents the increase in $[Ca^{2+}]_i$ and consequently produces a 70% inhibition of GroPIns4P-dependent ruffle formation. This data supported the idea that GroPIns4P activates a signalling pathway that, starting from the increase in $[Ca^{2+}]_i$, leads to ruffle formation. The inhibition of CaMKII completely impaired the GroPIns4P-dependent ruffle formation, thus confirming the fundamental role of this kinase in the pathway. The data also demonstrated that the Src/Ca^{2+}/CaMKII pathway is strongly required by GroPIns4P to produce ruffle formation. Both the inhibition of PLCs and of Src kinases cause a large, but not complete, blockage of ruffle formation. To explain the presence of this residual activity we could argue that CaMKII maintains a residual basal activity also after starvation, thus, GroPIns4P could allow the phosphorylation of TIAM1 and the consequent ruffle formation by modulating the activity of the kinase in another way, without increasing $[Ca^{2+}]_i$, for example by favouring the interaction of TIAM1 and CaMKII or the formation of protein complex that allowed the tethering of TIAM1 and Rac1 to the plasma membrane.

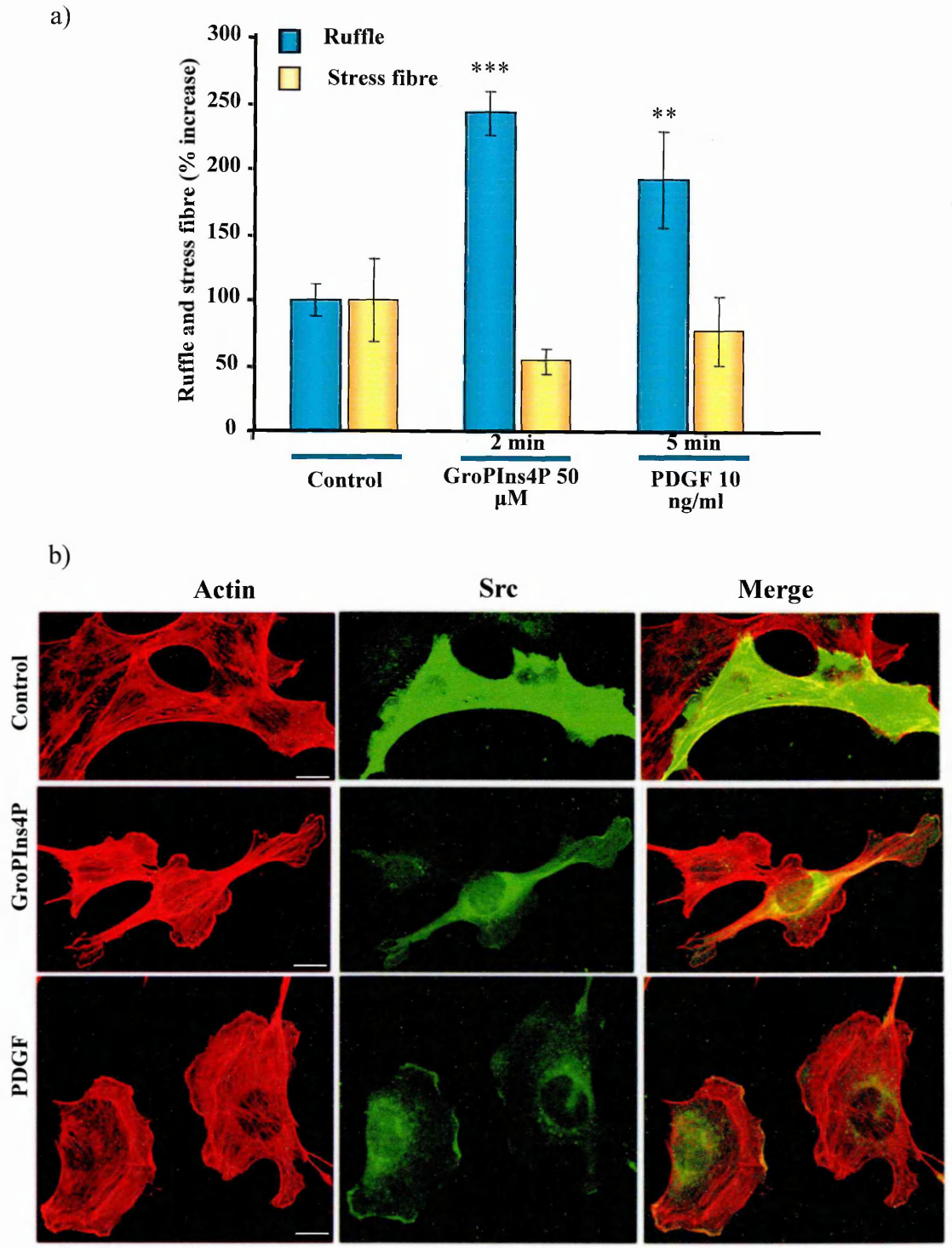

Figure 3.23 - GroPIns4P–dependent ruffle formation in SYF cells overexpressing Src. a) SYF cells were transfected with the pSM-c-Src construct as described in Section 2.6.5. Twenty four h after transfection, cells were serum starved for 12 h in DMEM, 0.1 % foetal bovine serum then were treated with 50 µM GroPIns4P for 2 min or 10 ng/ml PDGF for 5 min. Cells were then fixed and stained with the anti-c-Src ab (green) and TRITC-labelled phalloidin (red) and quantified blind for the extent of ruffle and stress fibre formation. The results shown are the means (±SD) of two independent experiments, each performed in duplicate. $^{**}P<0.01$, $^{***}P<0.001$, versus control (Section 1.14). **b)** Representative images of GroPIns4P- and PDGF-dependent modification of the actin cytoskeleton in SYF cells transfected with Src. Bar=20 µm

The importance of Src kinases for GroPIns4P activity was clearly demonstrated using SYF cells. In this case the absence of three isoforms of Src family kinases completely prevents the GroPIns4P-dependent ruffle formation; thus suggesting that in SYF cells Src kinases are fundamental for the activity of this compound.

3.10 Final discussion

The pathway that I am proposing is initiated by GroPIns4P, that activates a member of the Src family kinases (potentially Yes in NIH 3T3). This kinase then phosphorylates PLCγ1 allowing its activation and consequent IP_3 production and Ca^{2+} increase. This event triggers the activation of CaMKII that phosphorylates TIAM1, facilitating its translocation to the plasma membrane and enhancing its exchange activity versus Rac1. This small GTPase is also translocated to the plasma membrane upon treatment with GroPIns4P and, even if it is not clear, it is possible to hypothesise that the Ca^{2+} increase could facilitate this event. It has been shown that a Ca^{2+}-dependent activation of PKC can disrupt the Rac1-GDI complex via phosphorylation of GDI. This event favours the translocation of Rac1 to the plasma membrane and consequently its interaction with GEFs (Price et al., 2003); see Sections 1.2.3 and 1.2.3.1). Once activated at the level of plasma membrane, Rac1 can lead to the formation of membrane ruffles (Fig. 3.24).

Besides Src kinases there could be also another unknown target of GroPIns4P, able to cause ruffle formation, even if only at a low level, when Src kinases are inhibited. In normal conditions Src kinases and the other unknown element are both activated by GroPIns4P and this leads to the maximal effect that is 2.5-fold increase in ruffles versus the basal (Fig. 3.22). In the absence of active Src kinases, GroPIns4P induces only a 1.45-fold increase in ruffles that could correspond to the activation of the unknown target. In the case of SYF cells the absence of Src family kinases (Src, Fyn and Yes) completely abolished the GroPIns4P-dependent ruffle formation. This data also supports the idea that

Src kinases represent one of the main targets for GroPIns4P. In this case, however, the inhibition is complete and the transfection of c-Src, upon GroPIns4P treatment, cause a huge rescue of ruffle formation, which, in extent resembles the effect of PDGF. In fibroblasts, on the other hand, this growth factor is more active than GroPIns4P. Probably in SYF cells the second unidentified pathway is not present and the absence of Src completely abolishes the GroPIns4P-dependent ruffles formation.

It remains unclear how Src kinases can be activated by GroPIns4P. Src kinases are regulated by alternative phosphorylation/de-phosphorylation events: the chief phosphorylation sites of Src kinases include tyrosine 416, phosphorylation of which, results in activation *via* autophosphorylation, and tyrosine 527 that results in the inhibition of phosphorylation by C-terminal Src kinase (CSK). Protein-tyrosine phosphatases such as PTPα, Shp1, Shp2 and several other transmembrane enzymes, can remove the inhibitory phosphate from Src kinases causing their activation (see Section 1.3.5). GroPIns4P could directly interact with a Src kinase favouring its autophosphorylation on tyrosine 416 or alternatively activate a phosphatase that de-phosphorylates the tyrosine 527. It cannot be excluded that GroPIns4P could lead to the inhibition of CSK.

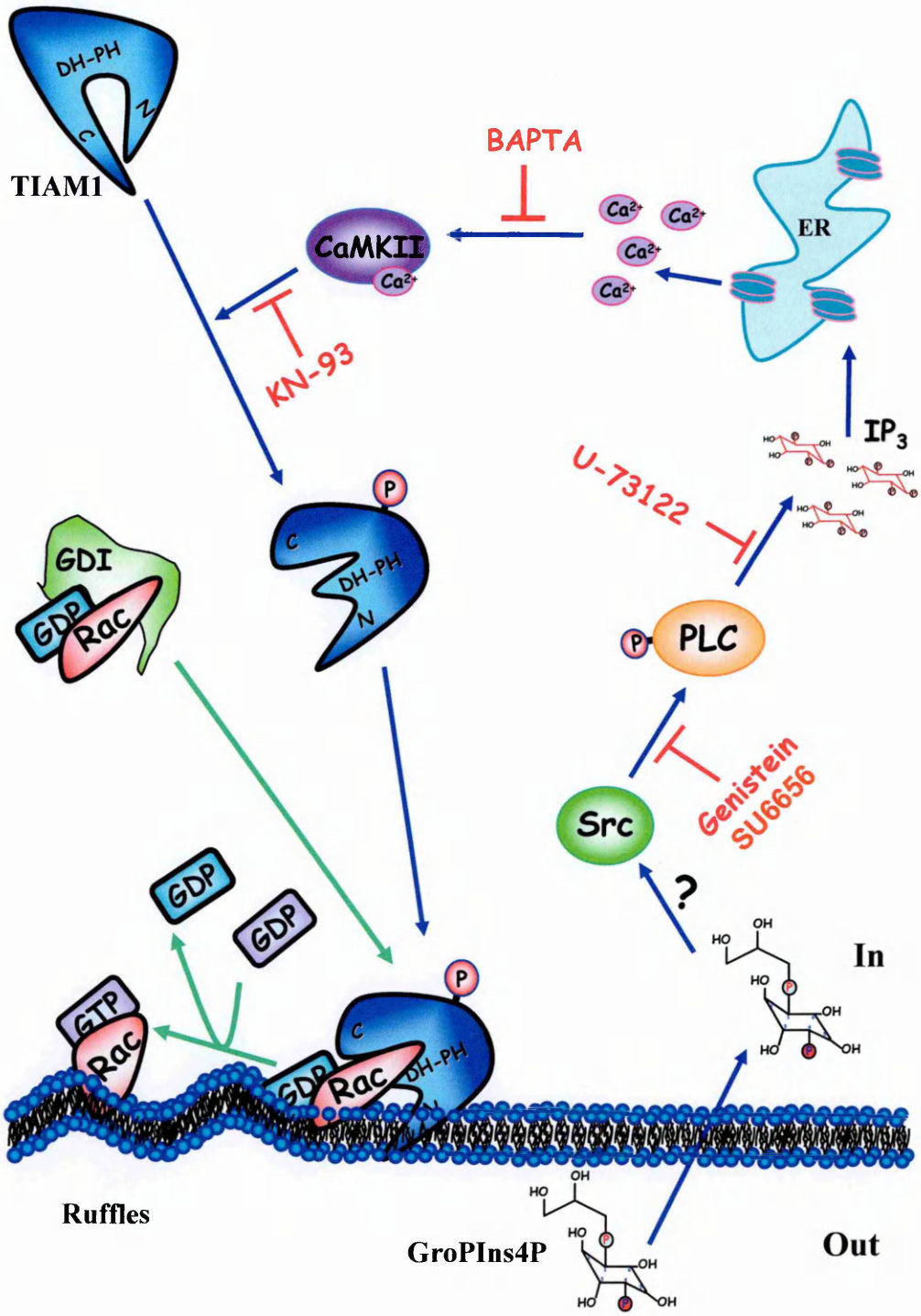

Figure 3.24 - Schematic representation of the pathway elucidated in Chapter 3. GroPIns4P activates a member of the Src family kinases (potentially Yes in NIH 3T3), this kinase phosphorylates PLCγ1 allowing its activation and the consequent IP_3 production and $[Ca^{2+}]_i$ increase. This event causes the activation of CaMKII that phosphorylates TIAM1, facilitating its translocation to the plasma membrane and enhancing its exchange activity versus Rac1. Once activated at the level of plasma membrane, Rac1 can lead to the formation of membrane ruffles.

CHAPTER 4

AN ALTERNATIVE MECHANISM OF ACTION OF GroPIns4P

4.1 Introduction

The pathways elucidated in Chapter 3 explain how exogenously added GroPIns4P induces ruffle formation in Swiss and NIH 3T3 cells. Its action involves CaMKII, which phosphorylates TIAM1, allowing the translocation of TIAM1 to the plasma membrane, where it can interact with and activate Rac1, which is responsible for ruffle formation. CaMKII is activated by GroPIns4P through a Src-dependent increase in $[Ca^{2+}]_i$. However, this increase can only partially explain GroPIns4P-dependent ruffle formation, as there is a residual response to GroPIns4P stimulation when Src kinases are blocked or a $[Ca^{2+}]_i$ increase is prevented (see Section 3.9).

Some important questions arise from these data: How does GroPIns4P activate Src kinases? Is their interaction direct or via a receptor-dependent process? What is the unknown Src-independent element that is involved in membrane ruffling produced by GroPIns4P?

To identify the specific targets of GroPIns4P, and in this way to elucidate the mechanisms by which this compound activates Src kinases and CaMKII, different methodological approaches were taken:

1) Uptake and binding assays for GroPIns4P in intact and permeabilised cells, and to membranes from NIH 3T3 cells. This should finally answer the question about the presence of a specific membrane receptor for GroPIns4P.
2) Pull-down assays to see if GroPIns4P can modulate the interaction between TIAM1 and Rac1

3) Immunoprecipitation and binding experiments to identify the interactors of GroPIns4P

4.2 Identification of a membrane receptor for GroPIns4P

4.2.1 General description

From previous results, it was clear that GroPIns4P enters cells, and there was no evidence for specific GroPIns4P binding to the membrane. Thus GroPIns4P was able to cross the plasma membrane of FRTL5 and Swiss 3T3 cells, and to rapidly reach equilibrium with the cell cytosol. Its concentration was high enough to allow the correlation of the biological effects of externally applied GroPIns4P (Berrie et al., 1999) with those of receptor-stimulated increases in intracellular levels of GroPIns4P (Falasca et al., 1997). However, to determine whether extracellularly applied GroPIns4P mediates these effects via a specific GroPIns4P receptor, a classic centrifugation binding assay on post-nuclear membranes obtained from Swiss 3T3 cells was carried out, and no significant specific "receptor" (high-affinity) binding sites were seen (Berrie et al., 1999).

To see if it is also possible to follow uptake of GroPIns4P in NIH 3T3 cells, and to conclusively understand if this compound can bind to the plasma membrane or enter cells, uptake experiments in intact and permeabilised NIH 3T3 cells were performed.

4.2.2 There is no evidence for the presence of a specific plasma membrane receptor for GroPIns4P

The uptake assay was performed in cell suspensions. Intact or tetanolysin-permeabilised cells (see Section 2.12.1) were incubated with [^{3}H]GroPIns4P for 10 min (the time needed for the maximal uptake of GroPIns4P, as reported in Berrie et al., 1999)

and then spotted onto nitrocellulose filters. The filters were then counted by β-scintillation counting (see Section 2.12.2.1). The amount of [^{3}H]GroPIns4P that was taken up within 10 min was compared to the time 0 sample (cells and [^{3}H]GroPIns4P were spotted separately on the same nitrocellulose filter). The non-specific binding to the filter was calculated by spotting the radioactive mixture directly onto the filters without the cells, and this was subtracted from the total bound [^{3}H]GroPIns4P obtained for each sample.

The aim of this assay was to determine if the uptake of GroPIns4P observed in intact cells was due to a real entry of the compound or to a binding at the level of the cell membrane. If an increase in GroPIns4P concentration is observed only in intact cells that would mean that GroPIns4P is able to enter the cells. However, if uptake is also observed in permeabilised cells that would mean that GroPIns4P binds to the cellular membranes or to a protein complex. The advantage of using permeabilisation with tetanolysin was to produce small pores at the plasma membrane that do not alter the structure of the cells, and do not allow the exit of the majority of the proteins (Riese et al., 2002).

It was possible to follow an increase in the intracellular concentration of GroPIns4P (even though different extents) both in intact and in permeabilised cells: the GroPIns4P concentration increased by 70% in intact cells (from 2.98±0.1 pmols at time 0 to 4.89±0.5 pmols after a 10-min incubation) and presented a 40% increase also in permeabilised cells (from 1.61±0.46 pmols at time 0 to 2.64±0.42 pmols after a 10-min incubation), as shown in Figure 4.1. With the permeabilisation, the portion of GroPIns4P that remains soluble in the cytosol or bound with a low affinity to a protein complex was lost. The 40% increase in GroPIns4P uptake in permeabilised cells represents the fraction that is tightly bound to its specific target (a protein complex or the membrane). These data indicated that GroPIns4P associated with NIH 3T3 cells represents the amount taken up and bound to intracellular elements or to the cellular membrane.

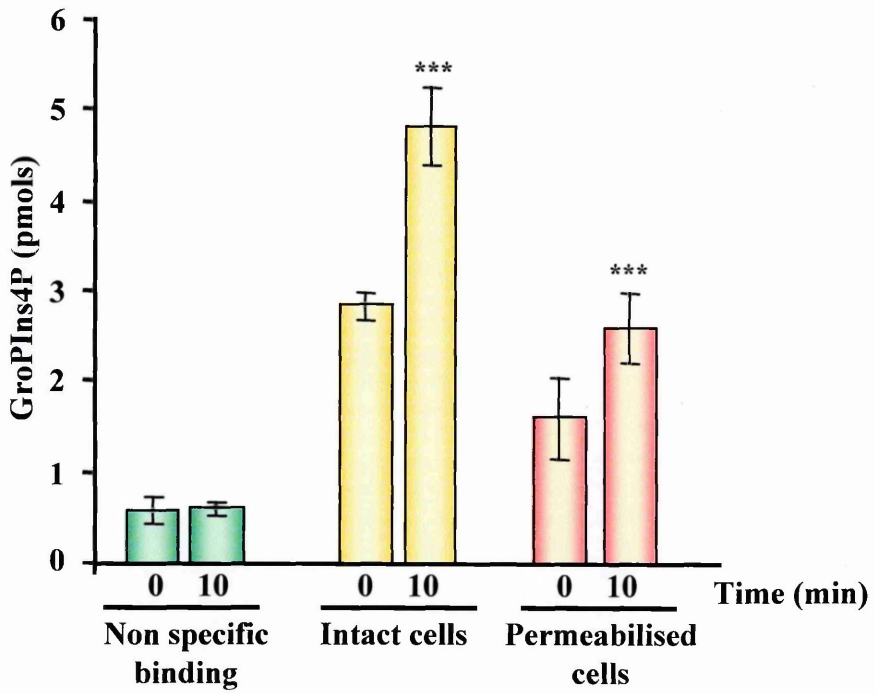

Figure 4.1 - GroPIns4P-uptake in NIH 3T3 cells. $1.5x10^6$ intact or permeabilised NIH 3T3 cells were diluted in 150 µl of growth medium plus 10 mM HEPES and incubated with 150 µl of growth medium plus [^{3}H]GroPIns4P (9 $x10^4$ cpm/sample), 10 µM GroPIns4P and 10 mM HEPES for 10 min. Then after 3 washes with a buffer containing HBSS, 2 mg/ml BSA and 10µM GroPIns4P, the samples were spotted onto nitrocellulose filters. Each sample was tested in quadruplicate. The filters were counted using a β-scintillation counter. The total pmols of GroPIns4P bound to the samples are reported in the y axis. The bars represent the mean (±SD) of three independent experiments. ***$P<0.001$, versus time 0 (Section 1.14).

4.2.3 GroPIns4P does not bind to membranes

To see if membranes could be providing the binding site for GroPIns4P, plasma membrane and total membranes of NIH 3T3 cells were used in the same binding assay. The assay was performed using the quantity of plasma membrane and total membranes that should be present in the amount of cells used for the equivalent cell assay. The theoretical amount of total membranes present in a single NIH 3T3 cell is about 80 pg (see Section 2.12.2.2). The uptake assay was performed with 1.5 x 10^6 cells per sample, and thus the amount of total membranes should be 120 μg, with 6 μg plasma membrane (in general, the plasma membrane represents 5% of the total membranes; Gettys et al., 1994).

The binding was performed comparing the amount of GroPIns4P bound after a 10-min incubation with that at time 0 (membranes and [^{3}H]GroPIns4P were spotted separately on the same nitrocellulose filter) (see Section 1.12.2). In terms of cpm, the specific binding to both plasma membrane and total membranes of [^{3}H]GroPIns4P (the tritiated compound was 9 x10^4 cpm/sample and represented 1/120 of the total GroPIns4P, used at a concentration of 10 μM) was very low. Here, 40 cpm (that corresponds to ~0.5 pmols of total GroPIns4P) represented the non-specific binding to the filters, and an increase of 40-50 cpm (0.8-0.9 pmols of total GroPIns4P) was observed in the presence of plasma membrane and total membranes, whereas the binding in intact and permeabilised cells ranged from a 400 cpm binding normal to 1100 cpm (from 1.61 to 4.89). At the same time, following the 10-min incubation, both the plasma membrane and total membranes do not show any increase in the binding of GroPIns4P, as shown in Figure 4.2. Therefore, the GroPIns4P associated with NIH 3T3 cells represents the amount taken up and bound to intracellular elements, and not to membranes. These data suggest that exogenously applied GroPIns4P can enter NIH 3T3 cells and remain tightly bound to a protein or protein complex inside the cells even performing cell permeabilisation.

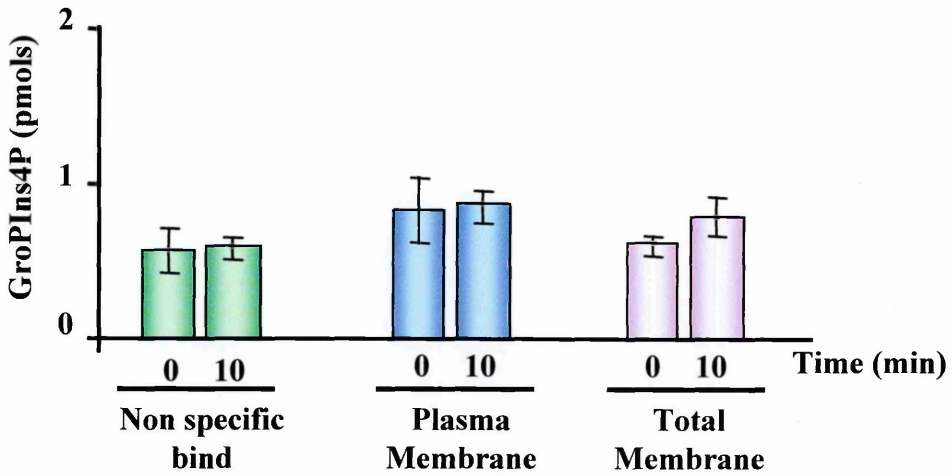

Figure 4.2 - GroPIns4P-binding to NIH 3T3 plasma and total membranes. Plasma membranes (6 μg) and total membranes (120 μg) of NIH 3T3 were diluted in 150 μl of growth medium plus 10 mM HEPES and incubated with 150 μl of growth medium plus [^{3}H]GroPIns4P (9 x10^4 cpm/sample), 10 μM GroPIns4P and 10 mM HPES for 10 min. Then the samples were spotted onto nitrocellulose filters and washed three times with a buffer containing HBSS, 2 mg/ml BSA and 10 μM GroPIns4P. Each sample was tested in quadruplicate. The filters were counted by β-scintillation counting. The total pmols of GroPIns4P bound to the samples are reported in the y axis, they correspond in terms of cpm to 100-150. The bars represent the mean (±SD) of two independent experiments.

4.2.4 Conclusion

This data thus indicates that GroPIns4P accumulates in cells and binds to an intracellular target, and there is no evidence for specific high affinity membrane receptor binding. Using uptake experiments, it was possible to follow an increase in the intracellular concentration of GroPIns4P, both in intact and permeabilised cells. Plasma membranes and total membranes of NIH 3T3 cells do not show any specific binding of GroPIns4P. At the same time, GroPIns4P is able to permeate into cells, rapidly reaching an equilibrium with the extracellular concentration (Berrie et al., 1999). The amount of GroPIns4P taken up in intact cells is twice the amount taken up in permeabilised cells; thus the portion of GroPIns4P that permeates into intact cells and remains soluble in the cytosol is lost in the permeabilised cells. This is consistent with the hypothesis that there is a protein complex to which GroPIns4P binds with a high affinity, and that this binding is not altered upon permeabilisation of the cells.

4.3 GroPIns4P increases the binding between Rac1 and TIAM1

4.3.1 General description

The exchange activity of TIAM1 implies its direct interaction with Rac1-GDP. GroPIns4P can favour the translocation of both Rac1 and TIAM1 to the plasma membrane, where the two proteins have been shown to co-localise (see Section 3.3.3). To evaluate if GroPIns4P can affect the binding between Rac1 and TIAM1, a biochemical approach, consisting of pull-down assays, was used. The results obtained have highlighted another possible mechanism of action of GroPIns4P that could act in parallel with the pathway described in Chapter 3.

4.3.2 The pull down assay

In the light of the data showing a GroPIns4P-dependent co-localization of TIAM1 and Rac1 at the level of the plasma membrane (see Section 3.3), the idea was to see if GroPIns4P can affect the formation of a complex between these two proteins. The pull-down assay was performed with cell cytosol from HEK293T cells overexpressing TIAM1-HA (the C-1199-TIAM1-HA) (see Section 2.8.1), incubated with GroPIns4P (50 μM) for 10 min at 37 °C. The purified GDP-bound form of Rac1-GST was then added to the samples, and the Rac1-GST was precipitated using the glutathione resin (see Section 2.11.2). The amount of TIAM1-HA that co-precipitated with Rac1-GST was evaluated by immuno-blotting with the anti-HA antibody and quantified by densitometric analysis with the NIH image analysis program. To remove the non-specific binding, the same experiment was performed with purified GST instead of Rac1-GST (see Section 2.11.2 for details). Upon incubation with 50 μM GroPIns4P, the binding between TIAM1-HA and Rac1-GST increased by 2.7-fold when compared with the untreated samples (as quantified in Figure 4.3b). GST did not produce any specific binding (Fig. 4.3a).

In the pull-down assay, the incubation between cell cytosol overexpressing TIAM1-HA and GroPIns4P was performed at 37 °C for 10 min. To see if there was a temperature-dependent effect of GroPIns4P, the incubation was performed at different temperatures: 0 °C, 20 °C and 37 °C for 10 min. However, the increase in binding between TIAM1 and Rac1 was observed only at 37 °C (Fig. 4.4a). If there was a physical interaction, the decrease in temperature would have lowered the rate of the interaction. Thus, to see if the effect was still present (even if delayed), the time of incubation was prolonged to 1 h. Here, a 2.7-fold increase in the binding was observed also at 20 °C, whereas at 0 °C no relevant effects were visible (Fig. 4.4b).

From these data it was not possible to conclude whether GroPIns4P acts on TIAM1 directly or indirectly through the activation of an enzymatic pathway. The temperature-

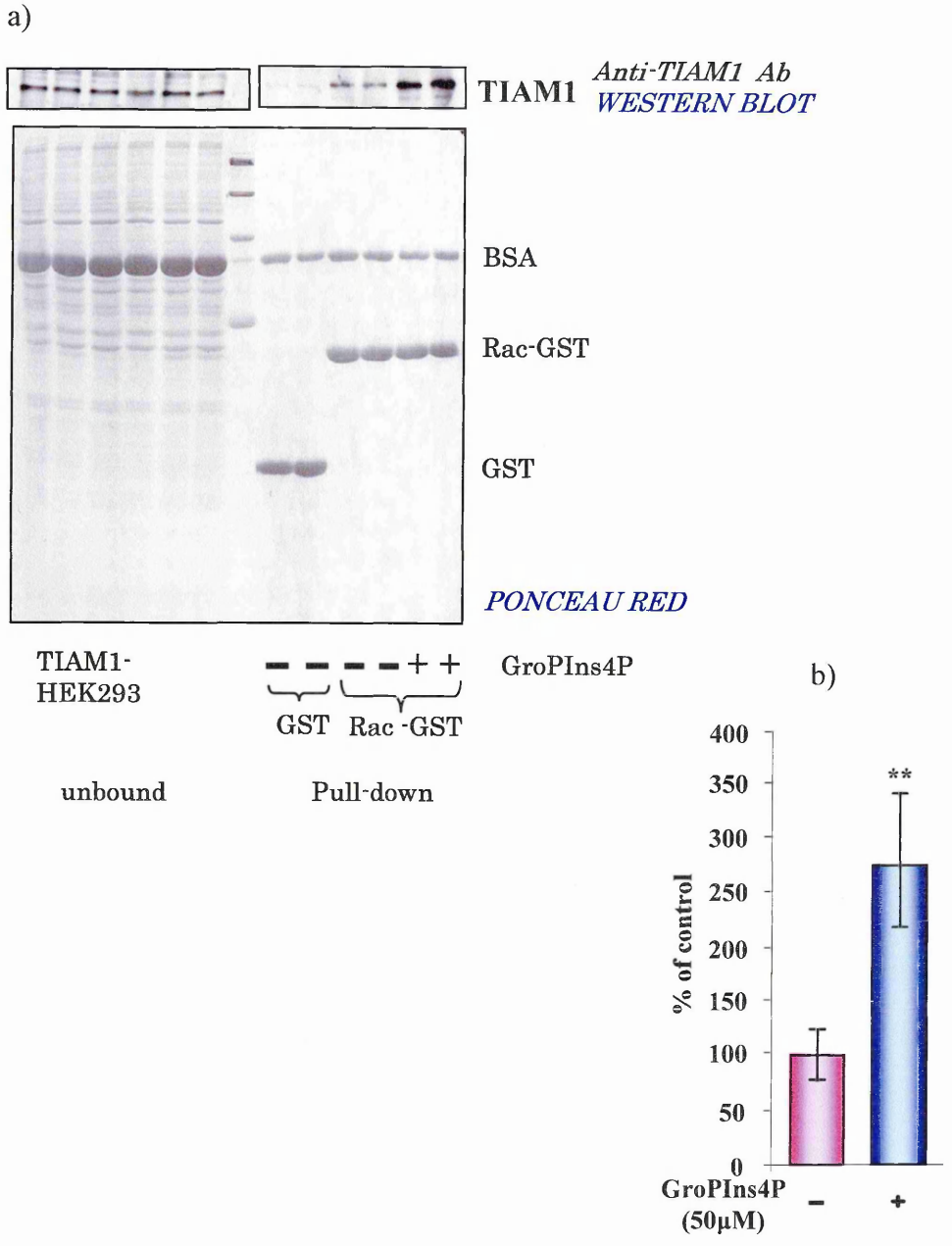

Figure 4.3 – Rac1-GST pull-down assay with cell cytosol overexpressing TIAM1. 120 µg of cell cytosol overexpressing TIAM1-HA (see Section 2.8.1) were first diluted (1:15) in reaction buffer (see Section 2.11.1). The cytosol was then pre-cleared with glutathione resin for 1 h at 4 °C on a rotating wheel (10 µl/sample) and then incubated for 10 min at 37 °C with 50 µM GroPIns4P. Finally, 4 µg of Rac1-GST purified protein, 10 µl glutathione resin and 20 µl of 2 mg/ml BSA (final volume 200 µl) were added to the samples and incubated for 1 h at 4 °C on a rotating wheel. The pellets were recovered and analysed by immuno-blotting with the antibody anti-TIAM1 (as described in Section 2.11.2). In a) the western blot of a representative pull-down assay is shown. In b) the quantification of the amount of TIAM1 co-precipitated with Rac1-GST, quantified by densitometric analysis with the NIH image program is shown. The effect of GroPIns4P is presented as percentage increase versus the untreated samples and the bars represent the mean (±SD) of four independent experiments, each performed in duplicate. $^{**}P<0.01$ versus control (w/o GroPIns4P)

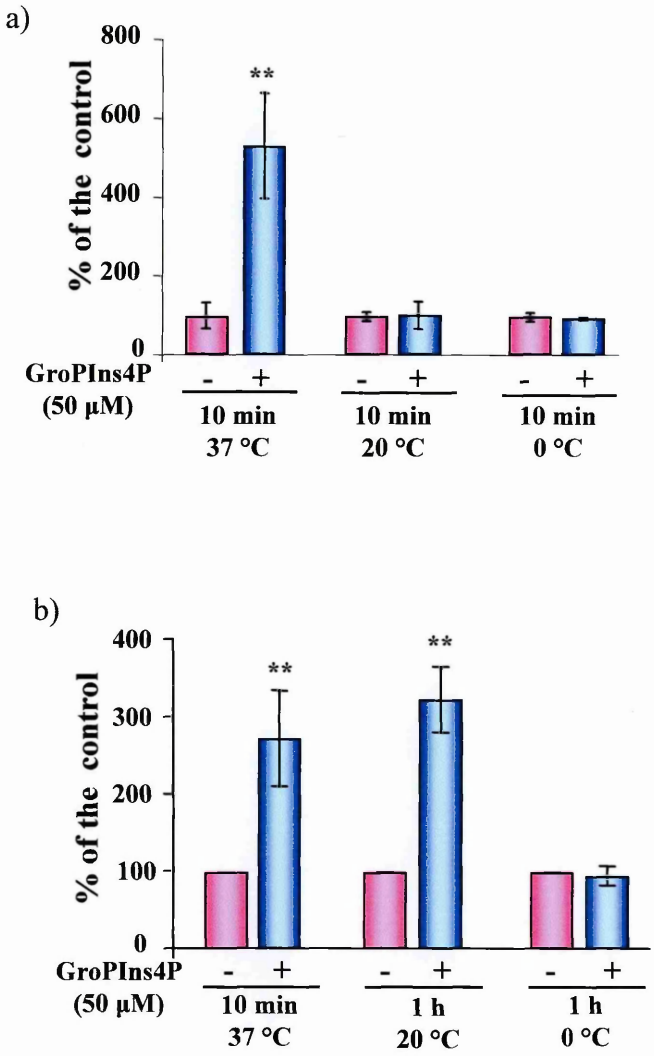

Figure 4.4 – Rac1-GST pull-down assay with cell cytosol overexpressing TIAM1. The pull down was performed as described in figure 4.3. In a) the samples were incubated with GroPIns4P for 10 min at different temperatures (37 °C, 20 °C and 0 °C). In b) the samples at 0 and 20 °C were incubated for 1 h. The quantification was performed by densitometric analysis with the NIH image program. The effect of GroPIns4P is presented as percentage increase versus the untreated samples and the bars represent the mean (±SD) of three independent experiments, each performed in duplicate. $^{**}P<0.01$ versus control (w/o GroPIns4P) (Section 1.14).

dependence would favour the second hypothesis, because at 0 °C there is no increase in binding between TIAM1 and Rac1 even increasing the time of incubation. However, the characteristics of the cytosol used tend to exclude the activation of an enzymatic pathway, since the $[Ca^{2+}]_i$ increase that is required for the initiation of the pathway from CaMKII activation that leads to TIAM1 and Rac1 activation cannot occur in this system. In fact, the cytosol is prepared in the presence of 1% NP-40 (which will solubilise all of the membranes) and with a 90,000 xg centrifugation (that eliminates any residual membrane complexes) (see Section 2.8.1; Labeta et al., 1988).

4.3.3 The pull-down assay with purified TIAM1

To see if GroPIns4P interacts directly with TIAM1, thus activating it and enhancing its binding to Rac1, a pull-down assay with purified TIAM1 was performed. Purified TIAM1 (C-1199-TIAM1) (see Section 2.9.2) was incubated for 10 min at 37 °C with GroPIns4P (50 μM). The pull down assay was performed as described for the cell cytosol (Section 4.3.2) and the TIAM1 was detected by immuno-blotting with the anti-TIAM1 antibody (as described in Section 2.11.3). Figure 4.5 shows the Western blot of an experiment (representative of three) in which it is clear that the binding between Rac1-GST and TIAM1 was not affected by the presence of GroPIns4P, as the amount of TIAM1 co-immunoprecipitated with Rac1 in the absence of GroPIns4P was similar to the amount precipitated in the presence of GroPIns4P. When GST was used instead of Rac1-GST, a signal for TIAM1 was not detectable (Fig. 4.5), thus suggesting that the binding between TIAM1 and Rac1-GST detected in the assay was specific.

These data exclude the hypothesis that a direct binding between GroPIns4P and TIAM1 could be enough to activate the exchange factor. However, it was still unclear how GroPIns4P increases the binding between TIAM1 and Rac1. The most probable hypothesis was the presence of a complex including TIAM1, Rac1 and other proteins that could have

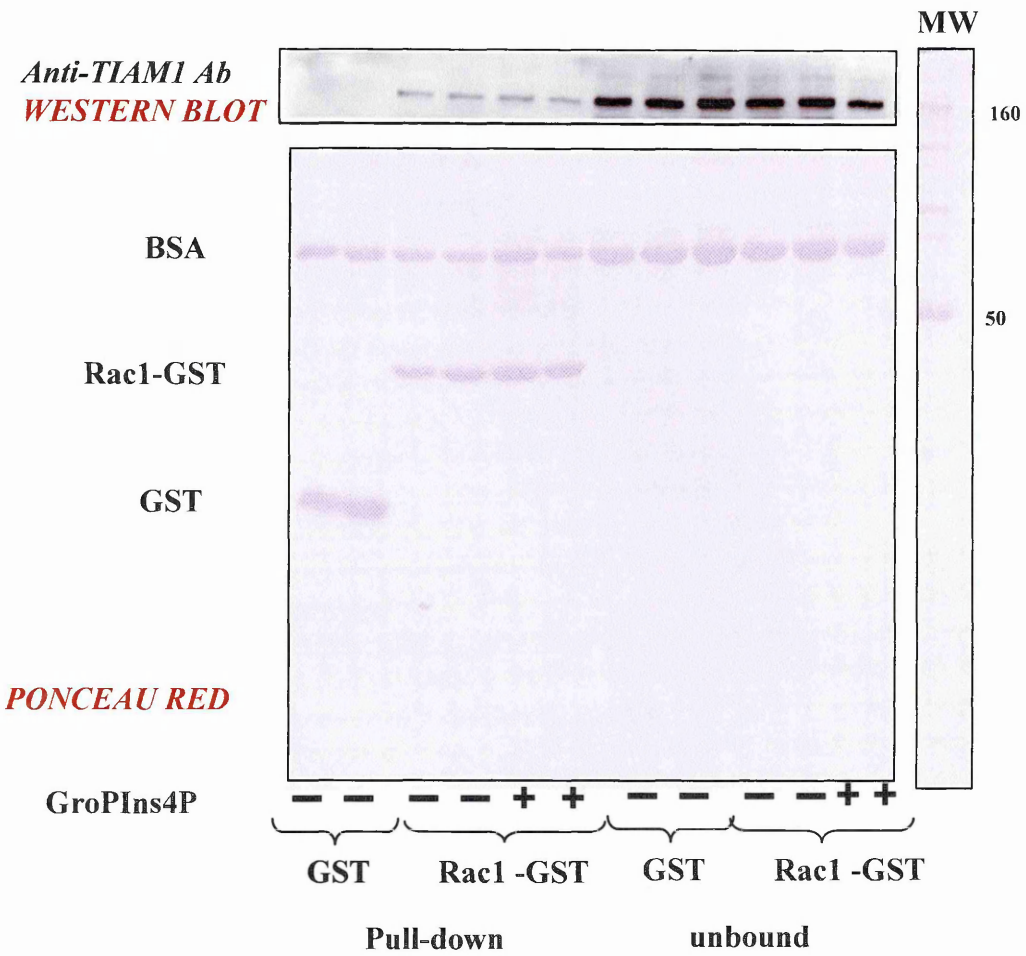

Figure 4.5 - Pull-down with purified TIAM1. 2 µg of purified TIAM1 (see Section 2.9.2) was incubated for 10 min at 37 °C with 50 µM GroPIns4P, then 2 µg of Rac1-GST or purified GST, 10 µl of 50% glutathione resin and the reaction buffer (see Section 2.11.3) were added to the samples (final volume 200 µl); finally the samples were incubated in a rotating wheel for 1 h at 4 °C. The pellets were recovered by centrifugation for 6 min at 800x *g* and then, after 3 steps of washing with the reaction buffer, analysed by immuno-blotting with the antibody anti-TIAM1 (as described in Section 2.11.3). The immuno-blot of TIAM1 (upper panel) and the ponceau red with the bands of Rac1-GST and GST (lower panel) are shown. This experiment is representative of three.

a role in favouring their interaction. Thus, the target of GroPIns4P could be a protein that, by interacting with TIAM1, favours its binding with Rac1, although it cannot be excluded that the interaction between GroPIns4P and TIAM1 itself allows a conformational change in TIAM1, which might result in interactions with other proteins (e.g. scaffolding proteins) that could increase the TIAM1 affinity for Rac1.

4.3.4 The effects of KN-93 in the pull-down assay

The pull-down assays indicated that GroPIns4P is able to increase the binding between Rac1 and TIAM1, but it is difficult to integrate this data into the pathway from PLC activation to membrane ruffle formation. The CaMKII-dependent phosphorylation of TIAM1 is important for its activation and favours its exchanging activity versus Rac1 (Michiels et al., 1997). As reported in Chapter 3, the activity of CaMKII can be modulated by GroPIns4P, and so it could be hypothesised that CaMKII is also involved in the GroPIns4P-dependent increase in Rac1-TIAM1 binding. To test this hypothesis, KN-93 (a specific inhibitor of CaMKII; see introduction, Section 1.3.4) was applied in the pull-down assay. The assay was performed with the same cell cytosol as for the previous pull-down assays, prepared from HEK293T cells transfected with TIAM1-HA (Section 4.3.2). The cytosol was incubated for 10 min at 37 °C with 50 μM GroPIns4P in the presence and absence of 20 μM KN-93 (the same concentration applied to completely prevent the translocation of TIAM1 to the plasma membrane; see Section 3.3.5). After the incubation, the pull-down assay was performed as described above (see Section 4.3.2).

The treatment with KN-93 completely prevented the GroPIns4P-dependent increase in Rac1-TIAM1 binding, as shown in Figure 4.6c, where the percentage increase in Rac1-TIAM1 binding is given with respect to the untreated samples. However, the treatment with KN-93 *per se* induced an increase in the basal level of interaction between Rac1 and TIAM1. The Western blotting with its relative quantification (Fig. 4.6a,b), revealed that

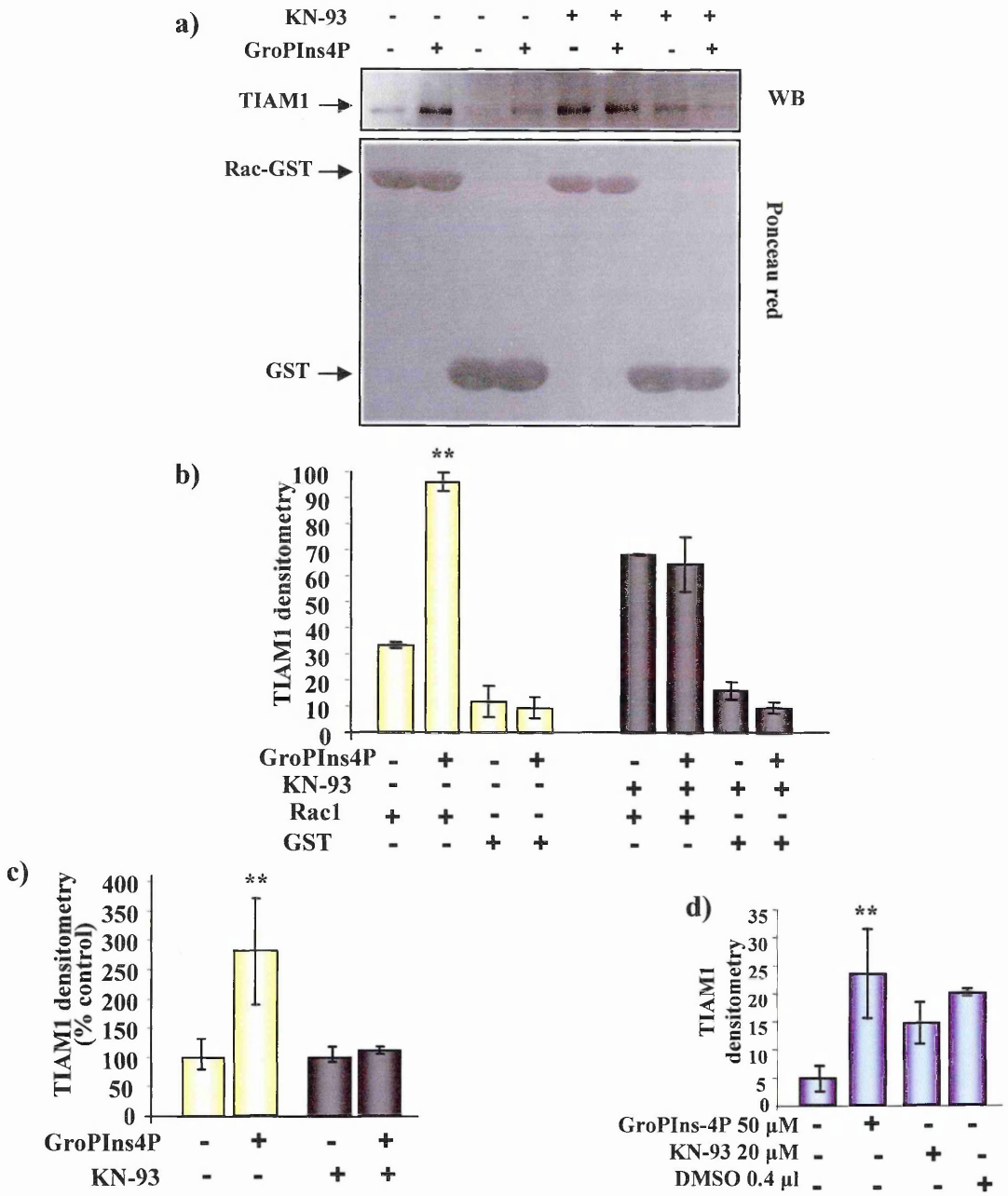

Figure 4.6 – Rac1-GST pull-down assay with cell cytosol overexpressing TIAM1. 120 µg of cell cytosol overexpressing TIAM1-HA (see Section 2.8.1) were first diluted (1:15) in reaction buffer (see Section 2.11.1), then the cytosol was pre-cleared with glutathione resin for 1 h at 4 °C on a rotating wheel (10 µl/sample) and incubated for 10 min at 37 °C with 50 µM GroPIns4P. Twenty µM KN-93 (CaMKII inhibitor) was added with the GroPIns4P during the 37 °C-incubation. Then the assay was performed as described in Figure 4.3 a) immuno-blot analysis of the experiment revealed with the Ab-anti TIAM1. b) quantification with the NIH program of the the experiment in a (was performed in duplicates). c) Average of three independent experiments; each sample was quantified by NIH image and then expressed as percentage of stimulation compared to the un-stimulated samples. d) Pull-down with KN-93 and DMSO: DMSO was added instead of KN-93, at the same concentration (0.4 µl of KN-93 were added to each sample to have a final concentration of 20 µM; thus 0.4 µl of DMSO were added as a control). $^{**}P<0.01$ versus control (w/o GroPIns4P) (Section 1.14).

the amount of TIAM1 co-precipitated with Rac1 upon treatment with KN-93 is similar to the amount obtained upon treatment with GroPIns4P. This increase in the basal interaction could explain why the GroPIns4P was not able to increase the binding between TIAM1 and Rac1 in the presence of KN-93. Thus, the CaMKII inhibitor appears to have a non-specific action in this assay and makes the results obtained difficult to interpret.

The KN-93 was dissolved in DMSO, which could also influence the final result; for this reason, the same pull-down assay was performed in the presence of DMSO. The cell cytosol overexpressing TIAM1-HA was incubated with GroPIns4P and KN-93 or with the same quantity of DMSO (control). DMSO itself produced an increase in the binding between TIAM1 and Rac1, thus confirming that the presence of DMSO could act in a non-specific way. The Figure 4.6d shows the densitometric quantification of the GroPIns4P-dependent binding between TIAM1 and Rac1 in the presence of KN-93 and DMSO. In conclusion, the KN-93-dependent reduction in the binding cannot be considered as an inhibition of the GroPIns4P effect, but as an increase in the basal level, due to the DMSO, that masks the activity of GroPIns4P.

There is still a possibility that CaMKII has an important role also in the GroPIns4P-dependent increase in Rac1-TIAM1 binding, and in this case, it remains to be elucidated how GroPIns4P activates this kinase. Neither direct activation of the kinase (the CaMKII activity assay performed with the purified enzyme does not shows any effect of GroPIns4P) nor a $[Ca^{2+}]_i$ increase appear to be the starting events that lead to the GroPIns4P-dependent increase in Rac1-TIAM1 binding in this *in vitro* pull-down assay.

4.3.4 Conclusion

The exchange activity of TIAM1 implies its direct interaction with Rac1-GDP. With the pull-down assay, it was possible to demonstrate that GroPIns4P facilitates the interaction between Rac1 and TIAM1. This action was temperature-dependent: there was

an increase in the binding with a short incubation at 37 °C or a long incubation at 20 °C, but not at 0 °C. From these data, it was not possible to conclude whether GroPIns4P acts on TIAM1 directly or indirectly through the activation of an enzymatic pathway. In addition, GroPIns4P was not active when the pull-down assay was performed with purified TIAM1, suggesting that GroPIns4P cannot act directly on the TIAM1. The attempt to evaluate if CaMKII is involved in the GroPIns4P-dependent increase in Rac1-TIAM1 binding was unsuccessful. There are no tools available to determine if GroPIns4P requires CaMKII to favour the binding between Rac1 and TIAM1, or if *per se*, by interacting with other proteins, GroPIns4P could be able to modulate this interaction. This second hypothesis is the most probable, even if to date we have not been able to find any specific interactor.

4.4 GroPIns4P interacts with a protein complex co-immunoprecipitated with TIAM1

4.4.1 General description

From the data obtained in the uptake experiments, the potential target of GroPIns4P should be a cytosolic protein that can also be complexed inside the cells in insoluble structures. Looking at the proteins involved in the GroPIns4P-dependent pathway that leads to ruffle formation and taking into consideration the data of the pull-down assay, which show that GroPIns4P favours the interaction between TIAM1 and Rac1, TIAM1 or a protein that binds this exchange factor could be good candidates.

A potential direct binding between GroPIns4P and TIAM1 could induce a change in the conformation of TIAM1 that favours its interaction with Rac1. However, this hypothesis is difficult to support, since much of the data are not in line with this direct interaction. First, the exchange activity of TIAM1 was not affected by GroPIns4P (as was

demonstrated by GEF assays performed in Mancini et al., 2003), and second, GroPIns4P does not bind with a high affinity to the two PH domains present in TIAM1 (as shown by the GroPIns4P competition assays with PC-liposomes containing 2% PIP_2, performed in this laboratory by Stefania Mariggiò, see Section 1.13.4). In addition, GroPIns4P was not able to increase the binding between purified TIAM1 and Rac1-GST in a pull-down assay. A potential interaction between Rac1 and GroPIns4P is also unlikely, since GroPIns4P is not able to affect the GEF or GAP activity of this small G-protein in *in vitro* assays (Mancini et al., 2003; see Section 1.4.3.2.2). Therefore, the presence of a third protein that interacts with TIAM1 and mediates the activation of TIAM1 by GroPIns4P, favouring the binding between Rac1 and its GEF, has to be considered the most plausible.

To further analyse the potential binding of GroPIns4P with a TIAM1-containing complex, binding experiments between immunoprecipitated or purified TIAM1 and GroPIns4P were performed, as reported in the following sections.

4.4.2 Binding experiments between GroPIns4P and TIAM1-HA immunoprecipitated from cell lysates.

TIAM1-HA was overexpressed in HEK293T cells, then immunoprecipitated from the cytosol with an anti-HA antibody, and finally, the immunoprecipitate was incubated with different concentrations of GroPIns4P in the presence of a tritiated tracer ([^{3}H]GroPIns4P) (see Sections 2.8.3 and 2.13.2). The specific binding was then calculated by subtracting the amount of [^{3}H]GroPIns4P bound to the cytosol of wild-type HEK293T cells incubated with the same antibody against the HA tag. The Western blot presented in Figure 4.7 shows the immunoprecipitation with the anti-HA antibody in the wild-type- and TIAM1-transfected cytosols. The incubation with [^{3}H]GroPIns4P was carried out at 37 °C for 45 min, then the samples were centrifuged and the pellets analysed by scintillation counting (see Section 2.13.2).

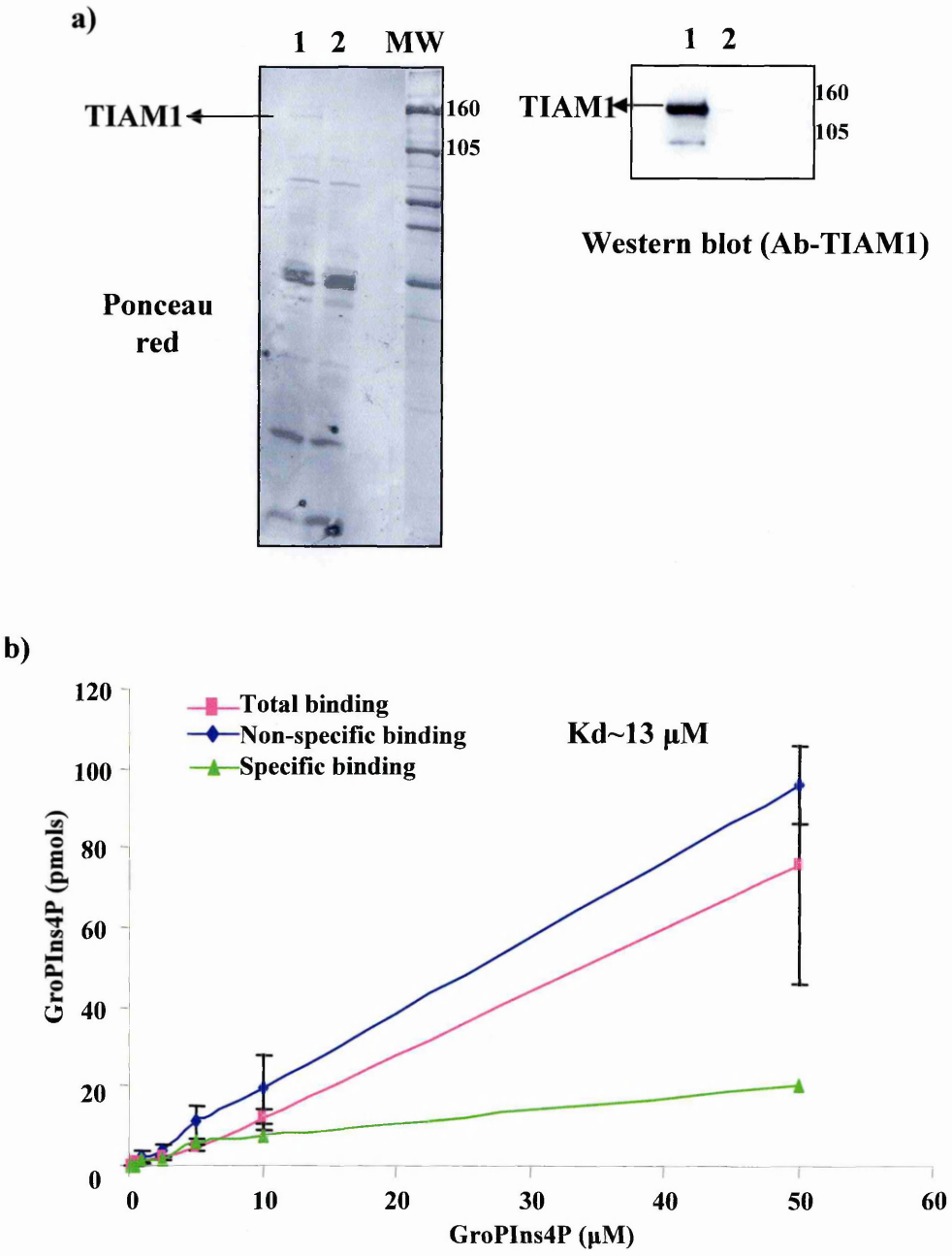

Figure 4.7 - Binding between a TIAM1-containing protein complex and GroPIns4P. a) Acrylamide gel of the immunoprecipitation. TIAM1-HA overexpressed in HEK293 cell lysate was immunoprecipitated with anti-HA antibody. The lanes represent the HEK293 wild type (2) and TIAM1-HA overexpressing (1) cell lysate immunoprecipitated with the antibody against the HA tag. Molecular weight markers (MW) are shown. **b**) The immunoprecipitates were incubated with GroPIns4P at different concentrations in the presence of a [^{3}H]GroPIns4P (see Section 2.13.2). The specific binding (—▲—) was calculated subtracting the non-specific (—◆—) from the total binding (—■—). The bars represent the mean (±SD) of two independent experiments, each performed in triplicates.

GroPIns4P was able to interact with the TIAM1 immunoprecipitate, thus supporting the idea that there is a potential binding between GroPIns4P and TIAM1 or a protein that co-precipitates with TIAM1. To calculate the affinity of GroPIns4P for this interactor, a dose-response curve was performed: GroPIns4P was applied to the samples in a range of concentrations from 0. 1 μM to 50 μM (see Section 2.13.2). This experiment showed that GroPIns4P was able to bind the immunoprecipitated TIAM1-HA with a Kd of ~13 μM (see Section 1.13.2), and thus the binding affinity is compatible with the GroPIns4P concentrations normally used and would support the hypothesis of the presence of specific binding between a complex containing TIAM1 and GroPIns4P in living cells (Fig. 4.7).

Thus, GroPIns4P could directly interact with TIAM1 or with another protein that is an interactor of TIAM1. This event could be the key point for our understanding of an alternative mechanism used by GroPIns4P to activate TIAM1 and Rac1.

4.4.3 Binding experiments between GroPIns4P and PH-domain-deleted mutants of TIAM1

If the interaction between GroPIns4P and TIAM1 is direct, it has to be understood where GroPIns4P binds TIAM1 and if there is a specific domain of interaction for GroPIns4P. If the interaction is not direct, the elucidation of the TIAM1 domain that could be responsible for the co-immunoprecipitation of the GroPIns4P-interactor may help us to understand the mechanism by which TIAM1 is activated by GroPIns4P.

This Rac1 exchange factor contains several sites of potential interaction with GroPIns4P. Besides the two PH domains (N- and C-terminal), a Ras binding domain (RBD) and a PDZ domain could be important for the interaction of TIAM1 with its effectors. TIAM1 activity can be modulated by different cellular events, like phosphorylation, interactions with phosphoinositides, and also with proteins (as discussed

in Section 1.2.3.2). Thus, one or more of these events could be important also for the activity of GroPIns4P.

As demonstrated by the GroPIns4P competition assays with PC-liposome containing 2% PIP_2 (Stefania Mariggiò, Section 2.13.4), GroPIns4P does not bind with a high affinity to the two PH domains of TIAM1. The PIP_2 binding assays were performed under different conditions to those using GroPIns4P (to follow the interaction between GroPIns4P and immunoprecipitated TIAM1), and thus it cannot be excluded that the PH domains are important for the binding of GroPIns4P either as sites of direct interaction or as binding elements of the protein that interacts with GroPIns4P. To solve this problem, PH-domain-deleted mutants of TIAM1 were used in the same binding assay. These mutants selectively lacked the N-terminal PH domain (ΔPHn-TIAM1), the C-terminal PH domain (ΔPHc-TIAM1) or both (ΔPH-TIAM1), as showed in Figure 3.7a (Chapter 3). The mutants were expressed in vectors that contain the GFP tag, thus the immunoprecipitation was performed using an antibody against GFP. Each mutant was compared with the GFP-tagged wild-type construct (TIAM1-GFP) for binding with GroPIns4P, and the non-specific binding was calculated by overexpressing and immunoprecipitating GFP alone in the same cell system.

Even if this comparison was affected by differences in the overexpression and immunoprecipitation efficiencies, the indication was that all the mutants were able to interact with the GroPIns4P. As shown in Figure 4.8b, both TIAM1-GFP and ΔPH-TIAM1 showed a 1.5-fold increase in [^{3}H]GroPIns4P binding when compared to GFP, thus suggesting that the absence of the PH domains does not affect the binding of GroPIns4P. The other two mutants showed lower levels of interaction, although in both cases the amount of overexpressed and immunoprecipitated protein was lower (Fig 4.8a). Thus, the data support the initial observation that the PH domains are not important for the activity of GroPIns4P. They appear not to be sites for direct interactions with GroPIns4P and they are most likely not important for the formation of a complex that contains TIAM1 and

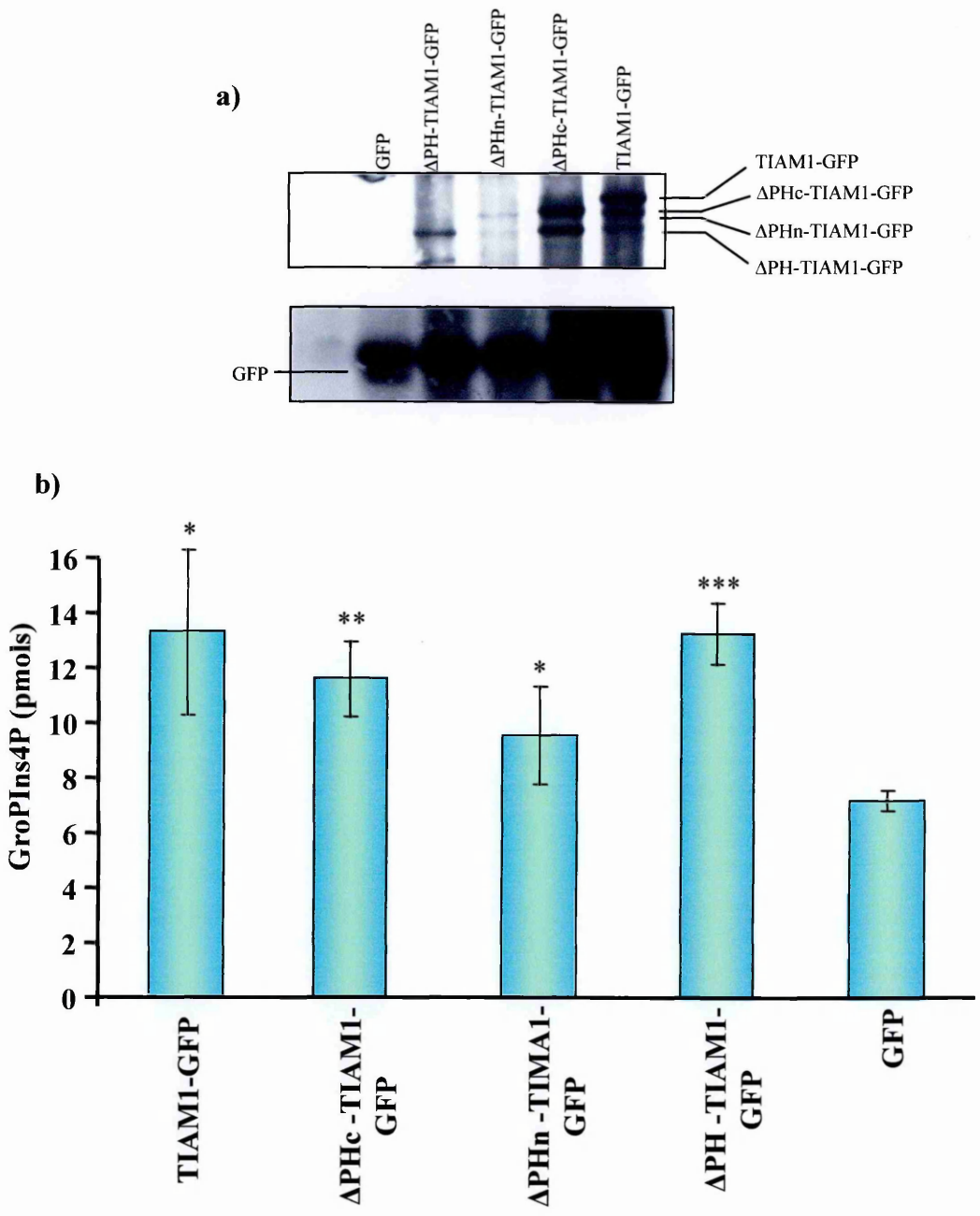

Figure 4.8 - Binding between GroPIns4P and TIAM1 or deleted mutants GFP-tagged (see Fig. 3.7a). HEK 293 cells were transfected with the GFP-tagged TIAM1 and its deletion mutants. The cells were then lysed after 48 h of transfection and the cytosol prepared (as described in Section 2.8.1). a) western blot of the immunoprecipitation performed using an antibody against the GFP. b) Binding assay. Each immunoprecipitated mutant was tested for the ability to bind GroPIns4P (as explained in Figure 4.7 and Section 2.13.2. Each mutant has to be compared with the GFP-tagged wild tipe construct for the binding to GroPIns4P and the non specific binding was calculated by overexpressing GFP in the same cell system. The bars represent the mean of two independent experiments, each performed in triplicate. **P*<0.05, ***P*<0.01, ****P*<0.001, versus GFP (Section 1.14).

GroPIns4P. Therefore, there should be another domain of TIAM1 that has an important role in this process. This domain should be a regulatory one that by interacting with different proteins, can modulate the behaviour of TIAM1.

4.4.4 GroPIns4P binding studies with purified TIAM1 and Rac1

The data obtained up to now tend to exclude the possibility that GroPIns4P interacts directly with TIAM1. However, to exclude this possibility by alternative approaches, binding assays were performed with purified GST-tagged TIAM1. Purified Rac1-GST was also tested in this assay, to check if it could interact with GroPIns4P.

The assay buffer, GroPIns4P concentration and time of incubation where the same as those used in the previous binding assays with immunoprecipitated TIAM1-HA (see Section 1.13.3). Two different approaches were used to determine if GroPIns4P binds directly to TIAM1-GST:

1. TIAM1-GST was incubated with [^{3}H]GroPIns4P (the tritiated compound was 9 x10^4 cpm/sample and represented 1/120 of the total GroPIns4P, used at a concentration of 10 μM) and then precipitated with glutathione resin to separate the unbound fraction. The non-specific binding was calculated by using purified GST instead of TIAM1-GST (see Section 2.13.3). There was no difference in the amount of GroPIns4P bound to TIAM1-GST or to GST alone, thus suggesting that GroPIns4P does not bind TIAM1 specifically (Fig 4.9a).
2. TIAM1-GST was incubated with [^{3}H]GroPIns4P as above, spotted onto nitrocellulose filters and washed twice using a vacuum filtration apparatus. Again, GST was used to evaluate the non-specific binding (see Section 2.13.3). However, no significant differences were seen between the samples with TIAM1-GST and those with GST (Fig. 4.9b). Purified Rac1-GST

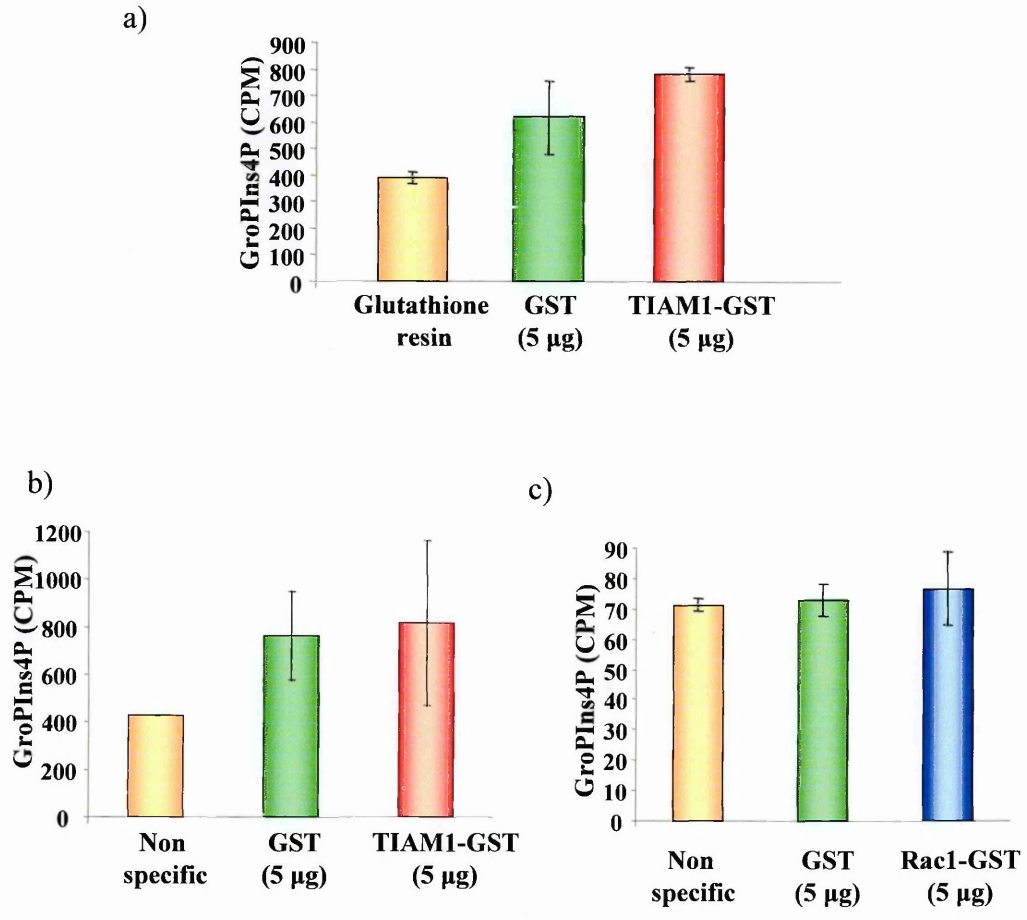

Figure 4.9 - Binding between GroPIns4P and purified TIAM1-GST or Rac1-GST. **a)** TIAM1-GST (5 µg), purified as reported in Section 2.9.2, was incubated with [^{3}H]GroPIns4P and then precipitated with the glutathione resin to separate the unbound fraction. The non-specific binding was calculated by using purified GST (5 µg, purified as described in Section 2.9.2) instead of TIAM1-GST (as described in Section 2.13.3. **b)** TIAM1-GST (5 µg) was incubated with [^{3}H]GroPIns4P, spotted on nitrocellulose filters and washed twice with a vacuum filtration apparatus. GST was used to evaluate the non specific binding (Section 2.13.3). **c)** the same assay with vacuum apparatus was used to test the binding between Rac1-GST (5 µg) (purified as described in Section 2.9.1) and GroPIns4P.

was also tested in this assay, and also in this case no specific binding was observed (Fig. 4.9c).

These data further confirmed the idea that GroPIns4P does not directly interact with TIAM1 or Rac1. It is presumably possible, however, that the conditions applied in the binding assay were not suitable to follow the interactions between TIAM1 or Rac1 and GroPIns4P.

4.4.5 CaMKII is co-immunoprecipitated with TIAM1

CaMKII was present in the complex that co-immunoprecipitated with TIAM1, as showed in Figure 4.10a. It could be hypothesized that CaMKII interacts directly with GroPIns4P, even if GroPIns4P was not able to directly activate the purified CaMKII (see Section 3.4.3). To verify if GroPIns4P can affect the activity of CaMKII co-immunoprecipitated with TIAM1, the ability of CaMKII to phosphorylate TIAM1 in the immunoprecipitated complex was analysed. After immunoprecipitation, the complex was incubated in the ADBII buffer and [γ^{32}P]ATP (see Section 2.6.2) in the presence of GroPIns4P (50 μM). The level of TIAM1 phosphorylation was then analysed by Western blotting and quantified by an analysis with the Instant Imager (see Section 2.6.2). GroPIns4P did not affect the level of CaMKII-dependent phosphorylation of TIAM1 under these conditions, as shown in Figure 4.10b. The specificity of the CaMKII activity was tested by adding KN-93 to the samples, which caused complete inhibition of the TIAM1 phosphorylation (Fig.4.10b).

The activity of CaMKII versus its substrate TIAM1 was not influenced by GroPIns4P. This observation was confirmed also when the assay was performed in the presence of purified TIAM1 and CaMKII instead of the immunoprecipitate. TIAM1-GST and CaMKII were incubated in ADBII buffer with [γ^{32}P]ATP (see Section 2.6.2), in the presence of GroPIns4P (50 μM). Then the samples were analysed by Westrn blotting and quantified by the instant imager. In Figure 4.10c is reported the autoradiography of a

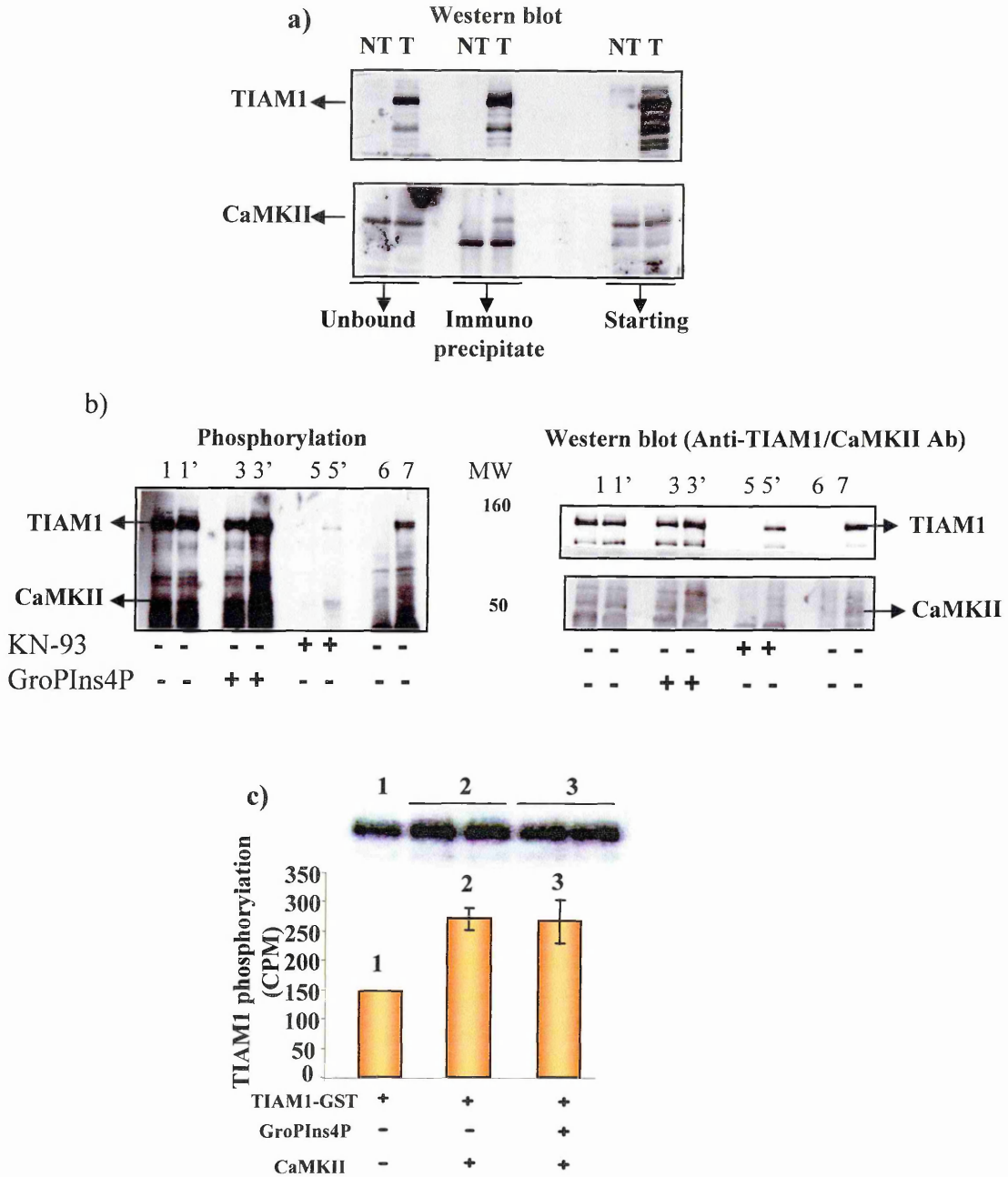

Figure 4.10 - CaMKII-dependent phosphorylation of TIAM1. a) Western blotting of the immunoprecipitation of TIAM1-HA (T) compared with the non transfected cytosol (NT) revealed with the antibody against TIAM1 and CaMKII. **b)** HEK293 cells were transfected with TIAM1-HA, then, after 48 h, treated for 24 h with KN-93 and lysed and immunoprecipitated with the anti-HA Ab. The immunoprecipitated samples were treated for 10 min with GroPIns4P prior to be used for the phosphorylation assay (Section 2.6.2). Samples 6 and 7 are respectively the negative (untrasfected cells) and positive controls (cell cytosol used for previous experiments overexpressing TIAM1) for the immunoprecipitation and phosphorylation. c) 2 µg of TIAM1 purified, 0.05 µg of purified CaMKII and [γ^{32}P] ATP were incubated in the absence and presence of 50 µM GroPIns4P for 45 min at 30 °C in the ADBII buffer, to follow the CaMKII-dependent TIAM1 phosphorylation (see Section 2.6.2). The figure shows a representative experiment, with the autoradiography and its relative quantification performed by Instant Imager. The plot represent the mean of each duplicate (2 and 3)

representative experiment with its relative quantification, from which it is clear that the CaMKII specifically phosphorylates TIAM1, but GroPIns4P does not affect the levels of TIAM1 phosphorylation. Thus, GroPIns4P can interact with a protein complex containing TIAM1, CaMKII and Rac1 without affecting the level of CaMKII-dependent phosphorylation of TIAM1.

4.4.6 Conclusion

The mechanism of action of GroPIns4P that could be hypothesized from the experimental evidence (obtained in Chapter 3) involves a PLC-dependent increase $[Ca^{2+}]_i$ that activates CaMKII; this kinase in turn phosphorylates TIAM1, allowing its translocation to the plasma membrane where Rac1 is activated, and consequently, where membrane ruffles are formed. Whether the binding between the TIAM1-containing complex and GroPIns4P is a crucial event for this pathway needs further analysis. In fact, the final effect (ruffle formation) could be the result of a double action of GroPIns4P, which on the one hand increases $[Ca^{2+}]_i$, activating in this way CaMKII, and on the other hand, modulates directly the activity of TIAM1 by bringing this GEF into contact with the relevant proteins. GroPIns4P could have a tethering function, allowing the formation of a large complex that could be responsible for the TIAM1/Rac1 activation, and consequently, ruffle formation.

4.5 Final discussion

When exogenously added to cells, GroPIns4P is able to equilibrate across the membrane due to the activity of a specific membrane transporter (as discussed in Section 1.4.4). Using uptake experiments it was possible to follow an increase in the intracellular concentration of GroPIns4P, both in intact and permeabilised cells. Plasma membranes and total membranes of NIH 3T3 cells do not show any specific binding of GroPIns4P. Thus

there is no experimental evidence that supports the presence of a specific membrane receptor, suggesting that the cellular effects of this compound are due to its action at the level of intracellular targets. Preliminary data, obtained form a competition assay between [^{3}H]GroPIns4P and unlabelled GroPIna4P, indicates that the affinity of GroPIns4P for its target is high because a complete displacement occurs in the range of 0.1-10 μM GroPIns4P (Fig. 4.11). Here the assay was performed by incubating permeabilised NIH 3T3 cells with a fixed amount of [^{3}H]GroPIns4P and then adding increasing amount of GroPIns4P. The uptake was followed as described in Section 2.12.2.1. The non specific binding was calculated by performing the same assay using total membranes (see Section 2.12.2.2). Further experiments will be performed in order to calculate the Kd for GroPIns4P and its unknown interactor.

As well as the Src-dependent pathway that starts from Src activation and *via* $[Ca^{2+}]_i$ increase, leads to the CaMKII-dependent TIAM1/Rac1 plasma membrane translocation and ruffle formation, GroPIns4P is able to increase the binding between Rac1 and TIAM1 and appears to interact directly with a protein complex associated with immunoprecipitated TIAM1-HA. How these two effects are connected is not yet clear. Three common elements are present: TIAM1, Rac1 and CaMKII.

Ruffle formation is strictly dependent on the localization of both TIAM1 and Rac1 at the plasma membrane and also on the activation of Rac1 by TIAM1. The action of GroPIns4P on these two proteins goes in two directions: on the one hand, it favours their translocation to the plasma membrane in a Src–dependent way, and on the other, it increases their interaction in a way that does not require Src-dependent signalling. TIAM1 is phosphorylated and thus activated by CaMKII, and GroPIns4P is able to activate this kinase by acting through Src. CaMKII is part of a complex that co-immunoprecipitates with TIAM1 and that interacts with GroPIns4P. The experimental evidence tends to exclude a direct interaction with or activation of CaMKII by GroPIns4P. In addition, the inhibition of CaMKII completely abolishes GroPIns4P-dependent ruffle formation,

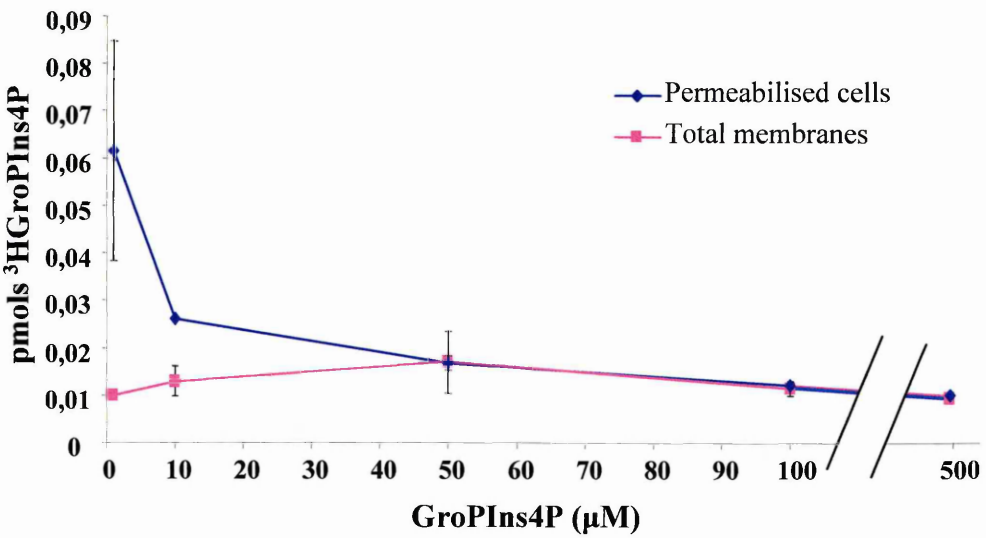

Figure 4.11 - Competition assay. Competition assay between the unlabelled and [^{3}H]GroPIns4P using permeabilised NIH 3T3 cells (1.5x10^6 cells) (◊). Total membrane (120 μg) of NIH 3T3 cells were used to see the non specific binding, (□) of GroPIns4P (see Figure 4.2 and Section 4.2.3). The concentration of GroPIns4P applied to the system was from 0.1 μM to 500 μM. The cells or the membranes were diluted in 150 μl of growth medium plus 10 μM HEPES and incubated with 150 μl of growth medium plus [^{3}H]GroPIns4P (9 x10^4 cpm/sample), 10 μM HEPES and GroPIns4P at the different concentrations for 10 min. After 3 washes with a buffer containing HBSS, 2 mg/ml BSA and GroPIns4P (each sample with the same concentration of GroPIns4P applied for the competition assay), the samples were spotted in nitrocellulose filters. Each sample was tested in quadruplicate. The filters were counted by β-scintillation counter. The total pmols of GroPIns4P bound to the samples are reported in the y axis. The bars represent the average (±SD) between the 4 samples analyzed for the experiment.

whereas the inhibition of Src still allows a 30% increase in ruffles (as shown in Section 3.9.3). The question that arises from these data is whether this residual activity of GroPIns4P is related to its ability to increase the binding between Rac1 and TIAM1, or to its ability to interact with a protein complex containing CaMKII and TIAM1. Coming back to the unknown target mentioned in Chapter 3 (Section 3.10), it is possible that what is co-immunoprecipitated with TIAM1 and specifically interacts with GroPIns4P is a scaffolding protein that tethers TIAM1, CaMKII and Rac1 together, forming a complex that has a fundamental role in ruffle formation. Under normal conditions, GroPIns4P can cause the full activation of CaMKII, by a Src-dependent pathway, thus reaching its maximal effect on ruffle formation (2.5-fold increase). When Src is blocked, the CaMKII portion that maintains a residual basal activity also after starvation, could be involved in the activation of TIAM1. GroPIns4P could interact with this unknown target, and in this way, favour the formation of a multi-protein complex, at the level of the membrane, containing TIAM1, Rac1 and CaMKII, which together cooperate in ruffle formation (Fig. 4.12).

This hypothesis needs to be challenged experimentally. First, the specific interactors of GroPIns4P have to be defined. New experimental approaches will be followed, such as two-dimensional gel electrophoresis to separate the proteins in the complex, followed by analysis by mass spectrometry to identify the proteins that are co-immunoprecipitated with TIAM1. However, this work is in progress and is not part of the present study.

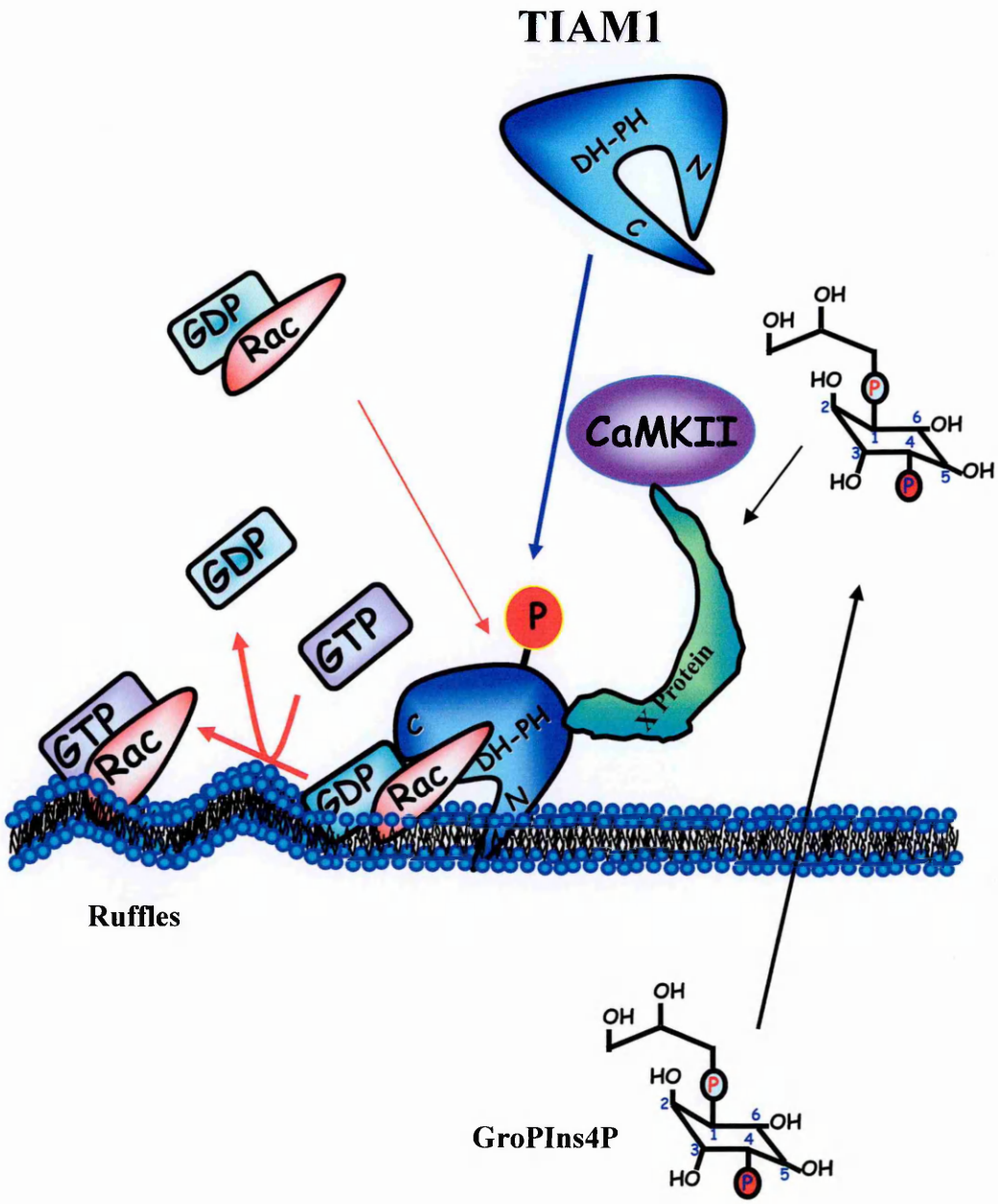

Figure 4.12 - Final scheme. GroPIns4P could interact with an unknown target (x protein), and in this way, favour the formation of a multi-protein complex containing TIAM1, Rac1 and CaMKII, which together cooperate in ruffle formation.

CHAPTER 5

OTHER BIOLOGICAL ACTIVITYES OF GroPIns4P

5.1 Introduction

As well as the pathway that leads to membrane ruffle formation described in Chapter 3 and 4, exogenously applied GroPIns4P causes other cellular events, such as the inhibition of G protein-activated adenylyl cyclase (AC) (Iacovelli et al., 1993), and stress fibre formation both in Swiss and NIH 3T3 cells. This latter event is dependent on the activation of the small GTPase RhoA (Mancini et al., 2003).

The aim of this Chapter is to describe the mechanisms by which GroPIns4P affects AC activation and stress fibre formation in fibroblasts and to discuss the correlation between the different effects that GroPIns4P can produce in cells.

5.2 GroPIns4P activates adenylyl cyclase acting through $G\alpha_i$ in NIH 3T3 cells

5.2.1 General description

The biological activities of the glycerophosphoinositols have been associated with G-proteins: it has been shown that exogenously applied GroPIns4P inhibits G_s-activated AC (Iacovelli et al., 1993). In thyroid cells, cholera toxin (CTX) or aluminium fluoride-activated AC was inhibited by GroPIns4P; moreover GroPIns4P was able to prevent CTX and forskolin-dependent activation of AC in Swiss 3T3 cells (Falasca et al., 1997). Several isoforms of AC exist, and they are regulated in different ways: isoforms I, III and VIII are activated synergistically by α_s, together with Ca^{2+}-calmodulin; isoforms II, IV and VII are activated synergistically by the α_s and $\beta\gamma$ subunits; and isoforms V and VI are inhibited by

α_i and Ca^{2+} (Sunahara and Taussig, 2002) (see Section 1.3.3). Considering that isoforms V and VI are expressed in NIH 3T3 cells (Smit et al., 1998), it can be hypothesized that the inhibition of AC operated by GroPIns4P is mediated by the activation of a $G\alpha_i$.

The mechanism by which GroPIns4P inhibits AC was investigated using different experimental approaches, including GTPγS binding to plasma membranes of NIH 3T3 cells, to see if GroPIns4P can activate the heterotrimeric G proteins, and cAMP measurements, to determine if GroPIns4P can inhibit AC.

5.2.2 GroPIns4P increases GTPγS binding to the plasma membranes of NIH 3T3 cells

To investigate a possible activation of heterotrimeric G proteins by GroPIns4P, assays of GTPγS binding to the plasma membranes of NIH 3T3 cells treated with GroPIns4P were performed. The plasma membranes were prepared from NIH 3T3 cells as reported in Section 2.10.2. The incubation with the stimuli was performed for 1 h at 37 °C in a GTPγS buffer containing [^{35}S]GTPγS (see Section 2.13.1). After the incubation, the samples were spotted onto nitrocellulose filters, washed 3 times with wash buffer, and then counted in a β-scintillation counter. The non-specific binding was calculated by spotting the radioactive mixture alone onto the filter (as described in Section 2.13.1).

The membranes were stimulated with 50 μM GroPIns4P, and to follow the activation of the heterotrimeric G-proteins, Mas7 (25 μM), a non-specific activator that mostly activates G_i, and LPA (10 μM), which can activate both G_i (for AC inhibition; van Corven et al., 1989) and G_{13} (for stress fibre formation; Ridley and Hall, 1992) were used. After 1 h of incubation of the plasma membranes with GroPIns4P, a 30% increase in

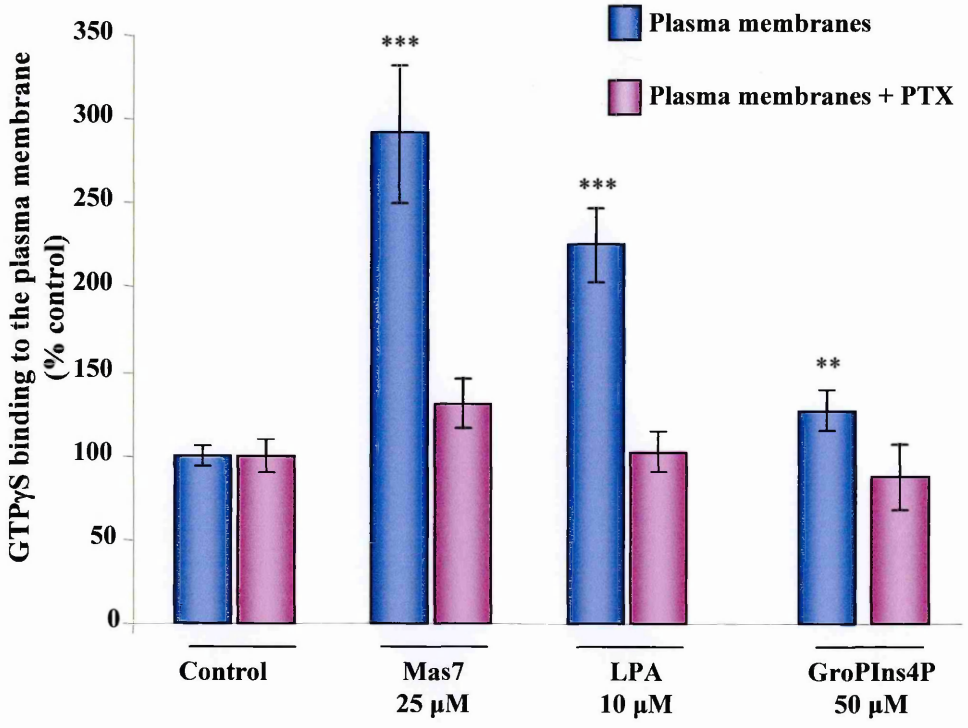

Figure 5.1 - GTPγS binding to the plasma membranes from NIH 3T3 cells. Plasma membranes from NIH 3T3 cells were untreated (blue) or treated (violet) with PTX (5 nM) and with different stimuli (25 μM Mas7, 10 μM LPA, and 50 μM GroPIns4P) for 30 min at 30 °C in the presence of [^{35}S]GTPγS. Then the samples were filtered using a vacuum filtration apparatus, and washed 3 times. The filters were added to scintillation fluid and counted in a β-scintillation counter, as described in Section 2.13.1. The data are presented as the percent response over untreated membranes (control). The bars represent the mean (±SD) of three independent experiments, each performed in triplicate. $^{**}P<0.01$ $^{***}P<0.001$, versus control (Section 1.14).

GTPγS binding was seen. This increase was lower than that obtained by stimuli like Mas7 (200%) and LPA (140%), as shown in Figure 5.1.

To identify which class of G proteins are activated by GroPIns4P, the same assay was performed using plasma membranes obtained from NIH 3T3 cells treated with pertussis toxin (PTX), which blocks all of the G_i/G_0 classes of G proteins. PTX has been widely used as a reagent to characterize the involvement of heterotrimeric G proteins in signalling. PTX catalyses the ADP-ribosylation of specific G protein α subunits of the G_i family, and this modification prevents the occurrence of the receptor-G protein interaction (Pittman, 1984). The NIH 3T3 cells were treated for 24 h with 5 nM PTX, and then harvested and the plasma membranes prepared as described in Section 2.10.2. This procedure leads to the full ribosylation of the $G\alpha_i$ subunits present in the membranes, as observed in the ADP-ribosylation assay reported in Figure 5.2. Here, the plasma membranes obtained from cells that were treated with (5 nM) PTX and from untreated cells were incubated with the catalytic subunit of PTX (100 nM) in the presence of [^{32}P]NAD, and the extent of ADP-ribosylation of the $G\alpha_i$ subunit was analysed (as described in Section 2.10.4). The treatment with the catalytic subunit of PTX caused a full ADP-ribosylation of the $G\alpha_i$ subunit of the plasma membranes obtained from the control cells, whereas the plasma membranes from the cells that were treated with PTX did not shown any ADP-ribosylation of the $G\alpha_i$ subunit (because $G\alpha_i$ was already ADP-ribosylated by treatment of the intact cells with PTX). This indicated that a 24 h-treatment with (5 nM) PTX of NIH 3T3 cells performed prior to the preparation of the plasma membranes was enough to obtain full ADP ribosylation of the $G\alpha_i$ subunit (Fig. 5.2).

The GroPIns4P-dependent increase in GTPγS binding to the plasma membranes was completely inhibited by PTX, and the same also happened for LPA and Mas7 (Fig. 5.1). Thus, GroPIns4P can act at the level of the G_i/G_0 family of heterotrimeric G proteins, and this action may be the key point for an explanation of its ability to inhibit AC in

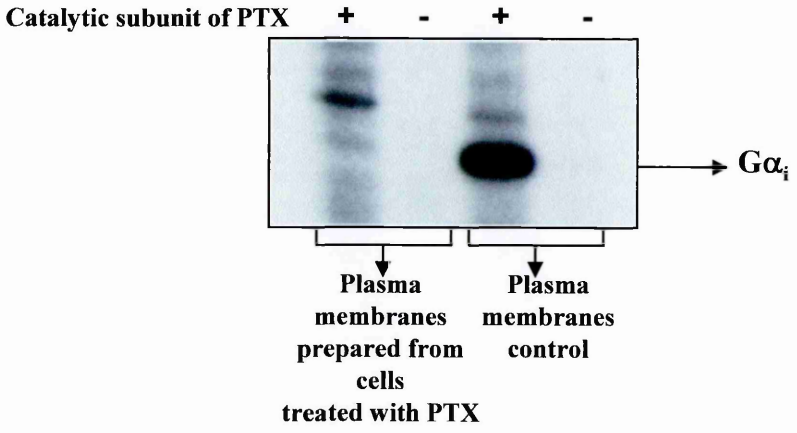

Figure 5.2 - PTX-dependent ADP-ribosylation of plasma membranes from NIH 3T3 cells. Plasma membranes were obtained from NIH 3T3 cells that were treated with 5 nM PTX (see Section 2.10.1) and from untreated cells. The membranes were incubated with the catalytic subunit of PTX (100 nM) in the presence of [^{32}P]NAD, and the extent of ADP-ribosylation of the Gα_i subunit was analysed (as described in Section 2.10.4). The ADP-ribosylation levels were analysed by autoradiography.
The experiment was performed by Nadia Dani, Di Girolamo' s laboratory (our department)

fibroblasts (Falasca et al., 1997).

5.2.3 The GroPIns4P-dependent inhibition of AC is prevented by PTX

To investigate whether after blocking the G_i/G_0 classes of G proteins, GroPIns4P can still prevent the activation of AC, cAMP measurements were carried out in the presence of PTX, in NIH 3T3 cells. AC was activated by CTX, which transfers the ADP-ribose to the $G\alpha_s$ subunit, forming a covalent bond with an arginine residue situated in close vicinity to the γ-phosphate of the bound GTP. This modification prevents the GTPase activity of $G\alpha_s$ and causes $G\alpha_s$ to remain activated (Gill and Meren, 1978). LPA was used to show $G\alpha_i$-dependent AC inhibition (van Corven et al., 1989). GroPIns4P (50 μM) and LPA (10 μM) were added to NIH 3T3 cells for 30 min, together with CTX (10 nM). In this way, it was possible to allow the blockage of AC inside the cells, and to prevent their CTX-dependent activation. The PTX (5 nM) was added 24 h before to prevent any residual activation of the $G\alpha_i$ proteins.

After the treatments, cAMP was extracted by the ethanol method (see Section 2.6.4) and measured using a commercial radioimmunoassay ("Cyclic AMP [^{3}H] assay system", from Amersham). This assay is based on competition between unlabelled cAMP and a fixed quantity of tritium labelled cAMP for binding to a protein which has a high specificity and affinity for cAMP. The amount of labelled protein-cAMP complex formed is inversely related to the amount of unlabelled cAMP present in the assay (see Section 2.6.4). The results are expressed as pmol of cAMP/well.

GroPIns4P was given for 30 min together with CTX and it caused a 30% inhibition of CTX-activated AC (Fig. 5.3). When LPA was applied under the same conditions as GoPIns4P, it caused a 70% inhibition. As shown in Figure 5.3, in the untreated samples, there were 4±1 pmols/well of cAMP, and upon treatment with CTX, the cAMP increased to 88±10 pmols/well. When CTX was given to the cells with the GroPIns4P, the amount of

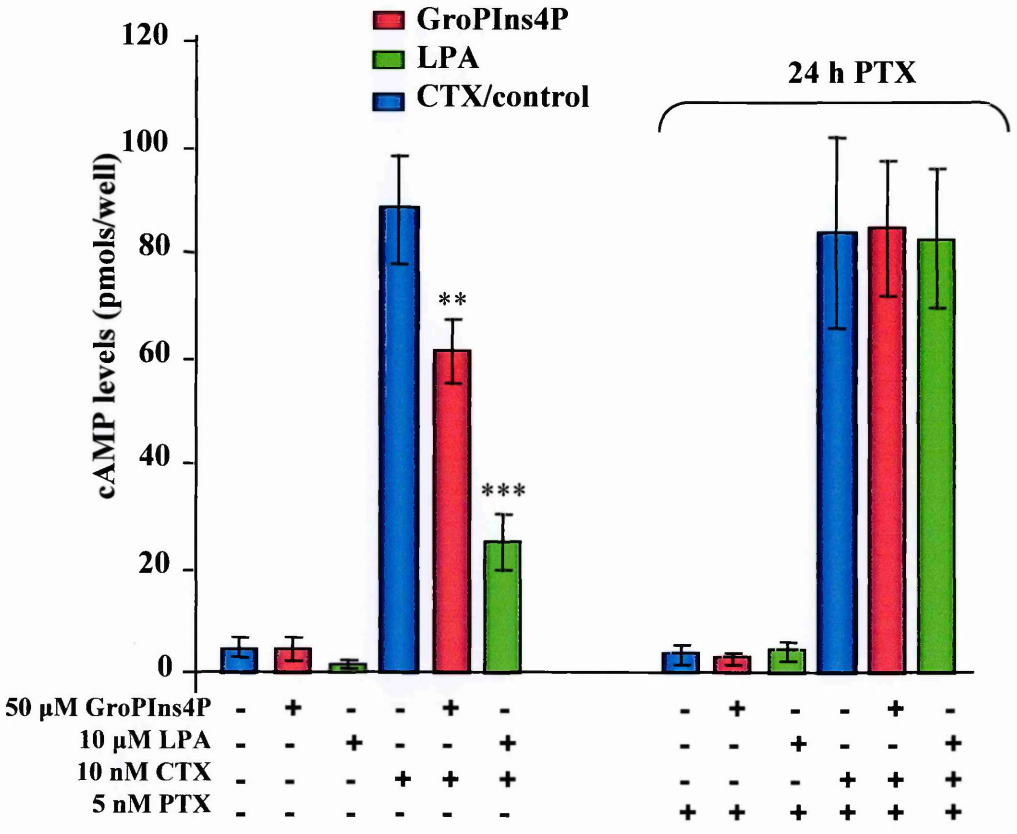

Figure 5.3 - Measurements of cAMP production in NIH 3T3 cells. NIH 3T3 cells were grown to confluence in 12-well plates in complete growth medium. Cells were then washed twice with HBSS and stimulated for different times at 37 °C in HBSS containing 0.4% BSA, 10 mM HEPES and 0.5 mM 3-isobutyl-1-methylxanthine (pH 7.4) in the presence of the various compounds to be assayed: CTX (10 nM), GroPIns4P (50 µM) and LPA (10 µM), as described in Section 2.6.4 The intracellular cAMP content was measured using a radioimmunoassay, as described in Section 2.6.4. The experiments were performed in triplicate, and the results are expressed as pmols of cAMP/well. The bars represent the mean (± SD) of three independent experiments, each performed in duplicate.
$^{**}P<0.01$ $^{***}P<0.001$ (versus the stimulation by CTX) (Section 1.14).

cAMP produced was 61±6 pmols/well, and in the presence of LPA, it was 25±5 pmols/well.

When NIH 3T3 cells were pre-treated with PTX for 24 h both the GroPIns4P- and the LPA-dependent inhibition of AC were impaired (Fig. 5.3). This result demonstrates that GroPIns4P inhibits the AC activity by acting at the level of the $G\alpha_i$ proteins.

5.2.4 Conclusion

GroPIns4P is able to increase the GTPγS binding to plasma membranes of NIH 3T3 cells, and this increase is prevented by pre-treating the cells with PTX. The data highlight the potential action of GroPIns4P through the $G\alpha_i$ proteins. The ability of GroPIns4P to inhibit AC was tested for its dependence on the $G\alpha_i$ proteins, and PTX treatment prevented the inhibition of AC produced by GroPIns4P. Thus, this inhibition of AC caused by GroPIns4P in NIH 3T3 cells depends on the activation of the $G\alpha_i$ proteins.

5.3 The potential involvement of $G\alpha_i$ proteins in GroPIns4P-dependent ruffle formation

5.3.1 General description

GroPIns4P acts through the $G\alpha_i$ class of heterotrimeric G proteins, at least with regard to AC inhibition. It cannot be excluded, however, that the activation of $G\alpha_i$ by GroPIns4P could be the key point in the pathway that leads from Src/PLCγ1 activation and a $[Ca^{2+}]_i$ increase to ruffle formation. There are interesting data that show how, by direct interaction, $G\alpha_i$ can activate Src (Ma et al., 2000) (Section 1.3.4). For this reason, an attempt was made to correlate all of the data obtained so far, from the Ca^{2+} measurements in the presence of inhibitors of the heterotrimeric G proteins to the immunofluorescence

assays, to see if GroPIns4P-dependent ruffle formation can be mediated by heterotrimeric G proteins.

5.3.2 GroPIns4P-dependent Ca^{2+} increases in the presence of PTX

NIH 3T3 cells were treated for 24 h with (5 nM) PTX to block all of the $G_{i/0}$ classes of heterotrimeric G proteins; then, the ability of GroPIns4P to increase $[Ca^{2+}]_i$ levels was investigated using the Till-Photonics live imaging of Fluo-3-loaded cells (as described in Section 2.5.1 and in Section 3.6). ATP was applied after GroPIns4P to check if the treatment with PTX alters the ability of the cells to increase their $[Ca^{2+}]_i$.

The PTX treatment did not prevent the $[Ca^{2+}]_i$ increases induced by adding GroPIns4P to the cells. In Figure 5.4, a representative experiment is shown, in which the cells were treated with GroPIns4P (50 μM) in the presence and absence of PTX; ATP (100 μM) was added to the samples as the positive control. The fluorescence changes, expressed as the pseudoratio ΔF/F0 (see Section 2.5.2 and 3.6), obtained in the control and PTX-treated cells were comparable, both for the GroPIns4P- and ATP-treated samples, as shown in Table 5.1.

There was no direct correlation between the GroPIns4P-dependent $G\alpha_i$ activation and $[Ca^{2+}]_i$ increases. Thus, these two effects of GroPIns4P ($[Ca^{2+}]_i$ increase and AC inhibition) cannot be associated with a single initial event like $G\alpha_i$ activation.

5.3.3 GroPIns4P-dependent ruffle formation in the presence of PTX

Even if the increase in $[Ca^{2+}]_i$ produced by GroPIns4P was not mediated by a $G\alpha_i$ protein, it could not be excluded that this heterotrimeric G-protein could be involved in GroPIns4P-dependent ruffle formation. As mentioned before (Chapter 3 and 4), the

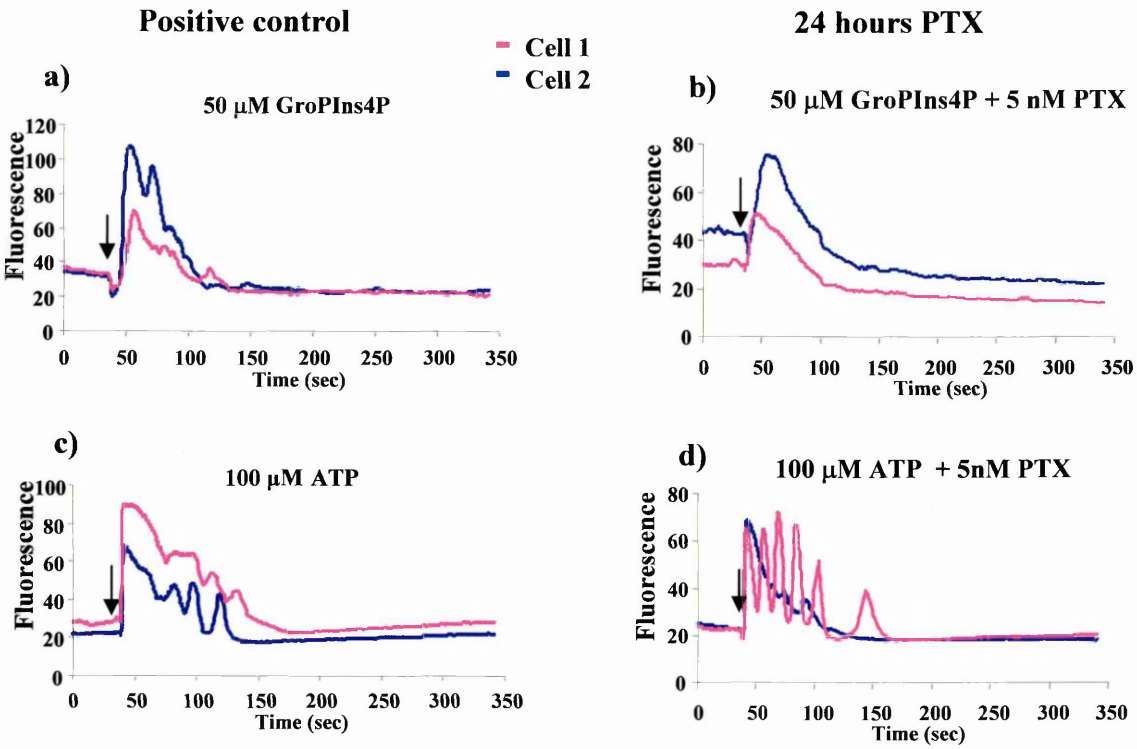

Figure 5.4 - Till photonics live imaging of Fluo3-AM loaded NIH 3T3 cells. The cells were incubated with 4 µM Fluo3-AM, for 30 min at 37 °C. After two washes in HEPES-buffered saline solution, the cells were placed in an open chamber at 37 °C with 1 ml of HEPES solution, and positioned on the stage of a Till photonics microscope (as described Section 2.5). For each experiment, the cells were monitored for at least 30 sec to establish a base-line fluorescence reading before the sequential addition of 50 µM GroPIns4P and 100 µM ATP. All of the incubations were carried out while monitoring the cells every 200 ms (first movie), and each second for 6 min (second movie) (as explained in Section 2.5). The treatment with PTX (5 nM) was performed 24 h before the stimulation, as explained in Section 2.3.5. The plots present the kinetics of $[Ca^{2+}]_i$ increases caused by 50 µM GroPIns4P (a, b) and 100 µM ATP (c, d) in the absence (a, c) and presence (b, d) of PTX. The arrows indicate the times at which the stimuli were given to the cells. The data shown are representative of four independent experiments. Each plot represents the behaviour of two cells (pink and blue).

	Control (ΔF/F0)	PTX (ΔF/F0)
GroPIns4P	1.42±0.44***	0.9±0.35***
ATP	1.7±0.4***	1.71±0.43***

Table 5.1 - Quantification of the changes in fluorescence relative to the baseline (pseudo ratio: ΔF/F0=(F-F0)/(F0-B)) (see Section 2.5.1). The values represent the means of 4 independent experiments. ***P<0.001, versus untreated samples (Section 1.14).

increase in $[Ca^{2+}]_i$ is not the only event that is involved in ruffle formation. There is a parallel event that, independently from this $[Ca^{2+}]_i$ increase, produces a GroPIns4P-dependent formation of a CaMKII-TIAM1-Rac1 complex and consequent ruffle formation (see Chapter 4). $G\alpha_i$ could be involved in this second event; for this reason the ability of GroPIns4P to induce membrane ruffles upon a 24 h-treatment with PTX was tested. After the incubation with (5 nM) PTX, the NIH 3T3 cells were treated with 50 μM GroPIns4P or 10 ng/ml PDGF for different times (2-30 min). The actin was stained with TRITC-phalloidin and the samples analysed blind for the presence of membrane ruffles.

Figure 5.5 presents the means of three independent experiments quantified blind, for the ability of GroPIns4P to induce ruffles (see Section 2.4.3). Within 2 min of treatment, GroPIns4P increased the ruffles by 1.7-1.8-fold versus the control, both under normal conditions and with the PTX treatment. Thus, the PTX treatment did not influence GroPIns4P-dependent ruffle formation; these data support the idea that $G\alpha_i$ activation cannot be associated with the pathway promoted by GroPIns4P that leads to Rac1-dependent actin cytoskeleton modifications.

5.3.4 Conclusion and discussion

GroPIns4P is able to inhibit AC by acting through the $G\alpha_i$ proteins. These proteins are involved in a variety of cellular events, which also include Src activation (Ma et al., 2000). For this reason, the involvement of the G_i proteins in the GroPIns4P-dependent Ca^{2+} increases and ruffle formation was analysed but neither cellular events was affected by G_i inhibition.

These results reveal that GroPIns4P is a multifunctional compound that is able to act inside the cells at different levels and to produce effects that are not always related to each other. There is a pathway that leads to ruffle formation (Fig. 3.24), and a different pathway that produces the $G\alpha_i$-dependent inhibition of AC (Fig. 5.6).

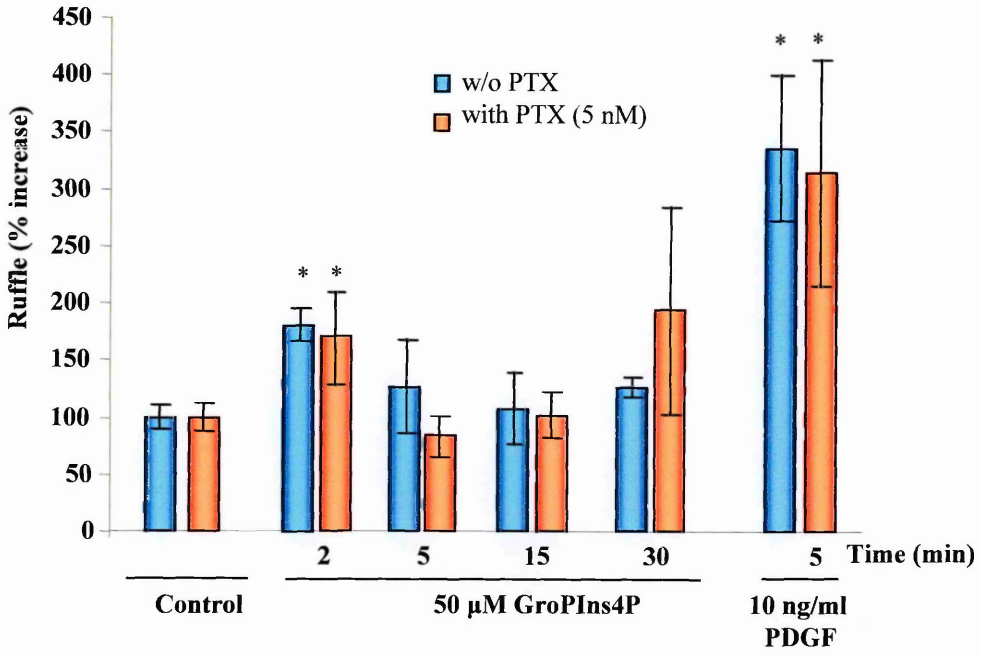

Figure 5.5 - Effect of PTX on ruffle formation in NIH 3T3 cells. Serum-starved NIH 3T3 cells were treated with GroPIns4P (50 µM) or PDGF (10 ng/ml) for different times (from 2 to 30 min), in the absence and presence of a 24 h treatment with 5 nM PTX. The cells were fixed and stained with TRITC-labelled phalloidin and quantified blind for the extent of ruffle formation, as described in Section 2.4.3. The results shown are means (±SD) of three independent experiments, each performed in duplicate. *P<0.05, versus the control (Section 1.14).

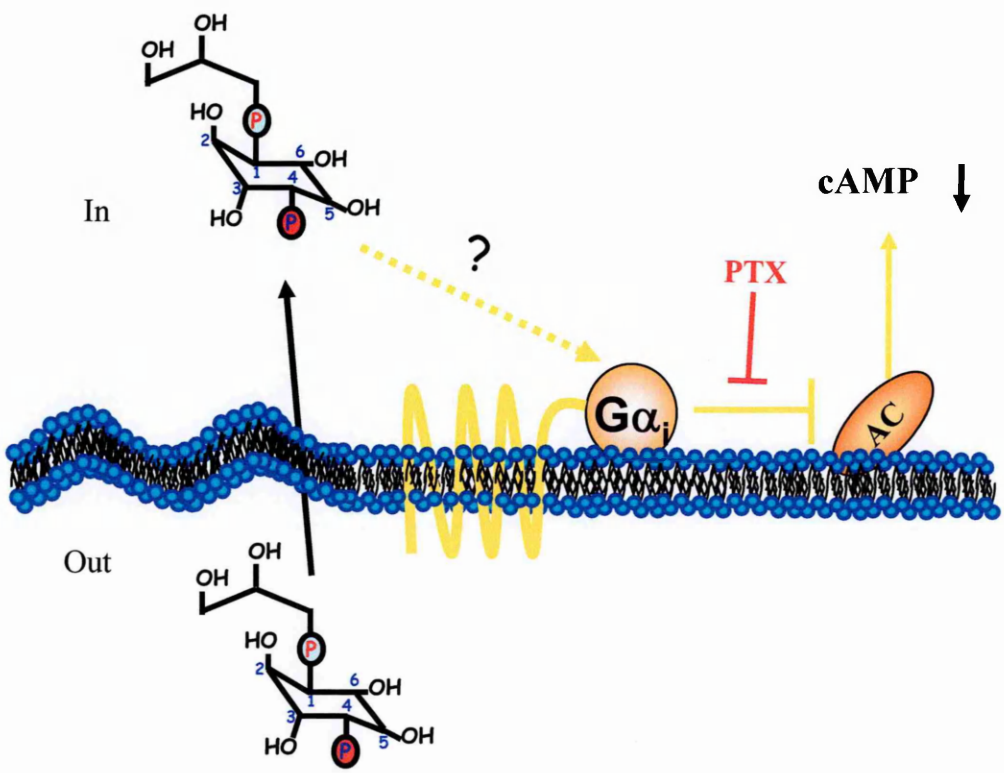

Figure 5.6 - GroPIns4P is able to inhibit AC by acting through G_i proteins. Schematic representation of the pathway involved.

It is still unclear how GroPIns4P activates the $G\alpha_i$ class of heterotrimeric G proteins. It is probably not through receptor-dependent signalling, as supported by the demonstration that GroPIns4P does not bind directly to plasma membrane and total membranes of NIH 3T3 cells (Berrie et al., 1999). One possibility could be a direct interaction between GroPIns4P and $G\alpha_i$, but so far there is no direct proof of this. An indirect activation of the G_i proteins through another unknown GroPIns4P-activated-element could be also plausible. In this case the presence of a common element cannot be excluded, which would be activated by GroPIns4P, and which would act on Src and induce ruffle formation on the one hand, and activate $G\alpha_i$, thus inhibiting AC on the other.

Several cAMP-elevating agents are known to inhibit cell migration towards chemoattractant (Armstrong, 1995; Harvath, 1991; Horio et al., 1995). Moreover, it has recently been demonstrated that an increase in cAMP can prevent Rac1 activation, thereby inhibiting membrane ruffling and chemotaxis; *vice versa*, an increase in Rac1 activity can go in parallel with a decrease in cAMP (Nagasawa et al., 2005). The two parallel effects of GroPIns4P that can activate Rac1 and inhibit AC could proceed in the same direction and lead to ruffle formation. Nevertheless, we do not have direct proof that the AC inhibition is relevant for GroPIns4P-dependent ruffle formation.

5.4 GroPIns4P induces stress fibre formation acting through RhoA

5.4.1 General description

GroPIns4P acts upstream of Rac1 and RhoA and requires active Rac1 (but not Cdc42 and RhoA) to form ruffles, and active RhoA (but not Rac1 and Cdc42) to form stress fibres (Mancini et al., 2003). The addition of GroPIns4P (50 μM) to serum-starved Swiss and NIH 3T3 fibroblasts caused the rapid formation of membrane ruffles, followed by the formation of stress fibres. The membrane ruffling induced by GroPIns4P is

dependent on a functional Rac1 protein, but the stress fibre formation is not. To examine whether the latter effect required RhoA, serum-starved Swiss 3T3 cells were microinjected with *C. botulinum* C3 transferase (160 μg/ml), which ADP ribosylates and inactivates RhoA, leaving the functions of Rac1 and Cdc42 unchanged (Ridley and Hall, 1992; Ridley et al., 1992). GroPIns4P-dependent stress fibre formation was completely inhibited by *C. botulinum* C3, indicating that this effect of GroPIns4P needs a functional RhoA protein. However, the formation of membrane ruffles induced by GroPIns4P was not influenced by C. botulinum C3 (Mancini et al., 2003).

GroPIns4P-dependent ruffle formation was addressed in the previous Chapters, whereas the study of the pathway from GroPIns4P stimulation to stress fibre formation has not been investigated here yet. The two pathways should be different, at least at the level of the small G protein involved, but the starting events that initiate the GroPIns4P-dependent signal cascade could be the same.

TIAM1 is specific for Rac1 and does not activate RhoA (see Section 1.2.3.2). Moreover there are no data that associate CaMKII with RhoA activation. There is a possibility that the increase of $[Ca^{+2}]_i$ stimulated by GroPIns4P is involved in stress fibre formation, even if no relevant indications that RhoA activity can be modulated by a $[Ca^{2+}]_i$ rise have been reported to date.

In some cellular systems RhoA can be activated via heterotrimeric G proteins. For example, upon treatment of cells with LPA, there is an increase in RhoA-dependent stress fibres in fibroblasts (Ridley and Hall, 1992). As demonstrated above, GroPIns4P can act through G_i proteins for its AC inhibition, and thus it is possible that RhoA-dependent stress fibre formation is a consequence of this G_i activation. Although many attempts have been made to clarify the mechanisms by which GroPIns4P induces stress fibres in fibroblasts, no definitive results have been obtained to date.

5.4.2 GroPIns4P does not produce any change in RhoA localization

It is well known that GroPIns4P can induce stress fibre formation in Swiss and NIH 3T3 cells *via* RhoA activation (Mancini et al., 2003), but nothing is known about the effects of GroPIns4P on RhoA localisation. By immunofluorescence experiments, an attempt was made to answer this question. NIH 3T3 cells were transfected with Myc tagged RhoA, and after 24 h of serum starvation, the cells were stimulated with 50 μM GroPIns4P for different times (from 2 to 30 min). Actin was stained with TRITC-phalloidin and the analysis was performed by confocal microscopy (as reported in Section 2.4.3). The aim of this experiment was to see if GroPIns4P can modulate the activity of RhoA by affecting its localisation, as was seen for Rac1 (Mancini et al., 2003). RhoA should also translocate to the plasma membranes upon activation, and it is known that RhoA can be found at the level of focal adhesions (Michaelson et al., 2001).

From this analysis it is evident that no particular changes in RhoA localisation occur upon treatment with GroPIns4P (Fig 5.7). The cells were treated for 2 to 30 min, but under all conditions the localisation of the RhoA-myc was cytosolic. Within 15 min of treatment with GroPIns4P (50 μM), the formation of stress fibres was seen, as expected, and a partial co-localisation of RhoA with the stress fibres was visible (Fig. 5.7).

5.4.3 Calcium mobilisation and $G\alpha_i$ activation are not involved in GroPIns4P-dependent stress fibre formation

If the GroPIns4P-dependent $[Ca^{2+}]_i$ increase is an event that initiates the signal cascade that leads to stress fibre formation, it should be possible to prevent the assembly of stress fibres by blocking the $[Ca^{2+}]_i$ increase. This blockage can be obtained by treating the cells either with a PLCs inhibitor (U-73122) or with a Src kinase inhibitor (PP2) (as shown in Section 3.6.3). The technical problems of using U-73122 is that it cannot be given to the

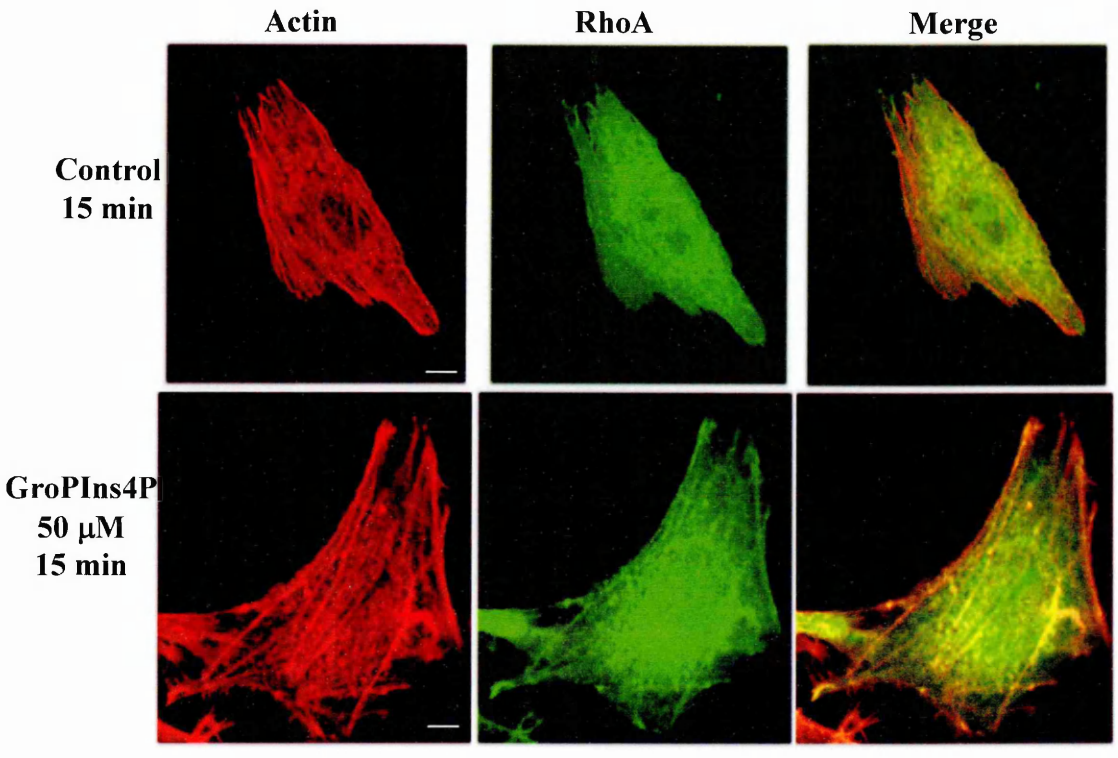

Figure 5.7 - RhoA localisation upon GroPIns4P treatment in NIH 3T3 cells. Sub-confluent NIH 3T3 cells were transfected with the RhoA-myc tagged expression construct, as described Section 2.3.4. Twenty-four h after transfection, the cells were serum-starved for 24 h and then treated with GroPIns4P (50 μM) for 15 min, fixed, and stained with an anti-myc antibody for RhoA visualization and TRITC-labelled phalloidin for actin visualization (as described in Section 2.4.3). Bar=20 μM

cells for longer than 20 min, otherwise the cells start to detach. For this reason, after pre-incubation with the inhibitor (for 10 min to allow its incorporation into the cells), stimuli longer than 5-10 min cannot be used. The time necessary to see GroPIns4P-dependent stress fibre formation is 15-30 min, thus, this was at the limit and too many cells detached during the experiments. As a consequence, U-73122 was not suitable for testing the effects of $[Ca^{2+}]_i$ on RhoA-dependent stress fibre formation produced by GroPIns4P. Instead, the Src family kinases inhibitor PP2, which can be applied to cells also for long incubations, was used in an immunofluorescence system.

NIH 3T3 cells were treated with 10 μM PP2 for 15 min, and then the cells were incubated with GroPIns4P (50 μM) for different times (2, 15, 30 min) (see Section 2.4.2). A two min incubation was used to check the functionality of the inhibitor, by following GroPIns4P-dependent ruffle formation and its inhibition by PP2. The longer time incubations (15-30 min) were used to follow the formation of stress fibres, which is maximal upon 15 min of treatment with 50 μM GroPIns4P (see Section 3.2).

Under normal conditions, the treatment with GroPIns4P caused the formation of membrane ruffles within 2 min (2.4-fold increase) and of stress fibres within 15 min (1.7-fold response over basal). LPA was applied at a concentration of 10 μM to follow the classical RhoA-dependent stress fibre formation, and it caused a 2.5-fold increase in stress fibres within 15 min of treatment (Fig. 5.8). The treatment with 10 μM PP2 caused the inhibition of GroPIns4P-induced ruffle formation as expected, and also the formation of stress fibres was altered both upon GroPIns4P and LPA treatment. GroPIns4P treatment showed a delayed and weaker increase in stress fibres (within 30 min there was only a 1.5-fold increase), and LPA produced a 1.6-fold increase in stress fibres within 15 min of treatment, lower when compared with the 2.5-fold increase obtained with LPA under normal conditions (Fig. 5.8)

The initial hypothesis was that blocking the $[Ca^{2+}]_i$ increase, could also prevent the GroPIns4P-dependent activation of RhoA and stress fibre formation, and the results

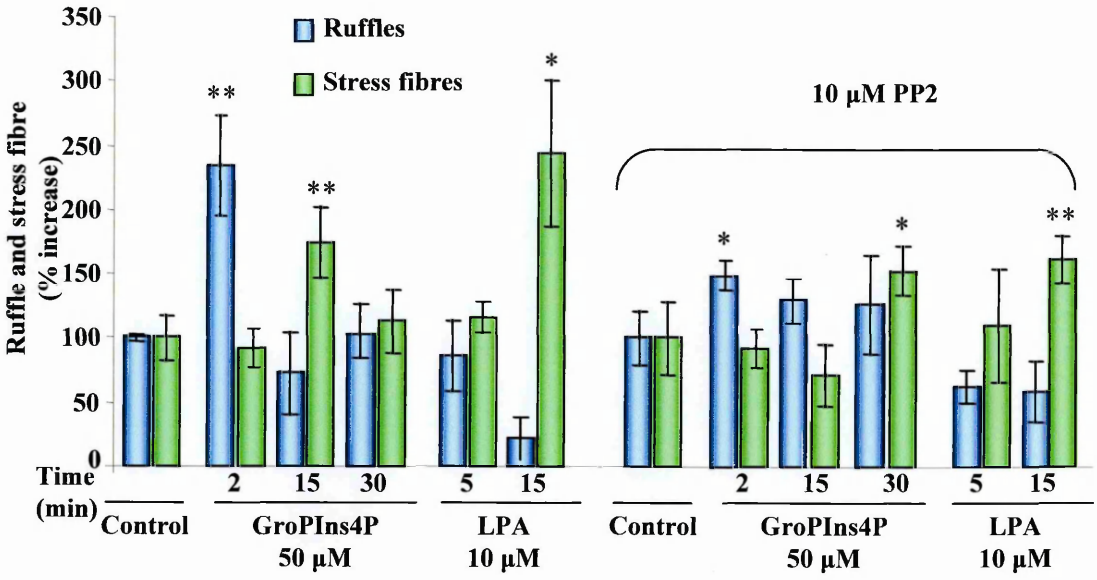

Figure 5.8 - Effects of the Src inhibitor PP2 on GroPIns4P-dependent stress fibre formation. Twenty-four hour starved NIH 3T3 were treated with PP2 (10 µM) for 15 min and then incubated with 50 µM GroPIns4P (2, 15 and 30 min) or 10 µM LPA (5 and 15 min). The cells were then fixed and stained with TRITC-labelled phalloidin and quantified blind for the extent of ruffle and stress fibre formation, as described in Section 2.4.3. The results shown are the means (±SD) of two independent experiments, each performed in duplicate.* $P<0.05$ **$P<0.01$ ***$P<0.001$, versus control (Section 1.14).

	Control (±SD)	PP2 10 µM (±SD)
CONTROL	69.5 ± 7.5	97±16
GroPIns4P (50 µM) 15 min	137 ± 1	82 ± 11
GroPIns4P (50 µM) 30 min	95.5 ± 4.5	146 ± 15
LPA (10 µM) 15 min	169.5 ± 25	156 ± 18.5

Table 5.2 - Scores of the quantification of stress fibre formation in the absence and presence of PP2. The quantification was performed by counting 200 cells and giving each one a score of 0 in the absence of stress fibre and of 1 or 2, depending on the quality of the stress fibres formed (1 if they were thin, and 2 if they were thick). The values presented in the Table are expressed as scores obtained with the quantification over a maximal value that is 400 (200 x2) (see Section 2.4.3 for details). The standard deviation is representative of the mean of four different samples.

obtained show that PP2 causes altered formation of stress fibres in response to the GroPIns4P treatment. However as the activity of LPA was also reduced, this indicates that the inhibition of Src can *per se* modify the behaviour of the cells. Indeed, LPA should activate the $G\alpha_{13}$ which directly interacts with and activates the p115RhoAGEF, thus favouring GDP/GTP exchange of RhoA and the consequent formation of stress fibres (without a $[Ca^{2+}]_i$ increase) (as reported in Section 1.2.3).

Src activity has been reported to be important for turnover of focal adhesions (see Section 1.2.2); it phosphorylates the focal adhesion kinase (FAK), causing the disassembly of focal adhesions (Timpson et al., 2001). Moreover, Src can activate the p190RhoGAP, which enhances the GTP hydrolysis of RhoA; the result is RhoA inactivation and the consequent disassembly of stress fibres (Brandt et al., 2002). Blocking Src there is a basal increase in stress fibres caused by the persistence of focal adhesions, and this increase could mask the effects of stimuli like LPA and GroPIns4P. As shown in Table 5.2, which gives the scores obtained in the quantification of stress fibre formation (see in Section 2.4.3) in absolute numbers, the basal stress fibres score was 69.5±7.5 over a maximum of 400 under normal conditions, and 97±16 in the presence of PP2. However, the values obtained upon stimulation with GroPIns4P and LPA were not so different from those treated and untreated with PP2. For GroPIns4P alone there was a delay in the formation of stress fibres due to the presence of the inhibitor (within 30 min), but in numbers, the extent of the increase was 146±15, which is comparable with that obtained under normal condition with 15 min of treatment (137 ±1) (Table 5.2).

This was also observed in SYF cells, in which the absence of Src kinase activity caused a basal increase in stress fibres and a parallel absence of stimulus-dependent stress fibre formation. Neither GroPIns4P (given at 50 μM for 15-30 min) nor LPA (given at 10 μM for 5-15 min) were able to induce stress fibre assembling, as shown in Figure 5.9.

From this data, it is not possible to determine whether the signal cascade that is activated by GroPIns4P and leads to a Src-dependent $[Ca^{2+}]_i$ increase and to ruffle

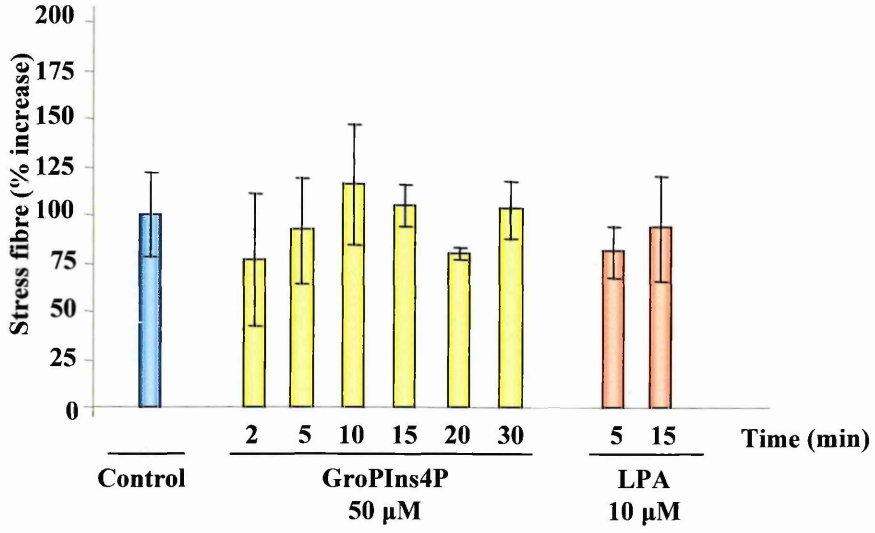

Figure 5.9 - GroPIns4P-dependent stress fibre formation in SYF cells. SYF cells were serum-starved for 12 h in DMEM, 0.1% foetal bovine serum, and then were treated with 50 µM GroPIns4P (from 2 to 30 min) or 10 µM LPA (5-15 min). The cells were then fixed and stained with TRITC-labelled phalloidin and quantified blind for the extent of ruffle formation as described in Section 2.4.3. The results shown are the means of two independent experiment, each performed in duplicate.

formation, can also favour RhoA-dependent stress fibre formation. Indeed, the Src kinases are involved in the turnover of focal adhesions, and the use of PP2 to inhibit the GroPIns4P-dependent $[Ca^{2+}]_i$ increase caused a basal increase in stress fibres that can affect the analysis. The best approach would be to treat the cells with PLC inhibitors, but as indicated above, during long incubations the cells tend to detach.

The same stress fibre quantification was performed in NIH 3T3 cells pre-treated with PTX, to inhibit all G_i proteins. Also in this case, the treatment with GroPIns4P was performed for different times (from 2 to 30 min). The GroPIns4-dependent stress fibre formation was not affected by the presence of PTX, thus excluding a correlation between $G\alpha_i$ activation and the RhoA dependent stress fibre formation induced by GroPIns4P (Fig. 5.10).

5.4.5 Conclusion and discussion

Exogenously added GroPIns4P is able to induce ruffle formation in a very short time, and stress fibre assembly after a prolonged treatment, in fibroblasts. The pathway that leads to ruffle formation was well elucidated in the previous Chapters, while for stress fibres no clear mechanism has been described. RhoA is involved in GroPIns4P-dependent stress fibre formation, as was well demonstrated in Mancini et al. (2003), but how GroPIns4P activates this small G protein and induces stress fibre formation is not yet understood.

We tested the hypothesis that GroPIns4P stimulation triggers ruffle and stress fibre formation *via* the same initial event. Since CaMKII and TIAM1 are specific for Rac1 activation, they can be excluded from the range of possible RhoA activators, whereas the $[Ca^{2+}]_i$ increase produced by GroPIns4P could be a potential signal that leads to Rac1 and RhoA activation; for this reason a possible involvement of PLCs was analysed. However, PLC inhibitors could not be used for long incubations, and so the inhibition of Src kinases

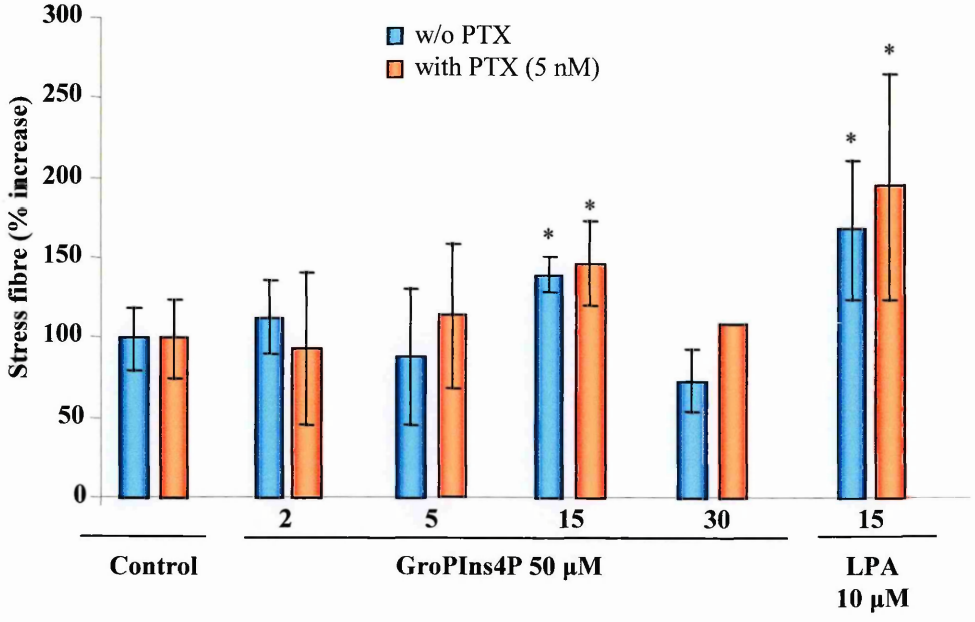

Figure 5.10 - Stress fibre formation in NIH 3T3 cells treated with PTX. Serum-starved NIH 3T3 cells were treated with GroPIns4P (50 µM) or LPA (10 µM) for different times (from 2 to 30 min), in the absence and presence of a 24 h treatment with 5 nM PTX. The cells were fixed and stained with TRITC-labelled phalloidin and quantified blind for the extent of stress fibre formation, as described in Section 2.4.3. The results shown are mean (±SD) of three independent experiments, each performed in duplicate. *P<0.05, versus the control (Section 1.14).

was used to prevent GroPIns4P-dependent $[Ca^{2+}]_i$ increase. Here, there was a basal increase in stress fibres that lowered the level of cellular response to either GroPIns4P and LPA treatments. Thus, we could not determine specifically whether the $[Ca^{2+}]_i$ increase is relevant also for RhoA activation. The potential involvement of $G\alpha_i$ was also analysed; indeed GroPIns4P could activate RhoA by acting through G_i proteins. However G_i was also not involved in GroPIns4P-dependent stress fibres formation.

Probably there is a net division between the signal cascades initiated by GroPIns4P that lead to ruffle versus stress fibre formation. These two events occur in different time frames and involve different proteins. There are also no similarities in the ways in which Rac1 and RhoA are activated: there is a translocation of Rac1 to the plasma membranes upon treatment with GroPIns4P, and this translocation defines Rac1 activation; the localisation of RhoA does not change upon addition of GroPIns4P however. There is only a partial co-localisation of RhoA with the stress fibres, and thus it is difficult to determine if this localisation is strictly dependent on GroPIns4P or occurs as consequence of RhoA activation.

The pathway of RhoA thus need further analysis to understand how GroPIns4P induces stress fibre formation.

CHAPTER 6

FINAL DISCUSSION

The main achievement of this study has been the identification of the mechanism of action of GroPIns4P. This compound is the product of the double deacylation of PI4P, which involves a PI-specific PLA_2. GroPIns4P is accumulated inside cells upon growth factor or Ca^{2+}-dependent Ras activation, or upon Ras transformation (see Section 1.4.3.1). When added exogenously to cells, GroPIns4P is able to equilibrate across the membrane, probably due to the activity of a membrane transporter specific for glycerophosphoinositols (as discussed in Section 1.4.4), and it has many biological effects. GroPIns4P can inhibit AC and PLA_2 (in thyroid cells and fibroblasts; see Section 1.4.3.2.1), can modulate the actin cytoskeleton organization (ruffle and stress fibre formation in fibroblasts; see Section 1.4.3.2.2), and can inhibit tumour cell invasion (see Section 1.4.3.2.3).

The pathway of ruffle formation has been characterized best in this work. In particular, I have shown how GroPIns4P is able to induce membrane ruffles in fibroblasts. It can act *via* two different mechanisms. On the one hand, GroPIns4P can activate a member of the Src kinase family (potentially Yes in NIH 3T3 cells), and this kinase phosphorylates and activates PLCγ1, resulting in IP_3 production and thus a $[Ca^{2+}]_i$ increase. The latter event promotes the activation of CaMKII, which in turn phosphorylates TIAM1, facilitating the translocation of this Rac1 GEF to the plasma membrane, and enhancing its exchange activity versus Rac1. The small GTPase Rac1 is also translocated to the plasma membrane upon treatment with GroPIns4P, where it can interact with TIAM1. Once activated at the level of plasma membrane, Rac1 can lead to the formation of membrane ruffles (as demonstrated in Chapter 3) (Fig. 6.1). On the other hand, GroPIns4P is able to increase the binding between Rac1 and TIAM1, and appears to interact directly with a

protein complex that is associated with immunoprecipitated TIAM1-HA (as shown in Chapter 4). How these two effects are interconnected is not yet clear. The common elements that are present in these two pathways are TIAM1 and Rac1, which are both necessary for ruffle formation, and CaMKII, which can be co-immunoprecipitated with TIAM1 (see Section 4.4.5). CaMKII is also fundamental in GroPIns4P-dependent ruffle formation, since the inhibition of CaMKII with its specific inhibitor completely abolished GroPIns4P-dependent ruffle formation. In contrast, blocking the Src kinases only reduces, rather than completely blocking, GroPIns4P-depent ruffle formation.

The hypothesis that I am proposing is that under normal conditions, GroPIns4P can cause the full activation of CaMKII, through a Src-dependent pathway, thus reaching its maximal effect on ruffle formation (2.5-fold response). When Src is inhibited, the CaMKII portion that maintains a residual basal activity also after starvation could still be involved in the activation of TIAM1. GroPIns4P would thus also interact with an as yet unknown target, and in this way, favour the formation of a multi-protein complex containing TIAM1, Rac1 and CaMKII, which together cooperate in ruffle formation (Fig. 6.1).

In fibroblasts, exogenously added GroPIns4P is able to rapidly induce ruffle formation, with stress fibre formation requiring a prolonged treatment with GroPIns4P. RhoA is involved in GroPIns4P-dependent stress fibre formation, as was demonstrated by Mancini et al. (2003). We tested the hypothesis that the initial event that follows GroPIns4P stimulation is the same for both ruffle and stress fibre formation pathways, and found that separate signalling cascades are activated (Chapter 5). These two events happened within different time frames, and they involve different signalling proteins. In addition, GroPIns4P can inhibit AC by acting through G_i proteins. However, this cannot be related to the ability of GroPIns4P to induce ruffles and stress fibres, since inhibition of G_i proteins does not affect the GroPIns4P-dependent actin cytoskeleton modifications (as described in Chapter 5) (Fig. 6.1).

These results reveal that GroPIns4P is a multifunctional compound, which is able to act inside cells at different levels, and to produce effects that are not always related to each other. There is a pathway that leads to ruffle formation, another that favours Rho-dependent stress fibre formation, and a third that causes the $G\alpha_i$-dependent inhibition of AC (Fig. 6.1).

Many points along these GroPIns4P signalling pathways remain unclear. Firstly, how are the Src kinases activated by GroPIns4P? The Src kinases are regulated by alternative phosphorylation/de-phosphorylation events (see Section 1.3.5), and thus GroPIns4P could either directly interact with a Src kinase to favour its autophosphorylation on Tyr-416, or alternatively, GroPIns4P could activate a phosphatase that de-phosphorylates the inhibitory Tyr-527. In the case of the kinase, CSK, that inhibits Src by phosphorylating Tyr-527 we can not exclude the possibility that it is inhibited by GroPIns4P. Secondly, what protein interacts with GroPIns4P? One possibility could be that it is a scaffolding protein that is able to hold TIAM1, CaMKII and Rac1 in a complex, in this way favouring the activation of TIAM1 and consequent Rac1-dependent ruffle formation. GroPIns4P could interact with this scaffolding protein, potentially causing changes in its conformation, and enhancing its affinity for TIAM1 and CaMKII. Thirdly, how does GroPIns4P activate RhoA to induce stress fibre formation? We have so far not been able to find a clear correlation between the pathway that leads to ruffle formation and that promotes the RhoA-dependent increase in stress fibres caused by GroPIns4P. Finally, how does GroPIns4P activate $G\alpha_i$? GroPIns4P could directly interact with G_i proteins, or it could activate proteins like the AGS (activators of G-protein signalling), that have been characterised as putative GEFs for $G\alpha$ subunits (Lanier, 2004). The possibility that GroPIns4P can inhibit the RGS (regulators of G-protein signalling) proteins, which are known to accelerate the GTP-hydrolysis of the $G\alpha$ subunits (Siderovski et al., 1996), has also to be considered.

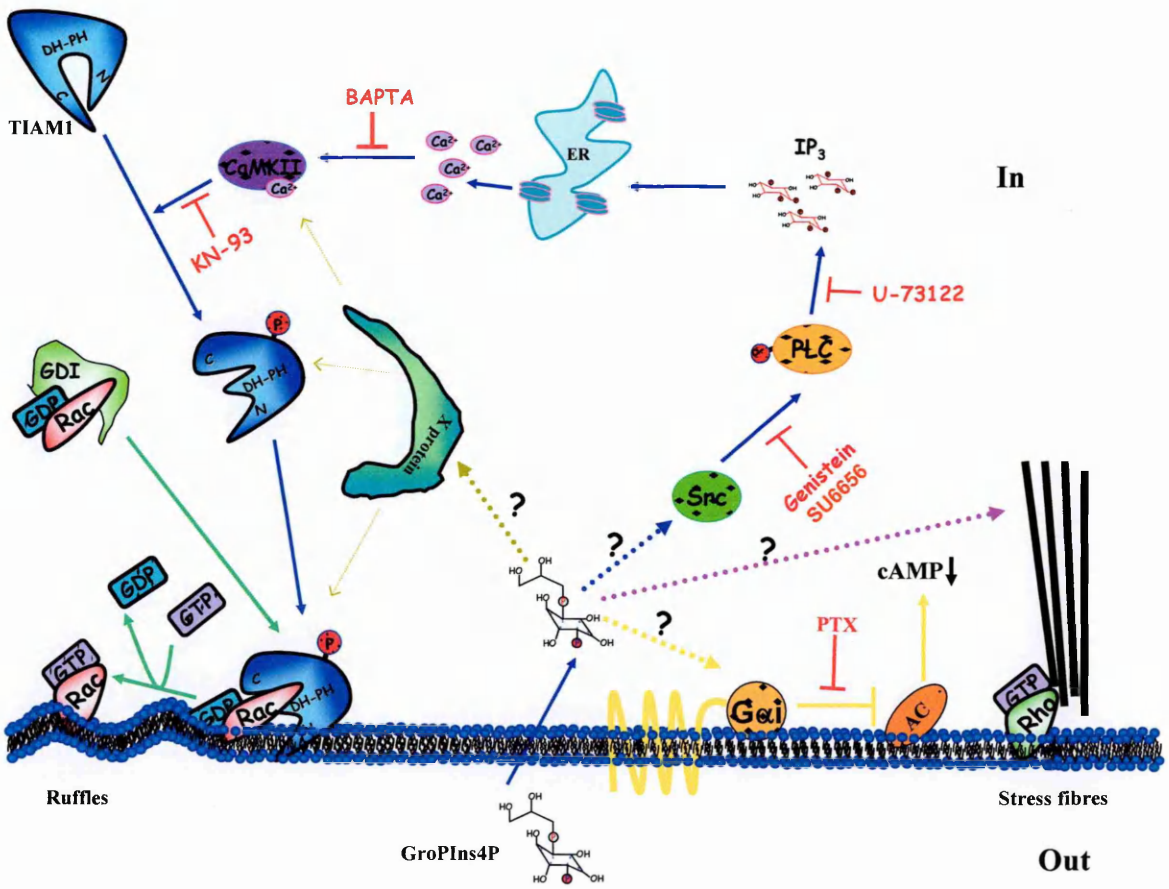

Figure 6.1 - Schematic representation of the regulatory cascades initiated by exogenously added GroPIns4P in cells.

The pathway elucidated in Chapter 3 that indicates that Src activation can lead to ruffle formation implies the activation of many different proteins, all of which are involved in the activation of other effectors that were not taken into direct consideration in the present study. For example, Src can activate VAV2, another specific exchange factor for Rac1, by phosphorylation. As with TIAM1, VAV2 is also ubiquitously expressed (also in fibroblasts), and it can be activated by Src, thus favouring ruffle formation (Arthur et al., 2004). However, there is evidence against the involvement of VAV2 in GroPIns4P-dependent ruffle formation: by blocking CaMKII, ruffle formation is completely prevented and TIAM1 is the only known exchange factor for Rac1 that can be activated by CaMKII. Nevertheless, there is no direct evidence that VAV2 is not involved in GroPIns4P-dependent ruffle formation, and thus further analysis will need to be carried out in order to clarify this possibility.

The most plausible explanation for the multiple effects of GroPIns4P would be the presence of a membrane receptor that is specific for this compound, even though there is no experimental evidence that supports such a hypothesis. Instead, GroPIns4P has been shown to enter the cells, where it can interact with a specific target or targets (as demonstrated in Chapter 4).

It is possible that one specific interactor for GroPIns4P initiates both Rac1- and RhoA-dependent actin cytoskeleton modifications, and also G_i-dependent AC inhibition. As described in Section 5.4.3, a decrease in cAMP is associated with an increased activity of Rac1 and the consequent augmentation of membrane ruffles (Nagasawa et al., 2005). The GroPIns4P-dependent sequential activation of Rac1 and RhoA could also be associated with a common final effect: cell movement. A moving cell creates new sites of adhesion at its leading edge, and disassembles trailing adhesions at its rear. Adhesion assemblies originate as 'focal complexes' (Nobes and Hall, 1995; Rottner et al., 1999) in association with lamellipodia (modulated *via* Rac) or filopodia (modulated *via* Cdc42). Focal complexes can exist briefly and turn over within a few minutes, or they can undergo

a transition into larger and longer-lived focal adhesions (modulated *via* Rho) (Kaverina et al., 2002). Both focal complexes and early focal adhesions remain stationary relative to the substrate and serve as traction points for the forward translocation of cells (Beningo et al., 2001). Without anchorage points, the actin cytoskeleton would not develop sufficiently at the rear to support the translocation of the cell body. This has been given as the reason for the requirement of at least low levels of Rho activity for cell migration (Nobes and Hall, 1999). Although Rac1 triggers the protrusion of lamellipodia, a recent study has shown that without appropriate adhesion, these lamellipodia are not able to support forward movement and are quickly retracted as membrane ruffles (Borm et al., 2005). So, to have active cell migration, the lamellipodial structure should persist for longer times, and RhoA can stabilise lamellipodia by creating stable focal adhesions. Thus, the sequential activation of Rac1 and RhoA that can be obtained upon treatment with GroPIns4P, together with the cAMP decrease, could be related to a single starting event (such as the interaction of GroPIns4P with a protein that is able to initiate all of the signal cascade), which thus leads to the actin reorganization that is necessary for cell movement.

On the other hand, the multiple effects observed upon treatment of cells with GroPIns4P could be independent of each other, and GroPIns4P could have many different targets inside cells, all of which might share sequence similarity. It would be very interesting to find a protein domain that is specific for GroPIns4P. There are many potential unknown interactors and effectors of GroPIns4P in cells, and they could all contain the same domain. The identification of all of the proteins that are present in the complex that can be co-immunoprecipitated with GroPIns4P should allow the final determination of which of these is the specific interactor for GroPIns4P, and also what form the machinery involved in TIAM1-dependent Rac1 activation and ruffle formation takes. As already mentioned in Section 4.5, new experimental approaches will be followed in the future, such as the use of two-dimensional gels to separate the proteins in the complex that co-immunoprecipitates with TIAM1, followed by their identification by mass

spectrometry. This will allow us to determine the specific interactor for GroPIns4P, as well as to identify all of the protein machineries that cooperate with TIAM1 for Rac1 activation and ruffle formation. The identification of a GroPIns4P-specific protein domain will significantly help in the definition of the multiple pathways modulated by GroPIns4P and should open the way to a further understanding of the reason why the activity of GroPIns4P cannot be mimicked by other similar compounds, such as GroPIns and GroPIns4,5P_2. Furthermore, the presence of a specific domain for GroPIns4P will allow us to also better understand its functions inside cells when GroPIns4P is produced upon receptor stimulation.

Ruffle formation is an event associated with cell protrusions (linear ruffles at the leading edge of lamellipodia) and macropinocytosis, and with structures involved in receptor internalization (dorsal ruffles or waves). This morphological feature is visible mostly upon growth factor stimulation (see Section 1.2.2). The action of GroPIns4P can thus mimic the activity of growth factors, even if it differs in the extent of its effects and the pathway that is activated. The production of GroPIns4P in fibroblasts has been seen upon growth-factor stimulation (Falasca et al., 1997). Thus it cannot be ruled out that GroPIns4P has a role as a second messenger in the pathway from growth-factor stimulation to actin cytoskeleton modification. GroPIns4P can induce a 50% increase in ruffle formation when compared to the extent of the PDGF-induced increase (see Section 3.2.2), but in terms of CaMKII activation or IP_3 production, both GroPIns4P and PDGF have similar effects (see Sections 3.4.2 and 3.7.2). It appears that there is a partial overlap of the two pathways and that PDGF also activates other proteins that can favour ruffle formation (Jimenez et al., 2000; Rosenmuller et al., 2001); in a CaMKII-independent way. Since GroPIns4P can be produced upon PDGF stimulation (Corda et al., 2002), it can be hypothesized that the production of GroPIns4P contributes to signalling by PDGF, maybe through activating CaMKII. At the moment, we are not able to say if GroPIns4P is indeed a second messenger, because we have no tools to block its production in a specific way.

Thus, it is not yet possible to separate the signalling associated with PDGF that leads to ruffle formation from the PDGF-dependent GroPIns4P production in cells.

Together with the search for a potential GroPIns4P-binding domain through its interaction with the CaMKII, TIAM1 and Rac1 complex, future work will focus on the definition of the metabolic pathways of the glycerophosphoinositols and their potential roles in pathological and physiological conditions. The identification of the specific PLA_2 involved in the synthesis of the glycerophosphoinositols will also provide further information that will help us to understand their roles in cells better. This will establish whether the glycerophosphoinositols, and GroPIns4P in particular, as well as being biologically active compounds able to enter the cells and to modulate many different cellular functions, can also be considered as novel second messengers produced upon Ras activation, and that can be associated with several cellular activities.

ABBREVIATIONS

$[Ca^{2+}]_i$	intracellular Ca^{2+}
AA	arachidonic acid
AA	arachidonic acid
ABP	actin binding protein
AC	adenylyl cyclases
ADF	actin depolymerising factor
AID	an auto-inhibitory domain
AIF^-_4	aluminium fluoride
Arp	Actin related protein
ATP	adenosine triphosphate
BAPTA-AM	1,2-bis-(o-Aminophenoxy)-ethane-N,N,-N',N'-tetraacetic acid tetraacetoxy-Methyl ester
BSA	bovine serum albumin
C3	Clostridium botulinum toxin
Ca^{2+}/CaM	Ca^{2+}/calmodulin complex
CaBP	calcium binding protein
cADPR	cyclic ADP ribose
CaMK	Ca^{2+}/calmodulin-dependent protein kinases
CaMKII	Ca^{2+}/calmodulin kinase II
cAMP	cyclic AMP
cAPKs	cAMP-dependent protein kinases
CC	coiled-coil region
CD44v3	hyaluronic acid (HA) receptor isoform
cDNA	complementary DNA

CS	calf serum
CSK	C-terminal Src kinase
CTX	cholera toxin
DAD	diaphanous auto-regulatory domain
DAG	Diacylglycerol
DAG	diacylglycerol
Dbl	diffuse B-cell lymphoma
DH	Dbl-homology
DID	diaphanous inhibitory domain
DMEM	Dulbecco's modified minimal essential medium
DMSO	Dimethyl Sulfoxide
DNA	deoxyribonuclease
DOCK180	180-kDa protein downstream of Crk,
Drfs	Diaphanous-related formins
DTT	dithiothreitol
EC_{50}	50% effective concentration
ECL	Enhanced chemiluminescence
ECM	extracellular matrix
EDTA	Ethylenediamine tetraacetic acid
EGF	epidermal growth factor
EGTA	thyleneglycol-bis-(2-aminoethyllether)-N,N,N',N'-tetracetic acid
Ena/VASP	Vasodilator stimulating phosphoprotein
ER	endoplasmic reticulum
EVH2	Ena/VASP homology domain
EX	extra sequence
FCS	foetal calf serum
FGD1	Faciogenital Dysplasia;

FIVE	Fab1, YOTB, Vac1 and EEA1
FRT-Fibro	Ras-transformed fibroblasts
FRTL-5	fisher rat thyroid cell line 5
GAP	GTPase-activating protein
GBD	GTPase-binding domains
GDI	GDP dissociation inhibitors
GDP	Guanosine 5'-diphosphate
GEF	guanine-nucleotide exchange factor
GFP	Green fluorescence protein
GIT1	glucose yeast transporter
GPCR	G-protein coupled receptors
GRK	G protein coupled receptor kinase
GroPIns	glycerophosphoinositol
GroPIns4,5P$_2$	glycerophosphoinositol 4,5-bisphosphate
GroPIns4P	glycerophosphoinositol 4-phosphate
GST	Glutathione S-transferase
GTP	guanosine 5'-triphosphate
GTPase	Guanosine triphosphatese
GTPγS	Guanosine 5'-0-(3-thiotriphosphate)
h	hour
HA	Hemagglutinin
HEPES	N-2-hydroxyethylpiperazine-N-2-ethanesulfonic acid
HF	Human fibroblast
HGF	hepatic growth factor
HKT	Buffer containing HEPES, KCl and Triton x-100
HPLC	High pressure liquid chromatography
Ib2/JIP2	pancreatic β-cell/brain-specific protein

Ins1:2cP	inositol 1:2-cyclic monophosphate
IP_3	1,4,5-trisphosphate
IPTG	Isopropyl β-D-thiogalactopyranoside
IRSp53	Insulin receptor tyrosine kinase substrate p53
JNK	c-Jun N-terminal kinase
Kd	dissociation constant
kDa	kilo Dalton
KiKi	K-Ras oncogene transformed thyroid cells
LB	Luria Broth
LIMK	activates LIM kinase
LPA	Lysophosphatidic acid
LPC	Lysophosphatidylcholine
LPI	lysophosphatidylinositol
LPIPs	phosphorylate derivatives, the LPI
MAFP	methyl arachidonil fluorophosphonate
MAPK	mitogen activated protein kinase
MMPs	matrix metallo proteases
MOPS	4-morpholinepropanesulfonic acid
MTOC	microtubule organizing center
NAADP	nicotinic acid adenine dinucleotide phosphate
NAD	Nicotinamide adenine dinucleotide
NIH 3T3	NIH Swiss mouse embryo
NP40	nonylphenoxy polyethoxy ethanol
p130Cas	Crk-associated substrate
p160ROCK	Rho associated kinase
PA	phosphatidic acid
PAF	platelet-activating factor

PAGE	polyacrylamide gel electrophoresis
PAK1	p21-activated protein kinase 1
PBS	phosphate buffered saline
PC	phosphatidylcholine
PDGF	platelet-derived growth factor
PDZ	PSD-95/DlgA/ZO-1
PE	phosphatidylethanolamine
PEST	sequences that are rich in proline-P- glutamic acid-E- serine-S- and threonine-T-)
PH	pleckstrin homology domain
PI	phosphatidylinositol
PI3,4,5P_3	phosphatidylinositol 3,4,5-triphosphate
PI3,4P_2	phosphatidylinositol 3,4-bisphosphate
PI3K	phosphatidylinositol 3-kinase
PI3P	phosphatidylinositol 3-phosphate
PI4,5P_2	phosphatidylinositol 4,5-bisphosphate
PI4K	phosphatidylinositol 4-kinase
PI4P	phosphatidylinositol 4-sphosphate
PIK	phosphatidylinositol kinase
PIKs	phosphoinositide kinases
PIP4K	phosphatidylinositol 5-phosphate 4-kinase
PIP5K	phosphatidylinositol 4-phosphate 5-kinase
PIPK	phosphatidylinositol monophosphate kinase
PIX	PAK-interactive exchange factor
PKC	protein kinase C
PLA_2	phospholipase A_2
PLC	phospholipase C

PLD	phospholipase D
PMA	Phorbol 12-Myristate 13-Acetate
PMSF	Phenylmethylsulphonyl fluoride
PTX	pertussis toxin
PX	phox homology domain
RBD	Ras-binding domain
rpm	revolutions per minute
RTK	Tyrosine kinase receptors
S1P	sphingosine-1- phosphate
SDS	Sodium dodecyl sulphate
SH	Src homology domain
SHD	N -terminal Scar homology domain. Subsequently,
Src	*Rous sarcoma* virus kinase
Swiss 3T3	3T3 Swiss albin, mouse fibroblast
TBS	150 mM NaCl, 50 mM Tris-HCl pH 7.5
TIAM1	T-lymphoma cells as an invasion- and metastasis-inducing gene
TRIS	tris(hydroxymethyl)aminomethane
TRITC	tetramethylrhodamineisothiocyanate
Ts	temperature sensitive
TTBS	0.05% Tween 20, 150 mM NaCl, 50 mM Tris-HCl pH 7.5
U	unit
VCA	verprolin-cofilin-homology-acidic
WASP	Wiskot-Aldrich-syndrome protein

BIBLIOGRAPHY

Akiyama, T., Ishida, J., Nakagawa, S., Ogawara, H., Watanabe, S., Itoh, N., Shibuya, M., and Fukami, Y. (1987). Genistein, a specific inhibitor of tyrosine-specific protein kinases. J Biol Chem *262*, 5592-5595.

Alberts, A. S. (2001). Identification of a carboxyl-terminal diaphanous-related formin homology protein autoregulatory domain. J Biol Chem *276*, 2824-2830.

Alblas, J., Ulfman, L., Hordijk, P., and Koenderman, L. (2001). Activation of Rhoa and ROCK are essential for detachment of migrating leukocytes. Mol Biol Cell *12*, 2137-2145.

Alonso, T., and Santos, E. (1990). Increased intracellular glycerophosphoinositol is a biochemical marker for transformation by membrane-associated and cytoplasmic oncogenes. Biochem Biophys Res Commun *171*, 14-19.

Arber, S., Barbayannis, F. A., Hanser, H., Schneider, C., Stanyon, C. A., Bernard, O., and Caroni, P. (1998). Regulation of actin dynamics through phosphorylation of cofilin by LIM-kinase. Nature *393*, 805-809.

Armstrong, R. A. (1995). Investigation of the inhibitory effects of PGE2 and selective EP agonists on chemotaxis of human neutrophils. Br J Pharmacol *116*, 2903-2908.

Arthur, W. T., Quilliam, L. A., and Cooper, J. A. (2004). Rap1 promotes cell spreading by localizing Rac1 guanine nucleotide exchange factors. J Cell Biol *167*, 111-122.

Asaoka, Y., Oka, M., Yoshida, K., and Nishizuka, Y. (1991). Lysophosphatidylcholine as a possible second messenger synergistic to diacylglycerol and calcium ion for T-lymphocyte activation. Biochem Biophys Res Commun *178*, 1378-1385.

Aspenstrom, P. (1999). The Rho GTPases have multiple effects on the actin cytoskeleton. Exp Cell Res *246*, 20-25.

Bae, S. S., Lee, Y. H., Chang, J. S., Galadari, S. H., Kim, Y. S., Ryu, S. H., and Suh, P. G. (1998a). Src homology domains of phospholipase C gamma1 inhibit nerve growth factor-induced differentiation of PC12 cells. J Neurochem *71*, 178-185.

Bae, Y. S., Cantley, L. G., Chen, C. S., Kim, S. R., Kwon, K. S., and Rhee, S. G. (1998b). Activation of phospholipase C-gamma by phosphatidylinositol 3,4,5-trisphosphate. J Biol Chem *273*, 4465-4469.

Bahnson, B. J. (2005). Structure, function and interfacial allosterism in phospholipase A2: insight from the anion-assisted dimer. Arch Biochem Biophys *433*, 96-106.

Bain, J., McLauchlan, H., Elliott, M., and Cohen, P. (2003). The specificities of protein kinase inhibitors: an update. Biochem J *371*, 199-204.

Bamburg, J. R., and Wiggan, O. P. (2002). ADF/cofilin and actin dynamics in disease. Trends Cell Biol *12*, 598-605.

Barfod, E. T., Moore, A. L., Melnick, R. F., and Lidofsky, S. D. (2005). Src regulates distinct pathways for cell volume control through Vav and phospholipase Cgamma. J Biol Chem *280*, 25548-25557.

Barkalow, K., Witke, W., Kwiatkowski, D. J., and Hartwig, J. H. (1996). Coordinated regulation of platelet actin filament barbed ends by gelsolin and capping protein. J Cell Biol *134*, 389-399.

Baumeister, M. A., Martinu, L., Rossman, K. L., Sondek, J., Lemmon, M. A., and Chou, M. M. (2003). Loss of phosphatidylinositol 3-phosphate binding by the C-terminal Tiam-1 pleckstrin homology domain prevents in vivo Rac1 activation without affecting membrane targeting. J Biol Chem *278*, 11457-11464.

Bayer, K. U., and Schulman, H. (2001). Regulation of signal transduction by protein targeting: the case for CaMKII. Biochem Biophys Res Commun *289*, 917-923.

Beeler, T. J., Jona, I., and Martonosi, A. (1979). The effect of ionomycin on calcium fluxes in sarcoplasmic reticulum vesicles and liposomes. J Biol Chem *254*, 6229-6231.

Beningo, K. A., Dembo, M., Kaverina, I., Small, J. V., and Wang, Y. L. (2001). Nascent focal adhesions are responsible for the generation of strong propulsive forces in migrating fibroblasts. J Cell Biol *153*, 881-888.

Berridge, M. J., Bootman, M. D., and Roderick, H. L. (2003). Calcium signalling: dynamics, homeostasis and remodelling. Nat Rev Mol Cell Biol *4*, 517-529.

Berrie, C. P., Dragani, L. K., van der Kaay, J., Iurisci, C., Brancaccio, A., Rotilio, D., and Corda, D. (2002). Maintenance of PtdIns45P2 pools under limiting inositol conditions, as assessed by liquid chromatography-tandem mass spectrometry and PtdIns45P2 mass evaluation in Ras-transformed cells. Eur J Cancer *38*, 2463-2475.

Berrie, C. P., and Falasca, M. (2000). Patterns within protein/polyphosphoinositide interactions provide specific targets for therapeutic intervention. Faseb J *14*, 2618-2622.

Berrie, C. P., Iurisci, C., and Corda, D. (1999). Membrane transport and in vitro metabolism of the Ras cascade messenger, glycerophosphoinositol 4-phosphate. Eur J Biochem *266*, 413-419.

Bleasdale, J. E., Thakur, N. R., Gremban, R. S., Bundy, G. L., Fitzpatrick, F. A., Smith, R. J., and Bunting, S. (1990). Selective inhibition of receptor-coupled phospholipase C-dependent processes in human platelets and polymorphonuclear neutrophils. J Pharmacol Exp Ther *255*, 756-768.

Boggon, T. J., and Eck, M. J. (2004). Structure and regulation of Src family kinases. Oncogene *23*, 7918-7927.

Bompard, G., and Caron, E. (2004). Regulation of WASP/WAVE proteins: making a long story short. J Cell Biol *166*, 957-962.

Bootman, M. D., Berridge, M. J., and Roderick, H. L. (2002). Activating calcium release through inositol 1,4,5-trisphosphate receptors without inositol 1,4,5-trisphosphate. Proc Natl Acad Sci U S A *99*, 7320-7322.

Borm, B., Requardt, R. P., Herzog, V., and Kirfel, G. (2005). Membrane ruffles in cell migration: indicators of inefficient lamellipodia adhesion and compartments of actin filament reorganization. Exp Cell Res *302*, 83-95.

Bosanac, I., Michikawa, T., Mikoshiba, K., and Ikura, M. (2004). Structural insights into the regulatory mechanism of IP3 receptor. Biochim Biophys Acta *1742*, 89-102.

Bourguignon, L. Y., Zhu, H., Shao, L., and Chen, Y. W. (2000). Ankyrin-Tiam1 interaction promotes Rac1 signaling and metastatic breast tumor cell invasion and migration. J Cell Biol *150*, 177-191.

Brandt, D., Gimona, M., Hillmann, M., Haller, H., and Mischak, H. (2002). Protein kinase C induces actin reorganization via a Src- and Rho-dependent pathway. J Biol Chem *277*, 20903-20910.

Braun, A. P., and Schulman, H. (1995). A non-selective cation current activated via the multifunctional Ca(2+)-calmodulin-dependent protein kinase in human epithelial cells. J Physiol *488 (Pt 1)*, 37-55.

Brown, M. T., and Cooper, J. A. (1996). Regulation, substrates and functions of src. Biochim Biophys Acta *1287*, 121-149.

Bryan, J., and Kurth, M. C. (1984). Actin-gelsolin interactions. Evidence for two actin-binding sites. J Biol Chem *259*, 7480-7487.

Buccione, R., Baldassarre, M., Trapani, V., Catalano, C., Pompeo, A., Brancaccio, A., Giavazzi, R., Luini, A., and Corda, D. (2005). Glycerophosphoinositols inhibit the ability of tumour cells to invade the extracellular matrix. Eur J Cancer *41*, 470-476.

Buccione, R., Orth, J. D., and McNiven, M. A. (2004). Foot and mouth: podosomes, invadopodia and circular dorsal ruffles. Nat Rev Mol Cell Biol *5*, 647-657.

Buchanan, F. G., Elliot, C. M., Gibbs, M., and Exton, J. H. (2000). Translocation of the Rac1 guanine nucleotide exchange factor Tiam1 induced by platelet-derived growth factor and lysophosphatidic acid. J Biol Chem *275*, 9742-9748.

Buchsbaum, R. J., Connolly, B. A., and Feig, L. A. (2002). Interaction of Rac exchange factors Tiam1 and Ras-GRF1 with a scaffold for the p38 mitogen-activated protein kinase cascade. Mol Cell Biol *22*, 4073-4085.

Buchsbaum, R. J., Connolly, B. A., and Feig, L. A. (2003). Regulation of p70 S6 kinase by complex formation between the Rac guanine nucleotide exchange factor (Rac-GEF) Tiam1 and the scaffold spinophilin. J Biol Chem *278*, 18833-18841.

Buday, L., Wunderlich, L., and Tamas, P. (2002). The Nck family of adapter proteins: regulators of actin cytoskeleton. Cell Signal *14*, 723-731.

Burd, C. G., and Emr, S. D. (1998). Phosphatidylinositol(3)-phosphate signaling mediated by specific binding to RING FYVE domains. Mol Cell *2*, 157-162.

Carlier, M. F., and Pantaloni, D. (1994). Actin assembly in response to extracellular signals: role of capping proteins, thymosin beta 4 and profilin. Semin Cell Biol *5*, 183-191.

Carlier, M. F., Pantaloni, D., and Korn, E. D. (1987). The mechanisms of ATP hydrolysis accompanying the polymerization of Mg-actin and Ca-actin. J Biol Chem *262*, 3052-3059.

Chaminade, B., Le Balle, F., Fourcade, O., Nauze, M., Delagebeaudeuf, C., Gassama-Diagne, A., Simon, M. F., Fauvel, J., and Chap, H. (1999). New developments in phospholipase A2. Lipids *34 Suppl*, S49-55.

Cheever, M. L., Sato, T. K., de Beer, T., Kutateladze, T. G., Emr, S. D., and Overduin, M. (2001). Phox domain interaction with PtdIns(3)P targets the Vam7 t-SNARE to vacuole membranes. Nat Cell Biol *3*, 613-618.

Chen, W. T. (1989). Proteolytic activity of specialized surface protrusions formed at rosette contact sites of transformed cells. J Exp Zool *251*, 167-185.

Chien, U. H., Lai, M., Shih, T. Y., Verma, I. M., Scolnick, E. M., Roy-Burman, P., and Davidson, N. (1979). Heteroduplex analysis of the sequence relationships between the genomes of Kirsten and Harvey sarcoma viruses, their respective parental murine leukemia viruses, and the rat endogenous 30S RNA. J Virol *31*, 752-760.

Ching, T. T., Wang, D. S., Hsu, A. L., Lu, P. J., and Chen, C. S. (1999). Identification of multiple phosphoinositide-specific phospholipases D as new regulatory enzymes for phosphatidylinositol 3,4, 5-trisphosphate. J Biol Chem *274*, 8611-8617.

Clarke, N. G., and Dawson, R. M. (1981). Alkaline O leads to N-transacylation. A new method for the quantitative deacylation of phospholipids. Biochem J *195*, 301-306.

Condeelis, J. (2001). How is actin polymerization nucleated in vivo? Trends Cell Biol *11*, 288-293.

Connolly, B. A., Rice, J., Feig, L. A., and Buchsbaum, R. J. (2005). Tiam1-IRSp53 complex formation directs specificity of rac-mediated actin cytoskeleton regulation. Mol Cell Biol *25*, 4602-4614.

Cooper, D. M. (2003). Regulation and organization of adenylyl cyclases and cAMP. Biochem J *375*, 517-529.

Corda, D., and Falasca, M. (1996). Glycerophosphoinositols as potential markers of ras-induced transformation and novel second messengers. Anticancer Res *16*, 1341-1350.

Corda, D., Iurisci, C., and Berrie, C. P. (2002). Biological activities and metabolism of the lysophosphoinositides and glycerophosphoinositols. Biochim Biophys Acta *1582*, 52-69.

De Cesare, D., Fimia, G. M., and Sassone-Corsi, P. (1999). Signaling routes to CREM and CREB: plasticity in transcriptional activation. Trends Biochem Sci *24*, 281-285.

Defilippi, P., Olivo, C., Venturino, M., Dolce, L., Silengo, L., and Tarone, G. (1999). Actin cytoskeleton organization in response to integrin-mediated adhesion. Microsc Res Tech *47*, 67-78.

De Matteis, M., Godi, A., and Corda, D. (2002). Phosphoinositides and the golgi complex. Curr Opin Cell Biol *14*, 434-447.

Dennis, E. A. (1994). Diversity of group types, regulation, and function of phospholipase A2. J Biol Chem *269*, 13057-13060.

Dennis, E. A. (1997). The growing phospholipase A2 superfamily of signal transduction enzymes. Trends Biochem Sci *22*, 1-2.

DePianto, D., and Coulombe, P. A. (2004). Intermediate filaments and tissue repair. Exp Cell Res *301*, 68-76.

Dogterom, M., Kerssemakers, J. W., Romet-Lemonne, G., and Janson, M. E. (2005). Force generation by dynamic microtubules. Curr Opin Cell Biol *17*, 67-74.

dos Remedios, C. G., Chhabra, D., Kekic, M., Dedova, I. V., Tsubakihara, M., Berry, D. A., and Nosworthy, N. J. (2003). Actin binding proteins: regulation of cytoskeletal microfilaments. Physiol Rev *83*, 433-473.

Dowler, S., Currie, R. A., Campbell, D. G., Deak, M., Kular, G., Downes, C. P., and Alessi, D. R. (2000). Identification of pleckstrin-homology-domain-containing proteins with novel phosphoinositide-binding specificities. Biochem J *351*, 19-31.

Dvorsky, R., and Ahmadian, M. R. (2004). Always look on the bright site of Rho: structural implications for a conserved intermolecular interface. EMBO Rep *5*, 1130-1136.

Edwards, D. C., Sanders, L. C., Bokoch, G. M., and Gill, G. N. (1999). Activation of LIM-kinase by Pak1 couples Rac/Cdc42 GTPase signalling to actin cytoskeletal dynamics. Nat Cell Biol *1*, 253-259.

Eva, A., and Aaronson, S. A. (1985). Isolation of a new human oncogene from a diffuse B-cell lymphoma. Nature *316*, 273-275.

Evangelista, M., Blundell, K., Longtine, M. S., Chow, C. J., Adames, N., Pringle, J. R., Peter, M., and Boone, C. (1997). Bni1p, a yeast formin linking cdc42p and the actin cytoskeleton during polarized morphogenesis. Science *276*, 118-122.

Falasca, M., Carvelli, A., Iurisci, C., Qiu, R. G., Symons, M. H., and Corda, D. (1997). Fast receptor-induced formation of glycerophosphoinositol-4-phosphate, a putative novel intracellular messenger in the Ras pathway. Mol Biol Cell *8*, 443-453.

Falasca, M., and Corda, D. (1994). Elevated levels and mitogenic activity of lysophosphatidylinositol in k-ras-transformed epithelial cells. Eur J Biochem *221*, 383-389.

Falasca, M., Iurisci, C., Carvelli, A., Sacchetti, A., and Corda, D. (1998). Release of the mitogen lysophosphatidylinositol from H-Ras-transformed fibroblasts; a possible mechanism of autocrine control of cell proliferation. Oncogene *16*, 2357-2365.

Falasca, M., Marino, M., Carvelli, A., Iurisci, C., Leoni, S., and Corda, D. (1996). Changes in the levels of glycerophosphoinositols during differentiation of hepatic and neuronal cells. Eur J Biochem *241*, 386-392.

Falasca, M., Silletta, M. G., Carvelli, A., Di Francesco, A. L., Fusco, A., Ramakrishna, V., and Corda, D. (1995). Signalling pathways involved in the mitogenic action of lysophosphatidylinositol. Oncogene *10*, 2113-2124.

Fang, X., Gaudette, D., Furui, T., Mao, M., Estrella, V., Eder, A., Pustilnik, T., Sasagawa, T., Lapushin, R., Yu, S., *et al.* (2000). Lysophospholipid growth factors in the initiation, progression, metastases, and management of ovarian cancer. Ann N Y Acad Sci *905*, 188-208.

Feller, S. M. (2001). Crk family adaptors-signalling complex formation and biological roles. Oncogene *20*, 6348-6371.

Feng, Y., and Walsh, C. A. (2004). The many faces of filamin: a versatile molecular scaffold for cell motility and signalling. Nat Cell Biol *6*, 1034-1038.

Ferry, X., Eichwald, V., Daeffler, L., and Landry, Y. (2001). Activation of betagamma subunits of G(i2) and G(i3) proteins by basic secretagogues induces exocytosis through phospholipase Cbeta and arachidonate release through phospholipase Cgamma in mast cells. J Immunol *167*, 4805-4813.

Fleming, I. N., Elliott, C. M., Buchanan, F. G., Downes, C. P., and Exton, J. H. (1999). Ca2+/calmodulin-dependent protein kinase II regulates Tiam1 by reversible protein phosphorylation. J Biol Chem *274*, 12753-12758.

Fleming, I. N., Elliott, C. M., and Exton, J. H. (1998). Phospholipase C-gamma, protein kinase C and Ca2+/calmodulin-dependent protein kinase II are involved in platelet-derived growth factor-induced phosphorylation of Tiam1. FEBS Lett *429*, 229-233.

Fleming, I. N., Gray, A., and Downes, C. P. (2000). Regulation of the Rac1-specific exchange factor Tiam1 involves both phosphoinositide 3-kinase-dependent and -independent components. Biochem J *351*, 173-182.

Fruman, D. A., Meyers, R. E., and Cantley, L. C. (1998). Phosphoinositide kinases. Annu Rev Biochem *67*, 481-507.

Gehrmann, T., and Heilmeyer, L. M., Jr. (1998). Phosphatidylinositol 4-kinases. Eur J Biochem *253*, 357-370.

Gettys, T. W., Fields, T. A., and Raymond, J. R. (1994). Selective activation of inhibitory G-protein alpha-subunits by partial agonists of the human 5-HT1A receptor. Biochemistry *33*, 4283-4290.

Ghosh, M., Song, X., Mouneimne, G., Sidani, M., Lawrence, D. S., and Condeelis, J. S. (2004). Cofilin promotes actin polymerization and defines the direction of cell motility. Science *304*, 743-746.

Gill, D. M., and Meren, R. (1978). ADP-ribosylation of membrane proteins catalyzed by cholera toxin: basis of the activation of adenylate cyclase. Proc Natl Acad Sci U S A *75*, 3050-3054.

Gillooly, D. J., Simonsen, A., and Stenmark, H. (2001). Cellular functions of phosphatidylinositol 3-phosphate and FYVE domain proteins. Biochem J *355*, 249-258.

Giovannardi, S., Racca, C., Bertollini, L., Sturani, E., and Peres, A. (1992). P2Y purinoceptors in normal NIH 3T3 and in NIH 3T3 overexpressing c-ras. Exp Cell Res *202*, 398-404.

Goetzl, E. J., Dolezalova, H., Kong, Y., and Zeng, L. (1999). Dual mechanisms for lysophospholipid induction of proliferation of human breast carcinoma cells. Cancer Res *59*, 4732-4737.

Gohla, A., Harhammer, R., and Schultz, G. (1998). The G-protein G13 but not G12 mediates signaling from lysophosphatidic acid receptor via epidermal growth factor receptor to Rho. J Biol Chem *273*, 4653-4659.

Goldschmidt-Clermont, P. J., Furman, M. I., Wachsstock, D., Safer, D., Nachmias, V. T., and Pollard, T. D. (1992). The control of actin nucleotide exchange by thymosin beta 4 and profilin. A potential regulatory mechanism for actin polymerization in cells. Mol Biol Cell *3*, 1015-1024.

Gotoh, T., Hattori, S., Nakamura, S., Kitayama, H., Noda, M., Takai, Y., Kaibuchi, K., Matsui, H., Hatase, O., Takahashi, H., and et al. (1995). Identification of Rap1 as a target for the Crk SH3 domain-binding guanine nucleotide-releasing factor C3G. Mol Cell Biol *15*, 6746-6753.

Goulding, E. H., Ngai, J., Kramer, R. H., Colicos, S., Axel, R., Siegelbaum, S. A., and Chess, A. (1992). Molecular cloning and single-channel properties of the cyclic nucleotide-gated channel from catfish olfactory neurons. Neuron *8*, 45-58.

Graham, F. L., and van der Eb, A. J. (1973). Transformation of rat cells by DNA of human adenovirus 5. Virology *54*, 536-539.

Habas, R., Kato, Y., and He, X. (2001). Wnt/Frizzled activation of Rho regulates vertebrate gastrulation and requires a novel Formin homology protein Daam1. Cell *107*, 843-854.

Habets, G. G., Scholtes, E. H., Zuydgeest, D., van der Kammen, R. A., Stam, J. C., Berns, A., and Collard, J. G. (1994). Identification of an invasion-inducing gene, Tiam-1, that encodes a protein with homology to GDP-GTP exchangers for Rho-like proteins. Cell *77*, 537-549.

Hall, A., Marshall, C. J., Spurr, N. K., and Weiss, R. A. (1983). Identification of transforming gene in two human sarcoma cell lines as a new member of the ras gene family located on chromosome 1. Nature *303*, 396-400.

Harrison, S. C. (2003). Variation on an Src-like theme. Cell *112*, 737-740.

Harvath, L. (1991). Neutrophil chemotactic factors. Exs *59*, 35-52.

Hasegawa, H., Kiyokawa, E., Tanaka, S., Nagashima, K., Gotoh, N., Shibuya, M., Kurata, T., and Matsuda, M. (1996). DOCK180, a major CRK-binding protein, alters cell morphology upon translocation to the cell membrane. Mol Cell Biol *16*, 1770-1776.

Hawkins, P. T., Stephens, L. R., and Piggott, J. R. (1993). Analysis of inositol metabolites produced by Saccharomyces cerevisiae in response to glucose stimulation. J Biol Chem *268*, 3374-3383.

Hibi, M., Lin, A., Smeal, T., Minden, A., and Karin, M. (1993). Identification of an oncoprotein- and UV-responsive protein kinase that binds and potentiates the c-Jun activation domain. Genes Dev *7*, 2135-2148.

Hirabayashi, T., Murayama, T., and Shimizu, T. (2004). Regulatory mechanism and physiological role of cytosolic phospholipase A2. Biol Pharm Bull *27*, 1168-1173.

Holmes, K. C., Popp, D., Gebhard, W., and Kabsch, W. (1990). Atomic model of the actin filament. Nature *347*, 44-49.

Honda, A., Nogami, M., Yokozeki, T., Yamazaki, M., Nakamura, H., Watanabe, H., Kawamoto, K., Nakayama, K., Morris, A. J., Frohman, M. A., and Kanaho, Y. (1999). Phosphatidylinositol 4-phosphate 5-kinase alpha is a downstream effector of the small G protein ARF6 in membrane ruffle formation. Cell *99*, 521-532.

Horio, T., Kohno, M., Kano, H., Ikeda, M., Yasunari, K., Yokokawa, K., Minami, M., and Takeda, T. (1995). Adrenomedullin as a novel antimigration factor of vascular smooth muscle cells. Circ Res *77*, 660-664.

Huff, T., Muller, C. S., Otto, A. M., Netzker, R., and Hannappel, E. (2001). beta-Thymosins, small acidic peptides with multiple functions. Int J Biochem Cell Biol *33*, 205-220.

Hunter, A. W., and Wordeman, L. (2000). How motor proteins influence microtubule polymerization dynamics. J Cell Sci *113 Pt 24*, 4379-4389.

Hwang, S. C., Jhon, D. Y., Bae, Y. S., Kim, J. H., and Rhee, S. G. (1996). Activation of phospholipase C-gamma by the concerted action of tau proteins and arachidonic acid. J Biol Chem *271*, 18342-18349.

Hyvonen, M., Macias, M. J., Nilges, M., Oschkinat, H., Saraste, M., and Wilmanns, M. (1995). Structure of the binding site for inositol phosphates in a PH domain. Embo J *14*, 4676-4685.

Iacovelli, L., Falasca, M., Valitutti, S., D'Arcangelo, D., and Corda, D. (1993). Glycerophosphoinositol 4-phosphate, a putative endogenous inhibitor of adenylylcyclase. J Biol Chem *268*, 20402-20407.

Imamura, H., Tanaka, K., Hihara, T., Umikawa, M., Kamei, T., Takahashi, K., Sasaki, T., and Takai, Y. (1997). Bni1p and Bnr1p: downstream targets of the Rho family small G-proteins which interact with profilin and regulate actin cytoskeleton in Saccharomyces cerevisiae. Embo J *16*, 2745-2755.

Irvine, R. F., Hemington, N., and Dawson, R. M. (1978). The hydrolysis of phosphatidylinositol by lysosomal enzymes of rat liver and brain. Biochem J *176*, 475-484.

Ishizaki, T., Naito, M., Fujisawa, K., Maekawa, M., Watanabe, N., Saito, Y., and Narumiya, S. (1997). p160ROCK, a Rho-associated coiled-coil forming protein kinase, works downstream of Rho and induces focal adhesions. FEBS Lett *404*, 118-124.

Jimenez, C., Portela, R. A., Mellado, M., Rodriguez-Frade, J. M., Collard, J., Serrano, A., Martinez, A. C., Avila, J., and Carrera, A. C. (2000). Role of the PI3K regulatory subunit in the control of actin organization and cell migration. J Cell Biol *151*, 249-262.

Jordan, M., Schallhorn, A., and Wurm, F. M. (1996). Transfecting mammalian cells: optimization of critical parameters affecting calcium-phosphate precipitate formation. Nucleic Acids Res *24*, 596-601.

Kabarowski, J.H., Zhu, K., Le, L.Q., Witte, O.N., and Xu, Y. (2001). Lysophosphatidylcholine as a ligand for the immunoregulatory receptor G2A. Science *293*, 702-705.

Kaibuchi, K. (1999). Regulation of cytoskeleton and cell adhesion by Rho targets. Prog Mol Subcell Biol *22*, 23-38.

Kaupp, U. B., Niidome, T., Tanabe, T., Terada, S., Bonigk, W., Stuhmer, W., Cook, N. J., Kangawa, K., Matsuo, H., Hirose, T., and et al. (1989). Primary structure and functional expression from complementary DNA of the rod photoreceptor cyclic GMP-gated channel. Nature *342*, 762-766.

Kaverina, I., Krylyshkina, O., and Small, J. V. (2002). Regulation of substrate adhesion dynamics during cell motility. Int J Biochem Cell Biol *34*, 746-761.

Kavran, J. M., Klein, D. E., Lee, A., Falasca, M., Isakoff, S. J., Skolnik, E. Y., and Lemmon, M. A. (1998). Specificity and promiscuity in phosphoinositide binding by pleckstrin homology domains. J Biol Chem *273*, 30497-30508.

Kawano, Y., Fukata, Y., Oshiro, N., Amano, M., Nakamura, T., Ito, M., Matsumura, F., Inagaki, M., and Kaibuchi, K. (1999). Phosphorylation of myosin-binding subunit (MBS) of myosin phosphatase by Rho-kinase in vivo. J Cell Biol *147*, 1023-1038.

Kawasaki, H., Springett, G. M., Mochizuki, N., Toki, S., Nakaya, M., Matsuda, M., Housman, D. E., and Graybiel, A. M. (1998). A family of cAMP-binding proteins that directly activate Rap1. Science *282*, 2275-2279.

Keely, P., Parise, L., and Juliano, R. (1998). Integrins and GTPases in tumour cell growth, motility and invasion. Trends Cell Biol *8*, 101-106.

Kemp, P., Hubscher, G., and Hawthorne, J. N. (1961). Phosphoinositides. 3. Enzymic hydrolysis of inositol-containing phospholipids. Biochem J *79*, 193-200.

Klein, P., Theibert, A., and Devreotes, P. (1988a). Identification and ligand-induced modification of the cAMP receptor in Dictyostelium. Methods Enzymol *159*, 267-278.

Klein, R. F., Nissenson, R. A., and Strewler, G. J. (1988b). Forskolin mimics the effects of calcitonin but not parathyroid hormone on bone resorption in vitro. Bone Miner *4*, 247-256.

Klepeis, V. E., Cornell-Bell, A., and Trinkaus-Randall, V. (2001). Growth factors but not gap junctions play a role in injury-induced Ca2+ waves in epithelial cells. J Cell Sci *114*, 4185-4195.

Klinghoffer, R. A., Sachsenmaier, C., Cooper, J. A., and Soriano, P. (1999). Src family kinases are required for integrin but not PDGFR signal transduction. Embo J *18*, 2459-2471.

Kobayashi, T., Kishimoto, M., and Okuyama, H. (1996). Phospholipases involved in lysophosphatidylinositol metabolism in rat brain. J Lipid Mediat Cell Signal *14*, 33-37.

Kohno, H., Tanaka, K., Mino, A., Umikawa, M., Imamura, H., Fujiwara, T., Fujita, Y., Hotta, K., Qadota, H., Watanabe, T., *et al.* (1996). Bni1p implicated in cytoskeletal control is a putative target of Rho1p small GTP binding protein in Saccharomyces cerevisiae. Embo J *15*, 6060-6068.

Korn, E. D., Carlier, M. F., and Pantaloni, D. (1987). Actin polymerization and ATP hydrolysis. Science *238*, 638-644.

Kraynov, V. S., Chamberlain, C., Bokoch, G. M., Schwartz, M. A., Slabaugh, S., and Hahn, K. M. (2000). Localized Rac activation dynamics visualized in living cells. Science *290*, 333-337.

Krugmann, S., Jordens, I., Gevaert, K., Driessens, M., Vandekerckhove, J., and Hall, A. (2001). Cdc42 induces filopodia by promoting the formation of an IRSp53:Mena complex. Curr Biol *11*, 1645-1655.

Kudo, I., and Murakami, M. (2002). Phospholipase A2 enzymes. Prostaglandins Other Lipid Mediat *68-69*, 3-58.

Kuriyama, S., Ohuchi, T., Yoshimura, N., and Honda, Y. (1991). Growth factor-induced cytosolic calcium ion transients in cultured human retinal pigment epithelial cells. Invest Ophthalmol Vis Sci *32*, 2882-2890.

Kushner, S. R. (1978). An improved method for transformation of Escherichia Coli with Col/EI derived plasmids. Elsevier/North Holland.

Labeta, M. O., Fernandez, N., and Festenstein, H. (1988). Solubilisation effect of Nonidet P-40, triton X-100 and CHAPS in the detection of MHC-like glycoproteins. J Immunol Methods *112*, 133-138.

Lambert, J. M., Lambert, Q. T., Reuther, G. W., Malliri, A., Siderovski, D. P., Sondek, J., Collard, J. G., and Der, C. J. (2002). Tiam1 mediates Ras activation of Rac by a PI(3)K-independent mechanism. Nat Cell Biol *4*, 621-625.

Lanier, S. M. (2004). AGS proteins, GPR motifs and the signals processed by heterotrimeric G proteins. Biol Cell *96*, 369-372.

Lassing, I., and Lindberg, U. (1985). Specific interaction between phosphatidylinositol 4,5-bisphosphate and profilactin. Nature *314*, 472-474.

Lauffenburger, D. A., and Horwitz, A. F. (1996). Cell migration: a physically integrated molecular process. Cell *84*, 359-369.

Lemmon, M. A., and Ferguson, K. M. (2000). Signal-dependent membrane targeting by pleckstrin homology (PH) domains. Biochem J *350 Pt 1*, 1-18.

Leslie, C. C. (1991). Kinetic properties of a high molecular mass arachidonoyl-hydrolyzing phospholipase A2 that exhibits lysophospholipase activity. J Biol Chem *266*, 11366-11371.

Lim, L., Manser, E., Leung, T., and Hall, C. (1996). Regulation of phosphorylation pathways by p21 GTPases. The p21 Ras-related Rho subfamily and its role in phosphorylation signalling pathways. Eur J Biochem *242*, 171-185.

Lio, Y. C., Reynolds, L. J., Balsinde, J., and Dennis, E. A. (1996). Irreversible inhibition of Ca(2+)-independent phospholipase A2 by methyl arachidonyl fluorophosphonate. Biochim Biophys Acta *1302*, 55-60.

Liu, P., Xu, Y., Hopfner, R. L., and Gopalakrishnan, V. (1999). Phosphatidic acid increases inositol-1,4,5,-trisphosphate and [Ca2+]i levels in neonatal rat cardiomyocytes. Biochim Biophys Acta *1440*, 89-99.

Loijens, J. C., Boronenkov, I. V., Parker, G. J., and Anderson, R. A. (1996). The phosphatidylinositol 4-phosphate 5-kinase family. Adv Enzyme Regul *36*, 115-140.

Lopez, I., Mak, E. C., Ding, J., Hamm, H. E., and Lomasney, J. W. (2001). A novel bifunctional phospholipase c that is regulated by Galpha 12 and stimulates the Ras/mitogen-activated protein kinase pathway. J Biol Chem *276*, 2758-2765.

Lupi, R., Corda, D., and Di Girolamo, M. (2000). Endogenous ADP-ribosylation of the G protein beta subunit prevents the inhibition of type 1 adenylyl cyclase. J Biol Chem *275*, 9418-9424.

Ma, Y. C., Huang, J., Ali, S., Lowry, W., and Huang, X. Y. (2000). Src tyrosine kinase is a novel direct effector of G proteins. Cell *102*, 635-646.

Machesky, L. M., Mullins, R. D., Higgs, H. N., Kaiser, D. A., Blanchoin, L., May, R. C., Hall, M. E., and Pollard, T. D. (1999). Scar, a WASp-related protein, activates nucleation of actin filaments by the Arp2/3 complex. Proc Natl Acad Sci U S A *96*, 3739-3744.

Maekawa, M., Ishizaki, T., Boku, S., Watanabe, N., Fujita, A., Iwamatsu, A., Obinata, T., Ohashi, K., Mizuno, K., and Narumiya, S. (1999). Signaling from Rho to the actin cytoskeleton through protein kinases ROCK and LIM-kinase. Science *285*, 895-898.

Mallik, R., and Gross, S. P. (2004). Molecular motors: strategies to get along. Curr Biol *14*, R971-982.

Manabe, R., Kovalenko, M., Webb, D. J., and Horwitz, A. R. (2002). GIT1 functions in a motile, multi-molecular signaling complex that regulates protrusive activity and cell migration. J Cell Sci *115*, 1497-1510.

Mancini, R., Piccolo, E., Mariggio, S., Filippi, B. M., Iurisci, C., Pertile, P., Berrie, C. P., and Corda, D. (2003). Reorganization of actin cytoskeleton by the phosphoinositide metabolite glycerophosphoinositol 4-phosphate. Mol Biol Cell *14*, 503-515.

Martin, G. S. (2001). The hunting of the Src. Nat Rev Mol Cell Biol *2*, 467-475.

McGough, A., Pope, B., Chiu, W., and Weeds, A. (1997). Cofilin changes the twist of F-actin: implications for actin filament dynamics and cellular function. J Cell Biol *138*, 771-781.

Mellor, H. (2004). Cell motility: Golgi signalling shapes up to ship out. Curr Biol *14*, R434-435.

Mellstrom, K., Heldin, C. H., and Westermark, B. (1988). Induction of circular membrane ruffling on human fibroblasts by platelet-derived growth factor. Exp Cell Res *177*, 347-359.

Mertens, A. E., Roovers, R. C., and Collard, J. G. (2003). Regulation of Tiam1-Rac signalling. FEBS Lett *546*, 11-16.

Michaelson, D., Silletti, J., Murphy, G., D'Eustachio, P., Rush, M., and Philips, M. R. (2001). Differential localization of Rho GTPases in live cells: regulation by hypervariable regions and RhoGDI binding. J Cell Biol *152*, 111-126.

Michell, R. H. (1992). Inositol lipids in cellular signalling mechanisms. Trends Biochem Sci *17*, 274-276.

Michiels, F., Stam, J. C., Hordijk, P. L., van der Kammen, R. A., Ruuls-Van Stalle, L., Feltkamp, C. A., and Collard, J. G. (1997). Regulated membrane localization of Tiam1, mediated by the NH2-terminal pleckstrin homology domain, is required for Rac-dependent membrane ruffling and C-Jun NH2-terminal kinase activation. J Cell Biol *137*, 387-398.

Miki, H., Yamaguchi, H., Suetsugu, S., and Takenawa, T. (2000). IRSp53 is an essential intermediate between Rac and WAVE in the regulation of membrane ruffling. Nature *408*, 732-735.

Mitchison, T. J., and Cramer, L. P. (1996). Actin-based cell motility and cell locomotion. Cell *84*, 371-379.

Moolenaar, W. H. (1999). Bioactive lysophospholipids and their G protein-coupled receptors. Exp Cell Res *253*, 230-238.

Moon, S. Y., and Zheng, Y. (2003). Rho GTPase-activating proteins in cell regulation. Trends Cell Biol *13*, 13-22.

Morris, E. P., and Torok, K. (2001). Oligomeric structure of alpha-calmodulin-dependent protein kinase II. J Mol Biol *308*, 1-8.

Mullins, R. D., Heuser, J. A., and Pollard, T. D. (1998). The interaction of Arp2/3 complex with actin: nucleation, high affinity pointed end capping, and formation of branching networks of filaments. Proc Natl Acad Sci U S A *95*, 6181-6186.

Nagasawa, S. Y., Takuwa, N., Sugimoto, N., Mabuchi, H., and Takuwa, Y. (2005). Inhibition of Rac activation as a mechanism for negative regulation of actin cytoskeletal reorganization and cell motility by cAMP. Biochem J *385*, 737-744.

Nakagawa, H., Miki, H., Ito, M., Ohashi, K., Takenawa, T., and Miyamoto, S. (2001). N-WASP, WAVE and Mena play different roles in the organization of actin cytoskeleton in lamellipodia. J Cell Sci *114*, 1555-1565.

Nakano, K., Takaishi, K., Kodama, A., Mammoto, A., Shiozaki, H., Monden, M., and Takai, Y. (1999). Distinct actions and cooperative roles of ROCK and mDia in Rho small G protein-induced reorganization of the actin cytoskeleton in Madin-Darby canine kidney cells. Mol Biol Cell *10*, 2481-2491.

Nobes, C. D., and Hall, A. (1995). Rho, rac and cdc42 GTPases: regulators of actin structures, cell adhesion and motility. Biochem Soc Trans *23*, 456-459.

Nobes, C. D., and Hall, A. (1999). Rho GTPases control polarity, protrusion, and adhesion during cell movement. J Cell Biol *144*, 1235-1244.

Nobes, C. D., Hawkins, P., Stephens, L., and Hall, A. (1995). Activation of the small GTP-binding proteins rho and rac by growth factor receptors. J Cell Sci *108 (Pt 1)*, 225-233.

Obermeier, A., Ahmed, S., Manser, E., Yen, S. C., Hall, C., and Lim, L. (1998). PAK promotes morphological changes by acting upstream of Rac. Embo J *17*, 4328-4339.

Otey, C. A., and Carpen, O. (2004). Alpha-actinin revisited: a fresh look at an old player. Cell Motil Cytoskeleton *58*, 104-111.

Paduch, M., Jelen, F., and Otlewski, J. (2001). Structure of small G proteins and their regulators. Acta Biochim Pol *48*, 829-850.

Palmer, F. B. (1986). Metabolism of lysopolyphosphoinositides by rat brain and liver microsomes. Biochem Cell Biol *64*, 117-125.

Pantaloni, D., Boujemaa, R., Didry, D., Gounon, P., and Carlier, M. F. (2000). The Arp2/3 complex branches filament barbed ends: functional antagonism with capping proteins. Nat Cell Biol *2*, 385-391.

Pantaloni, D., Le Clainche, C., and Carlier, M. F. (2001). Mechanism of actin-based motility. Science *292*, 1502-1506.

Parekh, D. B., Katso, R. M., Leslie, N. R., Downes, C. P., Procyk, K. J., Waterfield, M. D., and Parker, P. J. (2000). Beta1-integrin and PTEN control the phosphorylation of protein kinase C. Biochem J *352 Pt 2*, 425-433.

Parsons, S. J., and Parsons, J. T. (2004). Src family kinases, key regulators of signal transduction. Oncogene *23*, 7906-7909.

Pasteris, N. G., Cadle, A., Logie, L. J., Porteous, M. E., Schwartz, C. E., Stevenson, R. E., Glover, T. W., Wilroy, R. S., and Gorski, J. L. (1994). Isolation and characterization of the faciogenital dysplasia (Aarskog-Scott syndrome) gene: a putative Rho/Rac guanine nucleotide exchange factor. Cell *79*, 669-678.

Patki, V., Lawe, D. C., Corvera, S., Virbasius, J. V., and Chawla, A. (1998). A functional PtdIns(3)P-binding motif. Nature *394*, 433-434.

Patton-Vogt, J. L., and Henry, S. A. (1998). GIT1, a gene encoding a novel transporter for glycerophosphoinositol in Saccharomyces cerevisiae. Genetics *149*, 1707-1715.

Patton, J. L., Pessoa-Brandao, L., and Henry, S. A. (1995). Production and reutilization of an extracellular phosphatidylinositol catabolite, glycerophosphoinositol, by Saccharomyces cerevisiae. J Bacteriol *177*, 3379-3385.

Peppelenbosch, M. P., Qiu, R. G., de Vries-Smits, A. M., Tertoolen, L. G., de Laat, S. W., McCormick, F., Hall, A., Symons, M. H., and Bos, J. L. (1995). Rac mediates growth factor-induced arachidonic acid release. Cell *81*, 849-856.

Pittman, M. (1984). The concept of pertussis as a toxin-mediated disease. Pediatr Infect Dis *3*, 467-486.

Pollard, T. D., and Beltzner, C. C. (2002). Structure and function of the Arp2/3 complex. Curr Opin Struct Biol *12*, 768-774.

Pollard, T. D., Blanchoin, L., and Mullins, R. D. (2000). Molecular mechanisms controlling actin filament dynamics in nonmuscle cells. Annu Rev Biophys Biomol Struct *29*, 545-576.

Pollard, T. D., and Borisy, G. G. (2003). Cellular motility driven by assembly and disassembly of actin filaments. Cell *112*, 453-465.

Ponting, C. P. (1996). Novel domains in NADPH oxidase subunits, sorting nexins, and PtdIns 3-kinases: binding partners of SH3 domains? Protein Sci *5*, 2353-2357.

Price, J. T., Bonovich, M. T., and Kohn, E. C. (1997). The biochemistry of cancer dissemination. Crit Rev Biochem Mol Biol *32*, 175-253.

Price, L. S., Langeslag, M., ten Klooster, J. P., Hordijk, P. L., Jalink, K., and Collard, J. G. (2003). Calcium signaling regulates translocation and activation of Rac. J Biol Chem *278*, 39413-39421.

Raftopoulou, M., and Hall, A. (2004). Cell migration: Rho GTPases lead the way. Dev Biol *265*, 23-32.

Rameh, L. E., Arvidsson, A., Carraway, K. L., 3rd, Couvillon, A. D., Rathbun, G., Crompton, A., VanRenterghem, B., Czech, M. P., Ravichandran, K. S., Burakoff, S. J., *et al.* (1997). A comparative analysis of the phosphoinositide binding specificity of pleckstrin homology domains. J Biol Chem *272*, 22059-22066.

Rameh, L. E., Chen, C. S., and Cantley, L. C. (1995). Phosphatidylinositol (3,4,5)P3 interacts with SH2 domains and modulates PI 3-kinase association with tyrosine-phosphorylated proteins. Cell *83*, 821-830.

Rameh, L. E., Rhee, S. G., Spokes, K., Kazlauskas, A., Cantley, L. C., and Cantley, L. G. (1998). Phosphoinositide 3-kinase regulates phospholipase Cgamma-mediated calcium signaling. J Biol Chem *273*, 23750-23757.

Rebecchi, M. J., and Pentyala, S. N. (2000). Structure, function, and control of phosphoinositide-specific phospholipase C. Physiol Rev *80*, 1291-1335.

Rhee, S. G. (2001). Regulation of phosphoinositide-specific phospholipase C. Annu Rev Biochem *70*, 281-312.

Rhee, S. G., and Bae, Y. S. (1997). Regulation of phosphoinositide-specific phospholipase C isozymes. J Biol Chem *272*, 15045-15048.

Rhee, S. G., Suh, P. G., Ryu, S. H., and Lee, S. Y. (1989). Studies of inositol phospholipid-specific phospholipase C. Science *244*, 546-550.

Ridley, A. J. (1998). Mammalian cell microinjection assay to study the function of Rac and Rho. Methods Mol Biol *84*, 153-160.

Ridley, A. J. (1999). Stress fibres take shape. Nat Cell Biol *1*, E64-66.

Ridley, A. J., and Hall, A. (1992). The small GTP-binding protein rho regulates the assembly of focal adhesions and actin stress fibers in response to growth factors. Cell *70*, 389-399.

Ridley, A. J., Paterson, H. F., Johnston, C. L., Diekmann, D., and Hall, A. (1992). The small GTP-binding protein rac regulates growth factor-induced membrane ruffling. Cell *70*, 401-410.

Riese, M. J., Goehring, U. M., Ehrmantraut, M. E., Moss, J., Barbieri, J. T., Aktories, K., and Schmidt, G. (2002). Auto-ADP-ribosylation of Pseudomonas aeruginosa ExoS. J Biol Chem *277*, 12082-12088.

Rinnerthaler, G., Geiger, B., and Small, J. V. (1988). Contact formation during fibroblast locomotion: involvement of membrane ruffles and microtubules. J Cell Biol *106*, 747-760.

Rohatgi, R., Ho, H. Y., and Kirschner, M. W. (2000). Mechanism of N-WASP activation by CDC42 and phosphatidylinositol 4, 5-bisphosphate. J Cell Biol *150*, 1299-1310.

Rohatgi, R., Ma, L., Miki, H., Lopez, M., Kirchhausen, T., Takenawa, T., and Kirschner, M. W. (1999). The interaction between N-WASP and the Arp2/3 complex links Cdc42-dependent signals to actin assembly. Cell *97*, 221-231.

Ron, D., and Kazanietz, M. G. (1999). New insights into the regulation of protein kinase C and novel phorbol ester receptors. Faseb J *13*, 1658-1676.

Rosenmuller, T., Rydh, K., and Nanberg, E. (2001). Role of phosphoinositide 3OH-kinase in autocrine transformation by PDGF-BB. J Cell Physiol *188*, 369-382.

Roskoski, R., Jr. (2004). Src protein-tyrosine kinase structure and regulation. Biochem Biophys Res Commun *324*, 1155-1164.

Rottner, K., Hall, A., and Small, J. V. (1999). Interplay between Rac and Rho in the control of substrate contact dynamics. Curr Biol *9*, 640-648.

Ryu, J. K., Choi, H. B., Hatori, K., Heisel, R. L., Pelech, S. L., McLarnon, J. G., and Kim, S. U. (2003). Adenosine triphosphate induces proliferation of human neural stem cells: Role of calcium and p70 ribosomal protein S6 kinase. J Neurosci Res *72*, 352-362.

Schmidt, A., and Hall, A. (2002). Guanine nucleotide exchange factors for Rho GTPases: turning on the switch. Genes Dev *16*, 1587-1609.

Secrist, J. P., Sehgal, I., Powis, G., and Abraham, R. T. (1990). Preferential inhibition of the platelet-derived growth factor receptor tyrosine kinase by staurosporine. J Biol Chem *265*, 20394-20400.

Self, A. J., and Hall, A. (1995). Measurement of intrinsic nucleotide exchange and GTP hydrolysis rates. Methods Enzymol *256*, 67-76.

Sheng, M., Thompson, M. A., and Greenberg, M. E. (1991). CREB: a Ca(2+)-regulated transcription factor phosphorylated by calmodulin-dependent kinases. Science *252*, 1427-1430.

Shih, T. Y., Williams, D. R., Weeks, M. O., Maryak, J. M., Vass, W. C., and Scolnick, E. M. (1978). Comparison of the genomic organization of Kirsten and Harvey sarcoma viruses. J Virol *27*, 45-55.

Siderovski, D. P., Hessel, A., Chung, S., Mak, T. W., and Tyers, M. (1996). A new family of regulators of G-protein-coupled receptors? Curr Biol *6*, 211-212.

Silflow, C. D., and Lefebvre, P. A. (2001). Assembly and motility of eukaryotic cilia and flagella. Lessons from Chlamydomonas reinhardtii. Plant Physiol *127*, 1500-1507.

Small, J. V., Rottner, K., Kaverina, I., and Anderson, K. I. (1998). Assembling an actin cytoskeleton for cell attachment and movement. Biochim Biophys Acta *1404*, 271-281.

Small, J. V., Stradal, T., Vignal, E., and Rottner, K. (2002). The lamellipodium: where motility begins. Trends Cell Biol *12*, 112-120.

Smit, M. J., Verzijl, D., and Iyengar, R. (1998). Identity of adenylyl cyclase isoform determines the rate of cell cycle progression in NIH 3T3 cells. Proc Natl Acad Sci U S A *95*, 15084-15089.

Song, C., Chang, X. J., Bean, K. M., Proia, M. S., Knopf, J. L., and Kriz, R. W. (1999). Molecular characterization of cytosolic phospholipase A2-beta. J Biol Chem *274*, 17063-17067.

Song, X., Xu, W., Zhang, A., Huang, G., Liang, X., Virbasius, J. V., Czech, M. P., and Zhou, G. W. (2001). Phox homology domains specifically bind phosphatidylinositol phosphates. Biochemistry *40*, 8940-8944.

Stam, J. C., Sander, E. E., Michiels, F., van Leeuwen, F. N., Kain, H. E., van der Kammen, R. A., and Collard, J. G. (1997). Targeting of Tiam1 to the plasma membrane requires the cooperative function of the N-terminal pleckstrin homology domain and an adjacent protein interaction domain. J Biol Chem *272*, 28447-28454.

Stenmark, H., and Aasland, R. (1999). FYVE-finger proteins--effectors of an inositol lipid. J Cell Sci *112 (Pt 23)*, 4175-4183.

Stewart, A., Ghosh, M., Spencer, D. M., and Leslie, C. C. (2002). Enzymatic properties of human cytosolic phospholipase A(2)gamma. J Biol Chem *277*, 29526-29536.

Sumi, M., Kiuchi, K., Ishikawa, T., Ishii, A., Hagiwara, M., Nagatsu, T., and Hidaka, H. (1991). The newly synthesized selective Ca2+/calmodulin dependent protein kinase II inhibitor KN-93 reduces dopamine contents in PC12h cells. Biochem Biophys Res Commun *181*, 968-975.

Sumi, T., Matsumoto, K., and Nakamura, T. (2001). Specific activation of LIM kinase 2 via phosphorylation of threonine 505 by ROCK, a Rho-dependent protein kinase. J Biol Chem *276*, 670-676.

Sun, H. Q., Yamamoto, M., Mejillano, M., and Yin, H. L. (1999). Gelsolin, a multifunctional actin regulatory protein. J Biol Chem *274*, 33179-33182.

Sunahara, R. K., Dessauer, C. W., and Gilman, A. G. (1996). Complexity and diversity of mammalian adenylyl cyclases. Annu Rev Pharmacol Toxicol *36*, 461-480.

Sunahara, R. K., and Taussig, R. (2002). Isoforms of mammalian adenylyl cyclase: multiplicities of signaling. Mol Interv *2*, 168-184.

Sutherland, E. W. (1972). Studies on the mechanism of hormone action. Science *177*, 401-408.

Svoboda, K., Denk, W., Kleinfeld, D., and Tank, D. W. (1997). In vivo dendritic calcium dynamics in neocortical pyramidal neurons. Nature *385*, 161-165.

Takahashi, A., Camacho, P., Lechleiter, J. D., and Herman, B. (1999). Measurement of intracellular calcium. Physiol Rev *79*, 1089-1125.

Takahashi, K., Sasaki, T., Mammoto, A., Hotta, I., Takaishi, K., Imamura, H., Nakano, K., Kodama, A., and Takai, Y. (1998). Interaction of radixin with Rho small G protein GDP/GTP exchange protein Dbl. Oncogene *16*, 3279-3284.

Takai, Y., Sasaki, T., and Matozaki, T. (2001). Small GTP-binding proteins. Physiol Rev *81*, 153-208.

Takenawa, T., and Itoh, T. (2001). Phosphoinositides, key molecules for regulation of actin cytoskeletal organization and membrane traffic from the plasma membrane. Biochim Biophys Acta *1533*, 190-206.

Tapon, N., and Hall, A. (1997). Rho, Rac and Cdc42 GTPases regulate the organization of the actin cytoskeleton. Curr Opin Cell Biol *9*, 86-92.

Theriot, J. A. (1997). Accelerating on a treadmill: ADF/cofilin promotes rapid actin filament turnover in the dynamic cytoskeleton. J Cell Biol *136*, 1165-1168.

Thomas, G. H. (2001). Spectrin: the ghost in the machine. Bioessays *23*, 152-160.

Timpson, P., Jones, G. E., Frame, M. C., and Brunton, V. G. (2001). Coordination of cell polarization and migration by the Rho family GTPases requires Src tyrosine kinase activity. Curr Biol *11*, 1836-1846.

Toker, A. (2002). Phosphoinositides and signal transduction. Cell Mol Life Sci *59*, 761-779.

Tombes, R. M., Grant, S., Westin, E. H., and Krystal, G. (1995). G1 cell cycle arrest and apoptosis are induced in NIH 3T3 cells by KN-93, an inhibitor of CaMK-II (the multifunctional Ca2+/CaM kinase). Cell Growth Differ *6*, 1063-1070.

Ueda, H., Kobayashi, T., Kishimoto, M., Tsutsumi, T., and Okuyama, H. (1993). A possible pathway of phosphoinositide metabolism through EDTA-insensitive phospholipase A1 followed by lysophosphoinositide-specific phospholipase C in rat brain. J Neurochem *61*, 1874-1881.

Uehata, M., Ishizaki, T., Satoh, H., Ono, T., Kawahara, T., Morishita, T., Tamakawa, H., Yamagami, K., Inui, J., Maekawa, M., and Narumiya, S. (1997). Calcium sensitization of smooth muscle mediated by a Rho-associated protein kinase in hypertension. Nature *389*, 990-994.

Valitutti, S., Cucchi, P., Colletta, G., Di Filippo, C., and Corda, D. (1991). Transformation by the k-ras oncogene correlates with increases in phospholipase A2 activity, glycerophosphoinositol production and phosphoinositide synthesis in thyroid cells. Cell Signal *3*, 321-332.

van Corven, E. J., Groenink, A., Jalink, K., Eichholtz, T., and Moolenaar, W. H. (1989). Lysophosphatidate-induced cell proliferation: identification and dissection of signaling pathways mediated by G proteins. Cell *59*, 45-54.

Vanhaesebroeck, B., Leevers, S. J., Ahmadi, K., Timms, J., Katso, R., Driscoll, P. C., Woscholski, R., Parker, P. J., and Waterfield, M. D. (2001). Synthesis and function of 3-phosphorylated inositol lipids. Annu Rev Biochem *70*, 535-602.

Walsh, D. A., Perkins, J. P., and Krebs, E. G. (1968). An adenosine 3',5'-monophosphate-dependant protein kinase from rabbit skeletal muscle. J Biol Chem *243*, 3763-3765.

Wasserman, S. (1998). FH proteins as cytoskeletal organizers. Trends Cell Biol *8*, 111-115.

Watanabe, N., Kato, T., Fujita, A., Ishizaki, T., and Narumiya, S. (1999). Cooperation between mDia1 and ROCK in Rho-induced actin reorganization. Nat Cell Biol *1*, 136-143.

Watanabe, N., Madaule, P., Reid, T., Ishizaki, T., Watanabe, G., Kakizuka, A., Saito, Y., Nakao, K., Jockusch, B. M., and Narumiya, S. (1997). p140mDia, a mammalian homolog of Drosophila diaphanous, is a target protein for Rho small GTPase and is a ligand for profilin. Embo J *16*, 3044-3056.

Weiss, A. (1993). T cell antigen receptor signal transduction: a tale of tails and cytoplasmic protein-tyrosine kinases. Cell *73*, 209-212.

Weiss, R. A., Boettiger, D., and Murphy, H. M. (1977). Pseudotypes of avian sarcoma viruses with the envelope properties of vesicular stomatitis virus. Virology *76*, 808-825.

Wieland, C., Jakobs, K. H., and Wieland, T. (1994). Altered guanine nucleoside triphosphate binding to transducin by cholera toxin-catalysed ADP-ribosylation. Cell Signal *6*, 487-492.

Wishart, M. J., Taylor, G. S., and Dixon, J. E. (2001). Phoxy lipids: revealing PX domains as phosphoinositide binding modules. Cell *105*, 817-820.

Witke, W. (2004). The role of profilin complexes in cell motility and other cellular processes. Trends Cell Biol *14*, 461-469.

Worthylake, D. K., Rossman, K. L., and Sondek, J. (2000). Crystal structure of Rac1 in complex with the guanine nucleotide exchange region of Tiam1. Nature *408*, 682-688.

Wu, Y., Perisic, O., Williams, R. L., Katan, M., and Roberts, M. F. (1997). Phosphoinositide-specific phospholipase C delta1 activity toward micellar substrates, inositol 1,2-cyclic phosphate, and other water-soluble substrates: a sequential mechanism and allosteric activation. Biochemistry *36*, 11223-11233.

Xu, Y., Fang, X. J., Casey, G., and Mills, G. B. (1995). Lysophospholipids activate ovarian and breast cancer cells. Biochem J *309 (Pt 3)*, 933-940.

Yamamoto, T., Takeuchi, H., Kanematsu, T., Allen, V., Yagisawa, H., Kikkawa, U., Watanabe, Y., Nakasima, A., Katan, M., and Hirata, M. (1999). Involvement of EF hand motifs in the Ca(2+)-dependent binding of the pleckstrin homology domain to phosphoinositides. Eur J Biochem *265*, 481-490.

Yin, H. L., and Stossel, T. P. (1980). Purification and structural properties of gelsolin, a Ca2+-activated regulatory protein of macrophages. J Biol Chem *255*, 9490-9493.

Zeller, R., Haramis, A. G., Zuniga, A., McGuigan, C., Dono, R., Davidson, G., Chabanis, S., and Gibson, T. (1999). Formin defines a large family of morphoregulatory genes and functions in establishment of the polarising region. Cell Tissue Res *296*, 85-93.

Zheng, Y. (2001). Dbl family guanine nucleotide exchange factors. Trends Biochem Sci *26*, 724-732.

Zhou, K., Wang, Y., Gorski, J. L., Nomura, N., Collard, J., and Bokoch, G. M. (1998). Guanine nucleotide exchange factors regulate specificity of downstream signaling from Rac and Cdc42. J Biol Chem *273*, 16782-16786.

ACKNOWLEDGMENTS

I would like to start by thanking my Director of Studies Daniela Corda for her guidance and support during the course of these investigations and Viki Allan, my second Supervisor, for our fruitful discussions of my experimental work. I am also grateful to Stefania Mariggiò for the precious and constant scientific discussions during the course of my thesis. Particular thanks go to Chris Berrie for his supervision during the writing of my thesis. Thanks also go to the Open University and to Roberto Buccione for making my PhD possible. I would like also to mention my two discussants of my six monthly reports who gave to me many useful suggestion for my work, Roberto Buccione (again) and Michele Sallese, Mariella Di Girolamo for the discussions around my work, and finally, Alberto Luini for our 7 pm meetings together with Daniela;

Special thanks go to Nadia Dani, because she started her PhD with me and she was always near me, with her personal and scientific support.

Of course, I would like to thank all of my colleagues in the laboratory and also those who were here when I started: Cristiano, Pasquale, Valentina, Joirdi, Manu, Annalisa, Elena, Adriano and Cristina. I would also like to thank Massimiliano, Teo and Giuseppe for their help in setting up the conditions for some of my experiments.

A particular mention goes to my housemates: Antonella, Edy, Nadia and Cristina, and to all my friends here at the CMNS and in Loreto.

Finally, I want to thank Pino for his constant presence, and for always reminding me that there is more to life than just work, my sister Alessandra with her husband Matteo and my mother who have always been there for me and my father who was always the first with his support and encouragement.